MULTI-TARGET DRUG DISCOVERY AGAINST *STAPHYLOCOCCUS AUREUS* AND *TRYPANOSOMA BRUCEI* INFECTIONS

BY

YANG WANG

DISSERTATION

Submitted in partial fulfillment of the requirements
for the degree of Doctor of Philosophy in Chemistry
in the Graduate College of the
University of Illinois at Urbana-Champaign, 2016

Urbana, Illinois

Doctoral Committee:

Professor Eric Oldfield, Chair
Professor Robert B. Gennis
Professor Paul J. Hergenrother
Professor Steven C. Zimmerman

Abstract

The drug resistance has become a big threat to human health, and there is currently a dearth of new antibiotics being introduced. In order to find novel potent antibiotics against *Staphylococcus aureus*, a series of amidine and bisamidine compounds were synthesized and investigated against *Staphylococcus aureus*. The most active compounds are potent inhibitors against undecaprenyl diphosphate synthase (UPPS), an essential enzyme involved in cell wall biosynthesis pathway. Besides, they bound to an AT-rich DNA dodecamer $(CGCGAATTCGCG)_2$ and were found to increase the melting transition by up to 24 °C using differential scanning calorimetry (DSC). Good correlations ($R^2 = 0.89$, *S. aureus*) were found between experimental and predicted cell growth inhibition by using DNA ΔT_m and UPPS IC_{50} experimental results together with one computed descriptor. We also solved the structures of three bisamidines binding to DNA as well as three UPPS structures. Overall, the results are of general interest in the context of the development of resistance-resistant antibiotics that involve multi-targeting.

To extend the potential utility of this class of amidine compound, we tested them against *Trypanosoma brucei*, the causative agent of human African trypanosomiasis. The most active compound was a biphenyldiamidine which had an EC_{50} of 7.7 nM against bloodstream form parasites. There was little toxicity against two human cell lines with $CC_{50} > 100$ μM. There was also good *in vivo* activity in a mouse model of infection with 100% survival at 3 mg/kg i.p. The most potent lead blocked replication of kinetoplast DNA (k-DNA), but not nuclear DNA, in the parasite. Some compounds also inhibited the enzyme farnesyl diphosphate synthase (FPPS) and some were uncouplers of oxidative phosphorylation. We developed a computational model for *T. brucei* cell growth inhibition ($R^2 = 0.76$) using DNA ΔT_m values for inhibitor binding, combined with *T. brucei* FPPS IC_{50} values. Overall, the results suggest that it may be possible to develop multi-target drug leads against *T. brucei* that act by inhibiting both k-DNA replication and isoprenoid biosynthesis.

In the investigation of other novel inhibitors against *T. brucei*, we found out that the *Mycobacterium tuberculosis* cell growth inhibitor SQ109 showed potent activity against *T. brucei*. Then, I synthesized a library of 48 analogs of SQ109 in which the ethylene diamine linker was replaced by oxa-, thia- or heterocyclic species, and in some cases, the adamantyl

group was replaced by a 1,2-carborane or the N-geranyl group by another hydrophobic species. Compounds were tested against *Trypanosoma brucei* and two human cell lines (human embryonic kidney, HEK293T, and the hepatocellular carcinoma, HepG2). Most potent activity was found with a compound with a fixed positive charge (imidazolium ring), having IC_{50} values as low as 12 nM (5.5 ng/mL) and a selectivity index of ~300. In the investigation of ways of action, the best compound targeted the mitochondrial membrane potential, exhibiting stronger uncoupling effect and better cell growth inhibition activity compared with SQ109

In another project, we were looking for UPPS inhibitors as anti-infective by *in silico* screening. 12 UPPS crystal structures were used to validate virtual screening models then 100 virtual hits (from 450,000 compounds) were assayed against UPPS from *S. aureus* and *Escherichia coli.* The most promising inhibitors (IC_{50} ~2 μM) had activity against MRSA, *Listeria monocytogenes*, *Bacillus anthracis* and a vancomycin-resistant *Enterococcus* spp. with MIC or IC_{50} values in the 0.25-4 μg/mL range. Moreover, one compound, a rhodanine with close structural similarity to the commercial diabetes drug Epalrestat, exhibited good activity as well as a fractional inhibitory concentration index (FICI) of 0.1 with methicillin against the community-acquired MRSA USA300 strain, indicating strong synergism.

To further investigate antibacterial agents with novel motifs, I synthesized a series of benzoic acids and phenylphosphonic acids and investigated their effects on the growth of *Staphylococcus aureus* and *Bacillus subtilis*. One of the most active compounds acted synergistically with seven antibiotics known to target bacterial cell wall biosynthesis (a fractional inhibitory concentration index, FICI~0.35, on average) but had indifferent effects in combinations with six non cell-wall biosynthesis inhibitors (FICI~1.45, on average). The most active compounds were found to inhibit two enzymes in isoprenoid/bacterial cell wall biosynthesis: undecaprenyl diphosphate synthase (UPPS) and undecaprenyl diphophate phosphatase (UPPP), but not farnesyl diphosphate synthase, and there were good correlations between bacterial cell growth inhibition, UPPS inhibition and UPPP inhibition.

To My Parents, My Wife and My Child

Acknowledgments

It is my pleasure to express my gratitude to people who have been helping me throughout my Ph.D. studies.

First of all, I would like to thank my research advisor, Prof. Eric Oldfield for his constant support and guidance. He is a great mentor who teaches me how to become a good researcher. I am really grateful for the opportunity he gave me to work in the lab and the trust he has in me to pursue my own research ideas. It has been a really great experience interacting with Dr. Oldfield, both scientifically and personally.

Additionally, I am grateful to the members of the Oldfield group. I would like to thank Dr. Ke wang, Dr. Yonghui Zhang for training me in the lab, answering all my questions, and assisting me with my experiments. I thank Dr. Kai Li and Janish for collaboration. I also thank Francisco and Jikun for maintaining our internal website and make data processing much easier. I thank Xinxin, Lucas and Guodong for encouraging me along my way.

Moreover, I am very grateful to my collaborators from University of Illinois and other campus: Prof. Prof. J. Andrew McCammon, Dr. Joo-Hwan No, Prof. Michael Cynamon, Prof. Douglas Mitchell, Prof. Robert Gennis and Prof. Dean Crick, for their help and input on cell-based assays, respiration assays and molecular dynamics simulation, and X-ray crystallography.

Furthermore, I am very thankful to my thesis committee members, Prof. Robert Gennis, Prof. Paul J. Hergenrother and Professor Steven C. Zimmermanfor their suggestions during the committee meetings, as well as advice and support for my current and future career.

Last but not least, I would like to thank my parents, Mincai Guo and Zhidong Wang for their support and unconditional love throughout these years. I would also thank all my dear

friends for years of friendship, encouragement and support. And thank you, my dear baby, Yixin Wang, you are the miracle in my life. And lastly, I sincerely thank my wife, Yi Yu. You has been bringing me the greatest happiness in the world.

Table of Contents

Chapter 1: Introduction to the Multi-Target Drug Discovery Against *Staphylococcus aureus* and *Trypanosoma brucei* Infections

1.1 Multi-Targeting Drug Discovery

Drug resistance is on the rise but unfortunately, the number of new anti-infective drugs introduced is decreasing. The time line of dates of discovery of distinct classes of antibacterial is shown in figure 1.1.[1] The discovery of penicillin, the first natural product antibiotic, is a milestone in drug discovery, and it marks a true turning point in human history. Later there was a golden age of antibacterial discovery around 1940~60s. However, there have been no successful discoveries of novel agents since 1987. It means there has been a discovery void since then. On the other hand, the drug resistance has become a big threat to human health. According to the NIH data,[2] there are over 2 million of illnesses and 23 thousands of deaths are caused by antibiotic resistance every year in America. Also, there are additional illnesses and deaths caused indirectly by antibiotic resistance. Figure 1.2 shows time scale between the introduction of a new drug and the occurrence of the drug resistance.[3] Methicillin (Scheme 1.1), a derivative of penicillin, was introduced as the treatment to penicillin-resistant *Staphylococcus aureus* infections. However, only one year after the usage of methicillin,[4] the methicillin-resistant *Staphylococcus aureus* (MRSA) was observed in clinic. Even for vancomycin (Scheme 1.1), also called "the last defense of drug resistance", the resistance was obtained (vancomycin-resistant *enterococcus*) 32 years after the first clinical use of vancomycin. The average value of this time line is eight years, which is a relatively short period of time compared with the long time scale in drug discovery.

Scientists are looking for solutions to fight against drug resistance. On approach is to develop more antibiotics. In 2015, a new antibiotic was reported by nature, named Teixobactin (Scheme 1.1). In this work, the scientists did not obtain any mutants of *Staphylococcus aureus* or *Mycobacterium tuberculosis* resistant to this drug.[5] Another approach is the derivatization of existing antibiotics. One of the most famous example is the modification of beta lactam drugs. For example, methicillin was licensed in 1959 to treat penicillin-resistant *S. aureus* infections.[4] A third approach is multi-target therapy (Figure 1.3). Resistance occurred by the spontaneous generation of a point mutation in a target protein. While it is not possible to prevent mutations, it is logical to involve multiple targets into the therapy to reduce the likelihood of resistance. For example, combinational therapy was used in many commercialized drugs. In this case, two drugs with different targets are used in

one therapy. Moreover, if one drug would have two or more target, drug resistance is less likely to occur. As the development of multi-target drugs, the combination multi-target therapy would be a more powerful strategy to fight against drug resistance.

The multi-target drugs function in the following ways (Figure 1.3): "series inhibition"[6] (in which the targets are next to each other in a biosynthesis pathway and the product of one enzyme is the substrate for another, so an inhibitor might target both), "parallel inhibition"[7] (where the inhibitor targets unrelated pathways), or "network inhibition"[6] (which could involve both series and parallel inhibition). In my work, I will discuss the examples of these multi target drug leads.

1.2 Undecaprenyl Diphosphate Synthase

The cell wall biosynthesis pathway provides important targets for anti-bacterial drugs (such as vancomycin, methicillin). It begins at the tail end of either of the two isoprenoid biosynthesis pathways (Figure 1.4): the mevalonate pathway in *Staphylococcus aureus* or the methylerythritol phosphate (MEP) pathway in most other bacteria.[8] The products of the two pathways, dimethylallyl diphosphate (DMAPP) and isopentenyl diphosphate (IPP), are then converted to farnesyl diphosphate (FPP). In most bacteria, FPP condenses with 8 molecules of IPP to form *cis*-undecaprenyl diphosphate (UPP), a C_{55} precursor of peptidoglycan, and this reaction is catalyzed by undecaprenyl diphosphate synthase (UPPS).[9] UPP is converted to the monophosphate which then reacts with UDP-MurNAc pentapeptide to form Lipid I, then Lipid II, and finally peptidoglycan, *via* trans-glycosylation and trans-peptidylation.[10] Antibiotics such as methicillin and vancomycin block the last steps in peptidoglycan formation (Methicillin target the protein that catalyzes trans-peptidation, and vancomycin binds to the terminal D-Ala-D-Ala residues of the peptidoglycan precursor[11,12]). My work is focused on discovering drugs targeting isoprenoid biosynthesis, which is involved in the earliest steps of bacterial cell-wall biosynthesis (as shown in Figure 1.4).

UPPS is considered as an important drug target for the following reasons: First, the UPPS gene is the most up-regulated isoprenoid biosynthesis gene in *S. aureus* upon mevalonate pathway inhibition,[13] and in *Escherichia coli* upon non-mevalonate pathway inhibition,[14] indicating that UPPS is particularly important for cell survival; Second, there are no existing commercial drugs that inhibit this target, thus resistance will not be so easily acquired. Third, the UPPS inhibitors have the potential to synergize with other existing antibiotics whose targets are also in the same

biosynthetic pathway. Forth, UPPS is not used by humans,[15] so the possibility of UPPS inhibitors being toxic might be low.

Previously, we and others reported the discovery of several classes of UPPS inhibitors such as bisphosphonates[16] and diketoacids.[17] However, bisphosphonate inhibitors bind strongly to bone mineral and are readily removed from the circulation.[18] Thus, they are good for bone disease therapies, but not as anti-infectives. The diketoacid inhibitors suffer from instability and also have the disadvantage of low uptake and serum binding[19]. Thus, it is of interest to develop other UPPS inhibitors

Our group had determined how these inhibitors bind to UPPS by obtaining crystal structures of inhibitors bound to EcUPPS (Figure 1.5).[7] In the FPP binding site (site 1), a highly conserved Asp residue (D26) binds to the diphosphate group of substrate via Mg^{2+}.[20] The IPP binding site (site 2) is adjacent to D26 residue in site 1. It is expected that the anionic inhibitors with lipophilic side-chains (e.g. farnesyl S-thiolo-diphosphate, FSPP) would bind to site 1, as shown in Figure 1.5A. In the second structure, there are two FSPP molecules bound to the protein (Figure 1.5A).[7] One binds to site 1 and the other binds at the bottom of the protein (site 4). One additional binding site (site 3) was observed when the protein was crystallized with BPH-629,[21] a bisphosphonate inhibitor of UPPS, as shown in Figure 1.5B. In this structure, four molecules of the inhibitor bind to different sites (sites 1-4). The lipophilic side-chains of the four inhibitors occupy the large hydrophobic center of the protein that normally accommodates the lipophilic part of the C_{55} UPP product.

To distinguish the importance of these inhibitor binding sites, our group determined the structure of UPPS with different inhibitors. The less active benzoic acid inhibitors (inhibitors 1 and 2, Figure 1.6) bind to site 3 or sites 1, 2, 3, but activity is weak. Structures of more potent benzoic acid inhibitors (inhibitors 3 and 4, Figure 1.6) bound to UPPS were also determined. These inhibitors all have IC_{50} values against *E. coli* and *S. aureus* UPPS (EcUPPS and SaUPPS) of ~3 μM. In each of the X-ray structures, site 4 is occupied, together with one or more of sites 1, 2 or 3. These results suggest that the occupancy of site 4 is important for potent inhibition.[7]

1.3 Methicillin-Resistant *Staphylococcus aureus*

MRSA is the strain of *Staphylococcus aureus* that has developed resistance to beta-lactam antibiotics, which include the penicillins (methicillin, dicloxacillin, nafcillin, oxacillin, etc.) and

the cephalosporins.[22] Strains unable to resist these antibiotics are classified as methicillin-sensitive *Staphylococcus aureus*, or MSSA. The evolution of such resistance does not cause the organism to be more intrinsically virulent than strains of *S. aureus* that have no antibiotic resistance, but resistance does make MRSA infection more difficult to treat with standard types of antibiotics and thus more dangerous.

MRSA is especially troublesome in hospitals, prisons, and nursing homes, where patients with open wounds, invasive devices, and weakened immune systems are at greater risk of nosocomial infection than the general public (Figure 1.7).[23] MRSA infection has begun as a hospital-acquired infection, but has developed endemic status and is now sometimes community-acquired. MRSA causes 100000 severe infections, and is associated with 20000 death annually in USA.[24]

The general treatment of choice for *S. aureus* infection is penicillin and its derivatives, the class of beta lactam antibiotic.[25] Penicillin inhibits the formation of peptidoglycan cross-linkages that provide the rigidity and strength in a bacterial cell wall. MRSA strain is resistant to most β-lactam antibiotics. For this reason, vancomycin, a glycopeptide antibiotic, is commonly used to combat MRSA. Vancomycin binds to the terminal D-Ala-D-Ala residues of the peptidoglycan precursor, and prevents peptidoglycan cross-linkages from forming.[11] In this paper, I will develop novel compounds as antibiotics against MRSA.

1.4 *Trypanosoma brucei*

Human African trypanosomiasis (HAT), also known as sleeping sickness, is a parasitic disease of humans and other animals.[26] It is caused by protozoa of the species *Trypanosoma brucei*. HAT has two stages: haemo-lymphatic stage, accompanied by fever, headaches and itching, and neurological stage, appeared with changes of behavior, confusion and poor coordination. The population at risk is about 69 million with one third of this number being at a 'high' risk (Figure 1.8). 10000 new cases was reported in 2009.

Here shows the current treatment to sleeping sickness.[2] Suramin and pentamidine was developed more than 70 years ago and can only be used to treat the first stage of the disease. Meanwhile, they will result in strong side effect and sometimes the side effects are fetal. The Melarsoprol which is an arsenical compound, is effective to second stage, neurological stage of the disease. However, the compound is rather toxic and is lethal to 5-10 % of patient. Eflornithine is the only new drug against second stage of sleeping sickness during the past 50 years. And unfortunately, it also has

strong side effect. Moreover, drug resistance already occurred to these existing therapies. Moreover, since there are no vaccines available to prevent these diseases, there is a continuing need for new drugs.

1.5 SQ-109, a Tuberculosis Drug

Mycobacterium tuberculosis, the causative agent of tuberculosis, infects millions of people, resulting in 1-2 million deaths per year in the world. There is increasing resistance of *M. tuberculosis* to current antibiotics and in some cases, complete resistance is found.[27] Therefore, it is important to develop new drugs and drug leads. One of the oldest drugs for tuberculosis treatment is ethambutol (Scheme 1.2), an ethylene diamine derivative,[28] and recently, a series of 64000 analogs of ethambutol were synthesized and screened. From the screening, SQ-109 (Scheme 1.2) was found to be 4 fold more active than the other compounds made with an MIC of 0.7-1.56 μM against drug-resistant strains of *M. tuberculosis*.[29] It is of interest to us because it contains a geranyl group (C_{10}) together with a cationic center, making it a potential inhibitor of isoprenoid biosynthesis. The primary target of SQ-109 has been proposed to be the membrane protein MmpL3,[30] a trehalose monomycolate transporter. Several *M. tuberculosis* mutants produced via serial passage in the presence of other drugs had mutations in the MmpL3 gene and cross-resistance to SQ109, although the structural similarities between SQ109 and these compounds was not great, cross resistance was weak, and the mutation sites were quite spread out. It is puzzling that there have been no reports of spontaneous resistance to SQ-109, suggesting that SQ-109 may have multiple targets. Moreover, SQ-109 is active against other bacteria (e.g. *Helicobacter pylori*[31]) and yeasts (e.g. *Candida glabrata*[32]) that lack the MmpL3 gene, so there may be other targets or modes of action in *M. tuberculosis*.

SQ-109 contains a central ethylene diamine domain with pKa of ~10, therefore, is likely to be protonated at pH~7.4. This protonated molecule is a "hydrophobic-cationic-hydrophobic" species, indicating that it may inhibit the enzymes of which transition states or intermediates involve such a pharmacophore. The isoprenoid side-chain (the geranyl group) suggests the possibility of targeting enzymes in isoprenoid biosynthesis.

In other work carried out by Dr. Kai Li, a series of 11 SQ-109 analogs were synthesized and tested against *M. tuberculosis*.[6] The most active species was an ethanolamine analog (BPH-1283, Scheme 1.3) which was about 5 fold more active than was SQ-109 (MIC~0.02-0.05 μg/mL *versus* 0.1-0.2

μg/mL). His results suggested that in the structures of SQ-109 analogs, only one basic nitrogen is required for good activity against *M. tuberculosis.* SQ-109 and its analogs inhibit two enzymes (MenA and MenG) involved in menaquinone biosynthesis, the IC50 increases on rescue by menaquinone. Dean Crick's group discovered that our compounds inhibited electron transport and respiration. More recently, working with Dr. Dean Crick and Dr. Robert Gennis, we found that SQ109 and many of our compounds had potent activity on membranes, collapsing both pH gradients and the membrane potential (Figure 1.9). Here, I discuss the synthesis and activities of additional analogs of SQ-109.

1.6 Schemes, Charts, Tables and Figures

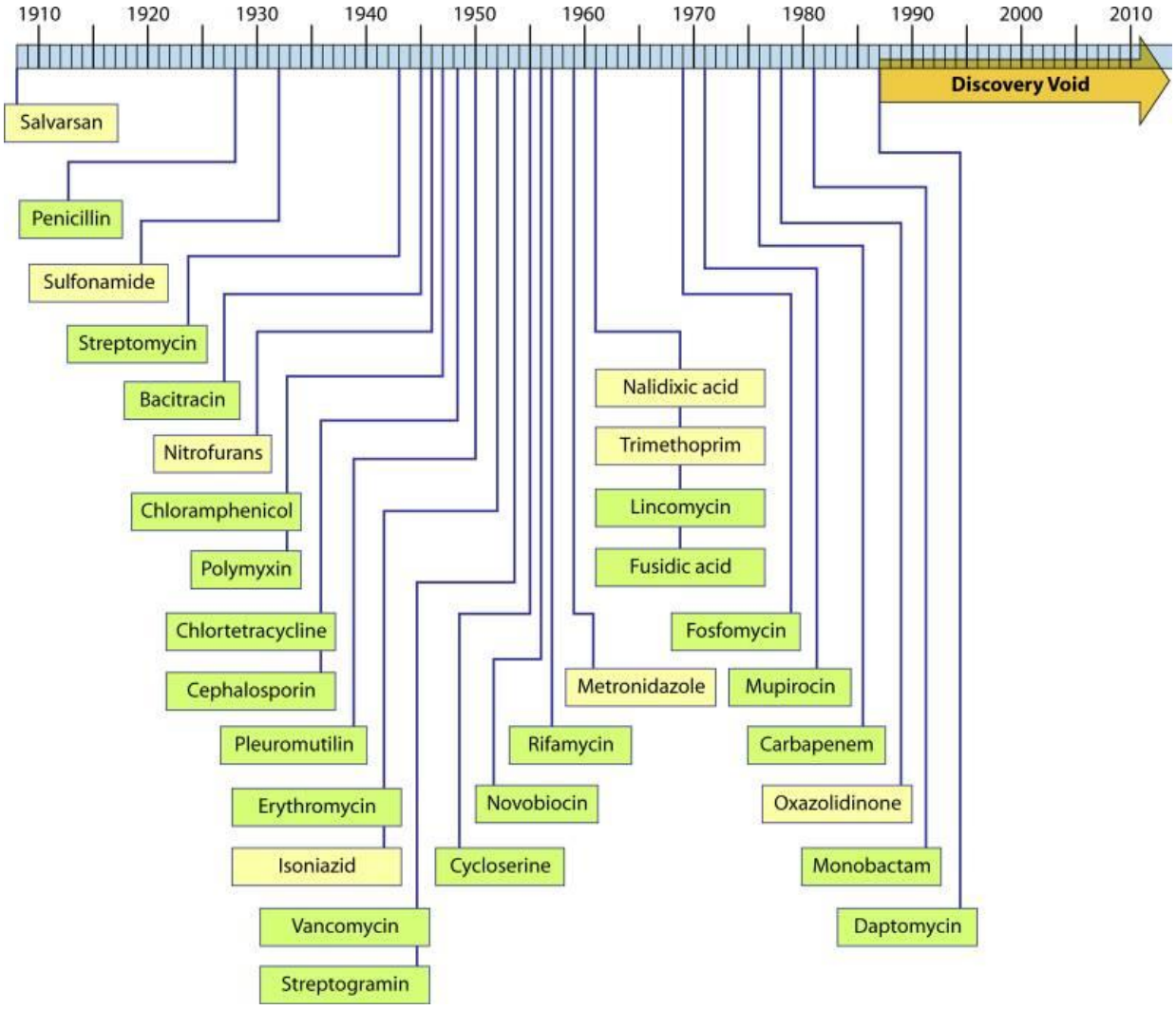

Figure 1.1. Illustration of the "discovery void." Dates indicated are those of reported initial discovery or patent. [1]

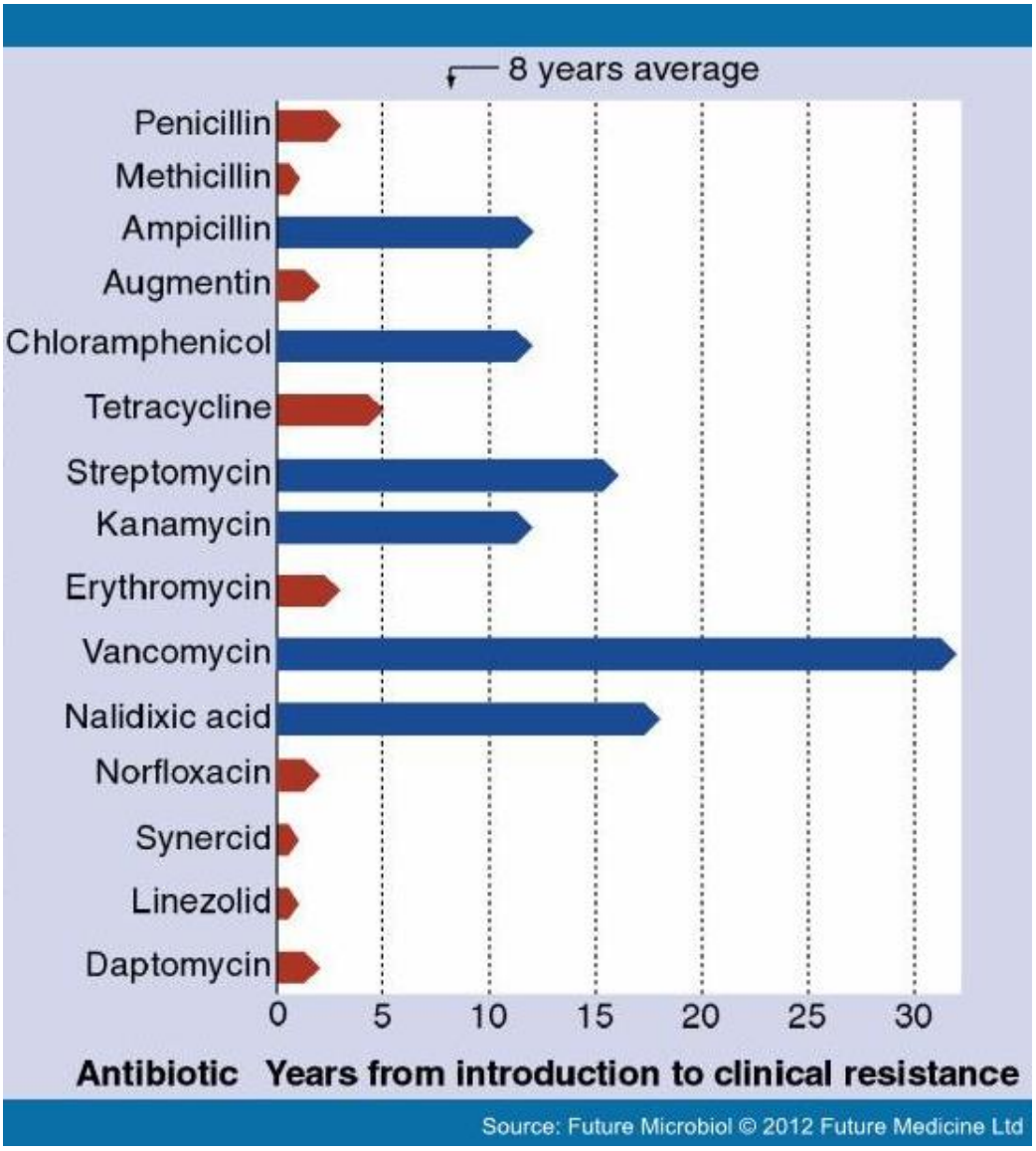

Figure 1.2. The time scale between the introduction of a new drug and the occurrence of the drug resistance.[33]

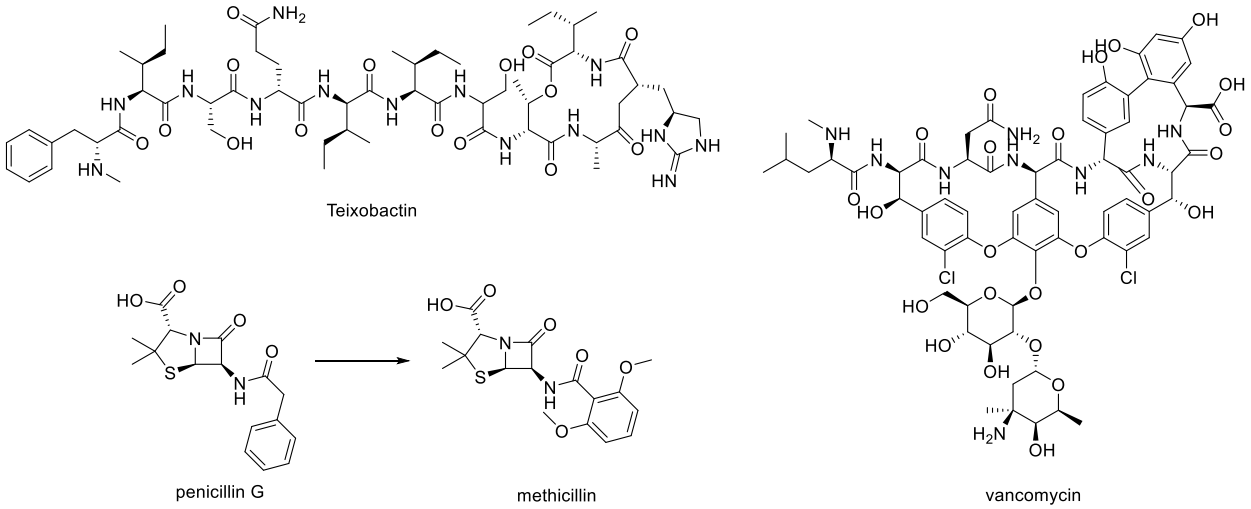

Scheme 1.1. Antibiotics discussed in the text.

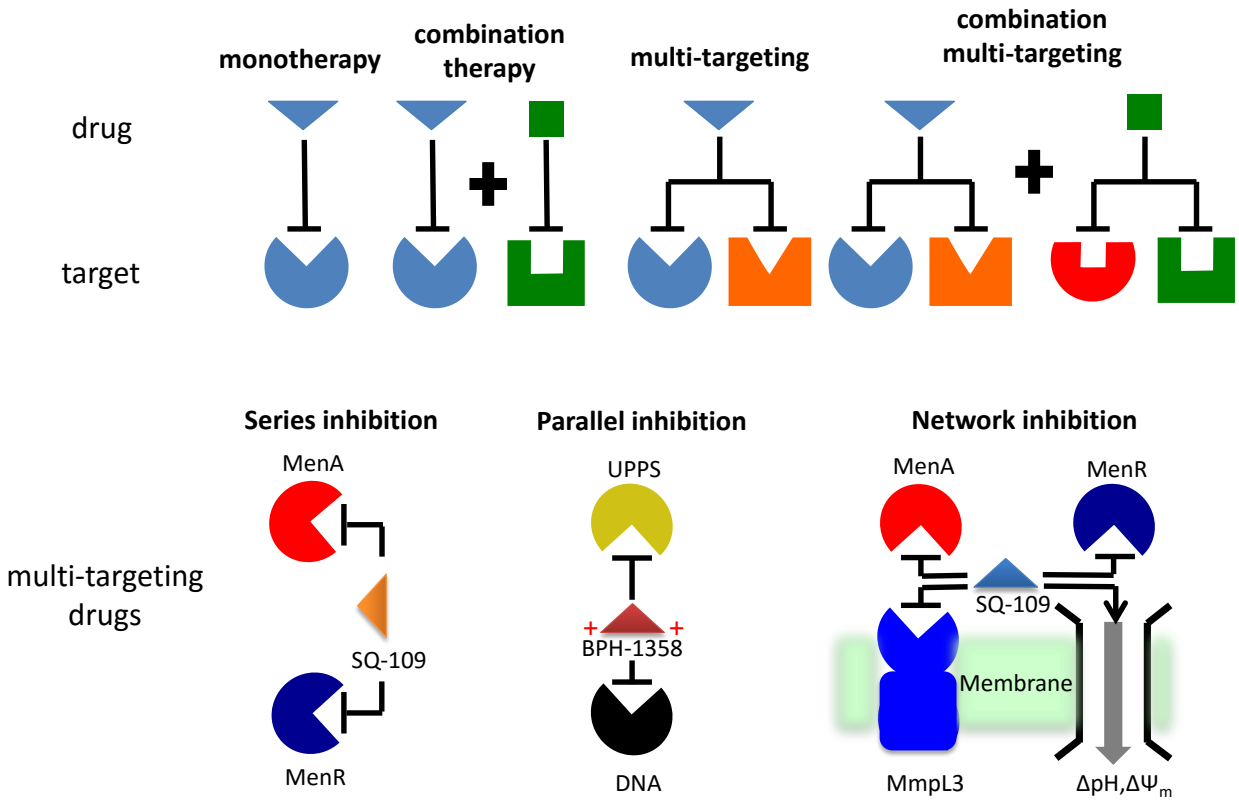

Figure 1.3. Schematic illustrations of multi-target therapies.

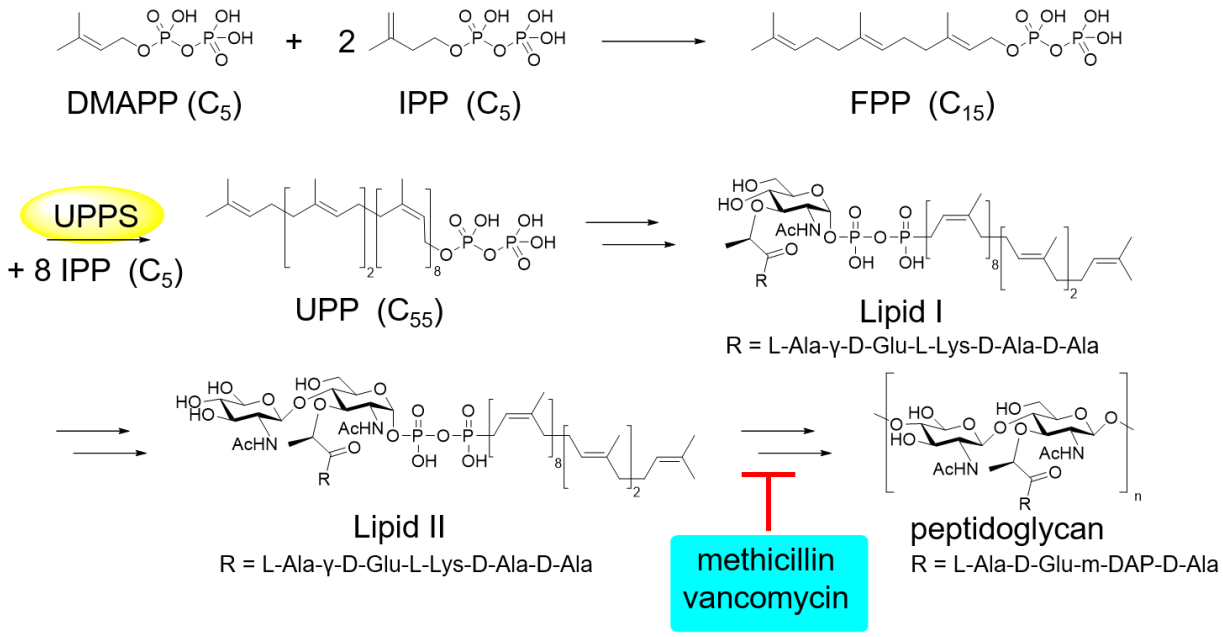

Figure 1.4. Schematic outline of cell wall biosynthesis (in most bacteria) showing involvement of isoprenoid biosynthesis in the early stages of peptidoglycan formation.[7]

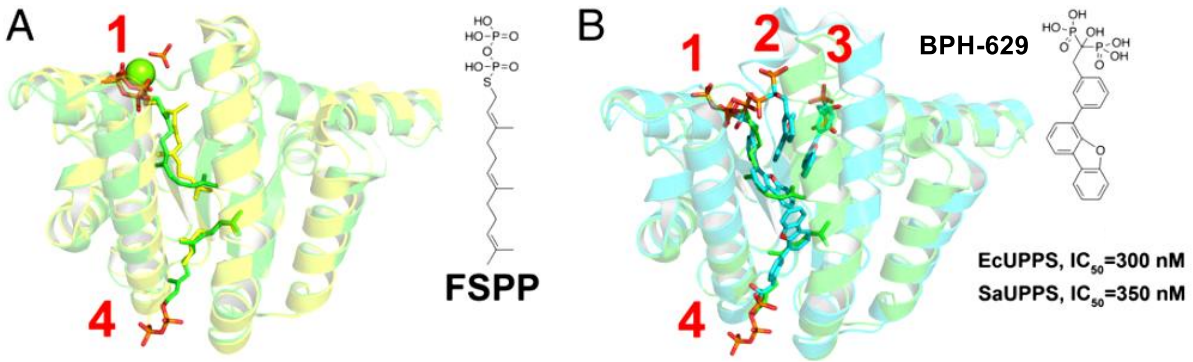

Figure 1.5. X-ray structures of *E. coli* UPPS showing substrate and inhibitor binding sites. (A) FSPP (yellow) binds to site 1 and FPP (green) binds to sites 1 and 4. (B) A bisphosphonate BPH-629 binds to sites 1~4.

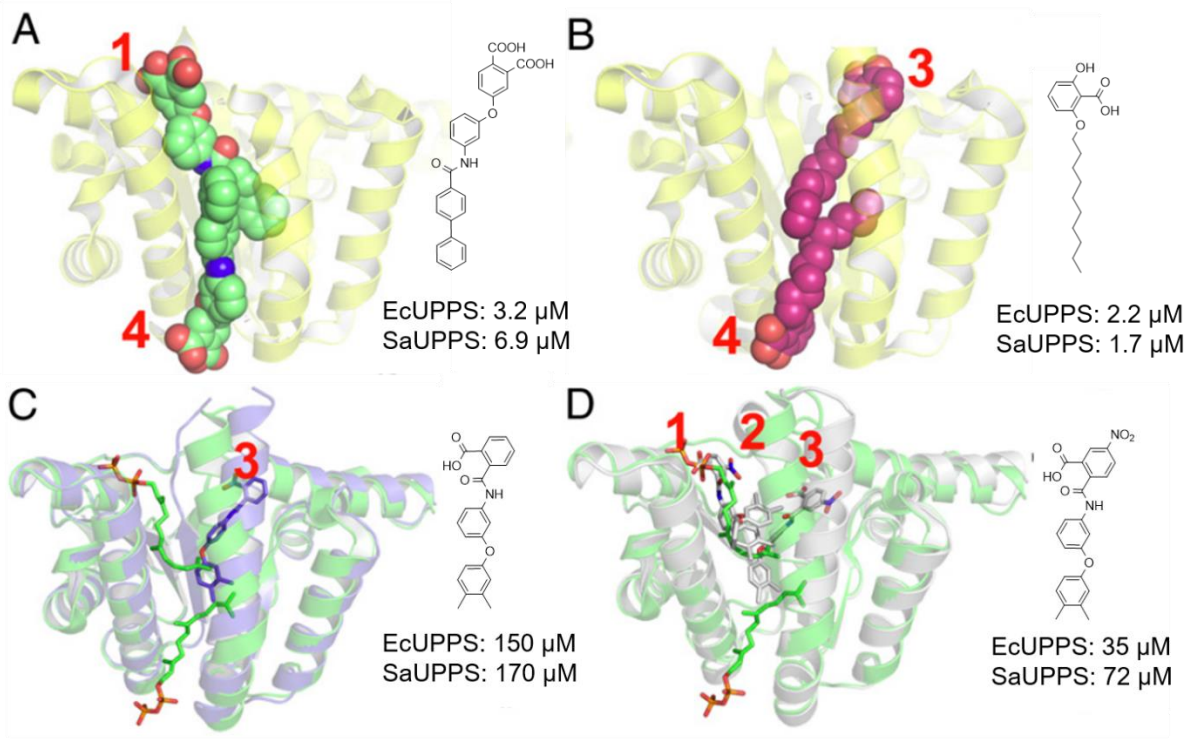

Figure 1.6. X-ray structures of *E. coli* UPPS showing substrate and benzoic acid inhibitor binding sites. (A) The potent inhibitor binds to site 1 and 4. (B) The potent inhibitor binds to site 3 and 4. (C) A weak inhibitor binds to sites 3. (C) A weak inhibitor binds to sites 1, 2 and 3.

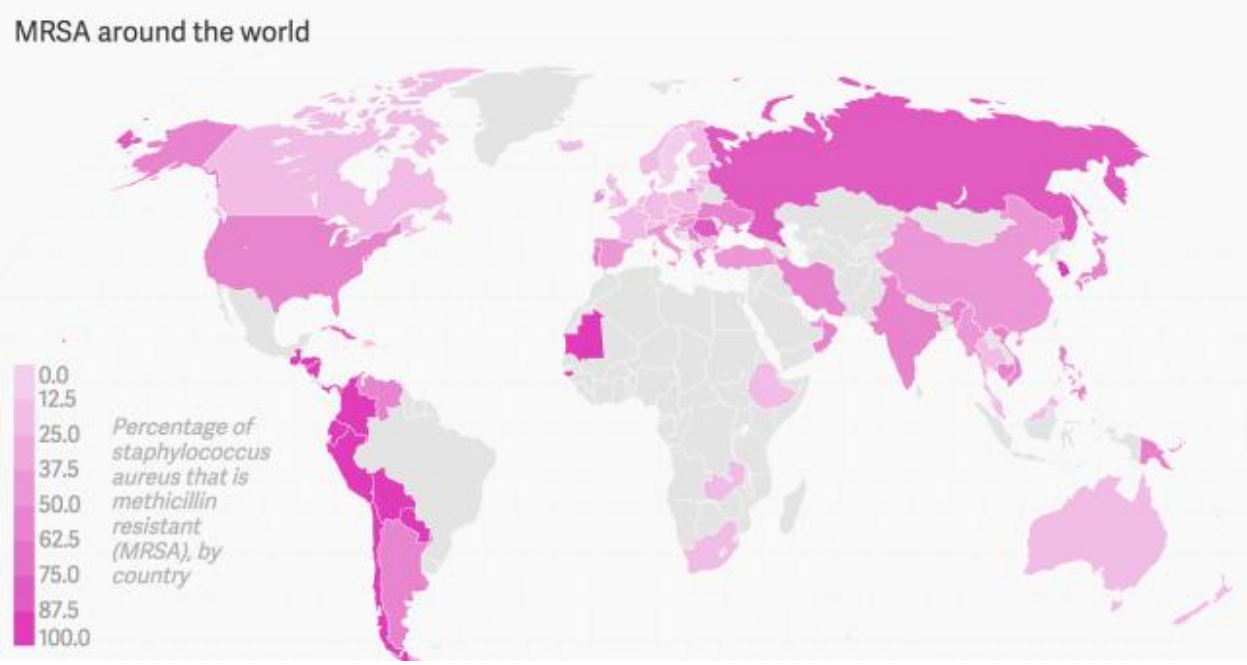

Figure 1.7. Percentage of *S. aureus* that is methicillin resistant (MRSA) by country.

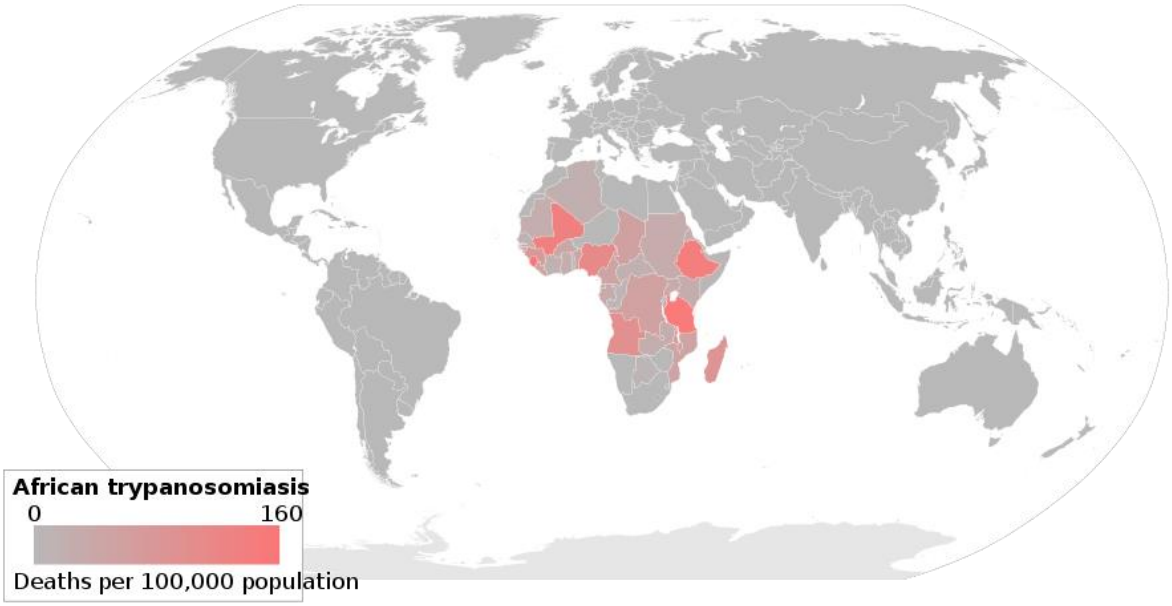

Figure 1.8. Deaths caused by *T. brucei* infection per 100,000 population.

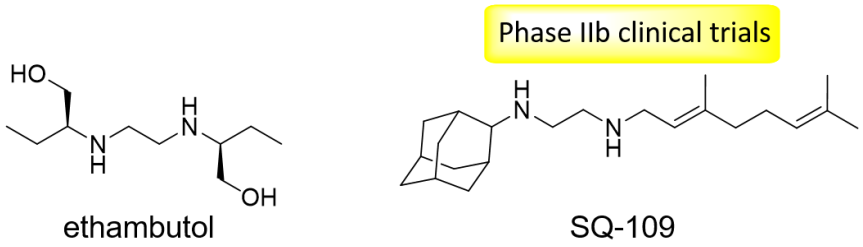

Scheme 1.2. Structure of ehambutol and SQ-109.

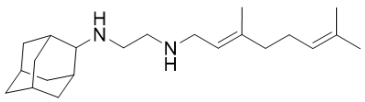

SQ 109 MIC_{90} = 0.15 µg/mL

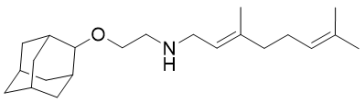

BPH 1283 MIC_{90} = 0.03 µg/mL

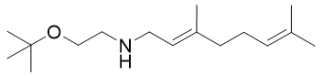

BPH 1398 MIC_{90} = 6.2 µg/mL

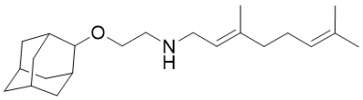

BPH 1283 MIC_{90} = 0.03 µg/mL

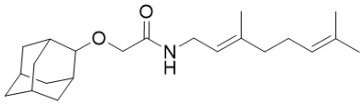

BPH 1282 MIC_{90} = 0.78 µg/mL

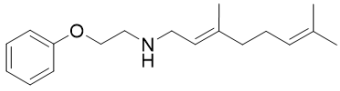

BPH 1399 MIC_{90} = 6.2 µg/mL

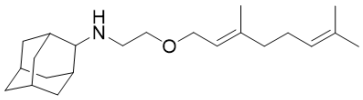

BPH 1281 MIC_{90} = 0.19 µg/mL

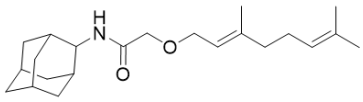

BPH 1284 MIC_{90} = 12 µg/mL

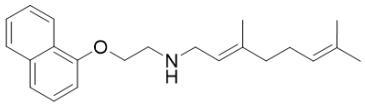

BPH 1400 MIC_{90} = 6.2 µg/mL

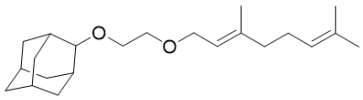

BPH 1280 MIC_{90} = 50 µg/mL

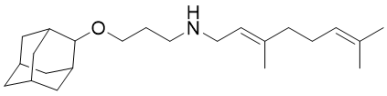

BPH 1304 MIC_{90} = 1.6 µg/mL

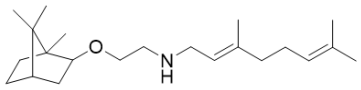

BPH 1402 MIC_{90} = 0.05 µg/mL

Scheme 1.3. SQ 109 analogs synthesized by Dr. Li and their activities against *M. tuberculosis*.

.

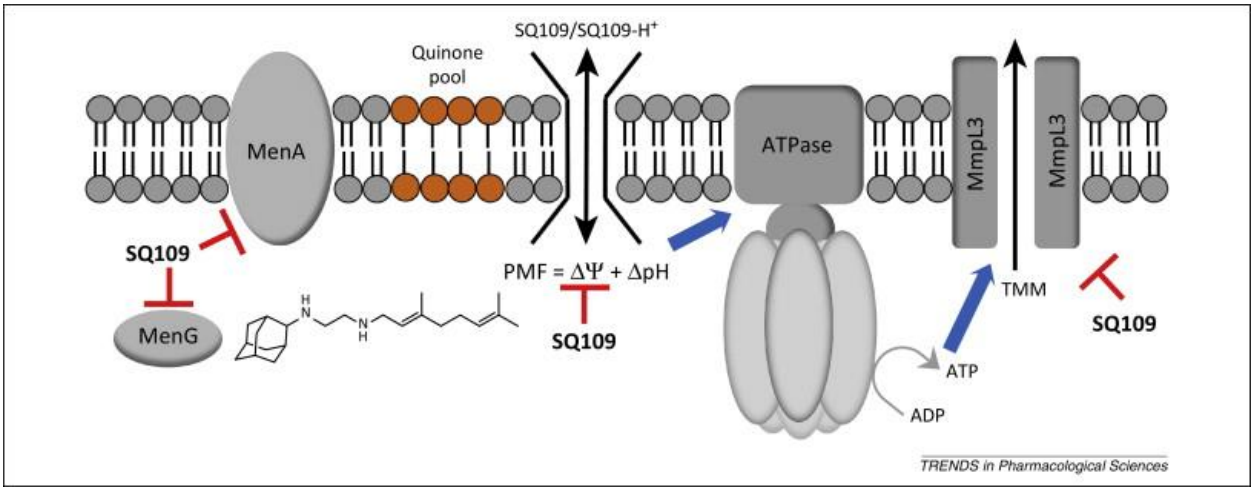

Figure 1.9. Investigation of ways of action of SQ-109.

1.7 References

1. Silver, L. L. Challenges of antibacterial discovery. *Clin. Microbiol. Rev.* **2011**, *24*, 71-109.
2. Baker, N.; de Koning, H. P.; Maser, P.; Horn, D. Drug resistance in African trypanosomiasis: the melarsoprol and pentamidine story. *Trends Parasitol.* **2013**, *29*, 110-118.
3. Gomes, E. S.; Schuch, V.; Lemos, E. G. D. Biotechnology of polyketides: New breath of life for the novel antibiotic genetic pathways discovery through metagenomics. *Braz. J. Microbiol.* **2013**, *44*.
4. Newsom, S. W. MRSA--past, present, future. *J. R. Soc. Med.* **2004**, *97*, 509-510.
5. Ling, L. L.; Schneider, T.; Peoples, A. J.; Spoering, A. L.; Engels, I.; Conlon, B. P.; Mueller, A.; Schaberle, T. F.; Hughes, D. E.; Epstein, S.; Jones, M.; Lazarides, L.; Steadman, V. A.; Cohen, D. R.; Felix, C. R.; Fetterman, K. A.; Millett, W. P.; Nitti, A. G.; Zullo, A. M.; Chen, C.; Lewis, K. A new antibiotic kills pathogens without detectable resistance. *Nature* **2015**, *517*, 455-459.
6. Li, K.; Schurig-Briccio, L. A.; Feng, X.; Upadhyay, A.; Pujari, V.; Lechartier, B.; Fontes, F. L.; Yang, H.; Rao, G.; Zhu, W.; Gulati, A.; No, J. H.; Cintra, G.; Bogue, S.; Liu, Y. L.; Molohon, K.; Orlean, P.; Mitchell, D. A.; Freitas-Junior, L.; Ren, F.; Sun, H.; Jiang, T.; Li, Y.; Guo, R. T.; Cole, S. T.; Gennis, R. B.; Crick, D. C.; Oldfield, E. Multitarget drug discovery for tuberculosis and other infectious diseases. *J. Med. Chem.* **2014**, *57*, 3126-3139.
7. Zhu, W.; Zhang, Y.; Sinko, W.; Hensler, M. E.; Olson, J.; Molohon, K. J.; Lindert, S.; Cao, R.; Li, K.; Wang, K.; Wang, Y.; Liu, Y. L.; Sankovsky, A.; de Oliveira, C. A.; Mitchell, D. A.; Nizet, V.; McCammon, J. A.; Oldfield, E. Antibacterial drug leads targeting isoprenoid biosynthesis. *Proc. Natl. Acad. Sci. U. S. A.* **2013**, *110*, 123-128.
8. Zhao, L.; Chang, W. C.; Xiao, Y.; Liu, H. W.; Liu, P. Methylerythritol phosphate pathway of isoprenoid biosynthesis. *Annu. Rev. Biochem* **2013**, *82*, 497-530.
9. Oldfield, E.; Lin, F. Y. Terpene biosynthesis: modularity rules. *Angew. Chem. Int. Ed. Engl.* **2012**, *51*, 1124-1137.
10. Bugg, T. D.; Braddick, D.; Dowson, C. G.; Roper, D. I. Bacterial cell wall assembly: still an attractive antibacterial target. *Trends Biotechnol.* **2011**, *29*, 167-173.
11. Small, P. M.; Chambers, H. F. Vancomycin for *Staphylococcus aureus* endocarditis in intravenous drug users. *Antimicrob. Agents Chemother.* **1990**, *34*, 1227-1231.
12. Hao, H. H.; Cheng, G. Y.; Dai, M. H.; Wu, Q. H.; Yuan, Z. H. Inhibitors targeting on cell wall biosynthesis pathway of MRSA. *Mol. Biosyst.* **2012**, *8*, 2828-2838.
13. Balibar, C. J.; Shen, X.; Tao, J. The mevalonate pathway of *Staphylococcus aureus*. *J. Bacteriol.* **2009**, *191*, 851-861.
14. Leon, A.; Liu, L.; Yang, Y.; Hudock, M. P.; Hall, P.; Yin, F.; Studer, D.; Puan, K. J.; Morita, C. T.; Oldfield, E. Isoprenoid biosynthesis as a drug target: bisphosphonate inhibition of *Escherichia coli* K12 growth and synergistic effects of fosmidomycin. *J. Med. Chem.* **2006**, *49*, 7331-7341.
15. Apfel, C. M.; Takacs, S.; Fountoulakis, M.; Stieger, M.; Keck, W. Use of genomics to identify bacterial undecaprenyl pyrophosphate synthetase: Cloning, expression, and characterization of the essential uppS gene. *J. Bacteriol.* **1999**, *181*, 483-492.

16. Guo, R. T.; Cao, R.; Liang, P. H.; Ko, T. P.; Chang, T. H.; Hudock, M. P.; Jeng, W. Y.; Chen, C. K. M.; Zhang, Y. H.; Song, Y. C.; Kuo, C. J.; Yin, F. L.; Oldfield, E.; Wang, A. H. J. Bisphosphonates target multiple sites in both cis- and trans-prenyltransferases. *Proc. Natl. Acad. Sci. U. S. A.* **2007**, *104*, 10022-10027.
17. Zhang, Y.; Fu-Yang, L.; Li, K.; Zhu, W.; Liu, Y. L.; Cao, R.; Pang, R.; Lee, E.; Axelson, J.; Hensler, M.; Wang, K.; Molohon, K. J.; Wang, Y.; Mitchell, D. A.; Nizet, V.; Oldfield, E. HIV-1 Integrase Inhibitor-Inspired Antibacterials Targeting Isoprenoid Biosynthesis. *ACS Med. Chem. Lett.* **2012**, *3*, 402-406.
18. Zhang, Y. H.; Cao, R.; Yin, F.; Hudock, M. P.; Guo, R. T.; Krysiak, K.; Mukherjee, S.; Gao, Y. G.; Robinson, H.; Song, Y.; No, J. H.; Bergan, K.; Leon, A.; Cass, L.; Goddard, A.; Chang, T. K.; Lin, F. Y.; Van Beek, E.; Papapoulos, S.; Wang, A. H. J.; Kubo, T.; Ochi, M.; Mukkamala, D.; Oldfield, E. Lipophilic Bisphosphonates as Dual Farnesyl/Geranylgeranyl Diphosphate Synthase Inhibitors: An X-ray and NMR Investigation. *J. Am. Chem. Soc.* **2009**, *131*, 5153-5162.
19. Neamati, N. *HIV-1 Intergrase: Mechanism and Inhibitor Design*; John Wiley & Sons, Inc.: John Wiley & Sons, Inc., 2011.
20. Lu, Y. P.; Liu, H. G.; Liang, P. H. Different reaction mechanisms for cis- and trans-prenyltransferases. *Biochem. Biophys. Res. Commun.* **2009**, *379*, 351-355.
21. Typas, A.; Banzhaf, M.; Gross, C. A.; Vollmer, W. From the regulation of peptidoglycan synthesis to bacterial growth and morphology. *Nat. Rev. Microbiol.* **2012**, *10*, 123-136.
22. McDougal, L. K.; Steward, C. D.; Killgore, G. E.; Chaitram, J. M.; McAllister, S. K.; Tenover, F. C. Pulsed-field gel electrophoresis typing of oxacillin-resistant *Staphylococcus aureus* isolates from the United States: establishing a national database. *J. Clin. Microbiol.* **2003**, *41*, 5113-5120.
23. *General Information About MRSA in the Community.* Centers for Disease Control and Prevention, 2013.
24. *Antimicrobial resistance.* World Health Organization, 2015.
25. *The development and discovery of penicillin 1928-1945*; American Chemistry Society and Royal Society of Chemistry
26. *Trypanosomiasis, human African (sleeping sickness).* World Health Organization, 2015.
27. *Global tuberculosis report 2015.* World Health Organization, 2015.
28. Koul, A.; Arnoult, E.; Lounis, N.; Guillemont, J.; Andries, K. The challenge of new drug discovery for tuberculosis. *Nature* **2011**, *469*, 483-490.
29. Lee, R. E.; Protopopova, M.; Crooks, E.; Slayden, R. A.; Terrot, M.; Barry, C. E. Combinatorial lead optimization of [1,2]-diamines based on ethambutol as potential antituberculosis preclinical candidates. *J. Comb. Chem.* **2003**, *5*, 172-187.
30. Tahlan, K.; Wilson, R.; Kastrinsky, D. B.; Arora, K.; Nair, V.; Fischer, E.; Barnes, S. W.; Walker, J. R.; Alland, D.; Barry, C. E.; Boshoff, H. I. SQ109 Targets MmpL3, a Membrane Transporter of Trehalose Monomycolate Involved in Mycolic Acid Donation to the Cell Wall Core of *Mycobacterium tuberculosis*. *Antimicrob. Agents Chemother.* **2012**, *56*, 1797-1809.
31. Makobongo, M. O.; Einck, L.; Peek, R. M.; Merrell, D. S. *In Vitro* Characterization of the Anti-Bacterial Activity of SQ109 against Helicobacter pylori. *PLoS One* **2013**, *8*, e68917.
32. *SQ109: A Broadly Active, Bactericidal, Small Molecule Antibiotic.*; Sequalla Incorporated Sequalla Incorporated 2013.
33. *Antimicrobial Resistance.*; National Institutes of Health, 2013.

Chapter 2: Multi-Targeting Drug Leads Against *Staphylococcus aureus* Infections

2.1 Notes and Acknowledgements

Y.W. and K.L. synthesized the compounds. W.Z. performed enzymatic and cell growth inhibition assays and DSC experiments; W.Z., J.G., C.-H.H., C.-C.C., T.-P.K., and R.-T.G. performed crystallographic experiments; K. Wang synthesized isopentenyl pyrophosphate, *trans*-farnesyl pyrophosphate and farnesyl thiopyrophosphate. Y.W., W.Z. and E.O. analyzed the data. I sincerely thank all the colleagues and collaborators.

This work was supported by United States Public Health Service (National Institutes of Health grant GM065307); a Harriet A. Harlin Professorship and the University of Illinois/Oldfield Research Fund; the National Basic Research Program of China (grants 2011CB710800 and 2011CBA00805) and the National Natural Science Foundation of China (grants 31200053 and 31300615). We thank Yigui Gao from the University of Illinois Macromolecular Crystallization Laboratory for providing crystallization facilities, and Professor T.E. Kehl-Fie (University of Illinois, Urbana−Champaign) for providing the *S. aureus* Newman strain. We thank the National Synchrotron Radiation Research Center of Taiwan for beamtime allocation and data collection assistance. Use of the Advanced Photon Source was supported by the US Department of Energy, Office of Science, Office of Basic Energy Sciences, under contract DE-AC02-06CH11357. Use of the Life Science Collaborative Access Team Sector 21 was supported by the Michigan Economic Development Corporation and Michigan Technology Tri-Corridor Grant 085P1000817.

This chapter was reproduced in part with permission from W. Zhu, E. Oldfield, *et al*. *J. Med. Chem.* **2015**, volume *58,* page 1215−1227, Copyright © 2015 American Chemical Society.

2.2 Introduction

There is currently a dearth of new antibiotics being introduced with both the United States Centers for Disease Control and Prevention[1] as well as the World Health Organization,[2] and others,[3] warning of the seriousness of the development of widespread antibiotic resistance. The problem is a multifaceted one with many factors such as use of antibiotics in feedstocks, unnecessary prescriptions, efflux pumps, and drug modifications all contributing to the problem. In addition, of course, random mutations in a target can occur, rendering a drug ineffective. One approach to ameliorate the latter problem is the use of combination therapies, and these are the norm for

malaria, HIV/AIDS, tuberculosis, as well as cancer therapeutics. While the development of just one new drug is a daunting prospect, the development of two new drugs (with new targets/mechanisms of action) will be even more challenging, hence the interest is new leads that act by multiple-targeting: one drug (drug lead) but two (or more) targets, an approach that can improve efficacy as well as decrease the likelihood of resistance developing. In our lab, we recently used computational screening to try and find novel inhibitors of two antibacterial drug targets, farnesyl diphosphate synthase (FPPS)[4,5] and undecaprenyl diphosphate synthase (UPPS),[6] that are involved in bacterial cell wall biosynthesis (and are not the targets of any currently FDA-approved anti-infective drugs). Inhibiting either of these targets would be of interest because it could lead to "resistance reversal" in, e.g., methicillin or vancomycin resistant bacteria (in a combination therapy), with UPPS inhibition being of particular interest because humans do not possess a UPPS gene. We found from our in silico and in vitro work that the bisamidine **1** (BPH-1358) was an inhibitor of both FPPS (IC_{50} ~2 μM) as well as UPPS (IC_{50} ~100 nM) and was active against *S. aureus* in vitro (MIC ~250 ng/mL) and in vivo (20/20 mice survived in an ip infection model with a MRSA strain) and, in addition, **1** (Scheme 2.1) acted synergistically with methicillin (with a fractional inhibitory concentration index, FICI = 0.25).

1 is, as noted above, a bisamidine (or a diamidine), and somewhat related compounds (derived from synthalin, **2**) have been developed as anti-infectives since ~1937.[7] For example, pentamidine (**3**) has been used against trypanosomatid infections and is still used against Pneumocystis jirovecii pneumonia in HIV/AIDS patients. It is, however, a rather toxic compound despite being on the World Health Organization's List of Essential Medicines. In later work (beginning in 1960), the A. Wander Company[8] developed large numbers of again generally related compounds, bisamidines such as **4**, primarily as antileukemia drug leads, but some were also found to have activity against *Trypanosoma brucei*, *Trypanosoma congolense*, the apicomplexan *Babesia rodaini*, as well as the bacterium *Mycobacterium tuberculosis*.[8] Other bisamidines were later developed and found to have promising activity against several other bacteria,[9] and **5** and related compounds[10] have been in clinical trials for human African trypanosomiasis. In many cases, the mechanism of action (or target) is not completely clear and, interestingly, it has been found with, for example **6** and **7**, that DNA synthesis as well as cell wall biosynthesis are targeted (based on macromolecular labeling studies).[11,12] In other cases, mitochondrial function is disrupted.[13] One possible inference from these results is that bisamidines may often have more than one target, with

so-called "multi-target" inhibitors being of interest because they could be less prone to the development of spontaneous resistance due to target mutations, with multi-target inhibition[14] being thought to be one of the main reasons that some antibiotics have been relatively successful in monotherapy.[15] The bisamidines **6**, **7**, and several related compounds have also been shown to bind to bacterial DNA (as observed by fluorescence: the DNA-bound ligands are highly fluorescent) and, more specifically, AT-rich DNA,[11,12,16] in which hydrogen bonding between the ligand and DNA bases can occur.[17] What is interesting here is that, in addition to these bisamidines binding to bacterial DNA, DNA-binding is also the proposed mechanism of action of several of the bisamidines that have been developed as anti-trypanosomatid drug leads (that reached clinical trials) where it is kinetoplast DNA (k-DNA) that is targeted.[16] DNA minor groove binders have also been developed to target a broad range of fungal and bacterial pathogens including Clostridium difficile,[18] so the possibility exists that it might be possible to develop compounds that target both DNA as well as a pathogen enzyme target (e.g., UPPS or FPPS), improving selectivity. In this work, I and coworkers synthesized a range of amidines and bisamidines and tested them, as well as other known bisamidines, for their binding to (or inhibition of) *Escherichia coli* UPPS, *Staphylococcus aureus* UPPS, and an AT-rich DNA duplex $(CGCGAATTCGCG)_2$ and correlated these results with their effects on *S. aureus* and *E. coli* cell growth. In some cases, we found both DNA minor groove binding as well as UPPS inhibition, leading to predictive models of cell growth inhibition. We also solved three X-ray structures of some of the leads bound to the DNA dodecamer duplex in addition to determining three UPPS X-ray structures.

2.3 Results and Discussion

We investigated the compounds shown in Figure 2.1 for their effects on enzyme (*E. coli* UPPS, *S. aureus* UPPS) inhibition, *E. coli* and *S. aureus* cell growth inhibition, and on the folded-unfolded transition of the AT-rich DNA dodecamer duplex, $(CGCGAATTCGCG)_2$. Compounds **6**–**8** have known antibacterial activity and were discovered or developed by Microbiotix (Worcester, MA) from a DTP/NCI (Developmental Therapeutics Program/National Cancer Institute) screening library (**6** = MBX-1162; **7** = MBX-1066 = NSC-317881; **8** = MBX-1090 = NSC-317880); **9** is the antibacterial netropsin; **1** is the bisamidine (NSC-50460) reported previously[5,6] to be a potent UPPS, FPPS inhibitor active against *S. aureus in vitro* and *in vivo*. Compounds **10**–**13** and **16**–**17** are all analogues of **1** or **10** containing various side chain or backbone modifications (see Experimental Section for synthesis and characterization); **14** is a Wander AG compound (NSC-

60340); **3** is pentamidine; **15** is an amidine based on the synthetic antimicrobial **18**[19] (which contains the "cationic− hydrophobic−cationic" motif found in the bisamidines). Compound **19** is a very potent UPPS inhibitor (IC_{50} ~400 nM) but is not expected to bind to DNA (because it is highly anionic).

Enzyme Inhibition. We first tested all 16 compounds against UPPS from *E. coli* and *S. aureus*. Results are shown in Table 2.1. The compounds are rank-ordered by their ΔT_m values, the strongest DNA-binder being at the top of the table. As can be seen in Table 2.1, **1** in the most potent inhibitor of both *E. coli* UPPS (EcUPPS) as well as *S. aureus* UPPS (SaUPPS), with an IC_{50} = 110 nM. The tetraphosphonate **19** is also a potent UPPS inhibitor with an IC_{50} ~400 nM against both enzymes. The bisindole **6** likewise has potent activity against both enzymes, and **7** (the same structure as **6** except for the replacement of the 6-membered bisamidine ring by a 5-membered ring) has good activity against EcUPPS (IC_{50} = 360 nM) but less (IC_{50} = 1.7 μM) against SaUPPS. Several other compounds (**13**, **18**) have low or submicromolar activity against SaUPPS but are less active against EcUPPS. Clearly, the overall most active compounds are **1**, **6**, **7**, and **19**. Compounds **1**, **6**, and **7** are bisamidines, while **19** is a tetraphosphonate. With the analogues of **1**, replacement of the 5-membered ring by a 6-membered ring reduced UPPS inhibition activity by 50-fold (Table 2.1) and replacement of the amide by a thioamide (**1** → **11**) reduced activity by a similar amount. Other side chain modifications all greatly reduced activity.

Cell Growth Inhibition Results. With these results on UPPS inhibition in hand, we next investigated the activity of all 16 compounds against two bacteria, the Gram-negative *E. coli* and the Gram-positive *S. aureus*. Cell growth inhibition results are shown in Table 2.1. As can be seen in Table 2.1, there are four compounds with <1 μM activity against both organisms **1**, **6**, **7**, and **10**, with similar results for **6**−**8** having been reported previously.[9,11,12,17] In most cases, these four compounds have good activities against UPPS, the exception being **10** (where UPPS IC_{50} values are ~5 μM). However, the potent UPPS inhibitor **19** had no cell activity, presumably because it has poor permeability, and in previous work[20] we found only one related (bisphosphonate) inhibitor having activity (EC_{50} = 33 μM) against *E. coli*. These results appear to be in accord with the idea that UPPS could be a target for the most potent cell growth inhibitors (some of which have been shown to inhibit cell wall biosynthesis). There is, however, only a very poor overall correlation between enzyme pIC_{50} (= $-\log_{10} IC_{50}$) and cell growth inhibition pEC_{50} values with R^2 = 0.25, p-value = 0.05 for *E. coli*/EcUPPS, and R^2 = 0.16, p-value = 0.12 for the *S. aureus*/SaUPPS

results. It thus seemed that there might be another, more important target, DNA, because as noted in the Introduction, in other work it has been shown that bisamidines bind to AT-rich DNA, both in bacteria11 as well as to kinetoplast DNA, in trypanosomatid parasites such as *T. brucei*.

DNA Binding: Calorimetry and Crystallography. We thus next investigated the binding of the 16 compounds shown in Table 2.1 to a DNA dodecamer duplex containing an AT-rich central domain: $(CGCGAATTCGCG)_2$, used previously to study the binding of Hoechst 33258,[21] propamidine[22] (pentamidine but with a C3 linker), and other ammonium compounds.[23] We used differential scanning calorimetry (DSC) to study the DNA−ligand interaction, and DSC thermograms for all 16 compounds are shown in Figure 2.2 (the results for the compounds having the largest ΔT_m values being shown at top left).

The changes in the DNA thermal unfolding temperatures, ΔT_m (where T_m is the maximum in the C_p vs T thermogram) are given in Table 2.1, and the DSC thermogram results are shown in Figure 2.2, ranked according to their ΔT_m values. In most cases, there was a single component observed, although in several instances there were two components (folded + unfolded), due presumably to solubility/incomplete mixing deficiencies. The two strongest binding ligands were **6** (ΔT_m = 24 °C) and **8** (ΔT_m = 20 °C), followed by **7** (ΔT_m = 16 °C) and **9** (netropsin, ΔTm = 16 °C). **1**, the 5-membered biphenyl bisamidine, had ΔT_m = 11 °C, essentially the same as the 6-membered ring analogue **10** (ΔT_m = 10 °C). The thioamide analogue of **1**, **11**, had worse binding (ΔT_m = 7.1 °C). Pentamidine (**3**) was also a poor binder (ΔT_m = 2.7 °C). Clearly, for most potent binding, the presence of a bisamidine is required, together with, perhaps, central groups that might H bond to the DNA bases. What is particularly interesting about these DSC results is that the most potent DNA binders are also some of the most the potent UPPS inhibitors, as well as the most potent cell growth inhibitors, suggesting, perhaps, dual target inhibition.

To see how some of the bisamidines actually bound to the $d(CGCGAATTCGCG)_2$ duplex, we used X-ray crystallography, cocrystallizing the DNA−ligand complexes as described in the Experimental Section..

As can be seen in Figure 2.3, **1**, **6**, and **10** all bound to the minor groove of the AT-rich dodecamer, and in each case there are H-bond contacts between the nitrogen atoms in the ligands, either in the amidine ring, amide bond (**1** and **10**), or in the indole group (**6**), with the bases in the DNA minor groove. Although there are only three structures, more interactions correlate with stronger

binding, that is, a bigger ΔT_m: **6** has 6 H-bond contacts and a ΔT_m = 24 °C; **1** and **10** have only 3−4 interactions and a $\Delta T_m \sim 10$ °C, Figure 2.3.

Models for Cell Growth Inhibition. These DSC ΔT_m results now enable us to test the hypothesis that the cell-based activity we see could be due to DNA binding, to UPPS binding, or to both DNA as well as UPPS binding. We first used a simple heat-map approach, Figure 2.4A, from which it can be seen that *S. aureus* cell growth inhibition can be quite potent and is most strongly correlated with ΔT_m (both in red/orange), with a weaker correlation with SaUPPS inhibition (Figure 2.4A). The trends are similar to *E. coli* (Figure 2.4A). The quantitative correlation between cell growth inhibition and either pIC_{50} (UPPS) or DNA ΔT_m results are, however, poor, varying from 0.16 to 0.62. We thus next employed the basic approach derived earlier[24] in which we used eq **1**:

$$pEC_{50}\ (\text{cell}) = a \cdot A + b \cdot B + c \cdot C + d\ 50\ (\mathbf{1})$$

where in this case A = UPPS pIC_{50}, B = DNA ΔT_m, and C is an (optional) computed descriptor (selected from 307 descriptors we computed in MOE[25]). With the UPPS pIC50 and DNA ΔT_m data together, the correlations improved to be $R^2 = 0.75$, p = 0.0001 for *S. aureus*, and $R^2 = 0.53$, p = 0.007 for *E. coli*. These results improved further with addition of a computed descriptor (vsurf_ID5 for *S. aureus*; GCUT_SMR_3 for *E. coli*) to $R^2 = 0.89$, $p = 6 \times 10^{-6}$ for *S. aureus* and $R^2 = 0.79$, p = 0.0002 for *E. coli*. The ΔT_m term was the major contributor to the *S. aureus* model while both UPPS inhibition and DNA binding contributed to the *E. coli* model. The experimental versus computed cell pEC_{50} results are shown in Figures 2.4B, C. There was no significant correlation between pIC_{50} (EcUPPS) and ΔT_m ($R^2 = 0.02$, p = 0.6) or between pIC_{50} (SaUPPS) and ΔT_m ($R^2 = 0.003$, p = 0.8) when data for all 16 compounds was used.

These results suggest, then, an extended model for the potent *S. aureus* growth inhibition reported previously[6] for 1 in which there is multi-target inhibition (DNA binding as well as UPPS inhibition), consistent with the observed synergistic interaction seen with methicillin in a methicillin-resistant strain of *S. aureus*.

X-ray Structures of SaUPPS and EcUPPS: Progress and Puzzles. Finally, we sought to investigate how some of the UPPS inhibitors bound to UPPS. The SaUPPS protein was of most interest because inhibitors such as **1** bind tightly to SaUPPS and are active *in vivo*. At present, there have been no reports of the structures of SaUPPS with (or without) inhibitors, although there are two reported structures of SaUPPS with its FPP substrate.[6] Unfortunately, we were not

successful in obtaining any bisamidine-bound SaUPPS Xray structures, We did succeed, however, in obtaining a structure of **19** bound to EcUPPS, Figure 2.5.

As reported previously, 29 small bisphosphonates bind to EcUPPS, with their lipophilic side chains binding to one or more of sites 1, 2, 3, or 4,[26] as shown for the inhibitor [2-(3-(dibenzofuran-2-yl-phenyl)-1-hydroxy-1-phosphono-ethyl]-phosphonic acid (BPH-629) in Figure 2.5A. However, with the bisamidine **14** (Figure 2.5B) as well as the diacetylenic amine species **18** (which would be expected to protonated), only a single molecule bound to UPPS, and these molecules were found to span both sites 2 and 4, the cationic groups being relatively solvent exposed, while the aromatic groups were buried in the hydrophobic interior of the protein. With **19**, we found that sites 1−3 were all occupied, Figure 2.5C.

2.4 Conclusions

The results we have reported here are of interest for a number of reasons. First, we synthesized and tested a range of amidine and bisamidine compounds against *E. coli* and *S. aureus* UPPS finding quite potent activity with some bisamidines. Second, we found that several bisamidines also bound to AT-rich DNA, shifting T_m by as much as 24 °C. Third, we developed computational models for cell growth inhibition using DNA ΔT_m and UPPS pIC_{50} values together with one mathematical descriptor that had $R^2 = 0.79-0.89$. Fourth, we determined the structures of three bisamidines bound to a synthetic DNA $(CGCGAATTCGCG)_2$ finding minor groove binding, with the largest ΔT_m correlating with the largest number of ligand−DNA interactions. Fifth, we solved three UPPS structures. Overall, the most important finding is that the compounds with best cell growth inhibition bind to AT-rich DNA in addition to inhibiting UPPS. This is a potentially important observation because it could lead to novel therapeutic leads that inhibit bacterial cell wall biosynthesis (targeting UPPS), synergize with existing drugs acting in these pathways (as does **1** with methicillin in a methicillin-resistant *S. aureus* strain), and also inhibit DNA replication: multiple-targeting leads that could in some cases help reverse resistance. It is, however, also possible that there may be toxicity against a potential host with such multitarget inhibitors although EC_{50} values against mammalian cells (manuscript in preparation) for compound **1** are >100 μM, leading to selectivity indices with *S. aureus* of >300. Moreover, **1** showed no adverse side-effects in the *S. aureus* mouse model of infection,**6** and **7** and **8** have been

reported to be effective in mice models of infection with both *Bacillus anthracis* as well as *Yersinia pestis*.[11]

2.5 Experimental Section

Chemical Syntheses: General Methods. All chemicals were reagent grade. Pentamidine and netropsin were purchased from Aldrich. ^{1}H NMR spectra were obtained on Varian (Palo Alto, CA) Unity spectrometers at 400 and 500 MHz. Elemental analyses were carried out in the University of Illinois Microanalysis Laboratory. HPLC/MS was performed using an Agilent LC/MSD Trap XCT Plus system (Agilent Technologies, Santa Clara, CA) with an 1100 series HPLC system including a degasser, an autosampler, a binary pump, and a multiple wavelength detector. All final compounds were ≥95% pure as determined by elemental analysis or analytical HPLC/MS analysis and were also characterized by ^{1}HNMR and HRMS.

N4,N4′-bis(3-(4,5-dihydro-1H-imidazol-2-yl)phenyl)-[1,1′-biphenyl]-4,4′-bicarboxamide (1)

To a mixture of 4,4′-diphenyl dicarbonyl chloride (1.39 g, 5 mmol), 3-aminobenzonitrile (1.18 g, 10 mmol) in anhydrous THF (20 mL) was added Et_3N (2.1 mL, 15 mmol) and the mixture was stirred at room temperature overnight. After filtration, the white solid was washed with water (20 mL) and ethyl acetate (10 mL) and then dried. Sodium hydrosulfide hydrate (100 mg), ethylenediamine (2 mL), and dimethylacetamide (10 mL) were then added and stirred overnight at 140 °C. Upon removal of the solvent, the solid was washed thoroughly with water and then ethyl acetate (10 mL). To the suspension of the crude product in 10 mL of water were added two equivalents of methanesulfonic acid. Removal of water afforded the final product **1** as its methanesulfonic acid salt (1.44 g, 40%). ^{1}H NMR (DMSO-d_6, 500 MHz) δ: 10.68 (s, 2 H), 10.52 (s, 4 H), 8.50 (s, 2 H), 8.12 (d, J = 9.0 Hz, 4 H), 8.02–7.98 (m, 2 H), 7.96 (d, J = 9 Hz, 4 H), 7.68–7.58 (m, 4 H), 4.00 (s, 8 H), 2.36 (s, 6 H). HRMS (ESI): m/z $[M + H]^+$ calculated for $C_{32}H_{29}N_6O_2$ 529.2361, found 529.2352. Purity of the product determined by HPLC (Phenomenex C6-Phenyl 110A. 100x2 mm, 3 μm, 300 nm, retention time = 5.6 min): 98.9%.

1,4-bis(6-(1,4,5,6-tetrahydropyrimidin-2-yl)-1*H*-indol-2-yl)benzene (6)

Terephthalaldehyde (1.34 g, 10 mmol) and 4-methyl-3-nitrobenzonitrile (3.24 g, 20 mmol) were added to a round-bottom flask and heated together to 150 ºC until the compounds melted. Piperidine (1.5 mL) and sulfolane (10 mL) were added and the resulting solution was stirred at 150 ºC overnight and cooled to room temperature to yield an orange solid (3.4 g, 80%) which was washed with methanol (15 mL × 3) and dried. The solid, 4,4'-(1*E*,1'*E*)-2,2'-(1,4-phenylene)bis(ethene-2,1-diyl)bis(3-nitrobenzonitrile) was utilized in the following steps without further purification. Product from last step was then suspended in triethyl phosphate (30 mL) and heated to reflux (160 ºC) for 72 h until the mixture turned from orange to yellow. The suspension was then filtered and the yellow solid washed with methanol (15 mL × 3) and dried (1.4 g, 55%). The solid, 2,2'-(1,4-phenylene)bis(1*H*-indole-6-carbonitrile) was utilized in the following steps without further purification. Product from last step was suspended in propane-1,3-diamine (15 mL) and heated to 130 ºC for 24 h. The suspension was filtered and the solid washed with water (15 mL × 3) and methanol (15 mL × 3). The final product **6** was a yellow solid. ^{1}H NMR (DMSO-d_6, 500 MHz) δ: 7.99 (s, 4 H), 7.79 (s, 2 H), 7.48 (d, J = 8.0 Hz, 2 H), 7.42 (d, J = 8.0 Hz, 2 H), 6.99 (s, 2 H), 3.37 (s, 8 H), 1,72 (m, 4 H). HRMS (ESI): m/z $[M + H]^+$ calculated for $C_{30}H_{29}N_6$ 473.2454, found 473.2450. Purity of the product determined by HPLC (Phenomenex C6-Phenyl 110A. 100x2 mm, 3 μm, 230 nm, retention time = 5.8 min): 99.1%.

1,4-bis(6-(4,5-dihydro-1*H*-imidazol-2-yl)-1*H*-indol-2-yl)benzene (7)

Terephthalaldehyde (1.34 g, 10 mmol) and 4-methyl-3-nitrobenzonitrile (3.24 g, 20 mmol) were added to a round-bottom flask and heated together to 150 ºC until the compounds melted. Piperidine (1.5 mL) and sulfolane (10 mL) were added and the resulting solution was stirred at 150 ºC overnight then cooled to room temperature to yield an orange solid (3.4 g, 80%) which was washed with methanol (15 mL × 3) and dried. The solid, 4,4'-(1*E*,1'*E*)-2,2'-(1,4-phenylene)bis(ethene-2,1-diyl)bis(3-nitrobenzonitrile) was utilized in the following steps without further purification. Product from last step was then suspended in triethyl phosphate (30 mL) and heated to reflux (160 ºC) for 72 h until the mixture turned from orange to yellow. The suspension was then filtered and the yellow solid washed with methanol (15 mL × 3) and dried (1.4 g, 55%). The solid, 2,2'-(1,4-phenylene)bis(1*H*-indole-6-carbonitrile) was utilized in the following steps without further purification. Product from last step was suspended in ethane-1,2-diamine (15 mL) and heated to 130 ºC for 24 h. The suspension was filtered and the solid washed with water (15

mL × 3) and methanol (15 mL × 3). The final product **7** was a yellow solid. ^{1}H NMR (DMSO-d_6, 500 MHz) δ: 11.73 (s, 2 H), 7.97 (s, 4 H), 7.85 (s, 2 H), 7.50 (s, 4 H), 7.00 (s, 2 H), 3.28 (s, 4 H). HRMS (ESI): m/z $[M + H]^+$ calculated for $C_{28}H_{25}N_6$ 445.2141, found 445.2139. Purity of the product determined by HPLC (Phenomenex C6-Phenyl 110A. 100x2 mm, 3 μm, 230 nm, retention time = 5.5 min): 99.3%.

1*H*-Indole, 2,2'-(1,2-ethenediyl)bis[6-(4,5-dihydro-1*H*-imidazol-2-yl)-, dihydrochloride (8)

The compound was requested from NCI. ^{1}H NMR (methanol-d_4, 400 MHz): 7.92 (s, 2H), 7.71 (d, 8.4 Hz, 2H), 7.45 (d, J = 8.8 Hz, 2H), 7.33 (s, 2H), 6.78 (s, 2H), 4.08 (s, 4H). HRMS (ESI): m/z $[M + H]^+$ calculated for $C_{24}H_{23}N_6$ 395.1984, found 395.1986. Purity of the product determined by HPLC (Phenomenex C6-Phenyl 110A. 100x2 mm, 3 μm, 230 nm, retention time = 5.6 min): 97.2%.

N4,N4'-bis(3-(1,4,5,6-tetrahydropyrimidin-2-yl)phenyl)biphenyl-4,4'-dicarboxamide (10)

To a mixture of 4,4′-diphenyl dicarbonyl chloride (1.39 g, 5 mmol), 3-aminobenzonitrile (1.18 g, 10 mmol) in anhydrous THF (20 mL) was added Et_3N (2.1 mL, 15 mmol) and the mixture stirred at room temperature overnight. After filtration, the white solid was washed with water (20 mL) and ethyl acetate (10 mL) and then dried. Sodium hydrosulfide hydrate (100 mg), propane-1,3-diamine (2 mL), and dimethylacetamide (10 mL) were then added and the mixture stirred overnight at 140 °C. Upon removal of the solvent, the solid was washed thoroughly with water and then ethyl acetate (10 mL). To the suspension of the crude product in 10 mL of water were added two equivalents of methanesulfonic acid. Removal of water afforded the final product as its methanesulfonic acid salt (1.50 g, 40%). ^{1}H NMR (DMSO-d_6, 500 MHz) δ: 10.68 (s, 2 H), 9.95 (s, 4 H), 8.38 (s, 2 H), 8.14 (d, J = 9.0 Hz, 4 H), 7.98 (m, 6 H), 7.62 (t, 2 H), 7.42 (d, 2 H), 3.50 (s, 8 H), 2.29 (s, 4 H). HRMS (ESI): m/z $[M + H]^+$ calculated for $C_{34}H_{33}N_6O_2$ 557.2665, found 557.2658. Purity of the product determined by HPLC (Phenomenex C6-Phenyl 110A. 100x2 mm, 3 μm, 230 nm, retention time = 5.3 min): 99.6%.

N4,N4'-bis(3-(4,5-dihydro-1*H*-imidazol-2-yl)phenyl)biphenyl-4,4'-bis(carbothioamide) (11)

N4, N4′-bis(3-(4,5-dihydro-1H-imidazol-2-yl)phenyl)-[1,1′-biphenyl]-4,4′-bicarboxamide (**1**, 560 mg, 1 mmol) was suspended in pyridine (5 mL). Lawesson's reagent (2,4-bis(4-methoxyphenyl)-1,3,2,4-dithiadiphosphetane-2,4-disulfide) (1.0 g, 2.5 mmol) was added and the mixture heated to

150 °C for 72 h until the mixture turned yellow. The suspension was then filtered and the solid washed with methanol (15 mL *3) and acetone (15 mL *3) and then dried under vacuum. The product **11** was obtained as a yellow solid. ^{1}H NMR (DMSO-d_6, 500 MHz) δ: 12.12 (s, 2 H), 10.60 (s, 4 H) 8.45 (s, 2 H), 7.90 (d, J = 9.0 Hz, 4 H), 8.00–7.98 (m, 2 H), 7.82 (d, J = 9 Hz, 4 H), 7.73 (m, 4 H), 4.00 (s, 8 H). HRMS (ESI): m/z [M + H]$^+$ calculated for $C_{32}H_{29}N_6S_2$ 561.1895, found 561.1896. Purity of the product determined by HPLC (Phenomenex C6-Phenyl 110A. 100x2 mm, 3 μm, 230 nm, retention time = 5.8 min): 97.6%.

N^4-(3-(4,5-dihydro-1*H*-imidazol-2-yl)phenyl)-$N^{4'}$-(3-(((2S,3R,4S,5S,6R)-3,4,5-trihydroxy-6-(hydroxymethyl)tetrahydro-2*H*-pyran-2-yl)oxy)phenyl)-[1,1 -biphenyl]-4,4 –dicarboxamide (12)

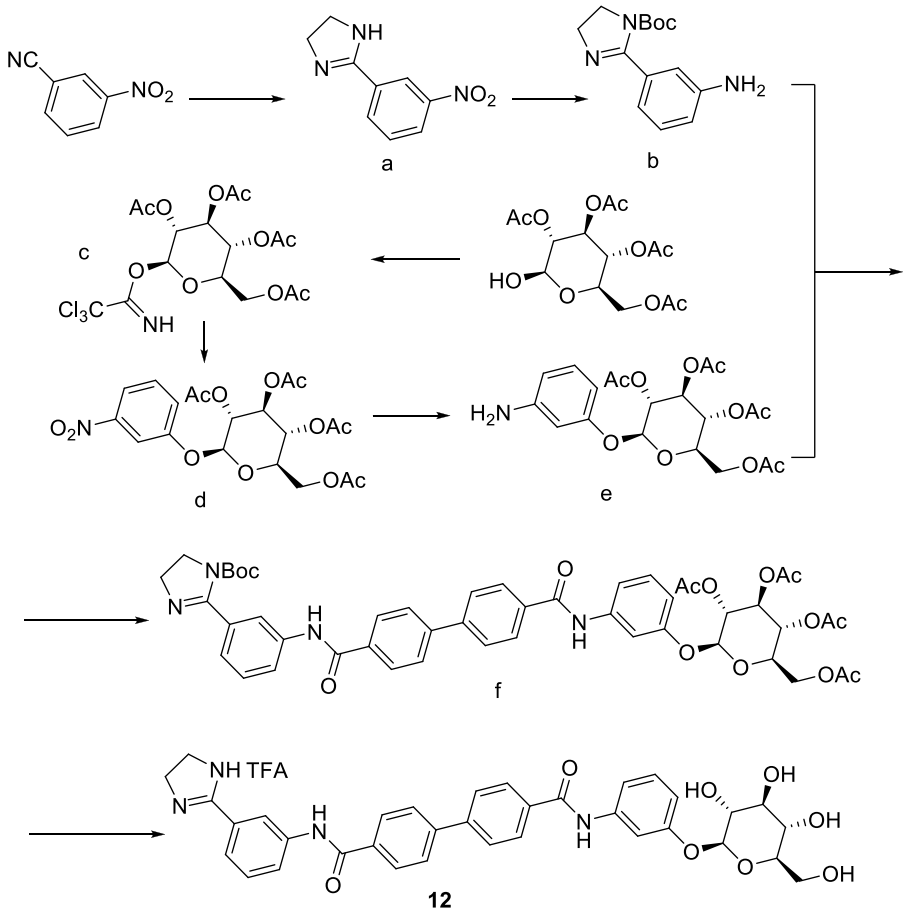

3-nitrobenzonitrile (3.6 g, 20 mmol) was treated with ethylene diamine (40 mL) and NaHS (200 mg). The solution was heated at 110 °C for 48 h and then quenched with water. The residue was extracted with ethyl acetate, dried under vacuum and purified by flash chromatography (silica gel,

hexane/ethyl acetate = 2/1) to give the dihydroimidazole compound **a** (2.6 g, 60%). To the solution of **a** (2.2 g, 10 mmol) and $NaHCO_3$ (3.6 mg, 40 mmol) in dichloromethane (20 mL) and water (20 mL) was added $(Boc)_2O$ (4.5 g, 20 mmol) with vigorous stirring at 0 ^oC. The stirring was continued for 12 h when the temperature rose to room temperature naturally. The dichloromethane phase was separated and concentrated to give the Boc protected. To the solution of the above nitro compound in ethyl acetate (40 mL) was added Pd/C (10% palladium on charcoal, 145 mg) under nitrogen at room temperature. The nitrogen was switched to H_2 using a balloon and stirring was continued for 12 h at room temperature. Filtration and concentration under reduced pressure gave the 3-aminophenyl imidazoline **b**. Glucose tetraacetate (3.5 g, 10 mmol) was treated with trichloroacetonitrile (14.4 g, 100 mmol), DBU (0.3 g, 2 mmol) and CH_2Cl_2 (40 mL). The solution was stirred at room temperature for 12 h and then washed with water. The residue was extracted with Et_2O, dried under vacuum and purified by flash chromatography (silica gel, hexane/ethyl acetate = 2/1) to give the peracetyl glucopyranosyl trichloroacetimidate **c** (4.4 g, 90%). A mixture of **c** (4.0 g, 8 mmol), 3-nitrophenol (1.1 g, 8 mmol), and freshly activated 4 Å molecular sieves in anhydrous CH_2Cl_2 (30 mL) was stirred under N_2 at 0 ^oC for 10 min, then BF_3Et_2O (40 μL, 0.8 mmol) was added via syringe. Stirring continued for 3 h, then Et_3N (2 mL) was added, and the resulting mixture was filtered through Celite. The filtrate was concentrated and purified by silica gel column chromatography (hexane/ethyl acetate = 3/1) to give 3-nitrophenol glycoside **d** (3.0 g, 80%). To the solution of **d** (2.3 g, 5 mmol) in ethyl acetate (20 mL) was added Pd/C (10% palladium on charcoal, 100 mg) under nitrogen at room temperature. The nitrogen was switched to H_2 using a balloon and stirring was continued for 12 h at room temperature. Filtration and concentration under reduced pressure gave 3-aminophenol glycoside **e**. To the solution of **b** (520 mg, 2 mmol), **e** (920 mg, 2 mmol) and Et_3N (1 mL) in dry dichloromethane (20 mL) was added [1,1'-biphenyl]-4,4'-dicarbonyl dichloride (560 mg, 2 mmol) at 0 ^oC. The stirring was continued for 4 h at 0 ^oC. The reaction mixture was washed with water (15 ml x 3), then concentrated under reduced pressure to give the residue. Purification of the residue by chromatography (silica gel, hexane/ethyl acetate = 2/1) gave product **f** (800 mg, 45%). To the solution of **f** (450 mg, 0.5 mmol) in MeOH (5 mL) was added MeONa (1 g) at room temperature. Stirring was continued for 4 h at room temperature and all the volatile components were removed under reduced pressure. The resulting residue was purified by chromatography (silica gel, ethyl acetate) to give the non-protected glycoside. To the solution of above free glycoside (360 mg, 0.5 mmol) in

dichloromethane (3 mL) was added trifluoroacetic acid (2 mL) with stirring at room temperature. The stirring was continued for 4 h then all volatile components were removed under reduced pressure. The resulting residue was purified by chromatography (silica gel, chloroform/MeOH = 5/1) to give the final product **12**(340 mg, 95%). ^{1}H NMR (methanol-d_4, 400 MHz) 8.48 (m, 1H), 8.06 (m, 4H), 7.96 (m, 5H), 7.61 (m, 2H), 7.55 (m, 1H), 7.37 (d, J = 8.0 Hz, 1H), 7.26 (t J = 8.0 Hz, 1H), 6.89 (dd, J = 1.6 Hz, 1H), 4.78 (s, 1H), 4.11 (s, 4H), 3.90 (dd, J = 12.0, 2.0 Hz, 1H), 3.71 (dd, J = 12.0, 7.6 Hz, 1H), 3.46-3.38 (m, 5H). HRMS (ESI): m/z $[M + H]^+$ calculated for $C_{35}H_{35}N_4O_8$, 639.2455; found 639.2446. Purity of the product determined by HPLC (Phenomenex C6-Phenyl 110A. 100x2 mm, 3 μm, 210 nm, retention time = 5.8 min): 97.9%.

N^4-(3-(4,5-dihydro-1*H*-imidazol-2-yl)phenyl)-$N^{4'}$-(3-methoxyphenyl)-[1,1-biphenyl]-4,4–dicarboxamide (13)

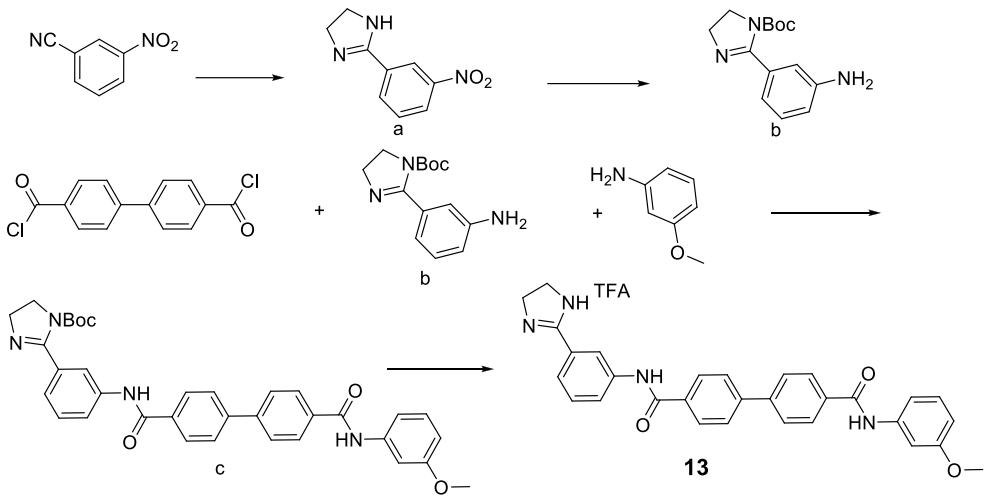

3-nitrobenzonitrile (3.6 g, 20 mmol) was treated with ethylene diamine (40 mL) and NaHS (200 mg). The solution was heated at 110 ^{o}C for 48 h and then quenched with water. The residue was extracted with ethyl acetate, dried under vacuum and purified by flash chromatography (silica gel, hexane/ethyl acetate = 2/1) to give the dihydroimidazole compound **a** (2.6 g, 60%). To a solution of **a** (2.2 g, 10 mmol) and $NaHCO_3$ (3.6 mg, 40 mmol) in dichloromethane (20 mL) and water (20 mL) was added $(Boc)_2O$ (4.5 g, 20 mmol) with vigorous stirring at 0 ^{o}C. The stirring was continued for 12 h at which point temperature had risen to room temperature naturally. The dichloromethane phase was separated and concentrated to give the Boc protected which was used in the next step. To a solution of the above nitro compound in ethyl acetate (40 mL) was added Pd/C (10%

palladium on charcoal, 145 mg) under nitrogen at room temperature. The nitrogen was switched to H_2 using a balloon and stirring was continued for 12 h at room temperature. Filtration and concentration under reduced pressure gave the crude 3-aminophenyl imidazoline **b**. To the solution of **b** (260 mg, 1 mmol), 3-methoxyaniline (120 mg, 1 mmol) and Et_3N (0.5 mL) in dry dichloromethane (10 mL) was added [1,1'-biphenyl]-4,4'-dicarbonyl dichloride (280 mg, 1 mmol) at 0 ^oC. The stirring was continued for 4 h at 0 ^oC then the reaction mixture was washed with water (5 ml × 3), and concentrated under reduced pressure. Purification of the residue by chromatography (silica gel, hexane/ethyl acetate = 2/1) gave the product **c** (240 mg, 42%). To the solution of **c** (115 mg, 0.2 mmol) in dichloromethane (1 mL) was added trifluoroacetic acid (1 mL) with stirring at room temperature. Stirring was continued for 4 h and all the volatile components were removed under reduced pressure. The resulting residue was purified by chromatography (silica gel, chloroform/MeOH = 5/1) to give the final product **13** (112 mg, 95%). ^1H NMR (methanol-d_4, 400 MHz) 8.45 (s, 1H), 8.03 (m, 4H), 7.90-7.80 (m, 6H), 7.59 (m, 2H), 7.30 (m, 1H), 6.71 (m, 1H), 4.09 (s, 4H), 3.78 (s, 3H). HRMS (ESI): m/z $[M + H]^+$ Calcd for $C_{30}H_{27}N_4O_3$, 491.2083; found 491.2084. Purity of the product determined by HPLC (Phenomenex C6-Phenyl 110A. 100x2 mm, 3 μm, 280 nm, retention time = 6.5 min): 97.5%.

N^1,N^4-bis(4-(4,5-dihydro-1*H*-imidazol-2-yl)phenyl)-2-nitroterephthalamide dihydrochloride (14)

The compound was requested from NCI. ^1H NMR (methanol-d_4, 400 MHz), 8.78 (d, J = 1.6 Hz, 2H), 8.42 (d, J = 8.0 Hz, 1H), 8.07 (dd, J = 8.8 Hz, 2H), 7.95-7.87 (m, 9H), 4.08 (s, 8H). HPLC-MS: m/z $[M + H]^+$ calculated for $C_{26}H_{24}N_7O_4$, 498.1890; found 498.1882. Purity of the product determined by HPLC (Phenomenex C6-Phenyl 110A. 100x2 mm, 3 μm, 280 nm, retention time = 5.0 min): 95.2%.

N^4-(3-(4,5-dihydro-1*H*-imidazol-2-yl)phenyl)-$N^{4'}$-(3-(hexyloxy)phenyl)-[1,1-biphenyl]-4,4–dicarboxamide (16)

The **16** was made with the same protocol for **13**. ^1H NMR (methanol-d_4, 400 MHz) 8.48 (s, 1H), 8.05 (m, 4H), 7.85 (m, 5H), 7.61 (m, 2H), 7.40 (s, 1H), 7.23 (m, 2H), 6.70 (m, 1H), 4.11 (s, 4H), 3.97 (t, J = 6.0 Hz, 2H), 1.77 (m, 2H), 1.48 (m, 2H), 1.36 (m, 4H), 0.91 (t, J = 6.8 Hz, 3H). HRMS (ESI): m/z $[M + H]^+$ Calcd for $C_{35}H_{37}N_4O_3$, 561.2866; found 561.2875. Purity of the product

determined by HPLC (Phenomenex C6-Phenyl 110A. 100x2 mm, 3 μm, 280 nm, retention time = 7.2 min): 97.9%.

N^4-(3-(4,5-dihydro-1*H*-imidazol-2-yl)phenyl)-$N^{4'}$-(3-phenoxyphenyl)biphenyl-4,4'-dicarboxamide (17)

The **17** was made with the same protocol for **13**. ^{1}H NMR (methanol-d_4, 400 MHz) 8.47 (d, *J* = 1.6 Hz, 1H), 8.07 (d, *J* = 8.4 Hz, 2H), 8.01 (d, *J* = 8.4 Hz, 2H), 7.90-7.81 (m, 5H), 7.6 (m, 2H), 7.48 (s, 1H), 7.44 (d, *J* = 12.4 Hz, 1H), 7.37-7.30 (m, 3H), 7.11 (t, *J* = 7.6 Hz, 1H), 7.03 (s, 1H), 7.01 (s, 1H), 6.77 (t, *J* = 8.0, 1.2 Hz, 1H), 4.11 (s, 4H). HRMS (ESI): m/z $[M + H]^+$ Calcd for $C_{35}H_{29}N4O_3$, 553.2240; found 553.2249. Purity of the product determined by HPLC (Phenomenex C6-Phenyl 110A. 100x2 mm, 3 μm, 210 nm, retention time = 6.3 min): 99.8%.

Protein Expression, Purification and Inhibition. EcUPPS and SaUPPS were expressed and purified as described previously.[6] UPPS inhibition assays were also carried out as described previously.[6] Briefly, the condensation of FPP with IPP catalyzed by UPPS was monitored by using a continuous spectrophotometric assay[27] in 96 well plates with 200 μL reaction mixtures containing 400 μM MESG, 25 μM IPP, 2.5 μM FPP, 25 μM Tris-HCl (pH 7.5), 0.01% Triton X-100 and 1 μM $MgCl_2$. The IC_{50} values were obtained by fitting the inhibition data to a standard rectangular hyperbolic dose-response function in GraphPad PRISM 4.0 software (Graphpad Software, San Diego, CA).

Cell Growth Inhibition Assay. The growth of *E. coli* (K12) and determination of IC_{50} values were carried out as described previously.[28] IC_{50} values for *S. aureus* growth inhibition were also determined as described previously.[29] Briefly, an overnight culture of *S. aureus* (Newman strain) was diluted 50-fold into fresh TSB (tryptic soy broth) and grown for 1 h at 37 °C and then diluted 100-fold into fresh TSB medium and 100 μL aliquots inoculated into each well of a 96-round-bottom culture plate (Corning Inc., Corning, NY) containing serially diluted compounds. Plates were incubated for 9 h with shaking at 37 °C. Absorbances were measured at 600 nm and dose-response curves constructed using GraphPad PRISM 4.0 software (Graphpad Software, San Diego, CA).

Differential Scanning Calorimetry. The DNA dodecamer $(CGCGAATTCGCG)_2$ was purchased from Intergrated DNA Technologies, Inc. and annealed into a duplex before use. DNA and ligand solutions were prepared in Mes buffer (0.01 M Mes, 0.001 M EDTA, 0.2 M NaCl, pH 6.2). All ligand solutions were prepared by adding appropriate amounts of compound powder into the 0.1 mM DNA solution and the final compound concentrations were 0.1 mM. DSC experiments were performed by using a Microcal VP-DSC instrument. The scans cover a 10 to 110 °C temperature range at a scan rate of 90 °C/h. DSC thermograms were analyzed using Origin 7.1 software. Buffer vs. buffer scans were used for baseline corrections.

X-Ray Crystallography. Native *E. coli* UPPS crystals for use in soaking were obtained by using the hanging-drop method (Hampton Research, Laguna Niguel, CA) by mixing 1 µL of UPPS protein solution (~10 mg/ml UPPS in 25 mM Tris-HCl, pH 7.5 and 150 mM NaCl) with 1 µL of mother liquor (25 mM Tris-HCl, pH 7.5, 150 mM NaCl and 5% PEG 2-4K) and then equilibrating with 400 µL mother liquor at room temperature. Tetragonal crystals appeared in 2 days and were then soaked in a cryoprotectant solution (30% EG and 5% PEG 35K) containing 1-5 mM inhibitors for 1 day.

S. aureus UPPS crystals with FSPP were obtained by using the hanging-drop method (Hampton Research, Laguna Niguel, CA) by mixing 1 µL of UPPS protein solution (~5 mg/ml UPPS in 1.5 mM $MgCl_2$, 1.5 mM FPP, 25 mM Tris-HCl, pH 7.5 and 150 mM NaCl) with 1 µL of mother liquor (100 mM NaMES, pH 6.5, 200 mM $(NH_4)SO_4$, and 25% PEG MME 5K) and then equilibrating with 400 µL mother liquor at room temperature. Bi-pyramidal crystals appeared overnight.

DNA/Ligand complex crystals were obtained via co-crystallization by mixing equivalent amount of 0.6 mM dodecamer and compounds (0.5-5 mM) and left on ice overnight. The mixtures were used to grow crystals from hanging drops against a reservoir of 40% MPD. Sheet-shaped crystals appeared in a month.

X-ray diffraction data were collected at the Life Science Collaborative Access Team (LS-CAT) 21-ID-D (G) at the Advanced Photon Source of Argonne National Laboratory. Diffraction data were processed and scaled by using the program HKL3000 (HKL Research Inc., Charlottesville, VA, USA). Structure refinements were carried out by using Refmac[30] and Coot.[31] All structure figures were prepared by using PyMOL.

2.6 Schemes, Charts, Tables and Figures

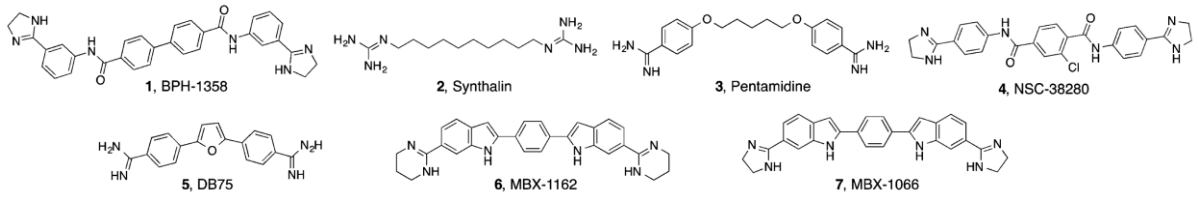

Scheme 2.1. Structures of bisamidines with anti-infective activity.

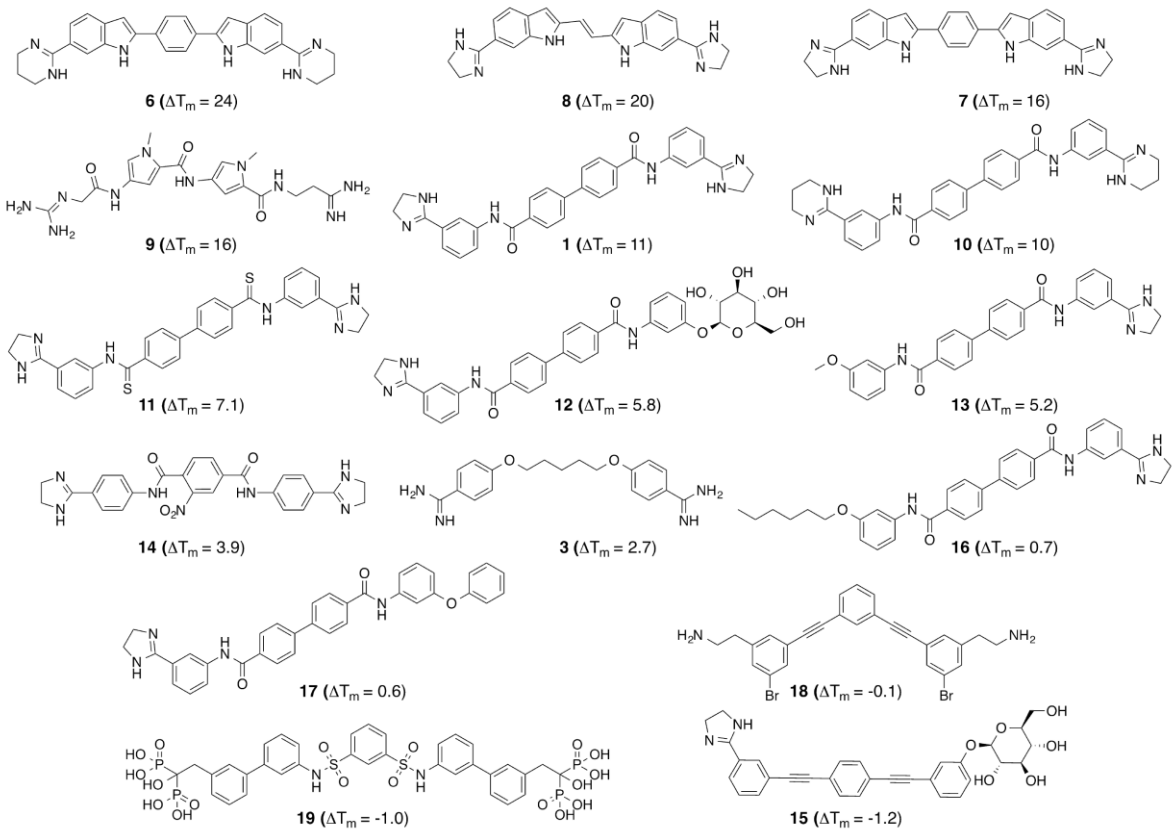

Figure 2.1. Structures of compounds of interest discussed in the text. Compounds are rank ordered (top left to bottom right) by their effects on the folded-unfolded transition (ΔT_m) of a DNA dodecamer duplex $(CGCGAATTCGCG)_2$, as determined by differential scanning calorimetry, the most potent binder being at the top left of the figure.

compounds	EcUPPS IC_{50} (μM)	SaUPPS IC_{50} (μM)	*E. coli* EC_{50} (μM)	*S. aureus* EC_{50} (μM)	ΔT_m (°C)
6	0.68	0.47	0.24	0.028	24
8	12	5.1	1.2	0.11	20
7	0.36	1.7	0.33	0.029	16
9	1400	1000	570	11	16
1	0.11	0.11	0.30	0.29	11
10	5.5	4.5	0.66	0.23	10
11	9.2	3.5	58	3.0	7.1
12	380	530	>1500	570	5.8
13	9.4	2.1	570	7.7	5.2
14	4.8	4.9	14	28	3.9
3	400	240	12	4.2	2.7
16	25	8.9	>1500	280	0.7
17	11	5.7	>1500	10	0.6
18	6.1	1.4	0.97	7.6	−0.1
19	0.36	0.39	>1500	100	−1.0
15	14	5.6	900	380	−1.2

Table 2.1. Enzyme inhibition, cell growth inhibition, and differential scanning calorimetry results.

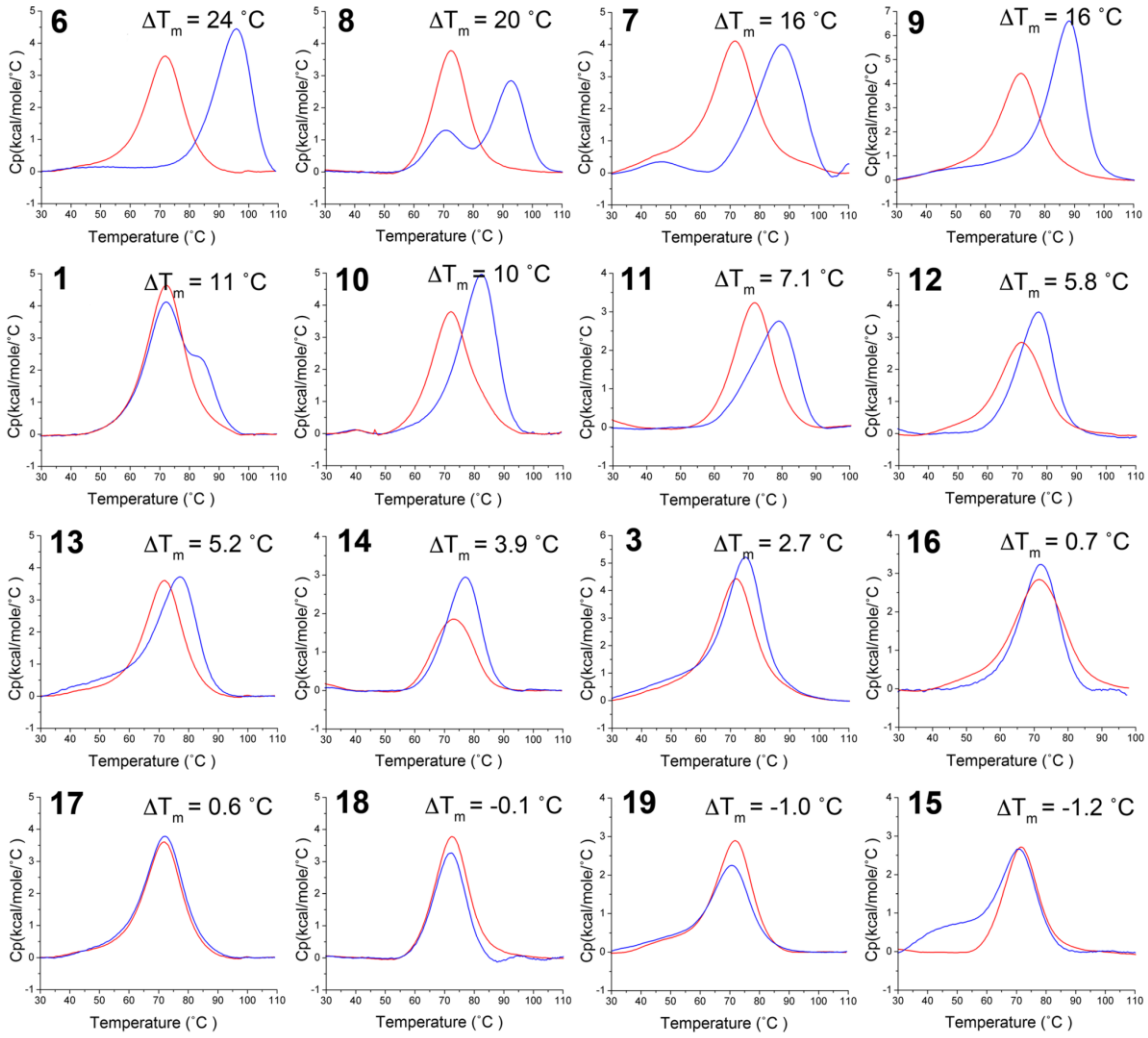

Figure 2.2. DSC thermograms for the 16 compounds shown in Figure 2.1 binding to the DNA dodecamer duplex $(CGCGAATTCGCG)_2$. The ΔT_m values are indicated. Apo-DNA thermograms of are shown in red, and DNA/ligand (1:1) thermograms are shown in blue.

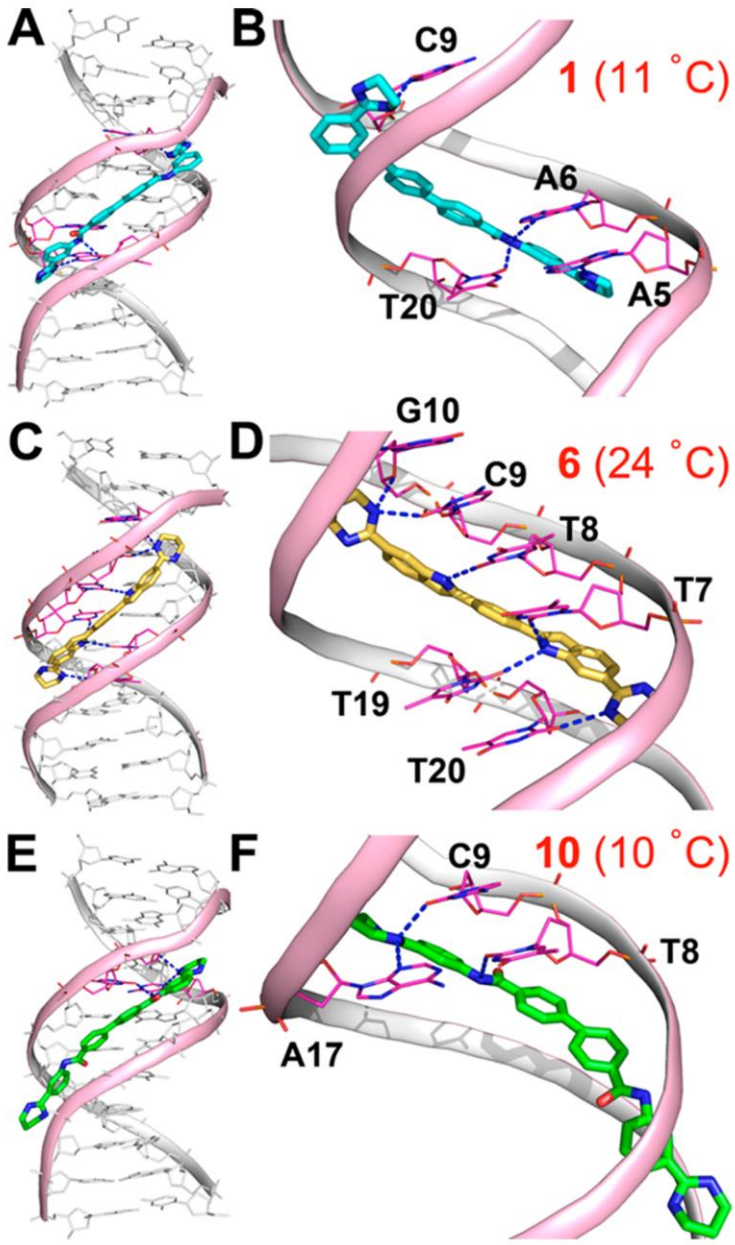

Figure 2.3. X-ray structures of DNA dodecamer duplex $(CGCGAATTCGCG)_2$ showing bisamidines bind to minor groove and interact with the nucleobases. (A) **1** (cyan) binds to the DNA minor groove, and (B) interacts with A5, A6, C9 and T20 (pink). (C) **6** (yellow) binds to the DNA minor groove, and (D) interacts with T7, T8, C9, G10, T19, and T20 (pink). (E) **10** (green) binds to the DNA minor groove, and (F) interacts with T8, C9, and A17 (pink). The largest number of bisamidine contacts correlates with the largest ΔT_m value (shown in parentheses).

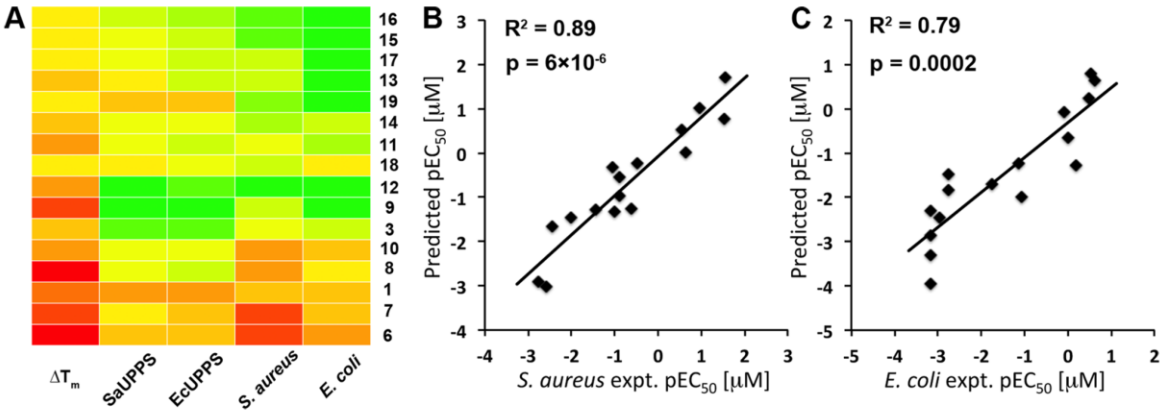

Figure 2.4. Heat-map and correlation plot. (A) Enzyme and cell growth inhibition and DNA binding heat-map. Red = strong activity, yellow = moderate activity, green = weak/no activity. (B) Correlation plot for *S. aureus* experimental and predicted cell activities based on UPPS IC50 and DNA ΔTm results in addition to one mathematical descriptor (vsurf_ID5). (C) Correlation plot for *E. coli* experimental and predicted cell activities based on UPPS IC50 and DNA ΔTm results in addition to one mathematical descriptor (GCUT_SMR_3).

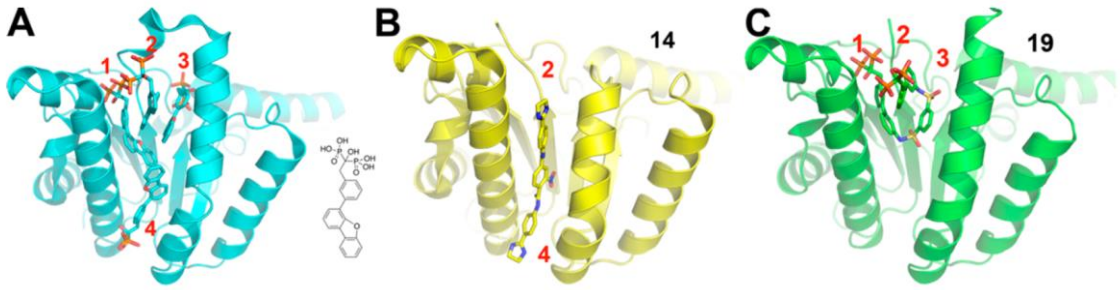

Figure 2.5. X-ray structures of *E. coli* UPPS showing ligand binding sites. (A) The bisphosphonate shown binds to sites 1−4 (PDB ID code 2E98). (B) Bisamidine **14** binds to sites 2 and 4 (PDB ID code 4H2J). (C) The tetraphosphonate **19** binds to sites 1−3 (PDB ID code 3WYJ).

2.7 References

1. *Antibiotic Resistance Threats in the United States*; Centers for Disease Control and Prevention: Atlanta, GA, 2013.
2. *Antimicrobial Resistance: Global Report on Surveillance*; World Health Organization: Geneva, 2014.
3. Davies, S.; Grant, J.; Catchpole, M. *The Drugs Don't Work: A Global Threat*; Penguin Books Ltd: London, 2013.
4. Durrant, J. D.; Cao, R.; Gorfe, A. A.; Zhu, W.; Li, J.; Sankovsky, A.; Oldfield, E.; McCammon, J. A. Non-bisphosphonate inhibitors of isoprenoid biosynthesis identified via computer-aided drug design. *Chem. Biol. Drug. Des.* **2011**, *78*, 323-332.
5. Lindert, S.; Zhu, W.; Liu, Y. L.; Pang, R.; Oldfield, E.; McCammon, J. A. Farnesyl diphosphate synthase inhibitors from *in silico* screening. *Chem. Biol. Drug. Des.* **2013**, *81*, 742-748.
6. Zhu, W.; Zhang, Y.; Sinko, W.; Hensler, M. E.; Olson, J.; Molohon, K. J.; Lindert, S.; Cao, R.; Li, K.; Wang, K.; Wang, Y.; Liu, Y. L.; Sankovsky, A.; de Oliveira, C. A.; Mitchell, D. A.; Nizet, V.; McCammon, J. A.; Oldfield, E. Antibacterial drug leads targeting isoprenoid biosynthesis. *Proc. Natl. Acad. Sci. U.S.A.* **2013**, *110*, 123-128.
7. Ashley, J. N.; Barber, H. J.; Ewins, A. J.; Newbery, G.; Self, A. D. H. A chemotherapeutic comparison of the trypanocidal action of some aromatic diamidines. *J. Chem. Soc.* **1942**, 103-116.
8. Fischer, R.; Hirt, R. US Patent 1971; Vol. No. 3, 622,596.
9. Williams, J. D.; Nguyen, S. T.; Gu, S.; Ding, X. Y.; Butler, M. M.; Tashjian, T. F.; Opperman, T. J.; Panchal, R. G.; Bavari, S.; Peet, N. P.; Moir, D. T.; Bowlin, T. L. Potent and broad-spectrum antibacterial activity of indole-based bisamidine antibiotics: Synthesis and SAR of novel analogs of MBX 1066 and MBX 1090. *Bioorg. Med. Chem.* **2013**, *21*, 7790-7806.
10. Steverding, D. The development of drugs for treatment of sleeping sickness: a historical review. *Parasit. Vectors* **2010**, *3*, 10.1186/1756-3305-1183-1115.
11. Panchal, R. G.; Ulrich, R. L.; Lane, D.; Butler, M. M.; Houseweart, C.; Opperman, T.; Williams, J. D.; Peet, N. P.; Moir, D. T.; Nguyen, T.; Gussio, R.; Bowlin, T.; Bavari, S. Novel Broad-Spectrum Bis-(Imidazolinylindole) Derivatives with Potent Antibacterial Activities against Antibiotic-Resistant Strains. *Antimicrob. Agents Chemother.* **2009**, *53*, 4283-4291.
12. Butler, M. M.; Williams, J. D.; Peet, N. P.; Moir, D. T.; Panchal, R. G.; Bavari, S.; Shinabarger, D. L.; Bowlin, T. L. Comparative *In Vitro* Activity Profiles of Novel Bis-Indole Antibacterials against Gram-Positive and Gram-Negative Clinical Isolates. *Antimicrob. Agents Chemother.* **2010**, *54*, 3974-3977.
13. Lanteri, C. A.; Trumpower, B. L.; Tidwell, R. R.; Meshnick, S. R. DB75, a novel trypanocidal agent, disrupts mitochondrial function in *Saccharomyces cerevisiae*. *Antimicrob. Agents Chemother.* **2004**, *48*, 3968-3974.
14. Oldfield, E.; Feng, X. X. Resistance-resistant antibiotics. *Trends Pharmacol. Sci.* **2014**, *35*, 664-674.
15. Silver, L. L. Challenges of Antibacterial Discovery. *Clin. Microbiol. Rev.* **2011**, *24*, 71-+.

16. Wilson, W. D.; Tanious, F. A.; Mathis, A.; Tevis, D.; Hall, J. E.; Boykin, D. W. Antiparasitic compounds that target DNA. *Biochimie* **2008**, *90*, 999-1014.
17. Chai, Y.; Paul, A.; Rettig, M.; Wilson, W. D.; Boykin, D. W. Design and Synthesis of Heterocyclic Cations for Specific DNA Recognition: From AT-Rich to Mixed-Base-Pair DNA Sequences. *J. Org. Chem.* **2014**, *79*, 852-866.
18. Barrett, M. P.; Gemmell, C. G.; Suckling, C. J. Minor groove binders as anti-infective agents. *Pharmacol. Ther.* **2013**, *139*, 12-23.
19. Scott, R. W.; DeGrado, W. F.; Tew, G. N. De novo designed synthetic mimics of antimicrobial peptides. *Curr. Opin. Biotechnol.* **2008**, *19*, 620-627.
20. Leon, A.; Liu, L.; Yang, Y.; Hudock, M. P.; Hall, P.; Yin, F. L.; Studer, D.; Puan, K. J.; Morita, C. T.; Oldfield, E. Isoprenoid biosynthesis as a drug target: Bisphosphonate inhibition of *Escherichia coli* K12 growth and synergistic effects of fosmidomycin. *J. Med. Chem.* **2006**, *49*, 7331-7341.
21. Teng, M.; Usman, N.; Frederick, C. A.; Wang, A. H. J. The Molecular-Structure of the Complex of Hoechst-33258 and the DNA Dodecamer D(Cgcgaattcgcg). *Nucleic Acids Res.* **1988**, *16*, 2671-2690.
22. Nunn, C. M.; Jenkins, T. C.; Neidle, S. Crystal-Structure of D(Cgcgaattcgcg) Complexed with Propamidine, a Short-Chain Homolog of the Drug Pentamidine. *Biochemistry* **1993**, *32*, 13838-13843.
23. Squire, C. J.; Clark, G. R.; Denny, W. A. Minor groove binding of a bis-quaternary ammonium compound: the crystal structure of SN 7167 bound to d(CGCGAATTCGCG)$_2$. *Nucleic Acids Res.* **1997**, *25*, 4072-4078.
24. Mukkamala, D.; No, J. H.; Cass, L. A.; Chang, T. K.; Oldfield, E. Bisphosphonate Inhibition of a *Plasmodium* Farnesyl Diphosphate Synthase and a General Method for Predicting Cell-Based Activity from Enzyme Data. *J. Med. Chem.* **2008**, *51*, 7827-7833.
25. *Molecular Operating Environment*; Chemical Computing Group Inc.: 1010 Sherbooke St. West, Suite #910, Montreal, QC, Canada, H3A 2R7, 2014, 2013.
26. Guo, R. T. C., R.; Liang, P. H.; Ko, T. P.; Chang, T. H.; Hudock, M. P.; Jeng, W. Y.; Chen, C. K.; Zhang, Y.; Song, Y.; Kuo, C. J.; Yin, F.; Oldfield, E.; Wang, A. H. Bisphosphonates target multiple sites in both cis- and trans-prenyltransferases. *Proc. Natl. Acad. Sci. U.S.A.* **2007**, *104*, 10022-10027.
27. Webb, M. R. A continuous spectrophotometric assay for inorganic phosphate and for measuring phosphate release kinetics in biological systems. *Proc. Natl. Acad. Sci. U.S.A.* **1992**, *89*, 4884-4887.
28. Li, K.; Schurig-Briccio, L. A.; Feng, X.; Upadhyay, A.; Pujari, V.; Lechartier, B.; Fontes, F. L.; Yang, H.; Rao, G.; Zhu, W.; Gulati, A.; No, J. H.; Cintra, G.; Bogue, S.; Liu, Y. L.; Molohon, K.; Orlean, P.; Mitchell, D. A.; Freitas-Junior, L.; Ren, F.; Sun, H.; Jiang, T.; Li, Y.; Guo, R. T.; Cole, S. T.; Gennis, R. B.; Crick, D. C.; Oldfield, E. Multitarget drug discovery for tuberculosis and other infectious diseases. *J. Med. Chem.* **2014**, *57*, 3126-3139.
29. Kehl-Fie, T. E.; Zhang, Y. F.; Moore, J. L.; Farrand, A. J.; Hood, M. I.; Rathi, S.; Chazin, W. J.; Caprioli, R. M.; Skaar, E. P. MntABC and MntH Contribute to Systemic *Staphylococcus aureus* Infection by Competing with Calprotectin for Nutrient Manganese. *Infect. Immun.* **2013**, *81*, 3395-3405.
30. Potterton, E.; Briggs, P.; Turkenburg, M.; Dodson, E. A graphical user interface to the CCP4 program suite. *Acta Crystallogr. Sect. D-Biol. Crystallogr.* **2003**, *59*, 1131-1137.

31. Emsley, P.; Cowtan, K. Coot: model-building tools for molecular graphics. *Acta Crystallogr. Sect. D-Biol. Crystallogr.* **2004**, *60*, 2126-2132.

Chapter 3: *In Vitro* and *In Vivo* Activity of Multi-Target Inhibitors Against *Trypanosoma brucei*

3.1 Notes and Acknowledgements

Y.W and K.L. synthesized compounds; G.Y., S.B., and G.C. performed cell growth inhibition assays and *in vivo* experiments; W.Z. and Z.H. performed enzyme inhibition assays; W.Z. performed DSC experiments and computational modeling; G.H. and S.B. performed membrane potential measurements; Y.W., G.Y., W.Z., R.D., E.O. and J.H.N. analyzed data.

This work was supported by the United States Public Health Service (National Institutes of Health grants GM065307, CA158191 and AI104120); a Harriet A. Harlin Professorship; the University of Illinois/Oldfield Research Fund; the National Research Foundation of Korea (NRF-2014K1A4A7A01074645), a grant funded by the Korean government (MSIP), Gyeonggi-do and KISTI.

This chapter was reproduced in part with permission from W. Zhu, E. Oldfield, *et al*. *ACS Infect. Dis.,* **2015***,* volume 1*,* page 388–398, Copyright © 2015 American Chemical Society.

3.2 Introduction

Diseases caused by trypanosomatid parasites afflict millions of individuals worldwide and are the causative agents of sleeping sickness in Africa, of Chagas disease in Latin America, and of the leishmaniases in India, the Middle East as well as in Latin America.[1] Many of the drugs used to treat these diseases are quite toxic (arsenicals, antimonials and benznidazole), or they are very expensive or difficult to administer in the field. Plus, many of the drugs that are in use are becoming ineffective due to resistance. Moreover, since there are no vaccines available to prevent these diseases, there is a continuing need for new drugs and new drug leads.

In this work, we focus on sleeping sickness, also known as human African trypanosomiasis (HAT). The disease is transmitted by the bite of the *tsetse* fly and is fatal if not treated, and resistance to currently used therapeutics is occurring.[2] There are two drugs used to treat the initial phase of the disease: suramin (**1**) and pentamidine (**2**), Figure 3.1, employed in the treatment of trypanosomiasis caused by *T. brucei rhodesiense* and *T. brucei gambiense*, respectively. Pentamidine therapy is rather toxic and the side effects can be fatal. For the treatment of the second or neurological phase, melarsoprol (**3**), an arsenical, is used for the treatment of both infections.

However, this drug likewise causes severe side effects and is lethal in ~5-10% of patients. Both drugs are taken up into cells by the *T. brucei* adenosine and aquaglyceroporin-2 transporters and cross-resistance to both drugs is increasing.[2] A newer drug, eflornithine (**4**), alone or in combination with nifurtimox (**5**), has recently been introduced but is effective only for the treatment of *T. brucei gambiense* infections. Other, less toxic, inexpensive drugs active against infections caused by both species are thus required. There are promising leads that are in clinical trials, such as fexinidazole[3] and oxaboroles,[4] but it is unfortunately true that most clinical trials fail, so there is almost always a need for new concepts, and new leads.

Another class of leads are the diamidines. These compounds (such as DB75 (**6**) and its prodrug DB289 (**7**)) have been developed from the diamidine pentamidine and are thought to bind to AT-rich DNA (primarily kinetoplast DNA, k-DNA), but may also have effects as uncouplers,[5,6] compounds that collapse the proton motive force and thus ATP synthesis. In our group, we recently found that other diamidines, such as BPH-1358 (NSC50460, **8**), had activity against two enzymes involved in isoprenoid biosynthesis, undecaprenyl diphosphate synthase (UPPS)[7] and farnesyl diphosphate synthase (FPPS).[8,9] There was potent (~100 nM) activity against *Staphylococcus aureus* UPPS[7] as well as against *S. aureus*, both *in vitro* and *in vivo* in a mouse model of infection with 20/20 mice surviving when treated with **8,**[7] while none survived without treatment.[7] In later work,[10] we found that **8** also bound to an AT-rich DNA dodecamer duplex, increasing the unfolding transition (ΔT_m) in a DSC (differential scanning calorimetry) experiment by ~11 ˚C. We found that we could quite accurately (R^2 ~ 0.89) model *S. aureus* cell growth inhibition by using ΔT_m and UPPS IC_{50} results together with one mathematical descriptor,[10] implying multi-target inhibition. Here, we investigated the activity of each of the compounds reported earlier as *S. aureus* cell growth inhibitors for potential activity against *T. brucei in vitro*, the most promising compound being tested *in vivo*. We also tested all compounds for activity against *T. brucei* farnesyl diphosphate synthase (TbFPPS), since **8** has been reported to inhibit human FPPS,[8] as well as for activity as uncouplers, since we have found that other lipophilic bases can act as potent uncouplers.[11]

3.3 Results and Discussion

***T. brucei* and human cell growth inhibition results.** We first investigated the activity of the sixteen compounds whose structures are shown in Figure 3.2 for activity against *T. brucei*

bloodstream form (BSF) parasites, as well as against two human cell lines: human embryonic kidney (HEK293T) and a human hepatocellular carcinoma (HepG2), as counter-screens for toxicity. The compounds were all from the batches whose synthesis and characterization were reported previously.[10] Representative dose-response results are shown in Figure 3.3. All EC_{50} (*T. brucei*) and cytotoxicity (CC_{50}; HEK293T, HepG2) values obtained are shown in Table 3.1. As can be seen in Table 3.1, there are 6 compounds (**2**, **8-11, 13**) that have promising activity with EC_{50} values of < 100 nM against *T. brucei* cell growth. The most potent compound was **8** which had an EC_{50} of 7.7 nM, essentially the same as found with pentamidine (**2**; EC_{50} = 5 nM). Perhaps more interesting is the observation that the activity of **8** against both human cell lines is > 100 μM, while that of pentamidine was < 0.4 μM. This leads to a "selectivity index" (SI), defined as:

$$SI = CC_{50} \text{ (human cell line)}/EC_{50} \text{ (}T.\ brucei\text{)}$$

of > 13000 for **8,** versus < 80 for pentamidine **2**, suggesting that **8** might be active *in vivo,* and could have less toxicity than does pentamidine (**2**).

Mechanism of action of diamidines and related compounds. How **8** and the other compounds inhibit *T. brucei* cell growth is of interest since it might eventually lead to more potent and/or selective inhibitors, something that is needed in light of the setbacks found with **7**[12] in clinical trials. All of the compounds described here that have significant activity against *S. aureus* bind to AT-rich DNA,[10] and we previously found that there was a correlation between the number of inhibitor-DNA hydrogen bonds and DNA-binding activity (as determined by ΔT_m, the shift in the maximum of the C_p-versus-T DSC thermogram upon inhibitor binding). Plus, in this earlier work[10] we found that there was a correlation between ΔT_m and *S. aureus* cell growth inhibition. Since binding of diamidines to AT-rich DNA has been implicated in the mechanism of action of other diamidine anti-bacterials[13], as well as in the inhibition of *T. brucei* cell growth, we sought to see whether the same mechanism was involved with the compounds described here. As can be seen in Table 3.1, the four compounds (**8-11**) with the largest AT-rich DNA ΔT_m values on ligand binding ($\Delta T_m \geq 10^{\circ}C$) are all potent *T. brucei* cell growth inhibitors with EC_{50} values ≤ 100 nM, suggesting a role of DNA binding in *T. brucei* cell growth inhibition. We thus next sought to see if **8** (the compound with the best *T. brucei* cell growth inhibition, and selectivity index) had any effects on nuclear DNA replication, kinetoplast DNA (k-DNA) replication, or both. k-DNA, located in the *T. brucei* mitochondrion, is an unique form of DNA found only in trypanosomatid parasites and is, therefore, a good drug target.

We found, using an EdU click chemistry reaction,[14,15,16] that there was a complete block of *T. brucei* k-DNA replication with **8**, as shown in Figure 3.4A. EdU is the thymidine-analog, 5-ethynyl-2′-deoxyuridine, which when detected using click chemistry with azide labeled Alexa•Fluor 488 leads to green fluorescence in replicating DNA/k-DNA. The bisamidine DAPI (4′,6-diamidino-2-phenylindole) when bound to DNA is a highly (blue) fluorescent compound, and is used to stain both nuclear and k-DNA. As can be seen in Figure 3.4A, in the presence of **8**, k-DNA replication in *T. brucei* is completely blocked, just as seen with the control, ethidium bromide (bottom panel in Figure 3.4A). These results show that the bisamidine **8** inhibits k-DNA replication, presumably by binding to AT-rich motifs in k-DNA. The kinetoplast in *T. brucei* is, however, relatively small when compared to that found in another trypanosomatid parasite, *Leishmania donovani*, and as expected, the results of the DAPI (nuclear and k-DNA) staining and the EdU click-chemistry (replicating DNA) reactions are much more readily seen with *L. donovani*, as shown in Figure 3.4B where clearly, as expected, **8** blocks k-DNA replication. Nevertheless, in both *T. brucei* as well as in *L. donovani*, it appears that **8** inhibits k-DNA replication but has no obvious effect on nuclear DNA replication. These results are consistent with k-DNA replication being one target for **8** in *T. brucei* cell growth inhibition. The actual number of kinetoplasts in the visual field also decreases as a function of drug concentration and incubation time, as shown in Figure 3.4C for *T. brucei*, indicating kinetoplast disruption.

When we compared the ΔT_m and *T. brucei* cell growth inhibition results (using $pEC_{50} = -\log_{10} EC_{50}$ values) there was only a poor correlation ($R^2 = 0.22$, Figure 3.5A). One possibility for this is that there are only relatively few compounds (n = 16) that are being investigated. Another possibility is that since there is considerable chemical diversity amongst the 16 structures, good correlations would not be expected because transport would be very variable. To test this possibility, we added a mathematical descriptor (one of 308 we calculated using the MOE program[17]), finding that the correlation between predicted and experimental *T. brucei* cell growth inhibition values increased to $R^2 = 0.66$ ($p = 0.001$), Figure 3.5B. The best mathematical descriptor, computed by using the MOE program[17], was vsurf_EWmin1. This descriptor is the lowest hydrophilic energy (and depends on both structure connectivity and conformation), and gave $R^2 = 0.60$, $p = 0.0004$. A third possibility is that multiple-targets are involved. This possibility is the one we reported[10] for *S. aureus* cell growth inhibition in which both DNA-binding (major) and UPPS inhibition (minor) were implicated, but there is no UPPS in *T. brucei*. There is, however, another

prenyl synthase that is a drug target in *T. brucei*,[18] farnesyl diphosphate synthase, and in earlier work we found that FPPS could be inhibited by diamidines.[8,9]

We thus next screened all sixteen compounds against an expressed *T. brucei* FPPS. All enzyme inhibition IC_{50} values are shown in Table 3.1. The IC_{50} values vary considerably, from ~490 nM to ~2 mM. When the *T. brucei* cell growth inhibition (pEC_{50}) results are compared with the *T. brucei* FPPS inhibition results there is essentially no correlation (Figure 3.5C), but the correlation improves to $R^2 = 0.71$ with the addition of 1 computed descriptor (PEOE_VSA_FPPOS, the fractional positive polar van der Waals surface area, computed by using the MOE program[17]), Figure 3.5D. When we use both ΔT_m and FPPS data to predict activity:

$$pEC_{50}\text{ (cell, predicted)} = a \bullet pIC_{50}\text{ (}Tb\text{FPPS)} + b \bullet \Delta T_m + c$$

the correlation is again poor ($R^2 = 0.28$; Figure 3.5E), but this improves to R^2=0.76 ($p = 0.0005$) with the addition of 1 computed descriptor, as shown in Figure 3.5F. These results support the idea that both k-DNA binding as well as FPPS inhibition may contribute to *T. brucei* cell growth inhibition. To put these R^2 values in perspective, in earlier work[19] we compared 10 sets of enzyme inhibition/cell assay results for diverse systems (anti-bacterial, anti-protozoal, anti-cancer, anti-viral) finding that on average, the enzyme/cell pIC_{50}/pEC_{50} correlations were remarkably poor, R^2 ~0.30,[19] even though in most cases highly homologous series of compounds were being investigated. The correlation greatly improved by adding mathematical descriptors (such as clogP) and, on average, the R^2 values increased to $R^2 = 0.70$ (with 2 added descriptors, and large data sets). The same general approach can be used with multiple experimental descriptors, and with *S. aureus* we found an $R^2 = 0.75$ using ΔT_m and UPPS inhibition data, which improved to $R^2 = 0.89$ with 1 computed descriptor.[10] It is possible that there are alternate targets whose inhibition is being reflected in the computational descriptors, although the use of the experimental ΔT_m and TbFPPS pIC_{50} values together with just 1 computed descriptor does give a very good prediction of activity ($R^2 = 0.76$, $p = 0.0005$). Interestingly, we also found that the IC_{50} of DB75 (**6**) against both human and *T. brucei* FPPS was ~50 μM. This seems a rather large value, but FPPS could be a target for this compound in *T. brucei* since it is likely to be taken up by transporters and could accumulate within the cells, contributing to the toxicity seen with the pro-drug DB289.[20]

In addition to k-DNA and FPPS as potential targets, there are of course other possibilities, suggested by the literature. Specifically, it has been found that pentamidine (**2**) is an

uncoupler of oxidative phosphorylation in isolated rat liver mitochondria,[21] and that the mitochondrion in *T. brucei* is the target of the trypanocidal action of the diamidine DB75.[22] We thus next tested the most promising lead **8** for its ability to collapse the proton motive force (here, primarily the mitochondrial membrane potential, $\Delta\psi_m$) in digitonin-permeabilized bloodstream form *T. brucei* (BSF) trypanosomes (Figure 3.6A) and procyclic form (PCF) trypanosomes (Figures 6 B-D) using the safranine method.[23,24] We chose compound **8** since is had no effect on the growth of either of the two human cell lines (CC_{50} > 100 μM), in addition to being the most potent *T. brucei* cell growth inhibitor and as we show below, it is active *in vivo*.

Figure 3.6A shows that addition of 10 μM **8** decreased $\Delta\psi_m$, which was further reduced by addition of 8 μM FCCP (carbonyl cyanide 4-(trifluoromethoxy)phenylhydrazone, 2 μg/mL), a potent protonophore uncoupler. Similar results were obtained with PCF, Figure 3.6B. *T. brucei* PCF mitochondria were able to phosphorylate ADP, as demonstrated by the small decrease in $\Delta\psi_m$ after its addition, Figure 3.6C. This activity was inhibited by the ATP synthase inhibitor oligomycin. In addition, the mitochondria were able to transport Ca^{2+}, as shown by the decrease in the $\Delta\psi_m$ after addition of $CaCl_2$, and the $\Delta\psi_m$ returned to basal levels after addition of the Ca^{2+}-chelator EGTA, Figure 3.6C. Further addition of **8** followed by FCCP again collapsed $\Delta\psi_m$, Figure 3.6C. **8** collapsed $\Delta\psi_m$ in a dose-dependent manner (Figure 3.6D) and **8** alone had no effect (Figure 3.6B). These results show that mitochondria in permeabilized *T. brucei* are able to develop a $\Delta\psi_m$, phosphorylate ATP and transport Ca^{2+} and that **8** collapses $\Delta\psi_m$. These effects on the proton motive force are rapid and are very similar to those observed for SQ109 in bacterial systems[11] and are likely to make a contribution to **8** inhibiting cell growth.

These observations then raise the question: do some of the other compounds affect the PMF? We thus next measured the collapse in $\Delta\psi_m$ for all compounds, but this time at just a single (5 μM) inhibitor concentration. Results are shown in Figure 3.7. As a control, we used FCCP. The three most potent uncouplers (from Figure 3.2) were all biphenyls: **13, 14** and **8**, Figure 3.7, with the 6-membered amidine **13** being the most effective species, albeit less so than was FCCP, 140 versus 230 (arbitrary) fluorescence units. The 6-membered ring species **13** was more effective than was **8**, which has 5-membered amidine rings. The next most active species were pentamidine and **9**. However, we did not obtain an improved growth inhibition models using the uncoupling results, although they may be important for individual compounds.

In addition to the effects on $\Delta\psi_m$, we find that there are deranged mitochondrial morphologies exhibited by *T. brucei* BSF on treatment with **8**. Figure 3.8 shows DMSO control cells and cells treated with 500 nM **8** for 24 hrs. DAPI (blue fluorescence) stains the nuclear and k-DNA while MitoTracker® Red (red fluorescence) is used to visualize the mitochondria, and its uptake depends on $\Delta\psi_m$. As can be seen in Figure 3.8, k-DNA is localized to the mitochondrion, however, the mitochondrial morphology is disrupted by **8**, changing from a normal tubular shaped organelle to a more condensed form, particularly towards the location near the k-DNA.

These uncoupling effects are clearly interesting, but they could lead to toxicity-as might human FPPS inhibition. However, in other work[11] we reported that the tuberculosis drug lead SQ109 acted at least in part as an uncoupler, and this work has now been extended [25] to numerous other TB drug leads including adamantyl ureas, indolecarboxamides, tetrahydropyrazolopyrimidines, and the 1,5-diarylpyrrole BM212,[25] all of which are now thought to function primarily as uncouplers. Moreover, drugs such as niclosamide function in the same way[26] and are of interest as diabetes drug leads.[27,28] We thus next sought to see if **8** had any efficacy *in vivo*, and/or if it was highly toxic.

***In vivo* activity in a mouse model of infection.** Compound **8** has the best computed SI in both cell lines and also has essentially the same activity as pentamidine (**2**), so was chosen for further investigation. We used the *T. brucei brucei* Lister 427 mouse model of infection in which all mice die ~6 days after infection, in the absence of any treatment. In an initial set of experiments, mice were treated with **8** at 10 or 3 mg/kg i.p. for 4 days. Figure 3.9A shows survival as a function of time, again with PBS, pentamidine and compound **8** treated mice. All **8** treated mice survive in this infection model at both 3 and 10 mg/kg after the 4-day treatment (and over the 25 day observational period), and there was no parasitemia observed in the **2** (pentamidine) or **8** treated mice, Figure 3.9B. We then carried out a second series of experiments, this time at 1 and 0.3 mg/kg i.p. for 4 days. Survival and parasitemia results are shown in Figures 9C, D and indicate (when compared with the results in Figures 9A, B) that the lowest effective dose is ~3 mg/kg. There is no weight loss during mice treatment.

3.4 Conclusions

The results presented here suggest that it may be possible to develop new multi-target inhibitors of *T. brucei* cell growth that target both parasite-specific kinetoplast DNA (k-DNA) as well as isoprenoid biosynthesis (FPPS) with such "multi-target" inhibition being of general interest

since it could lead to more effective and more "resistance-resistant" drugs.[29] Of particular interest is the observation that the lead **8** inhibits k-DNA replication, but not nuclear DNA replication. Some of the diamidine analogs also inhibited the isoprenoid biosynthesis enzyme, farnesyl diphosphate synthase. This is of interest since FPPS is an essential protein for *T. brucei* cell growth.[18] Plus, other compounds acted as uncouplers, of interest since other new drug leads against bacteria have been reported to act in this way. In a mouse model of infection, all mice survived upon treatment with **8** and a similar result (with **8**) has been reported with *S. aureus* infection in which both DNA and another isoprenoid biosynthesis enzyme, UPPS, were targeted.[7,10] **8** also acts as an uncoupler in both bloodstream and procyclic form parasites, rapidly collapsing the mitochondrial membrane potential, $\Delta\psi_m$. However, while **8** was a potent inhibitor of *T. brucei* cell growth, it was a poor inhibitor of the growth of two human cell lines and did not appear toxic in mice. The basic observation that k-DNA, FPPS as well as the proton motive force can be targeted is thus of general interest in the context of developing new anti-parasitic drug leads for treating infections caused by trypanosomatid parasites.

3.5 Experimental Section

Ethics Statement. All animal care and therapy studies were carried out in strict accordance with the guidelines and principles established by the Korean Animal Protection Law (http://animalrightskorea.org). Animal use protocol # IPK-13009-1 was reviewed and approved by the Institutional Animal Care and Use Committee (IACUC) of the Institut Pasteur Korea.

Inhibitors. Inhibitors were from the batches whose synthesis (or availability) as well as characterization were described previously.[10] All compounds were ≥ 95% pure as determined by elemental analysis or analytical HPLC/MS analysis and were also characterized by ^{1}H NMR and HRMS.

Parasites and Cell Culture. *Trypanosoma brucei brucei* Lister 427 (bloodstream form) was cultivated at 37 °C with a 5% CO_2 atmosphere in HMI-9 medium supplemented with 10% fetal bovine serum (FBS). *T. brucei* was subcultured every 3 or 4 d and maintained until the twentieth passage. The HEK239T and HepG2 cell lines used in the cytotoxicity testing were cultivated at 37 °C in a 5% CO_2 atmosphere in Dulbecco's modified Eagle's medium supplemented with 10% FBS.

***T. brucei* Growth Inhibition**. *T. brucei* cell growth inhibition was assayed by measuring the conversion of resazurin to resorufin. Assays were performed in duplicate in 384 well plates which were seeded with *T. brucei* (2.5×10^3 cells per well). After seeding the parasites, they were exposed to the compounds for 3 d. Resazurin sodium salt (120 μM; R7017; Sigma-Aldrich, St. Louis, MO, USA) was then added and plates incubated for 5h. After incubation, the parasites were fixed with 4% paraformaldehyde and the plates analyzed in a Victor 3^{TM} plate reader (PerkinElmer, Inc., Waltham, MA, USA) at 590 nm (emission) and 530 nm (excitation). Pentamidine was used as a reference drug in the *T. brucei* inhibition assay. The EC_{100} of pentamidine was taken as the concentration that produced 100% growth inhibition.

Cytotoxicity Assay. A resazurin cytotoxicity assay was performed in duplicate with HEK239T and HepG2 cell lines. Cells (4.0×10^3 cells per well) were seeded in 384 well plates and incubated for 72 h with selected compounds. Cells were then exposed to 40 μM resazurin for 5 h to allow for conversion to resorufin by aerobic respiration. After incubation, cells were fixed with 4% paraformaldehyde and the plates read with a Victor 3^{TM} plate reader (PerkinElmer, Inc., Waltham, MA, USA) at 530 nm (excitation) and 590 nm (emission). Chlorpromazine was used as a reference drug in the cytotoxicity assay. The EC_{100} of chlorpromazine was taken as the concentration that produced 100% growth inhibition.

Protein Expression and Purification. *Tb*FPPS was cloned and expressed as reported previously.[30] Briefly, DNA coding for *Tb*FPPS was cloned into the pET-28a vector (Novagen, Madison, WI, USA). The recombinant plasmid was transformed into an *Escherichia coli* BL21 (DE3) host to be expressed. Bacterial clones were grown in LB medium to an O.D. 600 of 0.8, and were induced with 1 mM isopropyl β-d-1-thiogalactopyranoside (IPTG) at 37 °C. After induction for 5 h, cells were re-suspended in binding buffer (500 mM NaCl, 20 mM Na_2HPO_4, pH 7.4) and incubated with 10 mg/mL lysozyme, 10 μg/mL protease inhibitor, and 1 μL/mL benzonase nuclease (Novagen) for 15 min, on ice. The supernatant was obtained by centrifugation at 15000 *g* for 1 h, at 4 °C. Lysates were applied to a nickel-chelated agarose affinity column and washed with binding buffer. Protein was eluted from the column using binding buffer containing 500 mM imidazole. The eluted fraction was desalted with a PD-10 desalting column (GE Life Sciences, Pittsburgh, PA, USA) and stored in 10 mM HEPES buffer (pH 7.4) containing 10 mM 2-mercaptoethanol.

***In vitro* Enzyme Assay**. *Tb*FPPS inhibition assays were carried out as described previously.[30] Briefly, the condensation of geranyl diphosphate (GPP) with isopentenyl diphosphate (IPP) catalyzed by FPPS was monitored by using a coupled colorimetric assay[31] in 96-well plates with 200-μL reaction mixtures containing 400 μM methylthioadenosine (MESG), 100 μM IPP and 100 μM GPP in 25 mM Tris-HCl (pH 7.4), 1 mM $MgCl_2$ and 0.01% Triton X-100. The highest concentration of the inhibitors in the assay was 316 μM.

Visualization of DNA Replication. After the treatment with inhibitors for 72 h, *T. brucei* BSF trypanosomes were incubated for 16 h with the thymidine analogue EdU (5-ethynyl-2'-deoxyuridine). EdU-labeled parasites were then washed with 1× PBS and fixed in 100% cold ethanol, and completely dried. Fixed parasites were washed with 1× PBS and incubated with Alexa Fluor® 488 Azide (Invitrogen, Grand Island, NY, USA) under Cu(I)-catalyzed click reaction conditions (100 μM of ascorbic acid and 1 μM of $CuSO_4$). EdU-labeled parasites were counterstained with 10 μg/ml DAPI before mounting in VECTASHIELD® mounting medium (Vector Laboratories, Burlingame, CA, USA). The images were analyzed using a Nikon Eclipse 90i fluorescence microscope (Nikon, Tokyo, Japan) and captured with a digital camera (DS-1QM, Nikon).

Visualization of Mitochondrial Membrane Potential. After the compound treatment for 24 h and 48 h, then parasites were incubated with 200 nM of Mitotracker® Red CMXRos (Invitrogen) for additional 30 min. BSF trypanosomes were washed in cold PBS and fixed with 3% PFA in PBS at 4 °C for 1 h. Fixed parasites were washed with PBS, and stained with 10 μg/ml of DAPI before mounting in VECTASHIELD® mounting medium (Vector Laboratories, Burlingame, CA, USA). Images were analyzed with a Nikon Eclipse 90i fluorescence microscope (Nikon, Tokyo, Japan) and captured with a digital camera (DS-1QM, Nikon).

***In vivo* Experiments**. BALB/C mice were infected with *T. brucei brucei* Lister 427 (3×10^4 cells) by i.p. injection. Mice were divided into groups (n = 5), and drug treatment carried out for 4 consecutive days by administering 10, 3, 1 or 0.3 mg/kg of compound **8** i.p. Parasitemia and survival were evaluated daily for 25 days. Mice showing impaired health status and/or with a parasite load > 10^8 cells per ml of blood were euthanized.

Analysis of Mitochondrial Membrane Potential. The mitochondrial membrane potential *in situ* was analyzed spectrofluorometrically by using safranine as the probe.[23,24] *T. brucei* PCF and BSF trypanosomes were incubated at 28 °C in reaction buffer (125 mM sucrose, 65 mM KCl,

10 mM HEPES–KOH buffer, pH 7.2, 1 mM $MgCl_2$, 2.5 mM potassium phosphate) with additions as described in the Figure legends. Fluorescence changes were monitored on a Hitachi 4500 spectrofluorometer (excitation wavelength = 496 nm; emission wavelength = 586 nm).

Computational Aspects. All mathematical modeling was performed in R (http://www.R-project.org). Descriptors were calculated by using MOE.[17]

Statistical Analyses. All IC_{50}/EC_{50} values were measured in duplicate. Dose-response curves were fitted by using a sigmoidal dose-response equation with a variable slope using GraphPad Prism 6 Software (GraphPad Software, San Diego, CA, USA).

Chemical Syntheses: General Methods. All chemicals were reagent grade. Pentamidine and netropsin were purchased from Aldrich. ^{1}H NMR and ^{13}C NMR spectra were obtained on Varian (Palo Alto, CA) Unity spectrometers at 400 and 500 MHz for ^{1}H and at 100 and 125 MHz for ^{13}C. Elemental analyses were carried out in the University of Illinois Microanalysis Laboratory. HPLC/MS was performed using an Agilent LC/MSD Trap XCT Plus system (Agilent Technologies, Santa Clara, CA) with an 1100 series HPLC system including a degasser, an autosampler, a binary pump, and a multiple wavelength detector. All final compounds were ≥95% pure as determined by elemental analysis or analytical HPLC/MS analysis and were also characterized by ^{1}HNMR and HRMS.

N4,N4′-bis(3-(4,5-dihydro-1H-imidazol-2-yl)phenyl)-[1,1′-biphenyl]-4,4′-bicarboxamide (1)

To a mixture of 4,4′-diphenyl dicarbonyl chloride (1.39 g, 5 mmol), 3-aminobenzonitrile (1.18 g, 10 mmol) in anhydrous THF (20 mL) was added Et_3N (2.1 mL, 15 mmol) and the mixture was stirred at room temperature overnight. After filtration, the white solid was washed with water (20 mL) and ethyl acetate (10 mL) and then dried. Sodium hydrosulfide hydrate (100 mg), ethylenediamine (2 mL), and dimethylacetamide (10 mL) were then added and stirred overnight at 140 °C. Upon removal of the solvent, the solid was washed thoroughly with water and then ethyl acetate (10 mL). To the suspension of the crude product in 10 mL of water were added two equivalents of methanesulfonic acid. Removal of water afforded the final product **1** as its methanesulfonic acid salt (1.44 g, 40%). ^{1}H NMR (DMSO-d_6, 500 MHz) δ: 10.68 (s, 2 H), 10.52

(s, 4 H), 8.50 (s, 2 H), 8.12 (d, J = 9.0 Hz, 4 H), 8.02–7.98 (m, 2 H), 7.96 (d, J = 9 Hz, 4 H), 7.68–7.58 (m, 4 H), 4.00 (s, 8 H), 2.36 (s, 6 H). HRMS (ESI): m/z $[M + H]^+$ calculated for $C_{32}H_{29}N_6O_2$ 529.2361, found 529.2352. Purity of the product determined by HPLC (Phenomenex C6-Phenyl 110A. 100x2 mm, 3 μm, 300 nm, retention time = 5.6 min): 98.9%.

1,4-bis(6-(1,4,5,6-tetrahydropyrimidin-2-yl)-1*H*-indol-2-yl)benzene (6)

Terephthalaldehyde (1.34 g, 10 mmol) and 4-methyl-3-nitrobenzonitrile (3.24 g, 20 mmol) were added to a round-bottom flask and heated together to 150 ºC until the compounds melted. Piperidine (1.5 mL) and sulfolane (10 mL) were added and the resulting solution was stirred at 150 ºC overnight and cooled to room temperature to yield an orange solid (3.4 g, 80%) which was washed with methanol (15 mL × 3) and dried. The solid, 4,4'-(1*E*,1'*E*)-2,2'-(1,4-phenylene)bis(ethene-2,1-diyl)bis(3-nitrobenzonitrile) was utilized in the following steps without further purification. Product from last step was then suspended in triethyl phosphate (30 mL) and heated to reflux (160 ºC) for 72 h until the mixture turned from orange to yellow. The suspension was then filtered and the yellow solid washed with methanol (15 mL × 3) and dried (1.4 g, 55%). The solid, 2,2'-(1,4-phenylene)bis(1*H*-indole-6-carbonitrile) was utilized in the following steps without further purification. Product from last step was suspended in propane-1,3-diamine (15 mL) and heated to 130 ºC for 24 h. The suspension was filtered and the solid washed with water (15 mL × 3) and methanol (15 mL × 3). The final product **6** was a yellow solid. ^{1}H NMR (DMSO-d_6, 500 MHz) δ: 7.99 (s, 4 H), 7.79 (s, 2 H), 7.48 (d, J = 8.0 Hz, 2 H), 7.42 (d, J = 8.0 Hz, 2 H), 6.99 (s, 2 H), 3.37 (s, 8 H), 1,72 (m, 4 H). HRMS (ESI): m/z $[M + H]^+$ calculated for $C_{30}H_{29}N_6$ 473.2454, found 473.2450. Purity of the product determined by HPLC (Phenomenex C6-Phenyl 110A. 100x2 mm, 3 μm, 230 nm, retention time = 5.8 min): 99.1%.

1,4-bis(6-(4,5-dihydro-1*H*-imidazol-2-yl)-1*H*-indol-2-yl)benzene (7)

Terephthalaldehyde (1.34 g, 10 mmol) and 4-methyl-3-nitrobenzonitrile (3.24 g, 20 mmol) were added to a round-bottom flask and heated together to 150 ºC until the compounds melted. Piperidine (1.5 mL) and sulfolane (10 mL) were added and the resulting solution was stirred at 150 ºC overnight then cooled to room temperature to yield an orange solid (3.4 g, 80%) which was washed with methanol (15 mL × 3) and dried. The solid, 4,4'-(1*E*,1'*E*)-2,2'-(1,4-phenylene)bis(ethene-2,1-diyl)bis(3-nitrobenzonitrile) was utilized in the following steps without

further purification. Product from last step was then suspended in triethyl phosphate (30 mL) and heated to reflux (160 ºC) for 72 h until the mixture turned from orange to yellow. The suspension was then filtered and the yellow solid washed with methanol (15 mL × 3) and dried (1.4 g, 55%). The solid, 2,2'-(1,4-phenylene)bis(1*H*-indole-6-carbonitrile) was utilized in the following steps without further purification. Product from last step was suspended in ethane-1,2-diamine (15 mL) and heated to 130 ºC for 24 h. The suspension was filtered and the solid washed with water (15 mL × 3) and methanol (15 mL × 3). The final product **7** was a yellow solid. ^{1}H NMR (DMSO-d_6, 500 MHz) δ: 11.73 (s, 2 H), 7.97 (s, 4 H), 7.85 (s, 2 H), 7.50 (s, 4 H), 7.00 (s, 2 H), 3.28 (s, 4 H). HRMS (ESI): m/z $[M + H]^+$ calculated for $C_{28}H_{25}N_6$ 445.2141, found 445.2139. Purity of the product determined by HPLC (Phenomenex C6-Phenyl 110A. 100x2 mm, 3 μm, 230 nm, retention time = 5.5 min): 99.3%.

1*H*-Indole, 2,2'-(1,2-ethenediyl)bis[6-(4,5-dihydro-1*H*-imidazol-2-yl)-, dihydrochloride (8)

The compound was requested from NCI. ^{1}H NMR (methanol-d_4, 400 MHz): 7.92 (s, 2H), 7.71 (d, 8.4 Hz, 2H), 7.45 (d, J = 8.8 Hz, 2H), 7.33 (s, 2H), 6.78 (s, 2H), 4.08 (s, 4H). HRMS (ESI): m/z $[M + H]^+$ calculated for $C_{24}H_{23}N_6$ 395.1984, found 395.1986. Purity of the product determined by HPLC (Phenomenex C6-Phenyl 110A. 100x2 mm, 3 μm, 230 nm, retention time = 5.6 min): 97.2%.

N4,N4'-bis(3-(1,4,5,6-tetrahydropyrimidin-2-yl)phenyl)biphenyl-4,4'-dicarboxamide (10)

To a mixture of 4,4′-diphenyl dicarbonyl chloride (1.39 g, 5 mmol), 3-aminobenzonitrile (1.18 g, 10 mmol) in anhydrous THF (20 mL) was added Et_3N (2.1 mL, 15 mmol) and the mixture stirred at room temperature overnight. After filtration, the white solid was washed with water (20 mL) and ethyl acetate (10 mL) and then dried. Sodium hydrosulfide hydrate (100 mg), propane-1,3-diamine (2 mL), and dimethylacetamide (10 mL) were then added and the mixture stirred overnight at 140 °C. Upon removal of the solvent, the solid was washed thoroughly with water and then ethyl acetate (10 mL). To the suspension of the crude product in 10 mL of water were added two equivalents of methanesulfonic acid. Removal of water afforded the final product as its methanesulfonic acid salt (1.50 g, 40%). ^{1}H NMR (DMSO-d_6, 500 MHz) δ: 10.68 (s, 2 H), 9.95 (s, 4 H), 8.38 (s, 2 H), 8.14 (d, J = 9.0 Hz, 4 H), 7.98 (m, 6 H), 7.62 (t, 2 H), 7.42 (d, 2 H), 3.50 (s, 8 H), 2.29 (s, 4 H). HRMS (ESI): m/z $[M + H]^+$ calculated for $C_{34}H_{33}N_6O_2$ 557.2665, found

557.2658. Purity of the product determined by HPLC (Phenomenex C6-Phenyl 110A. 100x2 mm, 3 μm, 230 nm, retention time = 5.3 min): 99.6%.

N4,N4'-bis(3-(4,5-dihydro-1*H*-imidazol-2-yl)phenyl)biphenyl-4,4'-bis(carbothioamide) (11)

N4, N4′-bis(3-(4,5-dihydro-1H-imidazol-2-yl)phenyl)-[1,1′-biphenyl]-4,4′-bicarboxamide (**1**, 560 mg, 1 mmol) was suspended in pyridine (5 mL). Lawesson's reagent (2,4-bis(4-methoxyphenyl)-1,3,2,4-dithiadiphosphetane-2,4-disulfide) (1.0 g, 2.5 mmol) was added and the mixture heated to 150 ^{o}C for 72 h until the mixture turned yellow. The suspension was then filtered and the solid washed with methanol (15 mL *3) and acetone (15 mL *3) and then dried under vacuum. The product **11** was obtained as a yellow solid. ^{1}H NMR (DMSO-d_6, 500 MHz) δ: 12.12 (s, 2 H), 10.60 (s, 4 H) 8.45 (s, 2 H), 7.90 (d, J = 9.0 Hz, 4 H), 8.00–7.98 (m, 2 H), 7.82 (d, J = 9 Hz, 4 H), 7.73 (m, 4 H), 4.00 (s, 8 H). HRMS (ESI): m/z $[M + H]^+$ calculated for $C_{32}H_{29}N_6S_2$ 561.1895, found 561.1896. Purity of the product determined by HPLC (Phenomenex C6-Phenyl 110A. 100x2 mm, 3 μm, 230 nm, retention time = 5.8 min): 97.6%.

***N*^{4}-(3-(4,5-dihydro-1*H*-imidazol-2-yl)phenyl)-*N*$^{4'}$-(3-(((2S,3R,4S,5S,6R)-3,4,5-trihydroxy-6-(hydroxymethyl)tetrahydro-2*H*-pyran-2-yl)oxy)phenyl)-[1,1 -biphenyl]-4,4 –dicarboxamide (12)**

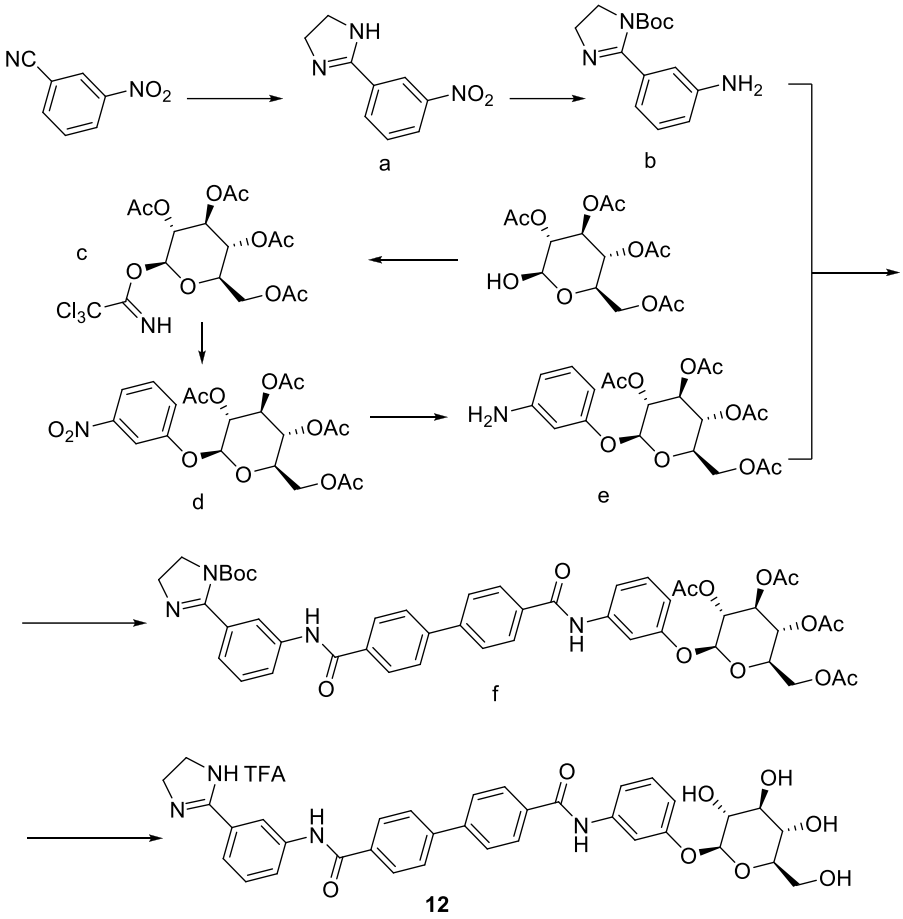

3-nitrobenzonitrile (3.6 g, 20 mmol) was treated with ethylene diamine (40 mL) and NaHS (200 mg). The solution was heated at 110 ^{o}C for 48 h and then quenched with water. The residue was extracted with ethyl acetate, dried under vacuum and purified by flash chromatography (silica gel, hexane/ethyl acetate = 2/1) to give the dihydroimidazole compound **a** (2.6 g, 60%). To the solution of **a** (2.2 g, 10 mmol) and $NaHCO_3$ (3.6 mg, 40 mmol) in dichloromethane (20 mL) and water (20 mL) was added $(Boc)_2O$ (4.5 g, 20 mmol) with vigorous stirring at 0 ^{o}C. The stirring was continued for 12 h when the temperature rose to room temperature naturally. The dichloromethane phase was separated and concentrated to give the Boc protected. To the solution of the above nitro compound in ethyl acetate (40 mL) was added Pd/C (10% palladium on charcoal, 145 mg) under nitrogen at room temperature. The nitrogen was switched to H_2 using a balloon and stirring was continued for 12 h at room temperature. Filtration and concentration under reduced pressure gave the 3-aminophenyl imidazoline **b**. Glucose tetraacetate (3.5 g, 10 mmol) was treated with trichloroacetonitrile (14.4 g, 100 mmol), DBU (0.3 g, 2 mmol) and CH_2Cl_2 (40 mL). The solution

was stirred at room temperature for 12 h and then washed with water. The residue was extracted with Et_2O, dried under vacuum and purified by flash chromatography (silica gel, hexane/ethyl acetate = 2/1) to give the peracetyl glucopyranosyl trichloroacetimidate **c** (4.4 g, 90%). A mixture of **c** (4.0 g, 8 mmol), 3-nitrophenol (1.1 g, 8 mmol), and freshly activated 4 Å molecular sieves in anhydrous CH_2Cl_2 (30 mL) was stirred under N_2 at 0 ^oC for 10 min, then BF_3Et_2O (40 μL, 0.8 mmol) was added via syringe. Stirring continued for 3 h, then Et_3N (2 mL) was added, and the resulting mixture was filtered through Celite. The filtrate was concentrated and purified by silica gel column chromatography (hexane/ethyl acetate = 3/1) to give 3-nitrophenol glycoside **d** (3.0 g, 80%). To the solution of **d** (2.3 g, 5 mmol) in ethyl acetate (20 mL) was added Pd/C (10% palladium on charcoal, 100 mg) under nitrogen at room temperature. The nitrogen was switched to H_2 using a balloon and stirring was continued for 12 h at room temperature. Filtration and concentration under reduced pressure gave 3-aminophenol glycoside **e**. To the solution of **b** (520 mg, 2 mmol), **e** (920 mg, 2 mmol) and Et_3N (1 mL) in dry dichloromethane (20 mL) was added [1,1'-biphenyl]-4,4'-dicarbonyl dichloride (560 mg, 2 mmol) at 0 ^oC. The stirring was continued for 4 h at 0 ^oC. The reaction mixture was washed with water (15 ml x 3), then concentrated under reduced pressure to give the residue. Purification of the residue by chromatography (silica gel, hexane/ethyl acetate = 2/1) gave product **f** (800 mg, 45%). To the solution of **f** (450 mg, 0.5 mmol) in MeOH (5 mL) was added MeONa (1 g) at room temperature. Stirring was continued for 4 h at room temperature and all the volatile components were removed under reduced pressure. The resulting residue was purified by chromatography (silica gel, ethyl acetate) to give the non-protected glycoside. To the solution of above free glycoside (360 mg, 0.5 mmol) in dichloromethane (3 mL) was added trifluoroacetic acid (2 mL) with stirring at room temperature. The stirring was continued for 4 h then all volatile components were removed under reduced pressure. The resulting residue was purified by chromatography (silica gel, chloroform/MeOH = 5/1) to give the final product **12**(340 mg, 95%). ^1H NMR (methanol-d_4, 400 MHz) 8.48 (m, 1H), 8.06 (m, 4H), 7.96 (m, 5H), 7.61 (m, 2H), 7.55 (m, 1H), 7.37 (d, J = 8.0 Hz, 1H), 7.26 (t J = 8.0 Hz, 1H), 6.89 (dd, J = 1.6 Hz, 1H), 4.78 (s, 1H), 4.11 (s, 4H), 3.90 (dd, J = 12.0, 2.0 Hz, 1H), 3.71 (dd, J = 12.0, 7.6 Hz, 1H), 3.46-3.38 (m, 5H). HRMS (ESI): m/z $[M + H]^+$ calculated for $C_{35}H_{35}N_4O_8$, 639.2455; found 639.2446. Purity of the product determined by HPLC (Phenomenex C6-Phenyl 110A. 100x2 mm, 3 μm, 210 nm, retention time = 5.8 min): 97.9%.

N^4-(3-(4,5-dihydro-1*H*-imidazol-2-yl)phenyl)-$N^{4'}$-(3-methoxyphenyl)-[1,1-biphenyl]-4,4–dicarboxamide (13)

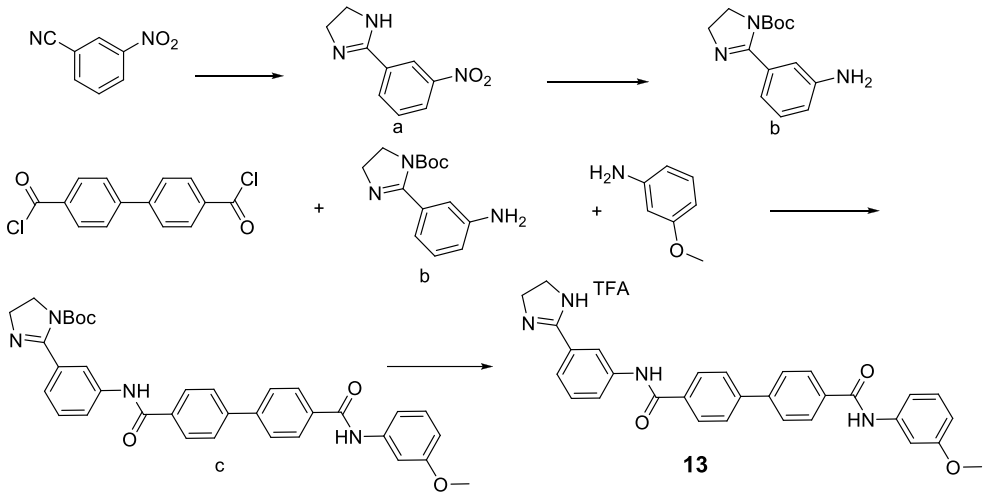

3-nitrobenzonitrile (3.6 g, 20 mmol) was treated with ethylene diamine (40 mL) and NaHS (200 mg). The solution was heated at 110 ^oC for 48 h and then quenched with water. The residue was extracted with ethyl acetate, dried under vacuum and purified by flash chromatography (silica gel, hexane/ethyl acetate = 2/1) to give the dihydroimidazole compound **a** (2.6 g, 60%). To a solution of **a** (2.2 g, 10 mmol) and $NaHCO_3$ (3.6 mg, 40 mmol) in dichloromethane (20 mL) and water (20 mL) was added $(Boc)_2O$ (4.5 g, 20 mmol) with vigorous stirring at 0 ^oC. The stirring was continued for 12 h at which point temperature had risen to room temperature naturally. The dichloromethane phase was separated and concentrated to give the Boc protected which was used in the next step. To a solution of the above nitro compound in ethyl acetate (40 mL) was added Pd/C (10% palladium on charcoal, 145 mg) under nitrogen at room temperature. The nitrogen was switched to H_2 using a balloon and stirring was continued for 12 h at room temperature. Filtration and concentration under reduced pressure gave the crude 3-aminophenyl imidazoline **b**. To the solution of **b** (260 mg, 1 mmol), 3-methoxyaniline (120 mg, 1 mmol) and Et_3N (0.5 mL) in dry dichloromethane (10 mL) was added [1,1'-biphenyl]-4,4'-dicarbonyl dichloride (280 mg, 1 mmol) at 0 ^oC. The stirring was continued for 4 h at 0 ^oC then the reaction mixture was washed with water (5 ml $\times$ 3), and concentrated under reduced pressure. Purification of the residue by chromatography (silica gel, hexane/ethyl acetate = 2/1) gave the product **c** (240 mg, 42%). To the solution of **c** (115 mg, 0.2 mmol) in dichloromethane (1 mL) was added trifluoroacetic acid (1 mL) with stirring at room temperature. Stirring was continued for 4 h and all the volatile components

were removed under reduced pressure. The resulting residue was purified by chromatography (silica gel, chloroform/MeOH = 5/1) to give the final product **13** (112 mg, 95%). ^{1}H NMR (methanol-d_4, 400 MHz) 8.45 (s, 1H), 8.03 (m, 4H), 7.90-7.80 (m, 6H), 7.59 (m, 2H), 7.30 (m, 1H), 6.71 (m, 1H), 4.09 (s, 4H), 3.78 (s, 3H). HRMS (ESI): m/z $[M + H]^+$ Calcd for $C_{30}H_{27}N_4O_3$, 491.2083; found 491.2084. Purity of the product determined by HPLC (Phenomenex C6-Phenyl 110A. 100x2 mm, 3 μm, 280 nm, retention time = 6.5 min): 97.5%.

N^1,N^4-bis(4-(4,5-dihydro-1*H*-imidazol-2-yl)phenyl)-2-nitroterephthalamide dihydrochloride (14)

The compound was requested from NCI. ^{1}H NMR (methanol-d_4, 400 MHz), 8.78 (d, J = 1.6 Hz, 2H), 8.42 (d, J = 8.0 Hz, 1H), 8.07 (dd, J = 8.8 Hz, 2H), 7.95-7.87 (m, 9H), 4.08 (s, 8H). HPLC-MS: m/z $[M + H]^+$ calculated for $C_{26}H_{24}N_7O_4$, 498.1890; found 498.1882. Purity of the product determined by HPLC (Phenomenex C6-Phenyl 110A. 100x2 mm, 3 μm, 280 nm, retention time = 5.0 min): 95.2%.

N^4-(3-(4,5-dihydro-1*H*-imidazol-2-yl)phenyl)-$N^{4'}$-(3-(hexyloxy)phenyl)-[1,1-biphenyl]-4,4–dicarboxamide (16)

The **16** was made with the same protocol for **13**. ^{1}H NMR (methanol-d_4, 400 MHz) 8.48 (s, 1H), 8.05 (m, 4H), 7.85 (m, 5H), 7.61 (m, 2H), 7.40 (s, 1H), 7.23 (m, 2H), 6.70 (m, 1H), 4.11 (s, 4H), 3.97 (t, J = 6.0 Hz, 2H), 1.77 (m, 2H), 1.48 (m, 2H), 1.36 (m, 4H), 0.91 (t, J = 6.8 Hz, 3H). HRMS (ESI): m/z $[M + H]^+$ Calcd for $C_{35}H_{37}N_4O_3$, 561.2866; found 561.2875. Purity of the product determined by HPLC (Phenomenex C6-Phenyl 110A. 100x2 mm, 3 μm, 280 nm, retention time = 7.2 min): 97.9%.

N^4-(3-(4,5-dihydro-1*H*-imidazol-2-yl)phenyl)-$N^{4'}$-(3-phenoxyphenyl)biphenyl-4,4'-dicarboxamide (17)

The **17** was made with the same protocol for **13**. ^{1}H NMR (methanol-d_4, 400 MHz) 8.47 (d, J = 1.6 Hz, 1H), 8.07 (d, J = 8.4 Hz, 2H), 8.01 (d, J = 8.4 Hz, 2H), 7.90-7.81 (m, 5H), 7.6 (m, 2H), 7.48 (s, 1H), 7.44 (d, J = 12.4 Hz, 1H), 7.37-7.30 (m, 3H), 7.11 (t, J = 7.6 Hz, 1H), 7.03 (s, 1H), 7.01 (s, 1H), 6.77 (t, J = 8.0, 1.2 Hz, 1H), 4.11 (s, 4H). HRMS (ESI): m/z $[M + H]^+$ Calcd for $C_{35}H_{29}N4O_3$, 553.2240; found 553.2249. Purity of the product determined by HPLC (Phenomenex C6-Phenyl 110A. 100x2 mm, 3 μm, 210 nm, retention time = 6.3 min): 99.8%.

Protein Expression, Purification and Inhibition. EcUPPS and SaUPPS were expressed and purified as described previously.[7] UPPS inhibition assays were also carried out as described previously.[7] Briefly, the condensation of FPP with IPP catalyzed by UPPS was monitored by using a continuous spectrophotometric assay[31] in 96 well plates with 200 μL reaction mixtures containing 400 μM MESG, 25 μM IPP, 2.5 μM FPP, 25 μM Tris-HCl (pH 7.5), 0.01% Triton X-100 and 1 μM $MgCl_2$. The IC_{50} values were obtained by fitting the inhibition data to a standard rectangular hyperbolic dose-response function in GraphPad PRISM 4.0 software (Graphpad Software, San Diego, CA).

Cell Growth Inhibition Assay. The growth of *E. coli* (K12) and determination of IC_{50} values were carried out as described previously.[11] IC_{50} values for *S. aureus* growth inhibition were also determined as described previously.[32] Briefly, an overnight culture of *S. aureus* (Newman strain) was diluted 50-fold into fresh TSB (tryptic soy broth) and grown for 1 h at 37 °C and then diluted 100-fold into fresh TSB medium and 100 μL aliquots inoculated into each well of a 96-round-bottom culture plate (Corning Inc., Corning, NY) containing serially diluted compounds. Plates were incubated for 9 h with shaking at 37 °C. Absorbances were measured at 600 nm and dose-response curves constructed using GraphPad PRISM 4.0 software (Graphpad Software, San Diego, CA).

Differential Scanning Calorimetry. The DNA dodecamer $(CGCGAATTCGCG)_2$ was purchased from Intergrated DNA Technologies, Inc. and annealed into a duplex before use. DNA and ligand solutions were prepared in Mes buffer (0.01 M Mes, 0.001 M EDTA, 0.2 M NaCl, pH 6.2). All ligand solutions were prepared by adding appropriate amounts of compound powder into the 0.1 mM DNA solution and the final compound concentrations were 0.1 mM. DSC experiments were performed by using a Microcal VP-DSC instrument. The scans cover a 10 to 110 °C temperature range at a scan rate of 90 °C/h. DSC thermograms were analyzed using Origin 7.1 software. Buffer vs. buffer scans were used for baseline corrections.

X-Ray Crystallography. Native *E. coli* UPPS crystals for use in soaking were obtained by using the hanging-drop method (Hampton Research, Laguna Niguel, CA) by mixing 1 μL of UPPS

protein solution (~10 mg/ml UPPS in 25 mM Tris-HCl, pH 7.5 and 150 mM NaCl) with 1 µL of mother liquor (25 mM Tris-HCl, pH 7.5, 150 mM NaCl and 5% PEG 2-4K) and then equilibrating with 400 µL mother liquor at room temperature. Tetragonal crystals appeared in 2 days and were then soaked in a cryoprotectant solution (30% EG and 5% PEG 35K) containing 1-5 mM inhibitors for 1 day.

S. aureus UPPS crystals with FSPP were obtained by using the hanging-drop method (Hampton Research, Laguna Niguel, CA) by mixing 1 µL of UPPS protein solution (~5 mg/ml UPPS in 1.5 mM $MgCl_2$, 1.5 mM FPP, 25 mM Tris-HCl, pH 7.5 and 150 mM NaCl) with 1 µL of mother liquor (100 mM NaMES, pH 6.5, 200 mM $(NH_4)SO_4$, and 25% PEG MME 5K) and then equilibrating with 400 µL mother liquor at room temperature. Bi-pyramidal crystals appeared overnight.

DNA/Ligand complex crystals were obtained via co-crystallization by mixing equivalent amount of 0.6 mM dodecamer and compounds (0.5-5 mM) and left on ice overnight. The mixtures were used to grow crystals from hanging drops against a reservoir of 40% MPD. Sheet-shaped crystals appeared in a month.

X-ray diffraction data were collected at the Life Science Collaborative Access Team (LS-CAT) 21-ID-D (G) at the Advanced Photon Source of Argonne National Laboratory. Diffraction data were processed and scaled by using the program HKL3000 (HKL Research Inc., Charlottesville, VA, USA).[33] Structure refinements were carried out by using Refmac,[34,35] Phenix[36] and Coot[37]. All structure figures were prepared by using PyMOL.[38]

3.6 Schemes, Charts, Tables and Figures

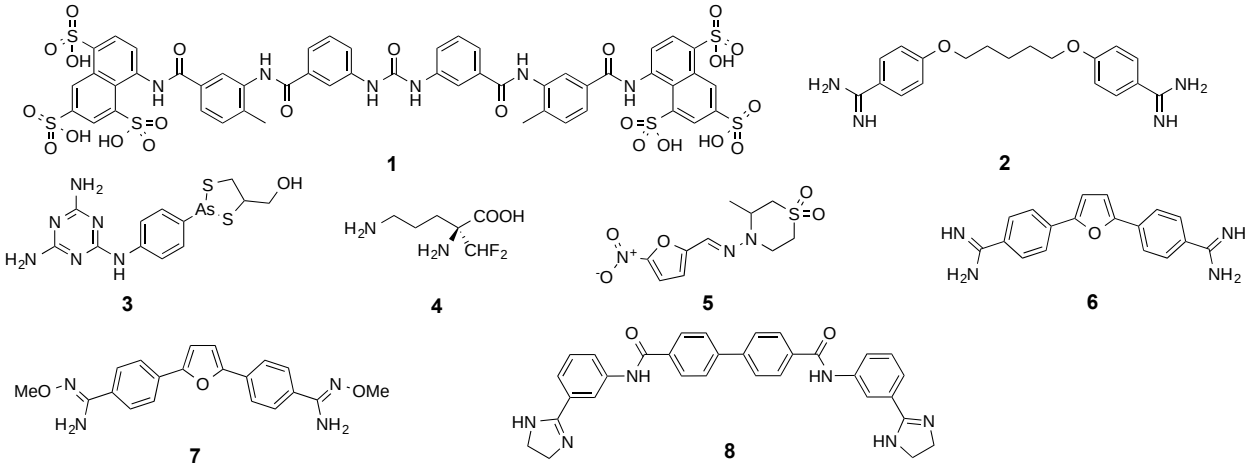

Figure 3.1. Structures of some *T. brucei* cell growth inhibitors.

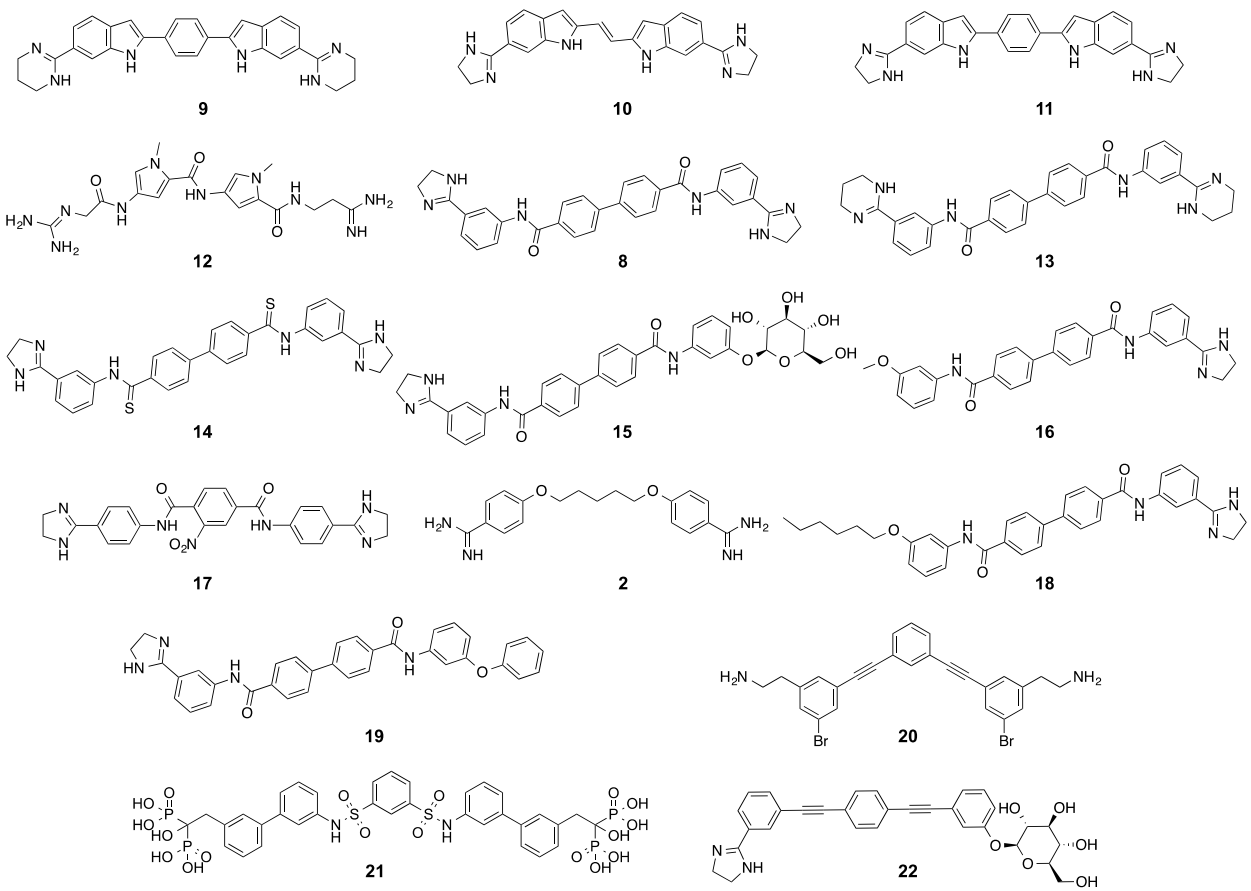

Figure 3.2. Structures of 16 compounds investigated here as *T. brucei* cell growth inhibitors.

ID	[a] *T. brucei* EC_{50} (μM)	[b] HEK293T CC_{50} (μM)	[c] HepG2 CC_{50} (μM)	[d] SI HEK/*Tb*	[e] SI Hep/*Tb*	[f] ΔT_m (°C)	[g] Fluor. A.U.	[h] TbFPPS IC_{50} (μM)
9	0.084	> 200	> 200	> 2400	> 2400	24	65 ± 5.0	3.5 ± 0.072
10	0.051	> 100	41	> 2000	810	20	12 ± 2.6	1.3 ± 0.017
11	0.020	> 100	> 100	> 5000	> 5000	16	25 ± 3.1	9.9 ± 0.50
12	2.1	> 200	> 200	> 96	> 96	16	13 ± 5.8	950 ± 230
8	0.0077	> 100	> 100	> 13000	> 13000	11	81 ± 2.9	27 ± 0.25
13	0.095	14	59	140	620	10	140 ± 16	310 ± 93
14	0.85	27	>100	32	118	7.1	110 ± 16	0.49 ± 0.0088
15	> 50	> 100	> 100	~ 2	~ 2	5.8	19 ± 4.5	21 ± 0.61
16	1.9	4.7	6.4	2.5	3.4	5.2	55 ± 2.5	18 ± 7.0
17	0.85	> 20	> 20	> 24	> 24	3.9	37 ± 4.4	240 ± 36
2	0.0055	< 0.4	< 0.4	< 80	< 80	2.7	64 ± 11	370 ± 7.2
18	0.42	14	33	35	80	0.7	18 ± 7.7	1800 ± 230
19	0.67	2	12	3	18	0.6	30 ± 3.3	45 ± 11
20	0.7	13	6.1	19	8.7	0.1	19 ± 8.3	4.4 ± 0.49
21	> 50	> 100	> 100	~ 2	~ 2	-1.0	7.1 ± 2.4	6.6 ± 2.8
22	23	> 100	> 100	> 4.4	> 4.4	-1.2	12 ± 2.6	1.9 ± 0.47

Table 3.1. Enzyme inhibition, cell growth inhibition, DSC and fluorescence results.

[a] *T. brucei* EC_{50} were determined from duplicate measurements by nonlinear regression analysis using GraphPad Prism 6. Values in parentheses are 95% confidence intervals.

Table 3.1 (cont.). Enzyme inhibition, cell growth inhibition, DSC and fluorescence results.

[b] HEK293T CC_{50} were determined from duplicate measurements. Values in parentheses are 95% confidence intervals.

[c] HepG2 CC_{50} were determined from duplicate measurements. Values in parentheses are 95% confidence intervals.

[d] Selective index: CC_{50} (HEK293T)/EC_{50} (*T. brucei*).

[e] Selective index: CC_{50} (HepG3)/EC_{50} (*T. brucei*).

[f] Data from ref. 10.

[g] Fluorescence intensity, arbitrary units. Larger values mean stronger uncoupling effects. Results shown are the average of triplicate experiments ± standard deviation.

[h] *T. brucei* FPPS IC_{50}. Data points are the average of duplicate experiment, ± standard deviation.

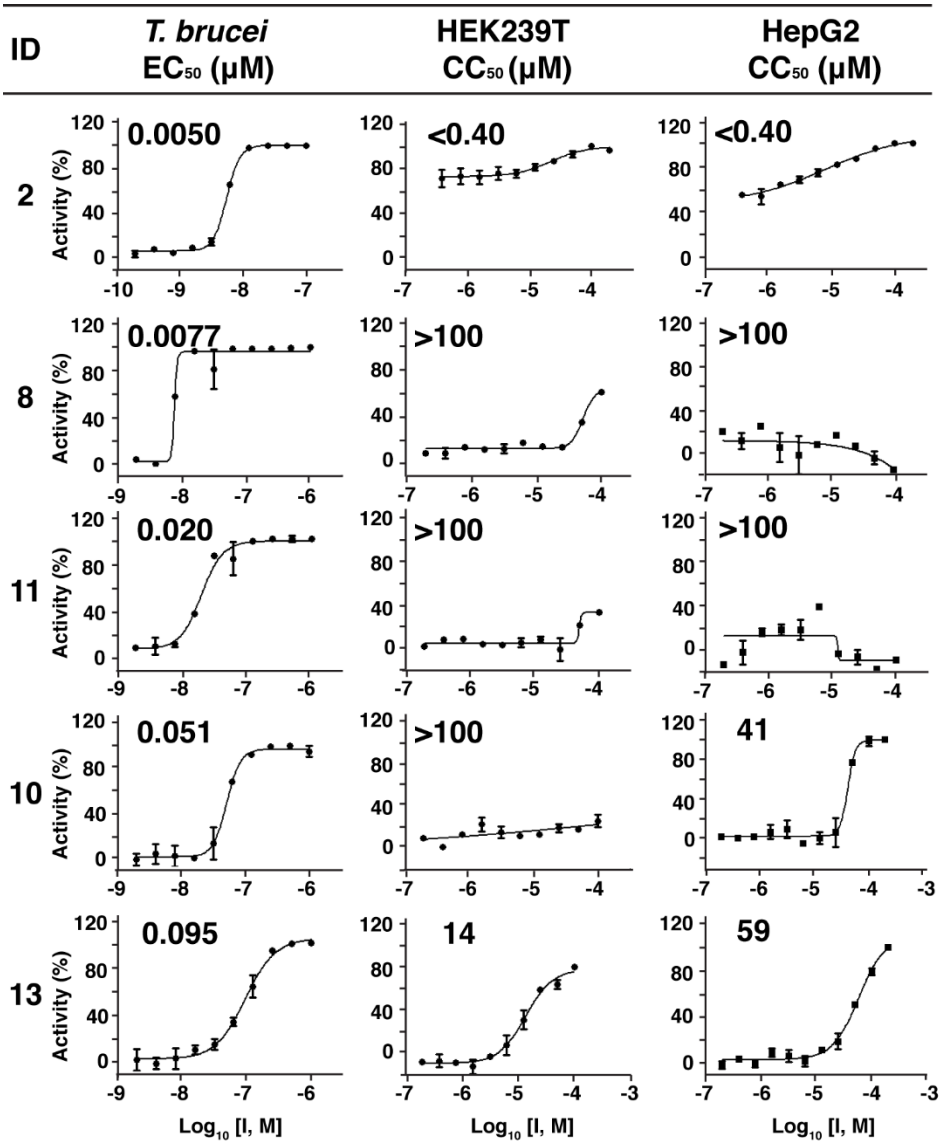

Figure 3.3. Representative dose-response results for some compounds of interest in *T. brucei*, HEK293T and HepG2 (human cell) growth inhibition, together with computed selectivity index (SI) values (SI = CC_{50} (human cell line)/EC_{50} *T. brucei*). Experiments were performed in duplicate.

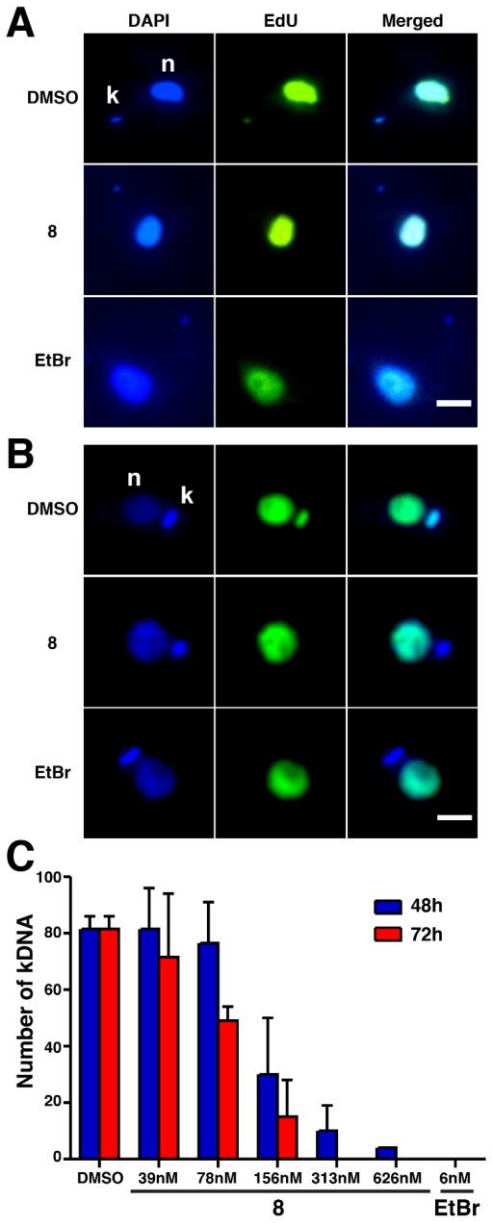

Figure 3.4. Effects of **8** on nuclear and k-DNA replication for *T. brucei* (A, C) and *L. donovani* (B). Shown at the top in A, B are control (DMSO vehicle) results with DAPI and EdU. DAPI stains all DNA and the bound compound exhibits a blue fluorescence. EdU is used to detect replicating DNA and fluoresces green. In the DMSO controls, both nuclear (n) and k-DNA (k) replicate in both organisms (green). In the middle row panels in A, B, cells are treated with **8**, which blocks k-DNA replication, so the (replicating) kinetoplast k-DNA signal is not observed (blue). The same k-DNA replication-inhibition result is found with the DNA intercalator ethidium bromide, shown in the bottom panels of the Figure. Scale bar, 2 μm. (C) Shows the number of kinetoplasts in the visual field as a function of **8** concentration (from 39 nM to 626 nM), and incubation time (48h or 72h). Values are means ± SD of duplicate experiments.

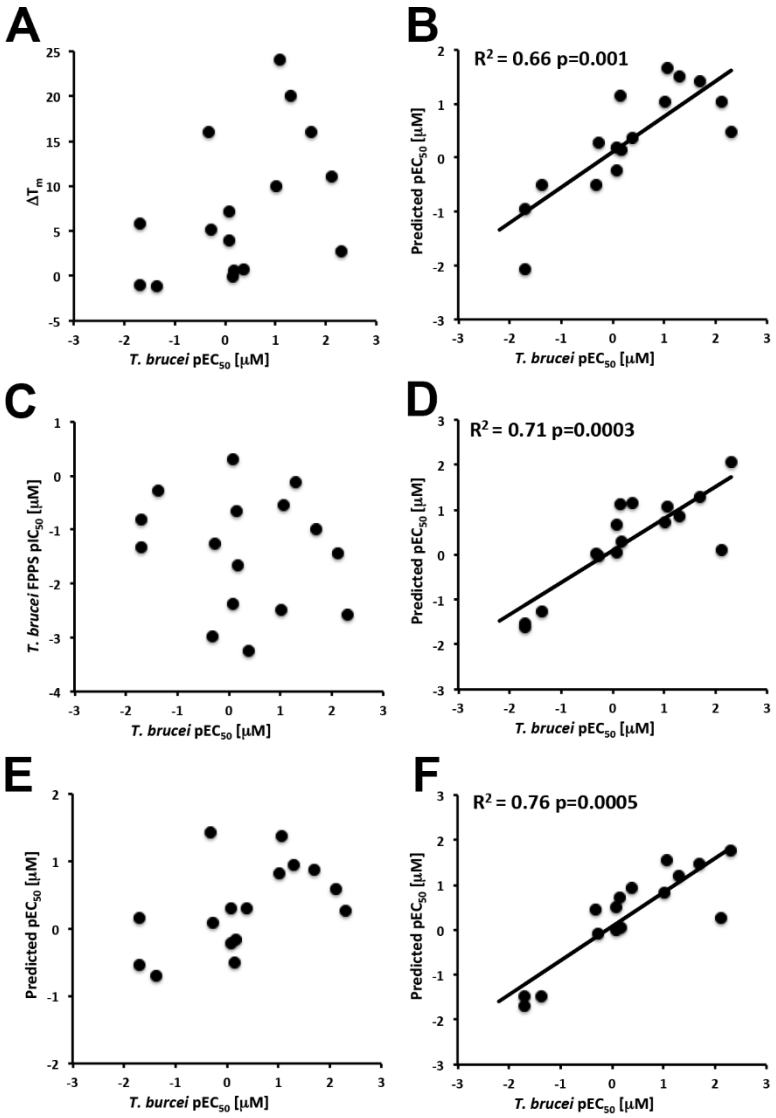

Figure 3.5. Plots between experimental *T. brucei* cell growth inhibition (pIC_{50} values) and experimental properties, and computed growth inhibition models. (A) ΔT_m, R^2=0.22, p=0.07. (B) ΔT_m+vsurf_EWmin1, R^2=0.66, p=0.001. (C) FPPS pIC_{50}, R^2=0.03, p=0.53. (D) FPPS pIC_{50}+PEOE_VSA_FPPOS, R^2=0.71, p=0.0003. (E) FPPS pIC_{50}+ΔT_m, R^2=0.28, p=0.12. (F) FPPS pIC_{50}+ΔT_m+ PEOE_VSA_FPPOS, R^2=0.76, p=0.0005.

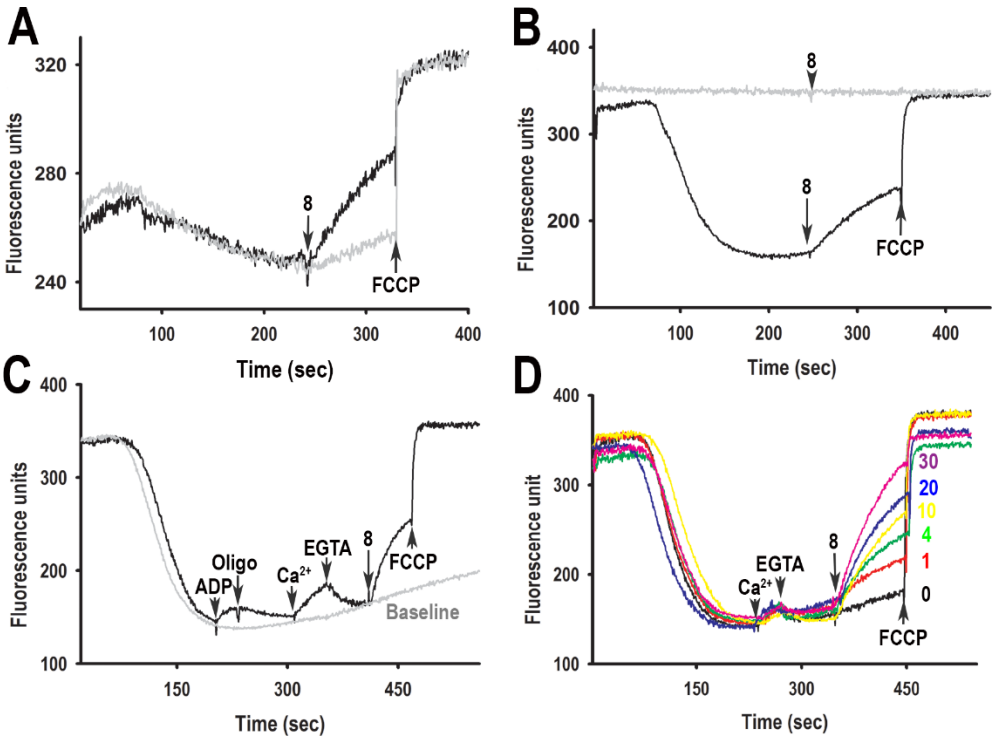

Figure 3.6. Effects of **8** on the mitochondrial membrane potential $\Delta\psi_m$ in digitonin-permeabilized *T. brucei*. (A) BSF trypanosomes ($2x10^8$ cells) were added to buffer (2 mL) containing 20 μM EGTA, 1 mM ATP, 500 μM sodium orthovanadate and 5 μM safranine, and the reaction initiated with 40 μM digitonin. **8** and FCCP were added where indicated. Grey line is baseline. (B) PCF trypanosomes ($5x10^7$ cells) were added to buffer (2.4 mL) containing 2 mM succinate and 5 μM safranine, and the reaction initiated with or without (grey trace) 50 μM digitonin. **8** (5 μM) and FCCP (8 μM) were added where indicated. (C) As (B) but ADP (10 μM), oligomycin (Oligo, 2 μg/ml), $CaCl_2$ (12 μM), EGTA (200 μM), **8** (10 μM), and FCCP (8 μM) were added where indicated. (D) As (B) but $CaCl_2$ (12 μM), EGTA (200 μM), various concentrations (0-30 μM) of **8** and FCCP (8 μM) were added where indicated.

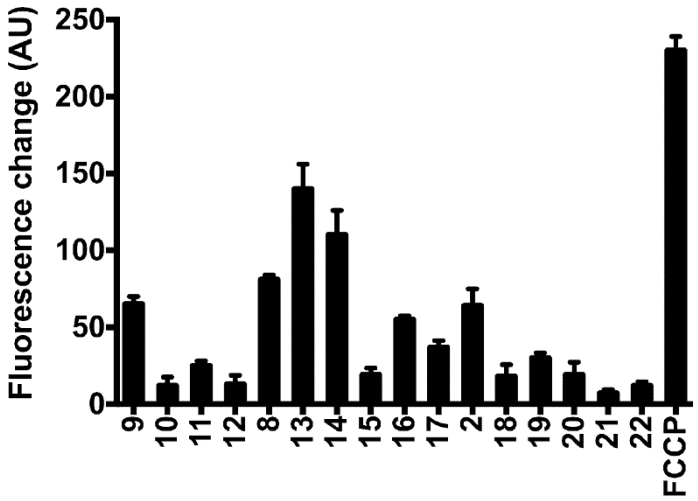

Figure 3.7. Effects of compounds on the mitochondrial membrane potential ($\Delta\psi_m$) in digitonin permeabilized *T. brucei* PCF trypanosomes. PCF trypanosomes ($5x10^7$ cells) were added to reaction buffer (1.95 mL) with additions as described in Figure 6 (B). The chart shows changes in safranine fluorescence (AU = arbitrary units) after addition of each compound (5 μM) or FCCP (5 μM). The results are means ± SD of three independent experiments.

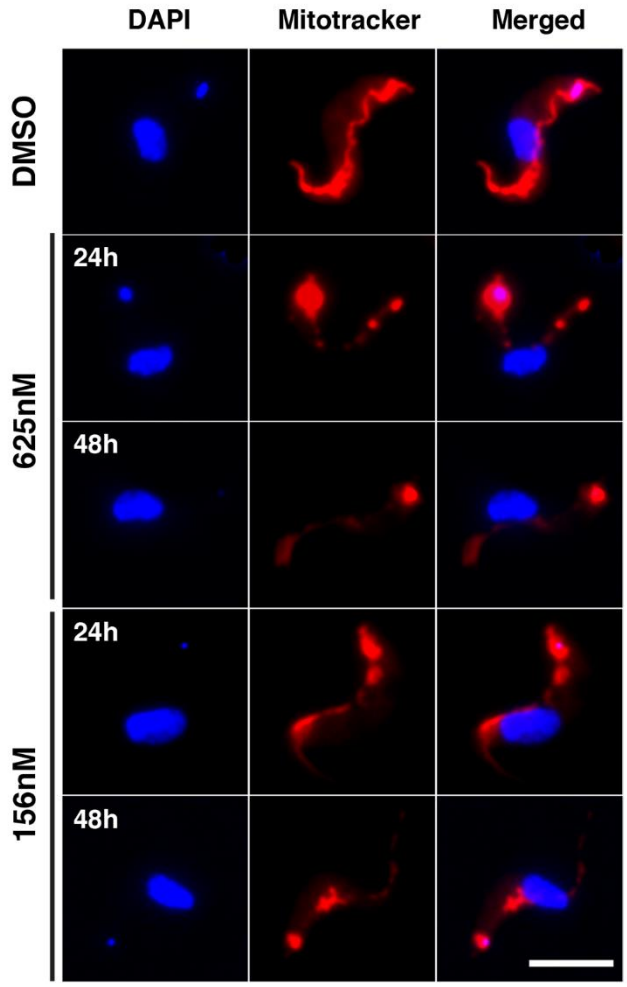

Figure 3.8. Effects of **8** (156 and 625 nM, 24 hrs and 48hrs) on *T. brucei* cells. DAPI fluoresces blue and stains DNA; Mitotracker Red fluoresces red and is used to locate the mitochondrion (Scale bar, 5 μm).

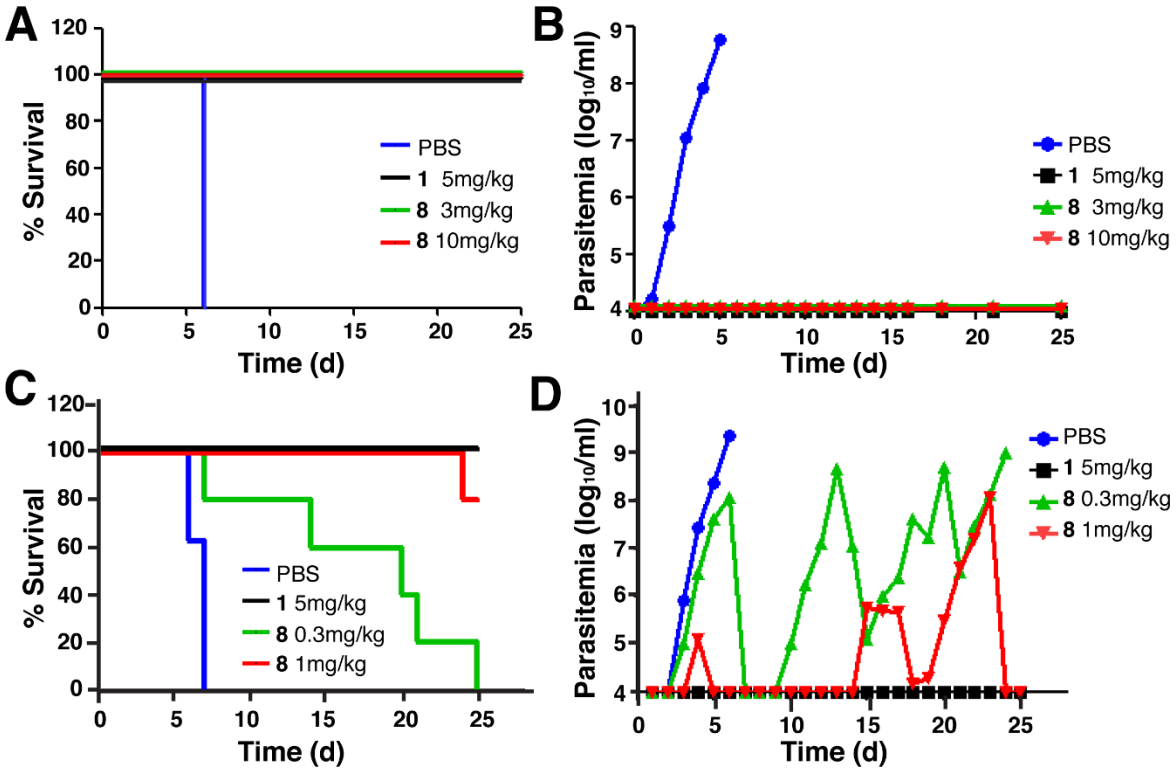

Figure 3.9. *In vivo* results for *T. brucei* brucei Lister 427 mouse model of infection. (A), Mouse survival after treatment at 3 and 10 mg/kg i.p. for 4 days. (B), Parasitemia as a function of time after treatment. (C-D) Same as (A-B) but at 0.3 and 1 mg/kg i.p. for 4 days.

3.7 References.

1. *About Parasites*; Centers for Disease Control and Prevention, 2014.
2. Baker, N.; de Koning, H. P.; Maser, P.; Horn, D. Drug resistance in African trypanosomiasis: the melarsoprol and pentamidine story. *Trends Parasitol.* **2013**, *29*, 110-118.
3. Torreele, E.; Bourdin Trunz, B.; Tweats, D.; Kaiser, M.; Brun, R.; Mazue, G.; Bray, M. A.; Pecoul, B. Fexinidazole--a new oral nitroimidazole drug candidate entering clinical development for the treatment of sleeping sickness. *PLoS Negl. Trop. Dis.* **2010**, *4*, e923.
4. Nare, B.; Wring, S.; Bacchi, C.; Beaudet, B.; Bowling, T.; Brun, R.; Chen, D.; Ding, C.; Freund, Y.; Gaukel, E.; Hussain, A.; Jarnagin, K.; Jenks, M.; Kaiser, M.; Mercer, L.; Mejia, E.; Noe, A.; Orr, M.; Parham, R.; Plattner, J.; Randolph, R.; Rattendi, D.; Rewerts, C.; Sligar, J.; Yarlett, N.; Don, R.; Jacobs, R. Discovery of novel orally bioavailable oxaborole 6-carboxamides that demonstrate cure in a murine model of late-stage central nervous system african trypanosomiasis. *Antimicrob. Agents Chemother.* **2010**, *54*, 4379-4388.
5. Mathis, A. M.; Holman, J. L.; Sturk, L. M.; Ismail, M. A.; Boykin, D. W.; Tidwell, R. R.; Hall, J. E. Accumulation and intracellular distribution of antitrypanosomal diamidine compounds DB75 and DB820 in African trypanosomes. *Antimicrob. Agents Chemother.* **2006**, *50*, 2185-2191.
6. Lanteri, C. A.; Trumpower, B. L.; Tidwell, R. R.; Meshnick, S. R. DB75, a novel trypanocidal agent, disrupts mitochondrial function in *Saccharomyces cerevisiae*. *Antimicrob. Agents Chemother.* **2004**, *48*, 3968-3974.
7. Zhu, W.; Zhang, Y.; Sinko, W.; Hensler, M. E.; Olson, J.; Molohon, K. J.; Lindert, S.; Cao, R.; Li, K.; Wang, K.; Wang, Y.; Liu, Y. L.; Sankovsky, A.; de Oliveira, C. A.; Mitchell, D. A.; Nizet, V.; McCammon, J. A.; Oldfield, E. Antibacterial drug leads targeting isoprenoid biosynthesis. *Proc. Natl. Acad. Sci. U. S. A.* **2013**, *110*, 123-128.
8. Lindert, S.; Zhu, W.; Liu, Y. L.; Pang, R.; Oldfield, E.; McCammon, J. A. Farnesyl diphosphate synthase inhibitors from in silico screening. *Chem. Biol. Drug Des.* **2013**, *81*, 742-748.
9. Liu, Y. L.; Cao, R.; Wang, Y.; Oldfield, E. Farnesyl diphosphate synthase inhibitors with unique ligand-binding geometries. *ACS Med. Chem. Lett.* **2015**.
10. Zhu, W.; Wang, Y.; Li, K.; Gao, J.; Huang, C. H.; Chen, C. C.; Ko, T. P.; Zhang, Y.; Guo, R. T.; Oldfield, E. Antibacterial Drug Leads: DNA and Enzyme Multitargeting. *J. Med. Chem.* **2015**.
11. Li, K.; Schurig-Briccio, L. A.; Feng, X. X.; Upadhyay, A.; Pujari, V.; Lechartier, B.; Fontes, F. L.; Yang, H. L.; Rao, G. D.; Zhu, W.; Gulati, A.; No, J. H.; Cintra, G.; Bogue, S.; Liu, Y. L.; Molohon, K.; Orlean, P.; Mitchell, D. A.; Freitas-Junior, L.; Ren, F. F.; Sun, H.; Jiang, T.; Li, Y. J.; Guo, R. T.; Cole, S. T.; Gennis, R. B.; Crick, D. C.; Oldfield, E. Multitarget drug discovery for tuberculosis and other infectious diseases. *Journal of Medicinal Chemistry* **2014**, *57*, 3126-3139.
12. Jacobs, R. T.; Nare, B.; Phillips, M. A. State of the art in African trypanosome drug discovery. *Curr. Top. Med. Chem.* **2011**, *11*, 1255-1274.
13. T.J. Opperman, C. H., D. Aiello, J.D. Williams, N.P. Peet, D.T. Moir, T.L. Bowlin. In *50th Interscience Conference on Antimicrobial Agents and Chemotherapy*, Boston, 2010.

14. Salic, A.; Mitchison, T. J. A chemical method for fast and sensitive detection of DNA synthesis *in vivo*. *Proc. Natl. Acad. Sci. U. S. A.* **2008**, *105*, 2415-2420.
15. Zeng, C.; Pan, F.; Jones, L. A.; Lim, M. M.; Griffin, E. A.; Sheline, Y. I.; Mintun, M. A.; Holtzman, D. M.; Mach, R. H. Evaluation of 5-ethynyl-2'-deoxyuridine staining as a sensitive and reliable method for studying cell proliferation in the adult nervous system. *Brain Res.* **2010**, *1319*, 21-32.
16. da Silva, M. S.; Monteiro, J. P.; Nunes, V. S.; Vasconcelos, E. J.; Perez, A. M.; Freitas-Junior Lde, H.; Elias, M. C.; Cano, M. I. Leishmania amazonensis promastigotes present two distinct modes of nucleus and kinetoplast segregation during cell cycle. *PLoS One* **2013**, *8*, e81397.
17. *Molecular Operating Environment (MOE), 2013.08*; Chemical Computing Group Inc., 2013.
18. Montalvetti, A.; Fernandez, A.; Sanders, J. M.; Ghosh, S.; Van Brussel, E.; Oldfield, E.; Docampo, R. Farnesyl pyrophosphate synthase is an essential enzyme in *Trypanosoma brucei* - *In vitro* RNA interference and *in vivo* inhibition studies. *J. Biol. Chem.* **2003**, *278*, 17075-17083.
19. *Epidemiology & Risk Factors*; Centers for Disease Control and Prevention, 2013.
20. Harrill, A. H.; DeSmet, K. D.; Wolf, K. K.; Bridges, A. S.; Eaddy, J. S.; Kurtz, C. L.; Hall, J. E.; Paine, M. F.; Tidwell, R. R.; Watkins, P. B. A mouse diversity panel approach reveals the potential for clinical kidney injury due to DB289 not predicted by classical rodent models. *Toxicol. Sci.* **2012**, *130*, 416-426.
21. Moreno, S. N. J. Pentamidine is an uncoupler of oxidative phosphorylation in rat liver mitochondria. *Arch. Biochem. Biophys.* **1996**, *326*, 15-20.
22. Lanteri, C. A.; Tidwell, R. R.; Meshnick, S. R. The mitochondrion is a site of trypanocidal action of the aromatic diamidine DB75 in bloodstream forms of *Trypanosoma brucei*. *Antimicrobial Agents and Chemotherapy* **2008**, *52*, 875-882.
23. Vercesi, A. E.; Bernardes, C. F.; Hoffmann, M. E.; Gadelha, F. R.; Docampo, R. Digitonin Permeabilization Does Not Affect Mitochondrial-Function and Allows the Determination of the Mitochondrial-Membrane Potential of Trypanosoma-Cruzi Insitu. *J. Biol. Chem.* **1991**, *266*, 14431-14434.
24. Huang, G.; Vercesi, A. E.; Docampo, R. Essential regulation of cell bioenergetics in *Trypanosoma brucei* by the mitochondrial calcium uniporter. *Nat. Commun.* **2013**, *4*, 2865.
25. Li, K.; Wang, Y.; Yang, G.; Byun, S. Y.; Rao, G.; Shoen, C.; Yang, H.; Gulati, A.; Crick, D. C.; Cynamon, M.; Huang, G.; Docampo, R.; No, J. H.; Oldfield, E. Oxa-, Thia-, Heterocycle and Carborane Analogs of SQ109: Bacterial and Protozoal Cell Growth Inhibitors. *ACS Infectious Diseases* **2014**.
26. Weinbach, E. C.; Garbus, J. Mechanism of Action of Reagents That Uncouple Oxidative Phosphorylation. *Nature* **1969**, *221*, 1016-&.
27. Tao, H.; Zhang, Y.; Zeng, X.; Shulman, G. I.; Jin, S. Niclosamide ethanolamine-induced mild mitochondrial uncoupling improves diabetic symptoms in mice. *Nat. Med.* **2014**, *20*, 1263-1269.
28. Crunkhorn, S. Metabolic disease: Mitochondrial uncoupler reverses diabetes. *Nat. Rev. Drug Discov.* **2014**, *13*, 885.
29. Oldfield, E.; Feng, X. Resistance-resistant antibiotics. *Trends Pharmacol. Sci.* **2014**.

30. Liu, Y. L.; Lindert, S.; Zhu, W.; Wang, K.; McCammon, J. A.; Oldfield, E. Taxodione and arenarone inhibit farnesyl diphosphate synthase by binding to the isopentenyl diphosphate site. *Proc. Natl. Acad. Sci. U. S. A.* **2014**, *111*, E2530-E2539.
31. Webb, M. R. A continuous spectrophotometric assay for inorganic phosphate and for measuring phosphate release kinetics in biological systems. *Proc. Natl. Acad. Sci. U. S. A.* **1992**, *89*, 4884-4887.
32. Kehl-Fie, T. E.; Zhang, Y.; Moore, J. L.; Farrand, A. J.; Hood, M. I.; Rathi, S.; Chazin, W. J.; Caprioli, R. M.; Skaar, E. P. MntABC and MntH contribute to systemic *Staphylococcus aureus* infection by competing with calprotectin for nutrient manganese. *Infect Immun* **2013**, *81*, 3395-3405.
33. Otwinowski, Z.; Minor, W. Processing of X-ray diffraction data collected in oscillation mode. *Methods Enzymol.* **1997**, *276*, 307-326.
34. Murshudov, G. N.; Vagin, A. A.; Dodson, E. J. Refinement of macromolecular structures by the maximum-likelihood method. *Acta. Crystallogr. D Biol. Crystallogr.* **1997**, *53*, 240-255.
35. Potterton, E.; Briggs, P.; Turkenburg, M.; Dodson, E. A graphical user interface to the CCP4 program suite. *Acta. Crystallogr. D Biol. Crystallogr.* **2003**, *59*, 1131-1137.
36. Adams, P. D.; Afonine, P. V.; Bunkoczi, G.; Chen, V. B.; Davis, I. W.; Echols, N.; Headd, J. J.; Hung, L. W.; Kapral, G. J.; Grosse-Kunstleve, R. W.; McCoy, A. J.; Moriarty, N. W.; Oeffner, R.; Read, R. J.; Richardson, D. C.; Richardson, J. S.; Terwilliger, T. C.; Zwart, P. H. PHENIX: a comprehensive Python-based system for macromolecular structure solution. *Acta. Crystallogr. D Biol. Crystallogr.* **2010**, *66*, 213-221.
37. Emsley, P.; Cowtan, K. Coot: model-building tools for molecular graphics. *Acta. Crystallogr. D Biol. Crystallogr.* **2004**, *60*, 2126-2132.
38. WL, D.; DeLano Scientific LLC: Palo Alto, CA, USA, 2008.

Chapter 4: Analogues of SQ109: Bacterial and Protozoal Cell Growth Inhibitors

4.1 Notes and Acknowledgements

Y.W. K.L. and E.O. designed research; Y.W. K.L. synthesized compounds; Y.W. G.Y. S.-Y.B. G.R. C.S. D.C. M.C. and J.-H.N. performed cell growth inhibition experiments; G.H. and R.D. performed mitochondrial membrane potential experiment; Y.W. and E.O. analyzed data. Y.W. and E.O. wrote the paper.

This work was supported by NIH grants GM065307 and AI049151; a National Research Foundation of Korea (NRF) grant funded by the Korean government (MSIP) (NO. 2007-00559), Gyeonggi-do and KISTI.

This chapter was reproduced in part with permission from K. Li, E. Oldfield, *et al*. *ACS Infect. Dis.,* **2015***,* volume 1*,* page 215-221, Copyright © 2015 American Chemical Society. Y.W. and K.L. contributed equally.

4.2 Introduction

The occurrence of drug resistance is a growing problem[1,2]. One serious threat is with tuberculosis since there are many millions of individuals infected with *Mycobacterium tuberculosis*, the causative agent of tuberculosis, resulting in ~1.5 million deaths per year[3]. Chemotherapy is lengthy and there is increasing resistance to antibiotics. New drugs and drug leads are thus needed. One of the oldest drugs for tuberculosis treatment is ethambutol (**1**), an ethylenediamine derivative, and in recent work some 74,000 analogs[4,5] of ethambutol including the ethylenediamine SQ109[4] (**2**) and the piperidine SQ609[5] have shown promise. One mechanism of action of SQ109 has been proposed to be inhibition of the membrane protein MmpL3[6], a trehalose monomycolate transporter[7]. There have been no reports of spontaneous resistance to SQ109 but resistance to somewhat similar species involving MmpL3 has been reported[8,9], and these *mmpL3* mutants have modest cross-resistance to SQ109[6]. SQ109 also has activity against other bacteria (e.g. *Helicobacter pylori*[10]), yeasts (e.g. *Candida abicans*[11]) as well as the malaria parasite *Plasmodium falciparum*, all of which lack the *mmpL3* gene, so in these organisms there must be other targets/mechanisms of action. SQ109 analogs might thus be of interest as anti-infective leads against a range of organisms. Here, we elected to synthesize four types of SQ109-inspired species that might have activity against bacteria, yeasts or protozoa.

4.3 Results and Discussion

We synthesized the SQ109 analogs (**3-50**) shown in Figures 1-3: a) 13 alkanolamine analogs (**3-15**, Figure 4.1); b) 3 thia analogs (**16-18**, Figure 4.1); c) 23 heterocycle-containing analogs (**19-41**, Figure 4.2) and d) 9 carborane-containing analogs (**42-50**, Figure 4.3). Full synthesis and characterization details are given in the Supporting Information.

In previous work, we found that compound **51** (Figure 4.1), the alkanolamine analog of SQ109, was more active (0.035 μg/mL) against *M. tuberculosis*) than was SQ109 (0.15 μg/mL)[12]. We therefore first synthesized and tested 13 alkanolamine-analogs of SQ109 (**3-15**, Figure 4.1) against *M. tuberculosis*, *M. smegmatis*, *B. subtilis*, *S. cerevisiae*, *E. coli*, *T. brucei*, HEK293T and HepG2 cells. MIC (*Mycobacterium tuberculosis* H37Rv, *Mycobacterium tuberculosis* Erdman), IC_{50} (*M. smegmatis*, *B. subtilis*, *E. coli*, *S. cerevisiae*, *T. brucei*) and CC_{50} (HEK293T and HepG2) values are given in Table 4.1 with the *M. tuberculosis* and *T. brucei* results shown, for convenience, below the structures in Figure 4.1.

There were several compounds with promising activity against *M. tuberculosis*. The most active compound was **5**, an analog of SQ109 (**2**) in which the ethylenediamine nitrogen attached to the adamantane group was replaced by an oxygen, and the geranyl (C_{10}) side-chain by a farnesyl (C_{15}) group. The MIC was 0.39 μg/mL for *M. tuberculosis* H37Rv and 1.0 μg/mL for *M. tuberculosis* Erdman (MtE), Figure 4.1 and Table 4.1, to be compared with 0.1-0.5 μg/mL for SQ109 (**2**), in both strains and 0.035 μg/mL for **51** in *M. tuberculosis* H37Rv[12]. The reduced side-chain species **6** was ~10-20x less active than was the farnesyl analog. The isopentenyl ethanolamine analog (**3**) was also less active than was **5**, and reduction (**4**) reduced activity further. Incorporation of a 1-Me or 1 *i*-Pr group (**8**, **9**) decreased activity when compared with **51**. The

presence of a 1-OH group (**7**) also resulted in decreased activity (0.78 μg/mL) over that found with SQ109. The O-methylated analogs (**10**, **11**) showed worse activity against MtE compared with the 1-OH species. Replacement of the isoprenoid side-chains with aromatic groups (**12-15**) blocked all activity and in other work[12] we found the diether analog of **2** was also inactive[12]. These results indicate that optimum activity is found with a single nitrogen and that the order of activity of these alkanolamines is geranyl>>farnesyl>>isopentenyl, and that the reduced side-chain containing species are all less active than the unsaturated species. In the other assays (*B. subtilis*, *E. coli* and *S. cerevisiae*) the most potent cell growth inhibitor (Table 4.1) was **5**, the N-farnesyl ethanolamine.

With the trypanosomatid parasite *T. brucei*, we found that SQ109 itself had quite potent activity against bloodstream form (BSF) parasites with an IC_{50} of 0.078 μg/mL and a selectivity index (SI), defined as SI = CC_{50} (HEK293T)/IC_{50} (*T. brucei*) or CC_{50} (HepG2)/IC_{50} (*T. brucei*) in the 15-24 range, Table 4.1. The most active SQ109 analogs were **10** (IC_{50} = 0.23 μg/mL), **8** (IC_{50} = 0.33 μg/mL) and **6** (IC_{50} = 0.50 μg/mL) with selectivity indices of 23, 21 (**10**), 19, 16 (**8**) and ~3-4 (**6**), so these analogs are less promising than is SQ109 against *T. brucei*. We also tested the SQ109 analog reported previously (**51**) to have potent activity against *M. tuberculosis*, but again it was slightly less active and had a worse SI as compared to SQ109 (Table 4.1).

We next investigated the 3 thia-analogs of SQ109 (**16-18**) in which the N attached to adamantane in SQ109 (O in the more active ethanolamine analog) was replaced by an S or SO_2 group (providing different H-bonding possibilities), and in two cases the geranyl group was reduced to the per-hydro species. Cell growth inhibition results are shown in Table 4.1.

As can be seen in Figure 4.1 and Table 4.1, the thio-ether **16** had potent activity against *M. tuberculosis* H37Rv with an MIC of 0.39 μg/mL. **16** is the closest analog to SQ109 in the compounds studied here and also had activity against *M. smegmatis* (1.2 μg/mL), *S. cerevisiae*

(0.38 μg/mL) and *E. coli* (1.4 μg/mL). Interestingly, in these organisms, the reduced species was even more active (Table 4.1). The sulfone had weak activity in all assays. The results in *M. tuberculosis* are consistent with the results found for the alkanolamines **5, 6** in that best activity is observed with the unsaturated side-chain containing species. With *T. brucei*, the most active thia-analog was **16** (IC_{50} = 0.31 μg/mL; SI 5-9), followed by **17** (IC_{50} = 0.69 μg/mL; SI 6-7) and **18** (IC_{50} = 0.89 μg/mL, SI = 4-5).

The results described above are of interest in that we show, for the first time, that SQ109 has activity against the parasitic protozoan *T. brucei*, but unlike the situation found with the alkanolamine analogs of SQ109 reported previously[12], none of the new analogs showed improved activity (over that seen with **51)** against *M. tuberculosis*, although **5**, **16** and **17** were all more active than was SQ109 against the Gram negative bacterium, *E. coli* (**5**, IC_{50} = 0.60 μg/mL; **16**, IC_{50} = 1.4 μg/mL; **17**, IC_{50} = 0.70 μg/mL, *versus* IC_{50} = 2.8 μg/mL for SQ109; Table 4.1), although the computed selectivity indices (using HEK293T and HepG2) are poor (~5).

In previous work[12] we also found that another SQ109 analog, a choline-derivative containing a quaternary ammonium instead of a protonable N, had the most potent activity against a different parasitic protozoan, the malaria parasite *P. falciparum*, in addition to being a very potent inhibitor of respiration, in *M. smegmatis*[12]. We thus reasoned that other cationic analogs of SQ109 might have better anti-bacterial and/or anti-protozoal activity, so we made and tested two further sets of analogs. We first synthesized a series of 23 SQ109 analogs with primarily protonatable (or fixed charge) heterocycle linker groups replacing the ethylenediamine fragment. The heterocycles investigated were neutral (the 1,2,3-triazoles **19, 20**); protonatable (guanidines and amidines, **21**, **40, 41;** and an imidazole, **38**), or they contained a fixed positive charge (imidazoliums and pyridiniums, **23-39**). The two neutral triazoles had low activity against *M. tuberculosis* (**19**, MIC

= 12, 25 μg/mL; **20**, MIC = 6.2 μg/mL) and *M. smegmatis* (IC_{50} ~5 μg/mL) and essentially no activity against the other bacteria or the yeast.

Of the other heterocyclic compounds investigated, most had some activity against *M. tuberculosis* Erdman (and *M. tuberculosis* H37Rv), Figure 4.2 and Table 4.1. However, there were only 3 compounds (**21**, **23, 24**) in which at least one of the *M. tuberculosis* MIC values was <2 μg/mL. Both **21** and **23** contain as a common structural feature the O-CH_2-CH_2-N group found in the potent alkanolamines and in both cases, the nitrogen is expected to have either a formal +1 charge (**23**) or a large positive charge density (**21**, due to the strong basicity of the ligand and charge delocalization), so both resemble the protonated ethanolamines. In **24,** the aliphatic "linker" group is absent, but we now see that this potent inhibitor resembles SQ109 in another way in that it contains the N-C-C-N group found in the ethylenediamine fragment which, in SQ109 is expected to carry a +1 charge (at pH~7), again delocalized most likely over both nitrogens. As can be seen in Table 4.1, many of the other heterocyclic analogs have activity against the other bacteria as well as the yeast *S. cerevisiae*, but they also inhibited the growth of the two human cell lines (Table 4.1), resulting in poor selectivity indices.

The results obtained against *T. brucei* were, however, much more encouraging, Table 4.1. Specifically, we found that there were 15 analogs of SQ109 that had better IC_{50} and SI values than did SQ109 (IC_{50} = 0.078 μg/mL; SI ~15-24, Table 4.1). A typical set of dose-response curves for the top five *T. brucei* cell growth inhibitors, together with their corresponding effects on HEK293T and HepG2 cell growth, are shown in Figure 4.5, and selectivity index *versus T. brucei* cell growth inhibition results (for both human cell lines) are shown in Figure 4.6. The best *T. brucei* IC_{50} value was 5.5 ng/mL, with corresponding SI values of 290 and 370 (Table 4.1). Clearly, these results are encouraging and as noted above, are reminiscent of the activity of the choline analog of SQ109

against *P. falciparum* in the intra-erythrocytic assay where an IC_{50} = 80 nM (35 ng/mL) was found (corresponding to a SI~400)[12], plus, activity against the two human cell lines is similar to that seen with SQ109 (which is already in advanced clinical trials for tuberculosis).

Next, we sought to see whether improved activity might be found by replacing the adamantyl group by a 1-*o*-carboranyl group, which is similar to the adamantyl group in terms of size, shape and hydrophobicity[13]. We produced the 9 carboranes (**42-50**) shown in Figure 4.3. None had potent activity against *M. tuberculosis* Erdman, Table 4.1. However, in almost all cases there was activity against *M. smegmatis*, *B. subtilis*, *S. cerevisiae* and more surprisingly against *E. coli*, with the ~2 μg/mL IC_{50} values found for **42**, **45** against *E. coli* being of interest since we found worse activity against this Gram negative with the other analogs. Reasons for the enhanced activity against *E. coli* are unknown. Three compounds (**45**, **47, 48**) also had IC_{50} < 0.5 μg/mL against *T. brucei*, although none approached the activity (and hence, SI values) seen with the adamantane-containing analogs.

The most potent compound against *M. tuberculosis* Erdman is thus **24** with an MIC of 0.50 μg/mL, and **24** also has a 0.78 μg/mL MIC against *M. tuberculosis* H37Rv (Table 4.1). What is of interest about **24** is that it closely resembles the structure of SQ109 in that there are adamantyl and geranyl groups and a N-C-C-N linker but here, the linker is an imidazolium, not an ethylenediamine group. The heterocycles (**19**-**41**) as a class have most potent activity against the trypanosomatid parasite *T. brucei* and are also most active against the 2 human cell lines. However, when selectivity index values are calculated it can be seen that **27, 28** have the best IC_{50} values of ~5-7 ng/mL and SI~300. All of the compounds with the best SI (**22**-**37**) also have fixed charge centers, raising the question as to their possible mechanism of action.

In earlier work we found that SQ109 acted as an uncoupler in *E. coli* as well as in *M. smegmatis* and we proposed that this uncoupling activity was important for its activity against *M. tuberculosis*[12]. Similar results have now been reported for a broader range of compounds which are now proposed to act as uncouplers, in *M. tuberculosis*[14], targeting ΔpH, Δψ, or both. We therefore tested SQ109 and the most interesting potential lead, **27**, in *T. brucei*, to see if similar effects were seen with either or both BSF and procyclic forms (PCF). We first tested whether SQ109 had effects on the proton motive force (more specifically, the inner mitochondrial membrane potential, **Δψ)** using the safranine method[15,16] with BSF parasites. Figure 4.4A shows that addition of 10 μM (3.3 μg/mL) SQ109 or 10 μM (4.5 μg/mL) **27** decreased Δψ, which was further reduced by addition of 8 μM (2 μg/mL) FCCP (carbonyl cyanide 4-(trifluoromethoxy)phenylhydrazone), a potent protonophore uncoupler. Similar results were obtained with PCF, Figure 4.4B. *T. brucei* mitochondria were able to phosphorylate ADP, as demonstrated by the small decrease in Δψ after its addition, Figure 4.4C. This activity was inhibited by the ATP synthase inhibitor oligomycin. In addition, the mitochondria were able to transport Ca^{2+}, as shown by the decrease in the Δψ after addition of $CaCl_2$, and the Δψ returned to basal levels after addition of the Ca^{2+}-chelator EGTA. Further addition of SQ109 or **27** followed by FCCP again collapsed the Δψ, Figure 4.4C. Both SQ109 and **27** collapsed Δψ in a dose-dependent manner (Figure 4.7) and SQ109 alone or solvent (0.2 % DMSO) had no effect. These results show that mitochondria in permeabilized *T. brucei* are able to develop a Δψ, phosphorylate ATP and transport Ca^{2+} and that SQ109 and **27** collapse Δψ. These effects on the proton motive force are rapid and are very similar to those observed for SQ109 in bacterial systems[17,18] and are likely to make a significant contribution to SQ109 and **27** inhibiting cell growth.

In addition to their effects on $\Delta\psi$, it seemed possible that some compounds might act by inhibiting quinone biosynthesis, in some systems, just as other SQ109 analogs did with the prenyl transferase MenA (1,4-dihydroxy-2-naphthoate octaprenyltransferase). We tested a representative set of compounds from the alkanolamine (**5**), imidazolium (**22**, **27**), imidazole (**39**) and carborane groups (**48**) against an expresssed *E. coli* MenA using the method reported previously[12]. Compounds **22** and **48** had no activity (IC_{50}>40 μM, 20 μg/mL), the IC_{50} for **27** was 19 μM (8.5 μg/mL), for **5**, 9.0 μM (3.6 μg/mL), while that for **39** was 1.5 μM (0.54 μg/mL), suggesting that MenA inhibition with **39** could be of importance in MtE cell growth inhibition (MIC = 3.1 μg/mL). However, **39** has a poor SI.

4.4 Conclusions

Overall, the results reported above are of interest since we synthesized a broad range of analogs of the *M. tuberculosis* growth inhibitor, the ethylene diamine SQ109, and tested their activity against bacteria, a yeast, as well as a protozoan parasite. Protonatable or cationic species had the most activity and the most potent leads against *M. tuberculosis* (MIC~0.4-0.5 μg/mL) contained ethanolamine, mercaptoethylamine or imidazolium linkers. The carboranes were less active against *M. tuberculosis* but surprisingly, had activity (IC_{50}~2 μg/mL) against the Gram negative, *E. coli*. However, we did not obtain compounds that were more active against *M. tuberculosis* than was the ethanolamine analog of SQ109 reported earlier. However, we did discover that the parent compound SQ109 had activity against the trypanosomatid parasite, *T. brucei*, the causative agent of human African trypanosomiasis, and that two SQ109 analogs had IC_{50} values in the ~5-7 ng/mL range against this organism with SI values of ~300.

4.5 Experimental Section

Cell growth inhibition assays: Cell Lines. *Mycobacterium tuberculosis* H37Rv, *Mycobacterium tuberculosis* Erdman, *Mycobacterium smegmatis* ATCC 700084, *Bacillus subtilis* subsp. *subtilis* ATCC 6051, *E. coli* ATCC 29425, and *Saccharomyces cerevisiae* ATCC 208352 were purchased from the American Type Culture Collection. *Trypanosoma brucei brucei* strain 427 (bloodstream form) was cultivated at 37 °C with a 5% CO_2 atmosphere in HMI-9 medium supplemented with 10% fetal bovine serum (FBS). *T. brucei* was subcultured every 3 or 4 d and maintained until the twentieth passage. The HEK293T, human embryonic kidney, and HepG2, the hepatocellular carcinoma cell line used in the cytotoxicity test was cultivated at 37 °C with a 5% CO_2 atmosphere in Dulbecco's modified Eagle's medium supplemented with 10% FBS.

***T. brucei* 427 (bloodstream forms) Growth Inhibition Assay.** *T. brucei* strain 427 bloodstream forms were cultivated at 37 °C with 5% CO_2 in HMI-9 medium supplemented with 10% FBS. *T. brucei* parasites (5 x 10^4/mL) were seeded in 384 well plates with or without a serial compound dilution. After 72 h of incubation, the parasites were exposed to 120 μM of resazurin sodium salt (Sigma, St. Louis, MO, USA) and were incubated for another 5 h. Then, the parasites were fixed with 4% PFA and the assay plates were read by using a Victor 3™ fluorimeter (PerkinElmer, Waltham, MA, USA) at an excitation wavelength of 530 nm and emission of 590 nm. Pentamidine was used as a reference drug and DMSO 0.5% was used as a drug-negative control. Two independent sets of experiments were carried out and the mean and standard deviations are shown in Table 4.1; the R^2 for the pIC_{50} correlation was 0.99.

***M. tuberculosis* H37Rv Growth Inhibition Assay**. The compounds were assayed for inhibition of *M. tuberculosis* H37Rv cell growth as described previously[19].

***M. tuberculosis* Erdman Growth Inhibition Assay**. The compounds were assayed for inhibition of *M. tuberculosis* Erdman cell growth as described previously[20].

***E. coli* ATCC 29425 Growth Inhibition Assay**. IC_{50} values for *E. coli* growth inhibition were determined by using a broth microdilution method. An overnight culture of *E. coli* was diluted 50-fold into fresh Luria−Bertani (LB) broth and incubated to an OD_{600} of ∼0.4. The culture was then diluted 500-fold into fresh LB medium and 100 μL inoculated into each well of a 96-well flat-bottom culture plate (Corning Inc., Corning, NY). The starting concentration of each compound was 200 μg/mL, and this was 2×serially diluted to 0.19 μg/mL. Plates were incubated for 3 h at 37 °C to midexponential phase. An MTT ((3-(4,5-dimethylthiazol-2-yl)-2,5-diphenyltetrazolium bromide) cell proliferation assay (ATCC) was then carried out to obtain bacterial viability dose−response curves. Briefly, 10 μL of MTT reagent was added into each well, followed by incubation for 2−4 h until a purple precipitate was visible. Then, 100 μL of detergent reagent was added, and the plates were incubated in the dark at 22 °C for 2 h. Absorbance was measured at 570 nm and a nonlinear regression analysis carried out using Origin 6.1 software. The average error was 11%.

***B. subtilis* ATCC® 6051TM growth inhibition assay**. A 16 h culture of *B. subtilis* was diluted 50-fold into fresh Luria-Bertani (LB) broth and incubated to an OD_{600} of ~ 0.4. The culture was then diluted 500-fold into fresh LB medium and 100 μL were inoculated into a 96 well flat bottom culture plate (Corning Inc., Corning, NY). The starting concentration of each compound was 0.5 μg/mL and was then serial diluted. Plates were incubated for 12-16 h at 37 °C. The absorbance was recorded at 570 nm. A non-linear regression analysis was carried out on the data obtained using Origin 6.1. The average error was 9%.

***S. cerevisiae* growth inhibition assay**. The protocol was the same as with the *B. subtilis* assay protocol except that YPD medium was used and the 96-well plate was incubated for 36 h instead of 12-16 h. A non-linear regression analysis was carried out on the data obtained using Origin 6.1. The average error was 14%.

M. smegmatis ATCC 700084 **growth inhibition assay**. The protocol was the same as with the *B. subtilis* assay protocol except that 7H9/ADC (9:1) medium was used. A non-linear regression analysis was carried out on the data obtained using Origin 6.1. The average error was 9%.

Analysis of mitochondrial membrane potential. We monitored the mitochondrial membrane potential spectrofluorometrically using safranine as the probe[15,16]. The reaction buffer contained 125 mM sucrose, 65 mM KCl, 10 mM Na-Hepes-KOH buffer, pH 7.2, 1 mM $MgCl_2$, 2.5 mM potassiumphosphate, and 5 µM safranine. *T. brucei* BSF (2×10^8 cells) were added to the reaction buffer (2.0) containing 1 mM ATP, 200 µM EGTA and 500 µM sodium orthovanadate, and the reaction was started by addition of 40 µM digitonin. PCF (5×10^7 cells) were added to the reaction buffer (2.4 ml) containing 2 mM succinate and the reaction started by addition of 50 µM digitonin. Incubations were at 28 ºC (PCF) or 37ºC (BSF). Drugs, ADP (10 µM), oligomycin (Oligo, 2 µg/ml), $CaCl_2$ (12 µM), EGTA (200 µM), and FCCP (8 µM) where added where indicated. Fluorescence changes were monitored using a Hitachi 4500 spectrofluorometer (excitation wavelength = 496 nm; emission wavelength = 586 nm).

Mammalian cell cytotoxicity assay. For evaluation of mammalian cell cytotoxicity, HEK293T and HepG2 cells were cultured at 37 °C with 5% CO_2 in Dulbecco's modified eagle medium containing 10% FBS. HEK293T and HepG2 cells were diluted to 8 X 10^4/mL and 4 X 10^4/mL, respectively, and were seeded in 384 well plates. The compounds at 2-fold dilution in 10-points concentration were tested and incubated for 72 h. To determine viability, 10 µL of a 280 µM

solution of resazurin sodium salt (final concentration, 40 μM of resazurin) was added to each well for 5 h. To assess cell viability, resazurin reduction was measured with a Victor 3^{TM} fluorimeter at an excitation wavelength of 530 nm and emission of 590 nm. Chloropromazine was used as a reference drug and DMSO 1% was used as a drug-negative control.

Chemical Syntheses: General Methods. All chemicals were reagent grade. ^{1}H NMR and ^{13}C NMR spectra were obtained on Varian (Palo Alto, CA) Unity spectrometers at 400 and 500 MHz for ^{1}H and at 100 and 125 MHz for ^{13}C. Elemental analyses were carried out in the University of Illinois Microanalysis Laboratory. HPLC/MS analyses were performed by using an Agilent LC/MSD Trap XCT Plus system (Agilent Technologies, Santa Clara, CA) with an 1100 series HPLC system including a degasser, an autosampler, a binary pump, and a multiple wavelength detector. All final compounds were ≥90% pure as determined by quantitative spin count NMR (qNMR) and structures were characterized by ^{1}H NMR and HRMS.

1-(2-(((1*r*,3*r*,5*r*,7*r*)-Adamantan-2-yl)oxy)ethyl)-4-hexyl-1*H*-1,2,3-triazole (19).

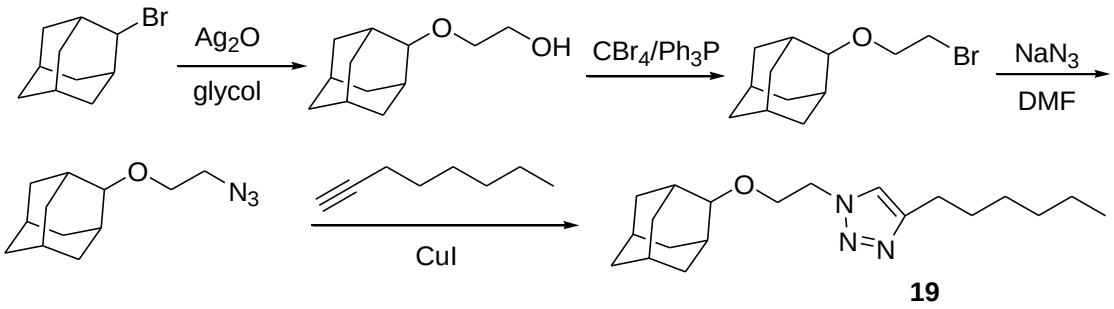

19

A mixture of 2-adamantyl bromide (215 mg, 1 mmol), Ag_2SO_4 (310 mg, 1 mmol) and ethylene glycol (1 ml) was heated for 1.5 h at 90 ^{o}C. The reaction mixture was then distributed between ethyl acetate and water. The ethyl acetate phase was separated and dried over anhydrous Na_2SO_4 then evaporated under reduced pressure to give a residue. Purification of the residue with flash chromatography (SiO_2, hexane/ethyl acetate = 6/1) gave the alcohol product (110 mg, yield: 56%).

To a solution of the alcohol (98 mg, 0.5 mmol) in dry DCM (3 mL) was added Ph_3P (183 mg, 0.7 mmol) and CBr_4 (232 mg, 0.7 mmol) at 0 ^oC with stirring. Stirring was continued for 30 min at 0 ^oC and 2 h at 25 ^oC. The reaction mixture was then concentrated and purified by using flash chromatography (SiO_2, hexane/ethyl acetate = 20/1) to give the bromide product (117 mg, yield: 91%). A mixture of the bromide product (103 mg, 0.4 mmol), NaN_3 (65 mg, 1 mmol) and DMF (1.5 mL) was heated for 1 h at 80 ^oC. The reaction mixture was then distributed between hexane and water. The hexane phase was separated and dried over anhydrous Na_2SO_4, then evaporated under reduced pressure to give the azide (83 mg, yield 95%). A mixture of the azide (44 mg, 0.2 mmol), CuI (7 mg, 0.04 mmol), 1-octyne (22 mg, 0.2 mmol) and sodium ascorbate (98 mg, 0.5 mmol) in H_2O/DCM (1 mL/2 mL) was then stirred for 12 h at 25 ^oC. The organic phase was concentrated and purified by using flash chromatography (SiO_2, hexane/ethyl acetate = 8/1) to give the product **19** (48 mg, yield: 72%). The HCl salt was obtained by neutralizing the triazole with HCl in toluene with quantitative yield. Purity of the product was determined by qNMR: 99.5%. ^{1}H NMR (500 MHz, chloroform-d_1) δ 7.58 (s, 1H), 4.57 (t, J = 4.9 Hz, 2H), 3.80 ((t, J = 4.9 Hz, 3H), 3.41 (s, 1H), 2.80 (t, J = 7.7 Hz, 2H), 2.02 – 1.22 (m, 22H), 0.88 ((t, J = 5.0 Hz, 3H). HRMS (ESI) m/z $[M + H]^+$ calculated for $[C_{20}H_{34}N_3O]^+$ 332.2702, found 332.2698.

1-(2-(((1*r*,3*r*,5*r*,7*r*)-Adamantan-2-yl)oxy)ethyl)-4-((((1*r*,3*r*,5*r*,7*r*)-adama-ntan-2-yl)oxy)methyl)-1*H*-1,2,3-triazole hydrochloride (20).

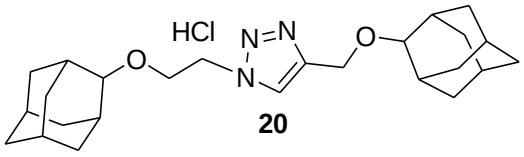

20

20 was made by following the protocol used for **19**. Purity of the product was determined by qNMR: 95.9%. ^{1}H NMR (500 MHz, chloroform-d_1) δ 7.89 (s, 1H), 4.77 (s, 2H), 4.61 (t,J = 5.0

Hz, 2H), 3.82 (t, *J* = 4.9 Hz, 2H), 3.59 (s, 1H), 3.42 (s, 1H), 2.23 – 1.34 (m, 28H). HRMS (ESI) m/z $[M + H]^+$ calculated for $[C_{25}H_{38}N_3O_2]^+$ 412.2964, found 412.2961.

***N*-(2-(((1*r*,3*r*,5*r*,7*r*)-Adamantan-2-yl)oxy)ethyl)-4-heptyl-4,5-dihydro-1*H*-imidazol-2-amine hydroiodide (21).**

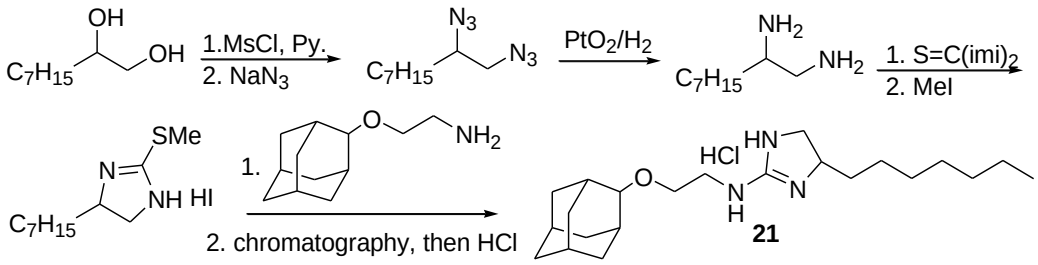

To a solution of 1,2-nonanediol (320 mg, 2 mmol) in dry DCM (6 mL) was added pyridine (480 mg, 6 mmol) and MsCl (342 mg, 3 mmol) at 0 ^oC with stirring. Stirring was continued for 1 h at 0 ^oC then the reaction was quenched by adding saturated aqueous $NaHCO_3$. The DCM phase was separated and concentrated to give the crude dimesylate. A mixture of the the crude dimesylate and NaN_3 (260 mg, 4 mmol) in DMF (4 mL) was heated at 80 ^oC for 2 h. The resulting mixture was distributed between hexane and water. The hexane phase was separated and dried over anhydrous Na_2SO_4 and solvents removed under reduced pressure to give the diazide. A mixture of diazide and PtO_2 (40 mg, 0.1 mmol) in MeOH (4 mL) was stirred under H_2 for 2 h at 25 ^oC. Filtration and evaporation gave the diamine (227 mg, 72%). To a solution of the diamine (227 mg, 1.44 mmol) in dry DCM was added 1,1'-thiocarbonyldiimidazole (356 mg, 2 mmol) at 0 ^oC. Stirring was continued for 2 h at 25 ^oC. The reaction mixture was purified by using flash chromatography (SiO_2, hexane/ethyl acetate = 6/1) to give the thiourea (216 mg, yield: 75%). A solution of the thiourea (216 mg, 1.08 mmol) and MeI (426 mg, 3 mmol) in methanol (4 mL) was refluxed for 4h. The solution was evaporated to give methylthioimidazole which was used in the next step. The amine (38 mg, 0.2 mmol) and methylthioimidazole (69 mg, 0.2 mmol) were refluxed

in isopropanol (2 mL) for 2 h. The reaction mixture was concentrated and purified with flash chromatography (SiO_2, $CHCl_3$/MeOH/Et_3N = 100/10/5) to give **21** (64 mg). The HCl salt of **21** was obtained by neutralizing it with HCl in toluene. Purity of the product was determined by qNMR: 95.6%. ^{1}H NMR (500 MHz, chloroform-*d1*) δ 8.99 (s, 1H), 8.42 (d, 1H), 7.05 (d, 1H), 4.51 – 3.80 (m, 2H), 3.74 – 3.57 (m, 2H), 3.53 (s, 1H), 3.49 – 3.10 (m, 3H), 2.09 – 1.66 (m, 11H), 1.62 – 1.15 (m, 15H), 0.89 (t, *J* = 5.0 Hz, 1H). HRMS (ESI) m/z $[M + H]^+$ calculated for $[C_{22}H_{40}N_3O]^+$ 362.3171, found 362.3171.

3-(2-(((1*r*,3*r*,5*r*,7*r*)-Adamantan-2-yl)oxy)ethyl)-1-((*E*)-3,7-dimethylocta-2,6-dien-1-yl)-1*H*-imidazol-3-ium methanesulfonate (22).

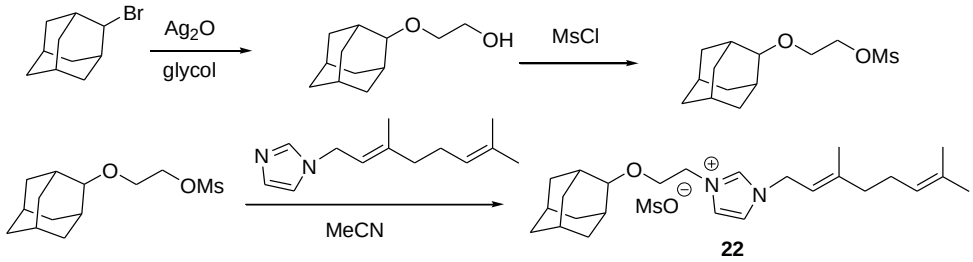

22

A mixture of 2-adamantyl bromide (215 mg, 1 mmol), Ag_2SO_4 (310 mg, 1 mmol) and ethylele glycol (1 mL) was heated for 1.5 h at 90 ^{o}C. The reaction mixture was distributed between ethyl acetate and water. The ethyl acetate phase was separated and dried over anhydrous Na_2SO_4 and solvents removed under reduced pressure to give the residue. Purification of the residue with flash chromatography (SiO_2, hexane/ethyl acetate = 6/1) gave the alcohol product (110 mg, yield: 56%). To a solution of the alcohol (110 mg, 0.56 mmol) in dry CH_2Cl_2 (3 mL) was added pyridine (158 mg, 2 mmol) and MsCl (91 mg, 0.8 mmol) at 0 ^{o}C with stirring. After stirring was continued for 2 h at 0 ^{o}C, all volatile components was removed under reduced pressure. The residue was purified by using flash chromatography (silica gel, hexane/ethyl acetate = 10/1) to give mesylate (146 mg, 95%). A mixture of the mesylate (27 mg, 0.1 mmol) and geranylimidazole (20 mg, 0.1 mmol) in

MeCN (2 mL) was refluxed for 5 h. Evaporation gave a quantitative yield of the product **22**. Purity of the product was determined by qNMR: 91.7%. ^{1}H NMR (500 MHz, chloroform-d_1) δ 9.96 (s, 1H), 7.47 (s, 1H), 7.08 (s, 1H), 5.37 (m, 1H), 5.03 (m, 1H), 4.88 (d, *J* = 7.5 Hz, 2H), 4.56 (m, 2H), 3.80 (m, 2H), 3.44 (s, 1H), 2.79 (s, 3H), 2.36 – 1.26 (m, 18H), 1.79 (s, ,3H), 1.68 (s, 3H), 1.60 (s, 3H). HRMS (ESI) m/z $[M]^+$ calculated for $[C_{25}H_{39}N_2O]^+$ 383.3062, found 383.3066.

1-(2-(((1*r*,3*r*,5*r*,7*r*)-Adamantan-2-yl)oxy)ethyl)-3-hexylpyridin-1-ium methanesulfonate (23).

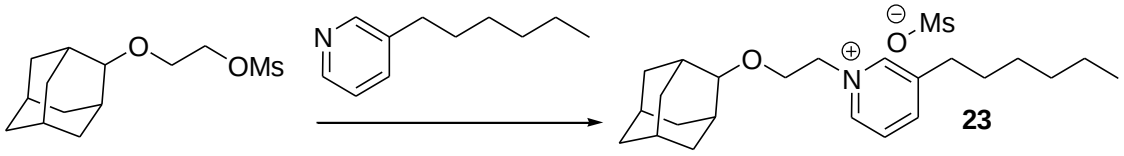

23

23 was made by following to the protocol used for **22**. Purity of the product was determined by qNMR: 96.11%. ^{1}H NMR (500 MHz, chloroform-d_1) δ 8.98 (m, 1H), 8.74 (s, 1H), 8.24 (d, *J* = 7.9, Hz, 1H), 7.99 (dd, *J* = 8.0, 6.0 Hz, 1H), 4.91 (t, *J* = 5.5 Hz, 2H), 3.91 (J = 5.5 Hz, 2H), 3.42 (s, 1H), 2.85 (t, *J* = 7.5 Hz, 2H), 2.75 (s, 3H), 2.03 – 1.11 (m, 22H), 0.90 (m, 3H). HRMS (ESI) m/z $[M]^+$ calculated for $[C_{23}H_{36}NO]^+$ 342.2797, found 342.2785.

1-((1r,3*r*,5*r*,7*r*)-Adamantan-2-yl)-3-((*E*)-3,7-dimethylocta-2,6-dien-1-yl)-1*H*-imidazol-3-ium bromide (24).

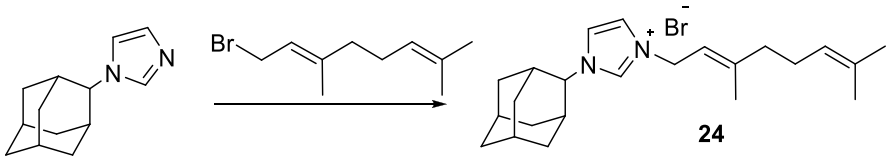

24

1-(1-Adamantyl)-1*H*-imidazole was made according to a reported protocol[22]. A mixture of adamantly-imidazole (40 mg, 0.2 mmol) and geranyl bromide (44 mg, 0.2 mmol) in DCM (0.5 mL) was stirred for 12 h at 25 ^{o}C. The solid resulting from evaporation was thoroughly washed with hexane to give the product **24** (50 mg, yield: 59%). Purity of the product was determined by

qNMR: 91.7%). ^{1}H NMR (500 MHz, Chloroform-*d*) δ 10.65 (s, 1H), 5.40 (t, *J* = 7.7 Hz, 1H), 5.17 (d, *J* = 7.6 Hz, 2H), 5.04 (s, 1H), 4.39 (s, 2H), 2.73 (s, 3H). HRMS (ESI) m/z $[M]^+$ calculated for $[C_{23}H_{35}N_2O]^+$ 339.2800, found 339.2797.

1-(((1*r*,3*r*,5*r*,7*r*)-Adamantan-2-yl)methyl)-3-octyl-1*H*-imidazol-3-ium bromide (25).

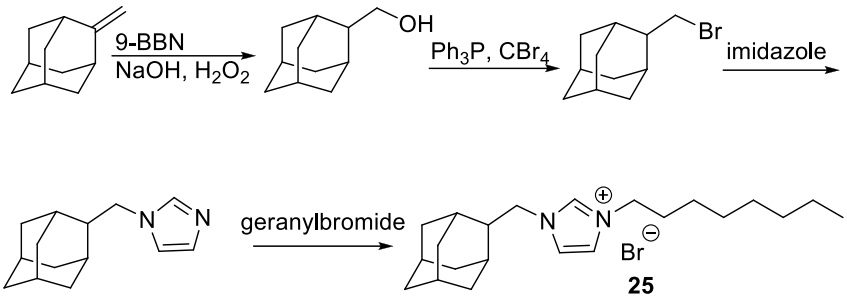

25

To a solution of methyleneadamantane[23] (296 mg, 2 mmol) in dry THF was added 9-BBN (0.5 M in THF, 4.4 mL) dropwise. Stirring was continued for 30 min at 0 °C and 1 h at 25 °C. The reaction flask was cooled in an ice-bath. To the resulting reaction mixture was added NaOH (3N in H_2O, 3 mL) and H_2O_2 (30% in water, 0.68 mL). Stirring was continued for 30 min at 0 °C and 1h at 25 °C. The reaction mixture was diluted with ethyl acetate and quenched with saturated aqueous Na_2SO_3 at 0 °C. The organic phase was dried over Na_2SO_4 and solvents removed under reduced pressure to give the crude hydroxymethyladamantane. To a solution of the 2-hydroxymethyladamantane in DCM (6 mL) was added Ph_3P (524 mg, 2 mmol) and CBr_4 (662 mg, 2 mmol) at 0 °C with stirring. Stirring was continued for 30 min at 0 °C and for 2 h at 25 °C. The reaction mixture was concentrated and purified by using flash chromatography (SiO_2, hexane/ethyl acetate = 20/1) to give the bromide product (274 mg, yield: 61%). To a solution of imidazole (134 mg, 2 mmol) in dry THF (7 mL) was added NaH (washed with hexane, 58 mg, 2.5 mmol) at 0 °C with stirring. Stirring was continued for 20 min at 25 °C and 30 min at 50 °C. To the resulting solution was added bromomethyladamantane (229 mg, 1 mmol) at 25 °C, with

stirring. Stirring was continued for 24 h at 50 °C. The reaction mixture was diluted with ethyl acetate and quenched with saturated aqueous NH_4Cl. The organic phase was separated and concentrated to give a residue. The residue was purified by using flash chromatography (SiO_2, ethyl acetate, 140 mg, 65%) to give the adamantanylmethylimidazole. A solution of adamantanylmethylimidazole (44 mg, 0.2 mmol) in octyl bromide (0.2 mL) was stirred for 4 h at 80 °C. To the reaction mixture was added 4 mL of hexane and the resulting precipitate was washed with hexane, three times, to give the product **25** (46 mg, yield: 56%). Purity of the product was determined by qNMR: 91.5%. ^{1}H NMR (500 MHz, Chloroform-*d*) δ 10.76 (s, 1H), 7.22 (s, 1H), 7.18 (s, 1H), 4.48 (d, *J* = 8.1 Hz, 2H), 4.38 (t, *J* = 7.5 Hz, 2H), 2.25 (t, *J* = 8.2 Hz, 1H), 2.10 – 1.07 (m, 26H), 0.87 (t, *J* = 6.9 Hz, 3H). HRMS (ESI) m/z $[M]^+$ calculated for $[C_{22}H_{37}N_2]^+$ 329.2957, found 329.2947.

1-(((1*r*,3*r*,5*r*,7*r*)-Adamantan-2-yl)methyl)-3-(3-phenoxybenzyl)-1*H*-imidazol-3-ium bromide (26).

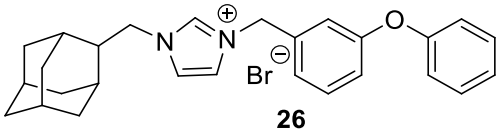

26

26 was made by following the protocol used for **25**. Purity of the product was determined by qNMR: 99.1%. ^{1}H NMR (500 MHz, chloroform-d_1) δ 10.86 (s, 1H), 7.39 – 7.31 (m, 3H), 7.24 – 7.19 (m, 1H), 7.19 – 7.10 (m, 3H), 7.04 – 6.92 (m, 4H), 5.64 (s, 2H), 4.41 (d, *J* = 8.0 Hz, 2H), 2.24 (t, *J* = 8.1 Hz, 1H), 2.02 – 1.57 (m, 14H). HRMS (ESI) m/z $[M]^+$ calculated for $[C_{27}H_{31}N_2O]^+$ 399.2436, found 399.2430.

1-(2-((3*r*,5*r*,7*r*)-Adamantan-1-yl)ethyl)-3-((*E*)-3,7-dimethylocta-2,6-dien-1-yl)-1*H*-imidazol-3-ium bromide (27).

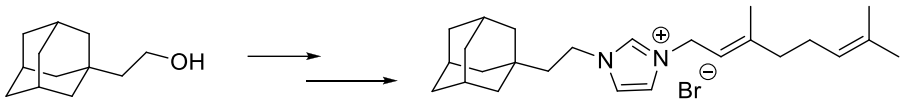

27

27 was made by following the protocol used for **25** using 1-(1-hydroxy-ethyl) adamantane as the starting material which is commercial available. Purity of the product was determined by qNMR: 91.9%. ^{1}H NMR (500 MHz, chloroform-d_1) δ 10.67 (s, 1H), 7.24 (s, 1H), 7.18 (s, 1H), 5.50 – 5.28 (m, 1H), 5.03 (m, 1H), 5.01 (d, J = 7.5 Hz, 2H), 4.49 – 4.19 (m, 2H), 2.17 – 1.22 (m, 21H), 1.60 (s, 3H), 1.57 (s, 6H). HRMS (ESI) m/z $[M]^+$ calculated for $[C_{25}H_{39}N_2]^+$ 367.3113, found 367.3128.

1-(2-((3*r*,5*r*,7*r*)-Adamantan-1-yl)ethyl)-3-octyl-1*H*-imidazol-3-ium bromide (28).

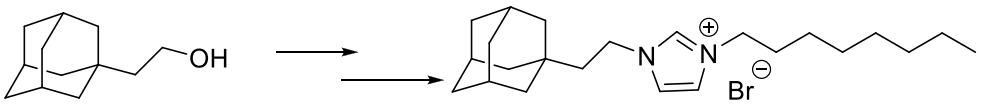

28

28 was made by following the protocol used for **25** using 1-(1-hydroxy-ethyl) adamantane as the starting material. Purity of the product was determined by qNMR: 98.1%. ^{1}H NMR (500 MHz, chloroform-d_1) δ 10.80 (s, 1H), 7.21 (m, 2H), 4.36 (m, 4H), 2.18 – 1.80 (m, 5H), 1.83 – 1.59 (m, 12H), 1.43 – 1.10 (m, 10H), 0.87 (t, J = 6.8 Hz, 3H). HRMS (ESI) m/z $[M]^+$ calculated for $[C_{23}H_{39}N_2]^+$ 343.3113, found 343.3111.

1-(2-((3*r*,5*r*,7*r*)-Adamantan-1-yl)ethyl)-3-(3-phenoxybenzyl)-1*H*-imidazol-3-ium bromide (29).

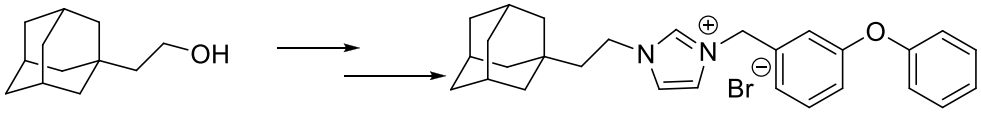

29

29 was made by following the protocol used for **26** using 1-(1-hydroxy-ethyl) adamantane as starting material. Purity of the product was determined by qNMR: 91.0%. ^{1}H NMR (500 MHz, chloroform-d_1) δ 10.83 (t, J = 1.6 Hz, 1H), 7.42 – 7.28 (m, 3H), 7.25 – 7.10 (m, 4H), 7.06 – 6.90

(m, 4H), 5.63 (s, 2H), 4.38 – 4.16 (m, 2H), 2.17 – 1.44 (m, 17H). HRMS (ESI) m/z $[M]^+$ calculated for $[C_{28}H_{33}N_2O]^+$ 413.2593, found 413.2595.

1-(3-((3*r*,5*r*,7*r*)-Adamantan-1-yl)propyl)-3-((*E*)-3,7-dimethylocta-2,6-dien-1-yl)-1*H*-imidazol-3-ium bromide (30).

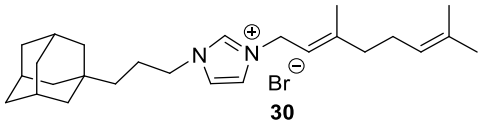

30

30 was made by following the protocol used for **25** using 1-(3-hydroxy-propyl)adamantane[24] as starting material. Purity of the product was determined by qNMR: 90.9%. ^{1}H NMR (500 MHz, chloroform-d_1) δ 10.61 (s, 1H), 7.21 (s, 1H), 7.16 (s, 1H), 5.38 (m, , 1H), 5.03 (t, m , 1H), 5.01 (d, J = 10.0 Hz, 2H), 4.30 (t, J = 7.5 Hz, 2H), 1.52 (m, 23H), 1.60 (s, 3), 1.44 (s, 6H). HRMS (ESI) m/z $[M]^+$ calculated for $[C_{26}H_{41}N_2]^+$: 381.3270, found : 381.3267.

1-(3-((3*r*,5*r*,7*r*)-Adamantan-1-yl)propyl)-3-octyl-1*H*-imidazol-3-ium bromide (31).

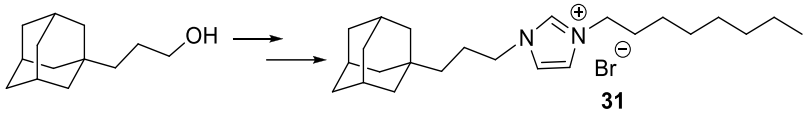

31

31 was made by following the protocol used for **25** using 1-(3-hydroxy-propyl) adamantaneas[24] starting material. Purity of the product was determined by qNMR: 97.2%. ^{1}H NMR (500 MHz, chloroform-d_1) δ 10.76 (s, 1H), 7.22 (s, 2H), 4.36 (t, J = 7.5 Hz, 2H), 4.32 (t, J = 7.5 Hz, 2H), 2.03 – 1.17 (m, 15H), 1.12 – 1.01 (m, 2H), 0.87 (t, J = 6.8 Hz, 3H). HRMS (ESI) m/z $[M]^+$ calculated for $[C_{24}H_{41}N_2]^+$ 357.3270, found 357.3258.

1-(3-((3*r*,5*r*,7*r*)-Adamantan-1-yl)propyl)-3-(3-phenoxybenzyl)-1*H*-imidazol-3-ium bromide (32).

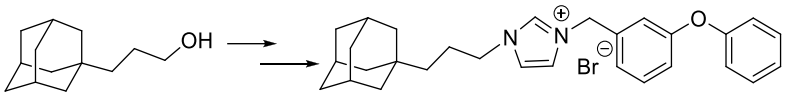

32

32 was made by following the protocol used for **26** using 1-(3-hydroxy-propyl)adamantane[24] as starting material. Purity of the product was determined by qNMR: 90.1%. ^{1}H NMR (500 MHz, chloroform-*d*$_1$) δ 10.90 (s, 1H), 7.35 (m, 3H), 7.24 – 7.11 (m, 3H), 6.99 (m, 5H), 5.62 (s, 2H), 4.27 (t, *J* = 7.5 Hz, 2H), 1.96 – 1.38 (m, 17H), 1.071 (m, 2H). HRMS (ESI) m/z $[M]^+$ calculated for $[C_{29}H_{35}N_2O]^+$ 427.2749, found 427.2754.

1-(3-((3*r*,5*r*,7*r*)-Adamantan-2-yl)propyl)-3-octyl-1*H*-imidazol-3-ium bromide (33)

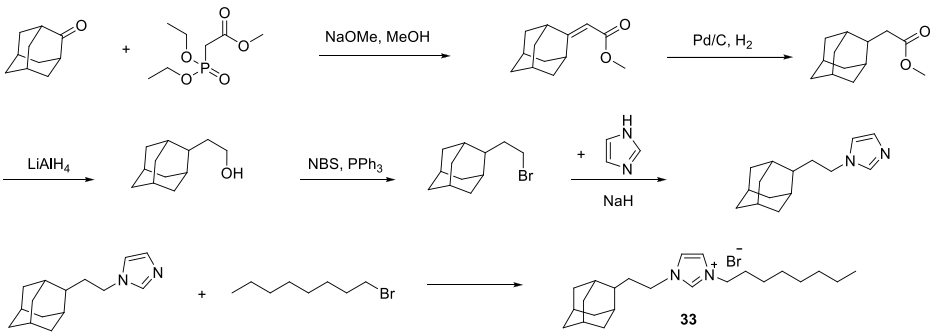

To a solution of 2-adamantanone (5 g, 33.28 mmol) in 32 mL of methanol was added methyl 2-diethoxyphosphoacetate (9 mL, 49.68 mmol). The reaction mixture was cooled at 0 ^{o}C and into it was slowly added sodium methoxide (solution of 30% wt in methanol). The mixture was stirred overnight at room temperature. The solvent was removed under reduced pressure and the crude was treated with ethyl acetate and water. The organic layer was dried over Na_2SO_4 and the solvent was removed under reduced pressure. The crude was purified by using column chromatography (silica gel, eluting with hexane/ethyl acetate 90:1) to give the unsaturated ester as a solid (6.41 g, 90%)**.** To a solution of the unsaturated ester (6.4 g, 31.07 mmol) in methanol (100 mL) was added ammonium formiate (7.8 g, 124.33 mmol), then was added palladium on charcoal (0.6 g, 10%) under nitrogen. The reaction mixture was stirred at room temperature for 3 h. Solvents were

removed under reduced pressure. The crude was treated with water and ethyl acetate, and the organic layer was separated, dried over Na_2SO_4 and solvent removed under reduced pressure. The ester product was obtained as a colourless oil (6.2 g, 95%). To a solution of lithium aluminum hydride (1.58 g, 41.63 mmol) in anhydrous tetrahydrofuran (THF) was slowly added a solution of the ester (6.2 g, 29.76 mmol) in THF (55 mL). The reaction mixture was stirred at room temperature overnight. Then water (12 mL), sodium hydroxide 4N (12 mL) and finally water (36 mL) were added into the solution at 0 ^oC. The mixture was stirred for some minutes and the resulting salts were filtered through a pad of celite washing with ethyl acetate (100 mL). The crude was treated with water and CH_2Cl_2 and the organic layer was separated, dried over Na_2SO_4 and solvents removed under reduced pressure to give the alcohol product as an oil (4.83 g, 90%). To a solution of the alcohol (4.8 g, 26 mmol) in 100 mL CH_2Cl_2 was added triphenylphosphine (13.6 g, 52 mmol). The reaction mixture was stirred at room temperature while N-bromosuccinimide (NBS, 6.9 g, 39 mmol) was added in small portions. The mixture was stirred overnight and then washed with water and extracted with hexane. The organic layer was separated, dried over Na_2SO_4 and solvents removed under reduced pressure to give the bromide product as a light yellow solid (6.0 g, 95%). Imidazole (1.0 g, 15 mmol) was dissolved in THF (30 mL) and NaH (240 mg, 10 mmol) was added. The reaction mixture was stirred at room temperature for 30 minutes and then the bromide product (1.2 g, 5 mmol) was added. The reaction mixture was then heated to 80 ^oC and stirred overnight. The reaction was quenched with water and the mixture extracted with diethyl ether. The organic layer was separated, dried over Na_2SO_4 and solvents removed under reduced pressure. The crude product was purified by silica flash chromatography (silica gel, hexane/ethyl acetate 2:1). The imidazole product was obtained as light yellow solid (0.6 g, 50%). The imidazole product was dissolved in 1-bromooctane and the reaction mixture stirred overnight under nitrogen

at 80 °C. The reaction mixture was treated with hexane and a white precipitate formed. The mixture was centrifuged and the solution discarded. The white precipitate was washed three times with hexane and gave the product **33** as a white solid. Purity of the product was determined by qNMR: 98.9%. ^{1}H NMR (500 MHz, chloroform-*d*$_1$) δ 10.638 (s, 1H), 7.35 (d, J = 10.5 Hz, 1H), 7.34 (d, J = 10.5 Hz 1H), 4.33 (m, 4H), 2.06 (m, 2H), 1.92-1.82 (m, 12H), 1.68 (m, 2H), 1.55 (m, 1H), 1.31-1.21 (m, 12H), 0.85 (t, J = 7.0 Hz, 3H). HRMS (ESI): m/z [M + H]$^+$ calculated for [$C_{23}H_{29}N_2$]$^+$ 343.3113, found 343.3119.

1-(3-((3*r*,5*r*,7*r*)-Adamantan-1-yl)propyl)-3-(3-phenoxybenzyl)-1*H*-imidazol-3-ium bromide (34).

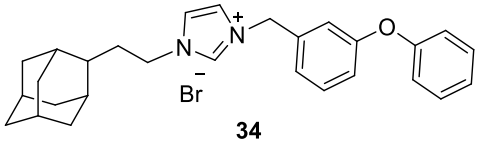

34

34 was made by following the protocol used for **33**. Purity of the product was determined by qNMR: 100%. ^{1}H NMR (500 MHz, chloroform-*d*$_1$) δ 10.77 (s, 1H), 7.33-6.90 (m, 11H), 5.62 (s, 2H), 4.29 (t, J = 7.5 Hz, 2H), 1.92-1.82 (m, 12H), 1.68 (m, 2H), 1.55 (m, 1H). HRMS (ESI) m/z [M]$^+$ calculated for [$C_{28}H_{33}N_2O$]$^+$ 413.2593, found 413.2586.

1-(3-((3*r*,5*r*,7*r*)-Adamantan-2-yl)propyl)-3-hexyl-1*H*-imidazol-3-ium bromide (35)

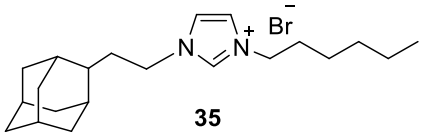

35

35 was made by following the protocol used for **33**. Purity of the product was determined by qNMR: 98.9%. ^{1}H NMR (500 MHz, chloroform-*d*$_1$) δ 10.86 (s, 1H), 7.35 (d, J = 10.5 Hz, 1H), 7.26 (d, J = 10.5 Hz 1H), 4.37 (m, 4H), 2.06 (m, 2H), 1.92-1.82 (m, 12H), 1.68 (m, 2H), 1.55 (m,

1H), 1.31-1.21 (m, 8H), 0.85 (t, J = 7.0 Hz, 3H). HRMS (ESI): m/z $[M + H]^+$ calculated for $[C_{21}H_{35}N_2]^+$ 315.2830, found 315.2834.

1-(3-((3*r*,5*r*,7*r*)-Adamantan-2-yl)propyl)-3-decyl-1*H*-imidazol-3-ium bromide (36)

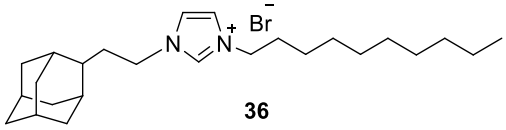

36

36 was made by following the protocol used for **33**. Purity of the product was determined by qNMR: 96.4%. ^{1}H NMR (500 MHz, chloroform-d_1) δ 10.86 (s, 1H), 7.35 (d, J = 10.5 Hz, 1H), 7.26 (d, J = 10.5 Hz 1H), 4.37 (m, 4H), 2.06 (m, 2H), 1.92-1.82 (m, 12H), 1.68 (m, 2H), 1.55 (m, 1H), 1.31-1.21 (m, 16H), 0.85 (t, J = 7.0 Hz, 3H). HRMS (ESI): m/z $[M + H]^+$ calculated for $[C_{25}H_{43}N_2]^+$ 371.3426, found 371.3430.

1-(3-((3*r*,5*r*,7*r*)-Adamantan-2-yl)propyl)-3-dodecyl-1*H*-imidazol-3-ium bromide (37)

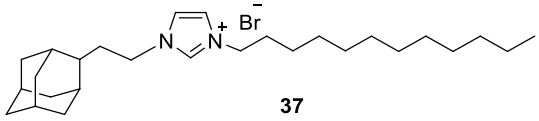

37

37 was made by following the protocol used for **33**. Purity of the product was determined by qNMR: 99.9%. ^{1}H NMR (500 MHz, chloroform-d_1) δ 10.85 (s, 1H), 7.35 (d, J = 10.5 Hz, 1H), 7.26 (d, J = 10.5 Hz 1H), 4.37 (m, 4H), 2.06 (m, 2H), 1.92-1.82 (m, 12H), 1.68 (m, 2H), 1.55 (m, 1H), 1.31-1.21 (m, 20H), 0.85 (t, J = 7.0 Hz, 3H). HRMS (ESI): m/z $[M + H]^+$ calculated for $[C_{27}H_{47}N_2]^+$ 399.3734, found 399.3739.

1-(-(1'-(1',2'-Dicarbaclosododecaboranyl))ethyl)-3-pentyl-1*H*-imidazol-3-ium bromide (43).

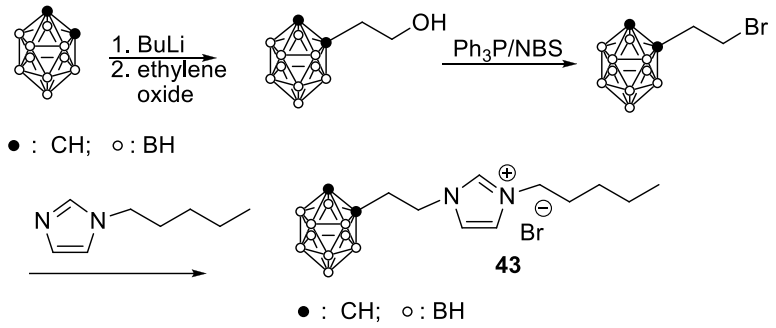

To a solution of *o*-carborane (268 mg, 2 mmol) in dry THF (6 mL, 2 mmol) was added BuLi (1.6 M in hexane, 1.25 mL, 2 mmol) at -78 ^{o}C under N_2. Stirring was continued for 30 min, then ethylene oxide (1.2 M in THF, 2.5 mL, 3 mmol) was added dropwise. Stirring was continued for 1 h at 0 ^{o}C, then the reaction was quenched by adding saturated aqueous NH_4Cl (2 mL). The aqueous phase was extracted with ethyl acetate (3 mL x 3) and the combined organic phase was dried over Na_2SO_4 and solvents removed under reduced pressure. The residue was purified by using flash chromatography (silica gel, hexane/ethyl acetate = 5/1) to give the carboranylethyl alcohol (303 mg, 85%). To a solution of the carboranylethyl alcohol (303 mg, 1.7 mmol) in dry CH_2Cl_2 (5 mL) was added Ph_3P (524 mg, 2 mmol) followed by NBS (356 mg, 2 mmol). Stirring was continued for 3 h at 0 ^{o}C, then all volatile components were removed under reduced pressure. The residue was purified by flash chromatography (silica gel, hexane/ethyl acetate = 15/1) to give the bromide product (328 mg, 80%). A mixture of the carboranylethyl bromide product (33 mg, 0.1 mmol), *N*-pentylimidazole (14 mg, 0.1 mmol) and chloroform (0.5 mL) was heated for 3 h at 120 ^{o}C in the sealed tube. The reaction mixture was cooled to room temperature and all volatile components removed under reduced pressure. The residue was purified by flash chromatography (silica gel, $CHCl_3$/MeOH = 10/1) to give the product **43** (30 mg, 65%). Purity of the product was determined by qNMR: 92.5%. ^{1}H NMR (500 MHz, chloroform-d_1) δ 10.60 (s, 1H), 7.52 (s, 1H), 7.20 (s, 1H), 5.11 (s, 1H), 4.58 (t, J = 10.0 Hz, 2H), 4.20 (t, J = 7.5 Hz, 2H), 3.22 (t, J = 10.0 Hz,,

2H), 2.80 – 1.71 (m, 10H), 1.93 (m, 2H), 1.36 (m, 4H), 0.92 (t, *J* = 7.0 Hz, 3H). HRMS (ESI) m/z $[M]^+$ calculated for $[C_{12}H_{29}B_{10}N_2]^+$ 311.3261, found 311.3232.

4.6 Schemes, Charts, Tables and Figures

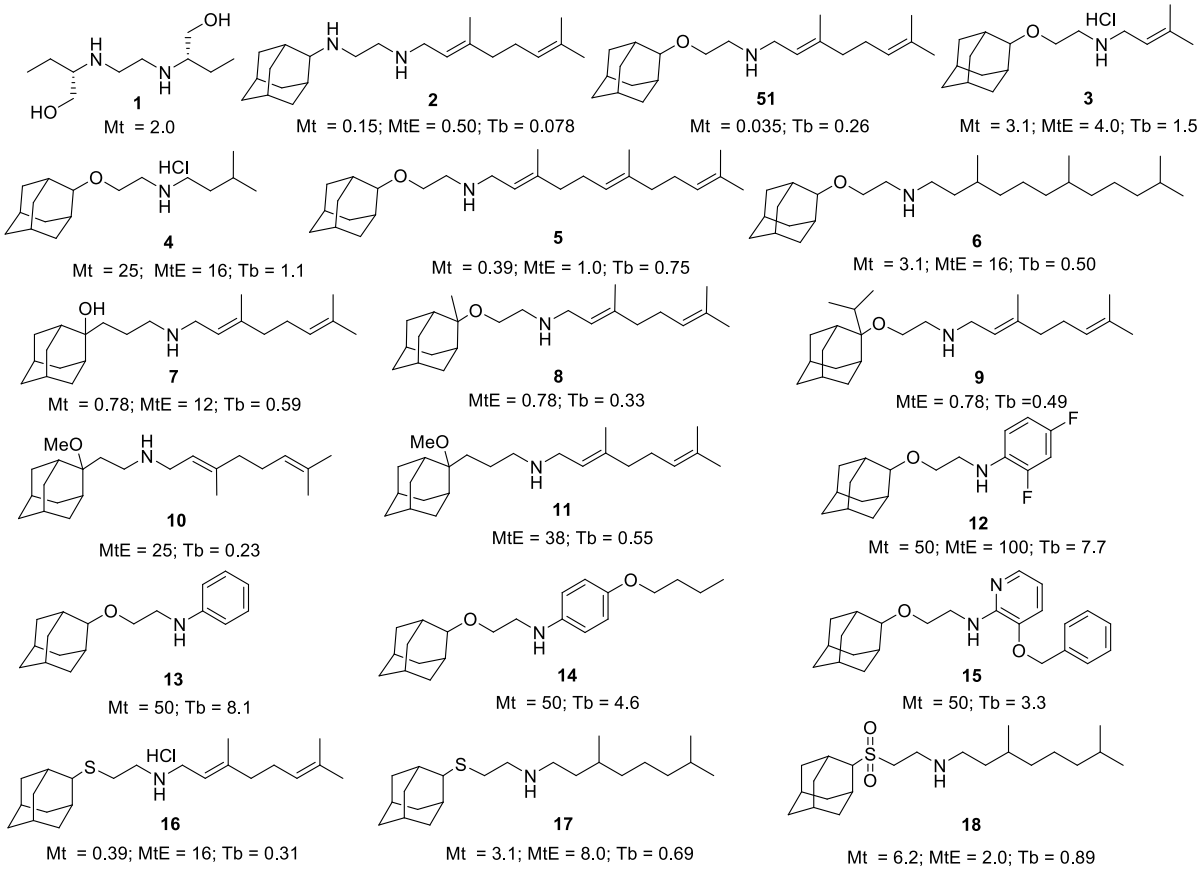

Figure 4.1. Alkanolamine and mercaptoethylamine analogs of SQ109 and their activities against *Mycobacterium tuberculosis* and *Trypanosoma brucei*. Mt = *M. tuberculosis* H37Rv; MtE = *M. tuberculosis* Erdman; Tb = *Trypanosoma brucei*. Values shown are in μg/mL and are MIC for the mycobacteria, and IC_{50} for *T. brucei*.

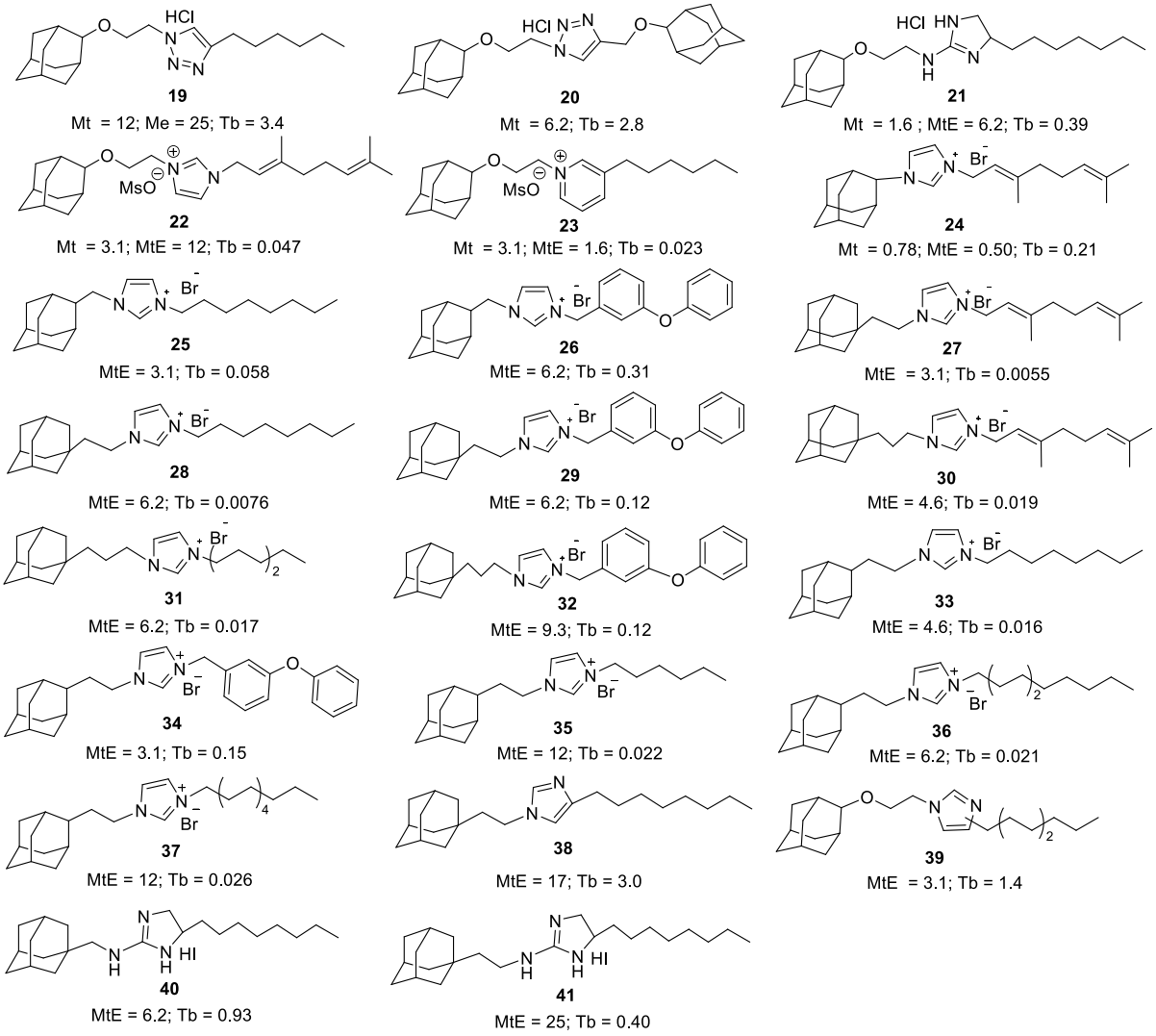

Figure 4.2. Heterocyclic analogs of SQ109 and their activities against *Mycobacterium tuberculosis* and *Trypanosoma brucei.* Mt = *M. tuberculosis* H37Rv; MtE = *M. tuberculosis* Erdman; Tb = *Trypanosoma brucei*; Values shown here are in μg/mL and are MIC for the mycobacteria and IC_{50} for *T. brucei*.

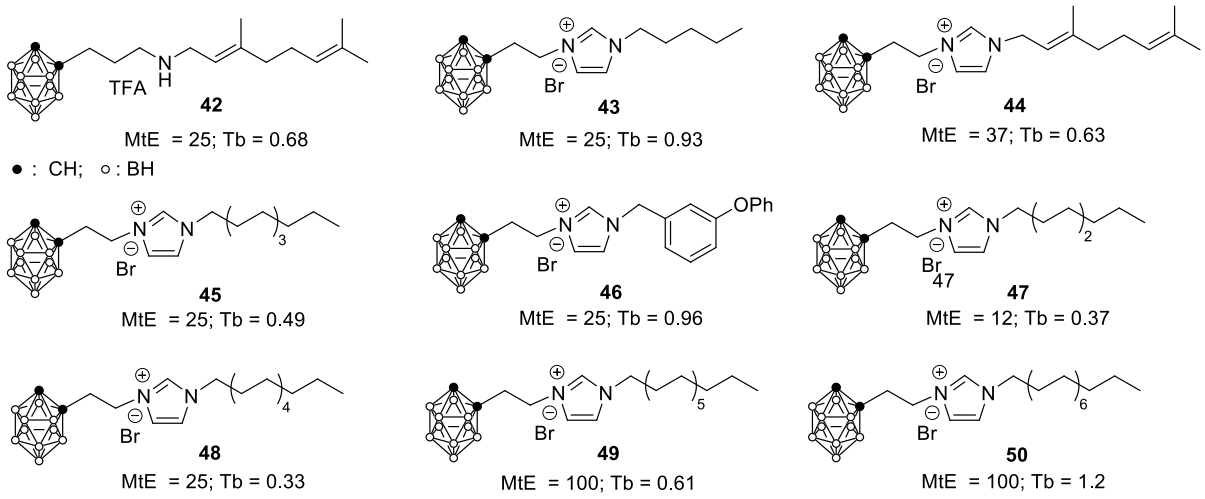

Figure 4.3. Carborane-containing analogs of SQ109 and their activities against *Mycobacterium tuberculosis* and *Trypanosoma brucei*. Mt = *M. tuberculosis* H37Rv; MtE = *M. tuberculosis* Erdman; Tb = *Trypanosoma brucei*; Values shown here are in μg/mL and are MIC for the mycobacteria and IC_{50} for *T. brucei*.

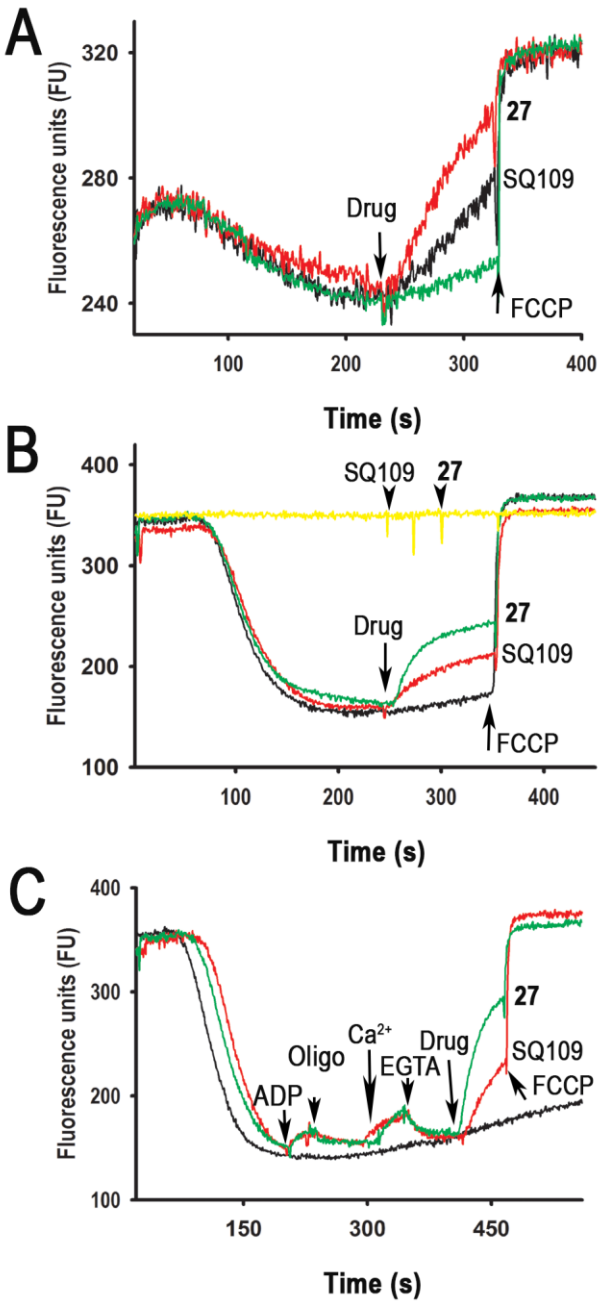

Figure 4.4. Effects of SQ109 or **27** on $\Delta\psi$ in digitonin-permeabilized *T. brucei*. (A) BSF trypanosomes ($2x10^8$ cells) were added to reaction buffer (125 mM sucrose, 65 mM KCl, 10 mM Hepes-KOH buffer, pH 7.2, 1 mM $MgCl_2$, 2.5 mM potassium phosphate; 2 mL) containing 20 µM EGTA, 1 mM ATP, 500 µM orthovanadate and 5 µM safranine, and the reaction started with 40 µM digitonin. (B, C) *T. brucei* PCF ($10x10^7$ cells) were added to the reaction buffer (2.4 mL) containing 2 mM succinate and 5 µM safranine, and the reaction initiated with or without (*yellow* trace in B) 50 µM digitonin. SQ109 (3.3 µg/mL), and **27** (4.5 µg/mL) (equimolar amounts), FCCP (8 µM), ADP (10 µM), oligomycin (Oligo, 2 µg/ml), $CaCl_2$ (12 µM), EGTA (200 µM) were added where indicated. No changes were detected in the absence of digitonin indicating lack of secondary effects of the drugs.

	Tb[a]	Mt[b]	MtE[c]	Ms[d]	Bs[e]	Ec[f]	Sc[g]	HEK 293T[h]	HepG2[i]	SI(HEK 293T/Tb)[j]	SI(HepG 2/Tb)[k]
1	ND	2.0	ND	1.0	ND	ND	ND	ND	ND	ND	ND
2	0.078±0.001	0.15	0.50	3.1	7.6	2.8	1.1	1.9	1.2	24	15
3	1.5±0.1	3.1	4.0	ND	>120	9.0	25	9.2	4.8	6.0	3.1
4	1.1±0.1	25	16	ND	>120	9.6	2.1	8.8	4.5	7.7	3.9
5	0.75±0.1	0.39	1.0	ND	0.8	0.6	0.7	11	9.4	15	13
6	0.50±0.1	3.1	16	ND	3.0	10	2.8	1.7	1.6	3.4	3.2
7	0.59±0.05	0.78	12	ND	2.1	12	3.2	4.6	2.9	7.8	4.9
8	0.33±0.06	ND	0.78	5.8	2.2	6.2	4.1	6.1	5.4	19	16
9	0.49±0.09	ND	0.78	5.7	3.3	8.0	4.1	9.5	5.6	20	12
10	0.23±0.03	ND	25	5.1	2.8	8.9	5.1	5.2	4.7	23	21
11	0.55±0.1	ND	38	5.2	3.9	9.2	6.1	5.5	3.6	10	6.6
12	7.7±1.5	50	100	ND	>60	>60	>60	18	12.0	2.3	1.6
13	8.1±0.1	50	ND	ND	>60	>60	>60	16	7.3	2.0	0.9
14	4.6±0.4	50	ND	ND	>60	>60	>60	16	12	3.5	2.6
15	3.3±0.5	25	ND	ND	>60	>60	>60	21	20	6.4	6.1
16	0.31±0.02	0.39	16	1.2	1.4	1.4	0.38	2.7	1.6	8.6	5.1
17	0.69±0.12	3.1	8.0	1.1	0.5	0.7	0.1	4.9	4.1	7.1	6.0
18	0.89±0.01	6.2	2.0	4.8	2.3	2.3	2.2	4.7	3.4	5.3	3.8
19	3.4±0.8	12	25	4.6	28	>74	>74	17	19	5.0	5.6
20	2.8±0.1	6.2	ND	5.6	>90	>90	>90	12	12	4.2	4.2
21	0.39±0.01	1.6	6.2	1.2	0.38	2.0	1.5	1.7	1.5	4.4	3.8
22	0.047±0.007	3.1	12	1.5	1.2	36	9.1	3.2	4.3	68	91
23	0.023±0.005	3.1	1.6	0.7	2.1	33	17	4.1	5.4	180	240
24	0.21±0.02	0.78	0.50	3.2	3.1	13	8.4	4.9	6.2	24	30
25	0.058±0.011	ND	3.1	1.2	2.1	12	5.7	2.6	3.1	45	53
26	0.31±0.05	ND	6.2	1.5	2.0	12	4.8	5.1	5.5	17	18
27	0.0055±0.0001	ND	3.1	0.9	0.88	7.2	4.4	1.6	2.0	290	370
28	0.0076±0.0004	ND	6.2	0.9	0.41	5.4	2.2	1.3	1.5	170	200
29	0.12±0.01	ND	6.2	1.6	0.78	5.6	3.8	3.7	3.7	30	30
30	0.019±0.001	ND	4.6	1.0	0.48	3.4	2.7	1.6	1.9	86	100
31	0.017±0.001	ND	6.2	1.0	0.37	2.0	1.6	1.6	1.5	92	86
32	0.12±0.02	ND	9.3	3.5	0.56	3.6	0.51	4.4	4.2	38	36
33	0.016±0.001	ND	4.6	0.8	0.59	6.7	1.9	1.8	2.1	110	130
34	0.15±0.02	ND	3.1	1.8	0.69	4.0	2.1	3.2	3.5	21	23
35	0.022±0.001	ND	12	2.3	3.3	35	12	3.2	5.4	97	160
36	0.021±0.004	ND	6.2	0.8	0.22	1.0	1.4	1.5	1.5	70	70
37	0.026±0.002	ND	12	0.5	0.24	1.0	1.8	1.9	1.6	73	61
38	3.0±0.5	ND	17	16	1.2	85	46	19	ND	6.3	ND
39	1.4±0.1	ND	3.1	1.1	0.36	4.6	4.5	5.2	6.3	3.8	4.7
40	0.93±0.10	ND	6.2	1.9	1.1	6.4	3.5	3.6	3.4	3.9	3.6
41	0.40±0.06	ND	25	7.3	3.8	19	16	6.3	4.9	16	12
42	0.68±0.07	ND	25	1.3	0.75	2.1	3.4	3.5	3.0	5.1	4.4
43	0.93±0.17	ND	25	3.8	1.6	11	29	7.2	5.1	7.7	5.5
44	0.63±0.09	ND	37	1.9	0.31	5.0	7.3	7.9	7.8	13	12
45	0.49±0.08	ND	25	0.8	0.2	1.8	3.0	4.1	3.7	8.4	7.6
46	0.96±0.09	ND	25	ND	ND	ND	ND	14	14	15	15
47	0.37±0.09	ND	12	ND	ND	ND	ND	2.5	3.1	6.8	8.4
48	0.33±0.05	ND	25	ND	ND	ND	ND	1.9	1.4	5.8	4.3
49	0.61±0.16	ND	100	ND	ND	ND	ND	4.7	4.2	7.6	6.8
50	1.2±0.2	ND	100	ND	ND	ND	ND	7.5	7.9	6.4	6.7
51	0.26±0.07	0.035	ND	1.6	16	2.8	1.8	1.3	1.0	4.9	3.8

Table 4.1. Growth inhibition of various cells by SQ109 and its analogs.

a. Tb = *Trypanosoma brucei*, IC_{50}; b. Mt = *M. tuberculosis* H37Rv, MIC; c. MtE = *M. tuberculosis* Erdman, MIC; d. Ms = *M. smegmatis*, IC_{50}; e. Bs = *B. subtilis*, IC_{50}; f. Ec = *E. coli*, IC_{50}; g. Sc = *S. cerevisiae*, IC_{50}; h. human embryonic kidney, HEK293T, CC_{50}; i. human hepatocellular carcinoma, HepG2, CC_{50}; j. SI = CC_{50}(HEK293T)/IC_{50}(Tb); k. SI = CC_{50}(HepG2)/IC_{50}(Tb). All units for MIC, IC_{50} and CC_{50} are μg/mL.

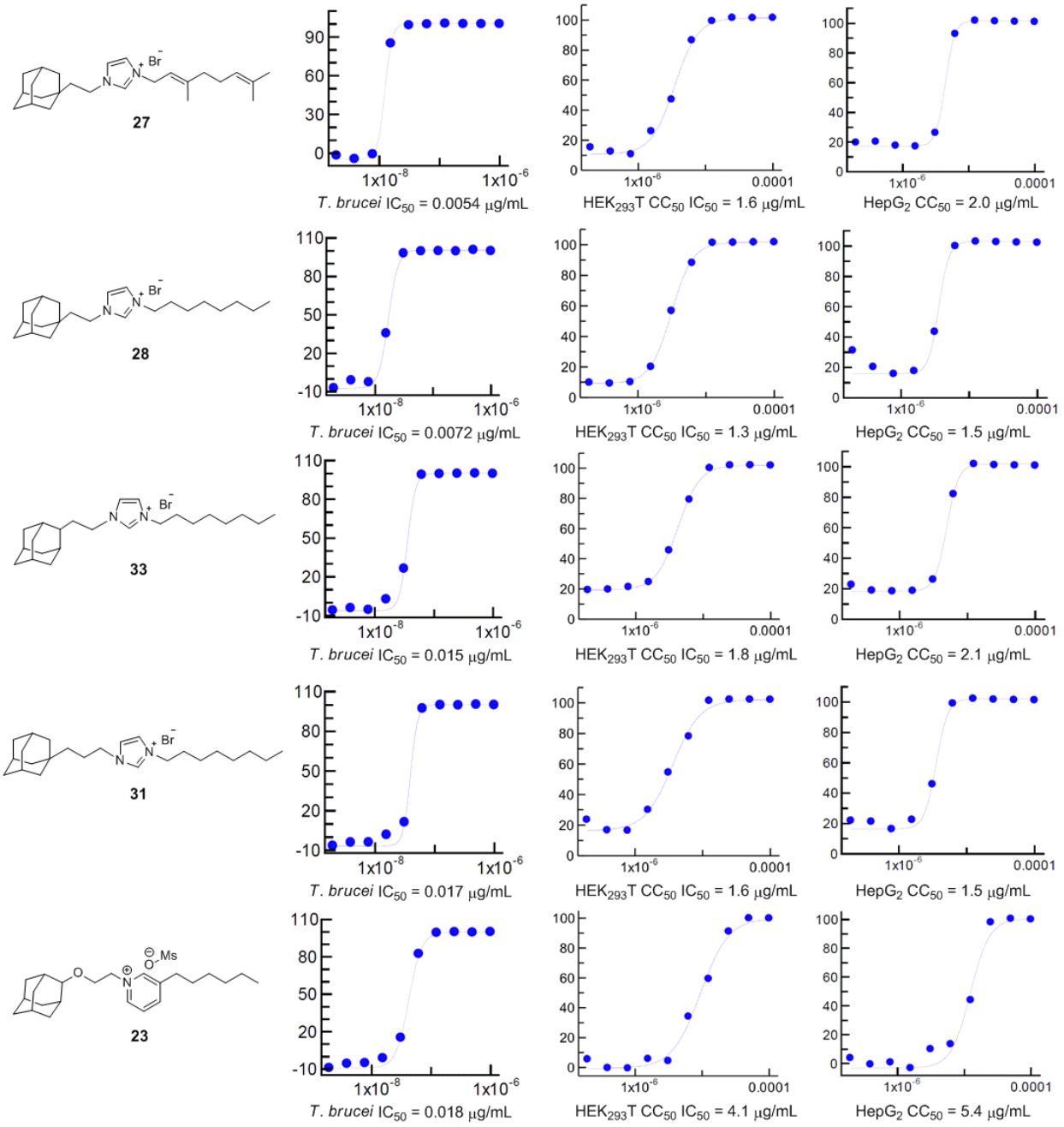

Figure 4.5. Dose-response curves for the top five *T. brucei* cell growth inhibitors and their corresponding effects on HEK293T and HepG2 cell growth.

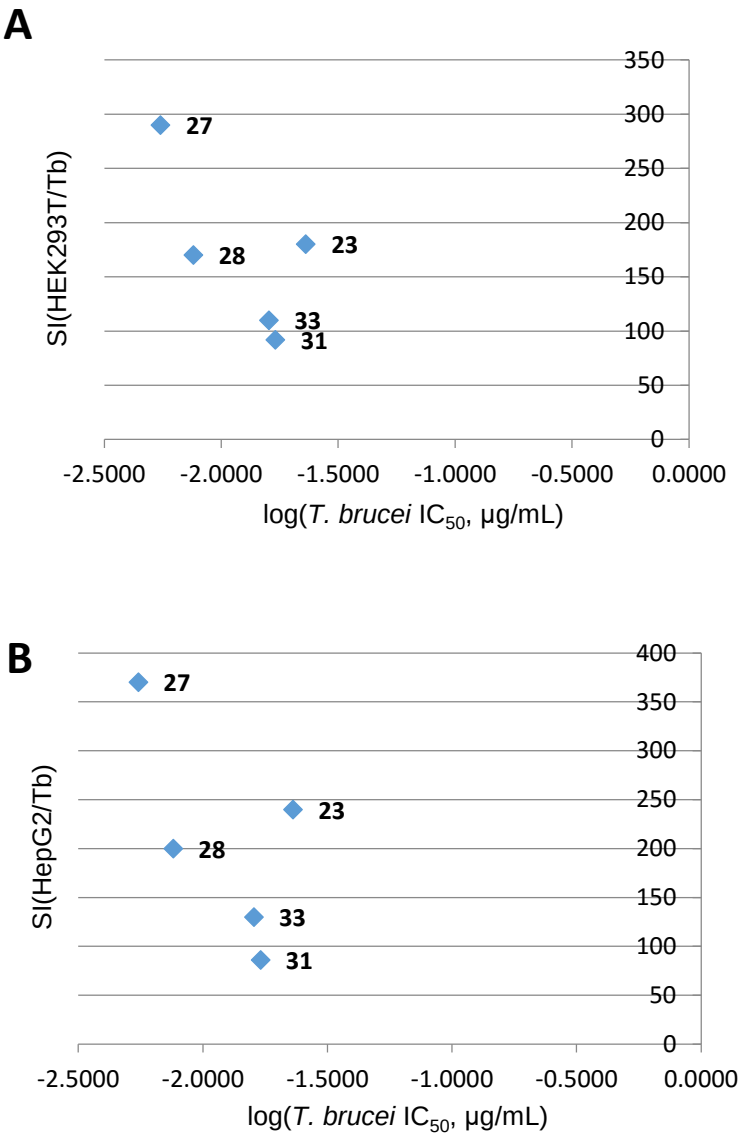

Figure 4.6. A. Plot of selectivity index (HEK293T CC_{50}/*T. brucei* IC_{50}) *versus* log(*T. brucei* IC_{50}, µg/mL). B. Plot of selectivity index (HepG2 CC_{50}/*T. brucei* IC_{50}) *versus* log(*T. brucei* IC_{50}, µg/mL).

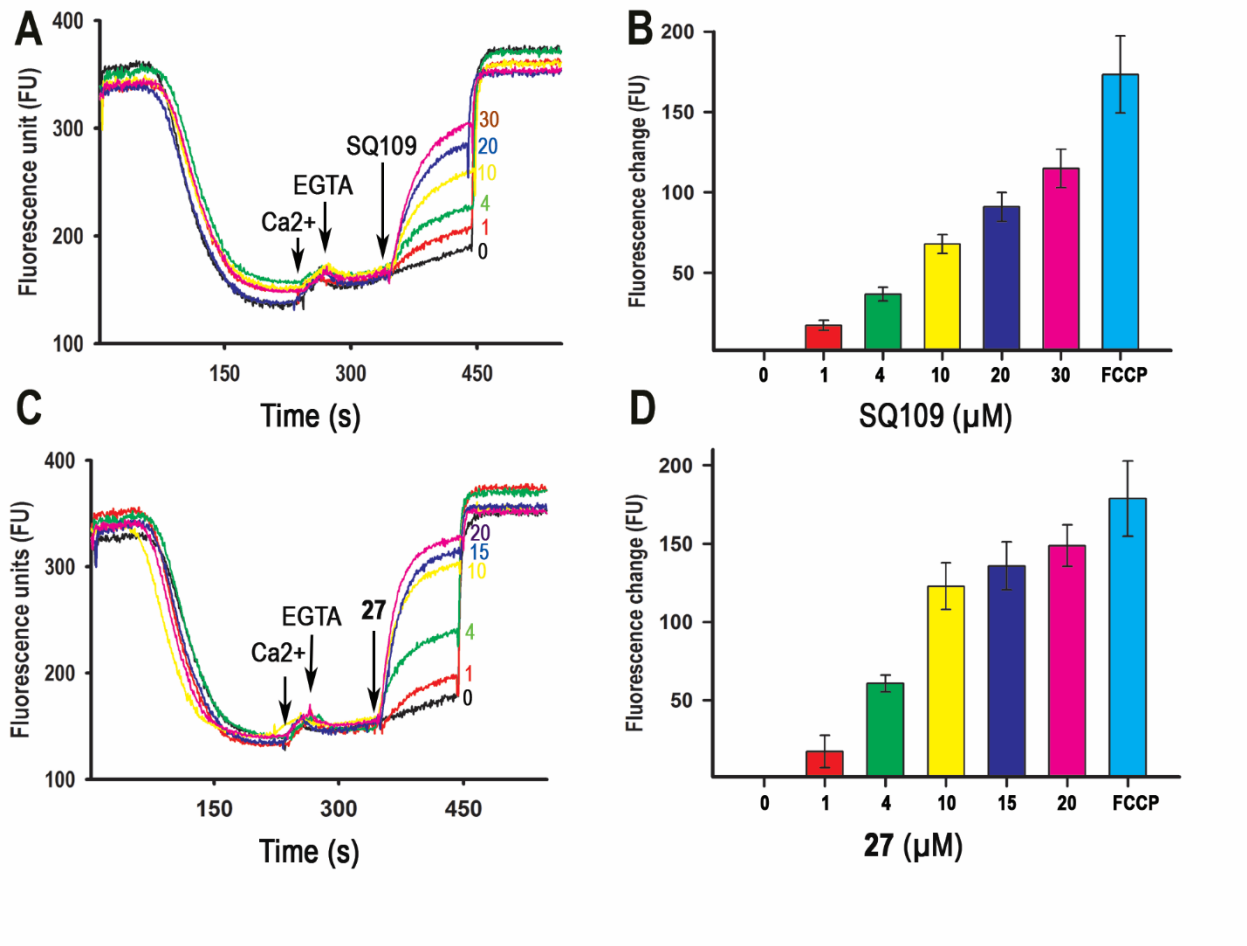

Figure 4.7. Effects of SQ109 (**2**) or **27** on the mitochondrial membrane potential of digitonin-permeabilized *T. brucei* procyclic forms. PCF trypanosomes (5 x 10^7 cells) were added to reaction buffer (2.4 mL) containing 2 mM succinate and 5 μM safranine, and the reaction initiated by addition of 50 μM digitonin. (A, C) $CaCl_2$ (12 μM), EGTA (200 μM), various concentrations of SQ109 (A) or **27** (C), and 8 μM FCCP were added where indicated. (B, D) Changes in safranine fluorescence after addition of SQ109 (1-30 μM, 0.33-10 μg/mL), **27** (1-20 μM, 0.45-9.0 μg/mL) or FCCP (8 μM), as shown in (A, C), respectively. The results are means ± SD of three independent experiments.

4.7 References

1. *Threat Report 2013: Antibiotic/Antimicrobial Resistance*; Centers for Disease Control and Prevention, 2013.
2. *Antimicrobial Resistance: Global Report on Surveillance 2014*; World Health Organization, 2014.
3. *Global tuberculosis report 2014*; World Health Organization, 2014.
4. Protopopova, M.; Hanrahan, C.; Nikonenko, B.; Samala, R.; Chen, P.; Gearhart, J.; Einck, L.; Nacy, C. A. Identification of a new antitubercular drug candidate, SQ109, from a combinatorial library of 1,2-ethylenediamines. *J. Antimicrob. Chemother.* **2005**, *56*, 968-974.
5. Bogatcheva, E.; Hanrahan, C.; Nikonenko, B.; de los Santos, G.; Reddy, V.; Chen, P.; Barbosa, F.; Einck, L.; Nacy, C.; Protopopova, M. Identification of SQ609 as a lead compound from a library of dipiperidines. *Bioorg. Med. Chem. Lett.* **2011**, *21*, 5353-5357.
6. Tahlan, K.; Wilson, R.; Kastrinsky, D. B.; Arora, K.; Nair, V.; Fischer, E.; Barnes, S. W.; Walker, J. R.; Alland, D.; Barry, C. E.; Boshoff, H. I. SQ109 Targets MmpL3, a Membrane Transporter of Trehalose Monomycolate Involved in Mycolic Acid Donation to the Cell Wall Core of *Mycobacterium tuberculosis*. *Antimicrob. Agents Chemother.* **2012**, *56*, 1797-1809.
7. Varela, C.; Rittmann, D.; Singh, A.; Krumbach, K.; Bhatt, K.; Eggeling, L.; Besra, G. S.; Bhatt, A. MmpL Genes Are Associated with Mycolic Acid Metabolism in Mycobacteria and Corynebacteria. *Chem. Biol.* **2012**, *19*, 498-506.
8. Owens, C. P.; Chim, N.; Goulding, C. W. Insights on how the *Mycobacterium tuberculosis* heme uptake pathway can be used as a drug target. *Future Med. Chem.* **2013**, *5*, 1391-1403.
9. Owens, C. P.; Chim, N.; Graves, A. B.; Harmston, C. A.; Iniguez, A.; Contreras‡, A.; Liptak, M. D.; Goulding, C. W. The *Mycobacterium tuberculosis* Secreted Protein Rv0203 Transfers Heme to Membrane Proteins MmpL3 and MmpL11. *J. Biol. Chem.* **2013**, *288*, 21714-21728.
10. Makobongo, M. O.; Einck, L.; Peek, R. M.; Merrell, D. S. *In Vitro* Characterization of the Anti-Bacterial Activity of SQ109 against *Helicobacter pylori*. *Plos One* **2013**, *8*, e68917.
11. Barbosa, e. a. In *Intersicence Conference on Antimicrobial Agents and Chemotherapy (ICAAC)* San Francisco, CA, 2006.
12. Li, K.; Schurig-Briccio, L. A.; Feng, X.; Upadhyay, A.; Pujari, V.; Lechartier, B.; Fontes, F. L.; Yang, H.; Rao, G.; Zhu, W.; Gulati, A.; No, J. H.; Cintra, G.; Bogue, S.; Liu, Y. L.; Molohon, K.; Orlean, P.; Mitchell, D. A.; Freitas-Junior, L.; Ren, F.; Sun, H.; Jiang, T.; Li, Y.; Guo, R. T.; Cole, S. T.; Gennis, R. B.; Crick, D. C.; Oldfield, E. Multitarget drug discovery for tuberculosis and other infectious diseases. *J. Med. Chem.* **2014**, *57*, 3126-3139.
13. Brynda, J., Mader, P., Šícha, V., Fábry, M., Poncová, K., Bakardiev, M., Grüner, B., Cígler, P. and Řezáčová, P. Carborane-Based Carbonic Anhydrase Inhibitors. *Angew. Chem. Int. Ed.* **2013**, *52*.
14. Li, W.; Upadhyay, A.; Fontes, F. L.; North, E. J.; Wang, Y.; Crans, D. C.; Grzegorzewicz, A. E.; Jones, V.; Franzblau, S. G.; Lee, R. E.; Crick, D. C.; Jackson, M. Novel insights into the mechanism of inhibition of MmpL3, a target of multiple pharmacophores in *Mycobacterium tuberculosis*. *Antimicrob. Agents Chemother.* **2014**, *58*, 6413-6423.

15. Vercesi, A. E.; Bernardes, C. F.; Hoffmann, M. E.; Gadelha, F. R.; Docampo, R. Digitonin permeabilization does not affect mitochondrial function and allows the determination of the mitochondrial membrane potential of *Trypanosoma cruzi in situ*. *J. Biol. Chem.* **1991**, *266*, 14431-14434.
16. Huang, G.; Vercesi, A. E.; Docampo, R. Essential regulation of cell bioenergetics in Trypanosoma brucei by the mitochondrial calcium uniporter. *Nat. Commun.* **2013**, *4*, 2865.
17. Haagsma, A. C.; Podasca, I.; Koul, A.; Andries, K.; Guillemont, J.; Lill, H.; Bald, D. Probing the interaction of the diarylquinoline TMC207 with its target mycobacterial ATP synthase. *Plos One* **2011**, *6*, e23575.
18. Boshoff, H. I.; Myers, T. G.; Copp, B. R.; McNeil, M. R.; Wilson, M. A.; Barry, C. E., 3rd The transcriptional responses of *Mycobacterium tuberculosis* to inhibitors of metabolism: novel insights into drug mechanisms of action. *J. Biol. Chem.* **2004**, *279*, 40174-40184.
19. Gruppo, V.; Johnson, C. M.; Marietta, K. S.; Scherman, H.; Zink, E. E.; Crick, D. C.; Adams, L. B.; Orme, I. M.; Lenaerts, A. J. Rapid microbiologic and pharmacologic evaluation of experimental compounds against *Mycobacterium tuberculosis*. *Antimicrob. Agents Chemother.* **2006**, *50*, 1245-1250.
20. Hoffman, A. E.; DeStefano, M.; Shoen, C.; Gopinath, K.; Warner, D. F.; Cynamon, M.; Doyle, R. P. Co(II) and Cu(II) pyrophosphate complexes have selectivity and potency against Mycobacteria including *Mycobacterium tuberculosis*. *Eur. J. Med. Chem.* **2013**, *70*, 589-593.
21. Greidanus, J. W. Chemistry of 2-substituted adamantanes. Preparation of Zadamantanethiol and some of its derivatives. Aromatic solvent-induced shifts in their n.m.r. spectra. *Can. J. Chem.* **1970**, *48*, 3593-3597.
22. Perry, M. C.; Cui, X.; Powell, M. T.; Hou, D. R.; Reibenspies, J. H.; Burgess, K. Optically active iridium imidazol-2-ylidene-oxazoline complexes: preparation and use in asymmetric hydrogenation of arylalkenes. *J. Am. Chem. Soc.* **2003**, *125*, 113-123.
23. Hughes, L.; Ingold, K. U.; Walton, J. C. ycloalkylmethyl radicals. 6. The unexpectedly high barrier to the rotation of axial CH2.cntdot. groups in cyclohexylmethyl radicals. *J. Am. Chem. Soc.* **1988**, *110*, 7494-7499.
24. Victor, G. m.; Carlos, P. d. *Derivatives of 4-(2-amino-1 -hydroxyethyl)phenol as agonists of the SS2 adrenergic receptor* Patent WO2008EP09469 20081110, 2009.

Chapter 5: Undecaprenyl Diphosphate Synthase Inhibitors: Antibacterial Drug Leads

5.1 Notes and Acknowledgements

Y.W. W.S. and E.O. designed research; Y.W. obtained the compounds; Y.W. performed enzyme inhibition experiments; Y.W. and C.C. performed cell growth inhibition experiments; Y.W. W.S. and E.O. analyzed data.

This work was supported by the United States Public Health Service (National Institutes of Health Grants GM065307, CA158191, GM08326, GM31749 and HD071600); the National Science Foundation (Grant MCB-1020765); a Packard Fellowship for Science and Engineering (D.A.M.), the National Biomedical Computation Resource, the UCSD Center for Theoretical Biological Physics, the Howard Hughes Medical Institute, and the NSF Supercomputer Centers. F. F. acknowledges financial support of the Beatriu de Pinós program from AGAUR for a postdoctoral grant (2010 BP_A 00339). We thank the Drug Synthesis and Chemistry Branch, Developmental Therapeutics Program, Division of Cancer Treatment and Diagnosis, National Cancer Institute, for providing chemicals, and Professors James Wells and Paul Hergenrother for providing bacteria.

This chapter was reproduced in part with permission from W. Sinko, E. Oldfield, *et al*. *J. Med. Chem.* **2014***,* volume 57, page 5693−5701, Copyright © 2015 American Chemical Society.

5.2 Introduction

The need for new antibiotics has arisen due to the widespread resistance to current drugs.[1] Despite this need, the antibiotic pipeline in the past few decades has been relatively dry in terms of new antibacterial classes when compared with progress against other diseases.[2] One strategy to fight bacterial resistance is to inhibit enzymes that are not the targets of current antibiotics but instead, act in the same pathways as existing drugs since this might enable the restoration of drug sensitivity via combination therapy. Undecaprenyl diphosphate synthase (UPPS) is one such target. The undecaprenyl diphosphate product (UPP) is essential for bacterial cell growth because of its role in the formation of bacterial cell wall peptidoglycan,[1,3] Figure 5.1, and it is not produced by humans.[2,4]

SmithKline Beecham screened their compound collection against UPPS but reported no chemically tractable low micromolar hits.[5] Novartis pursued tetramic and tetronic acids and dihydropyridin-2-ones, but noted issues associated with human serum albumin binding and a lack

of *in vivo* activity.[6,7] Previously, we reported several potent UPPS inhibitors together with X-ray crystallographic (or modeled) binding modes for a variety of chemical classes including lipophilic bisphosphonates,[8] phthalic acids,[9] diketo acids,[10] anthranilic acids, benzoic acids,[11] aryl phosphonates, bis-amines, and bis-amidines.[12] The most promising of these compounds, a bis-amidine, was shown to have potent activity in biochemical assays, cellular assays, and in a murine model of MRSA infection.[12]

Since UPPS must bind multiple substrates (IPP, FPP or more elongated prenyl-PP intermediates) and many inhibitors are to some degree substrate mimics, it is common to observe numerous inhibitors simultaneously bound to UPPS, with up to 4 binding sites being occupied.[8] However, it is unclear whether inhibitory activity is due to binding to one specific site, or to multiple sites. It has been shown that some inhibitors occupy only site 4, an allosteric site distant from the catalytic center, while others bind to site 1, the substrate binding site,[12] complicating docking studies and, regardless of the inhibitor-binding mode, the flexibility of UPPS creates challenges for virtual screening. Here, to help reduce these problems we employed the 12 crystallographic structures described in previous work[8,12] to select those that provided maximal enrichment in retrospective virtual screening studies. We then made prospective predictions using these structures, leading to novel UPPS inhibitors, some with promising anti-bacterial activity.

5.3 Results and Discussion

In previous work, we obtained moderate correlations between enzyme inhibition activity and docking scores within a congeneric series of UPPS inhibitors (lipophilic bisphosphonates)[8,13] using docking methods, so we first examined whether we could obtain similar correlations between docking scores and experimentally determined IC_{50} values for the 112 known actives. There was no significant correlation between docking scores and pIC_{50} values ($pIC_{50} = -\log(IC_{50})$). The wide variety of potential binding modes (Sites 1, 2, 3 and 4[8,12]) and protein conformations would be expected to make it difficult to achieve a good correlation between a scoring function and the experimentally determined pIC_{50} values, in addition to the assumptions made in scoring functions that cause inaccuracy when compared to experimental affinities. Nevertheless, docking studies can provide enrichment of active compounds from large libraries, even though docking scores rarely correlate well with activity when structurally diverse compounds are involved. We thus next employed an area-under-the-curve (AUC) analysis, also known as the receiver-operating-

characteristic (ROC), a method that has been shown to be useful in validating structure-based virtual screening protocols[14] and is a standard method for evaluating such protocols.[15]

We therefore tested 12 EcUPPS X-ray structures for their ability to separate actives (IC_{50} <100 μM) from decoys (presumed inactive compounds in the decoy library). Several EcUPPS X-ray structures showed a good separation of active from decoy compounds, with AUC values of ~0.8. These structures also demonstrated early enrichment, as evidenced by the steep initial slope of the curve. This means that the best scores were given primarily to active compounds, and suggests that in screening a large compound library, the best scoring compounds would be enriched in UPPS inhibitors. We thus picked the two X-ray structures (PDB codes 2E98 and 4H3A) that provided significant early enrichment and a high AUC in the validation studies, for predictive studies. Using these two X-ray structures, we screened the Chembridge EXPRESS-pick compound library (after filtering) and determined ~400 hits with GlideXP scores less than -7 kcal/mol (lower energy is better). Since many highly ranked compounds were chemically very similar, we clustered the top scoring compounds and selected representatives from each cluster to ensure chemical diversity among the compounds to be tested.

Discovery of novel UPPS inhibitor cores. The screening of the Chembridge EXPRESS-pick compound library using the validated docking protocol resulted in the discovery of three new UPPS inhibitor classes: the 4-oxo-2-thioxo-1,3-thiazolidines, also known as rhodanines (*e.g.* compound **1**), dihydroxyphenyls (the resorcinol, compound **2**), and pyrimidinetrione (a barbiturate analog, compound **3**). None of these have been previously reported to be UPPS inhibitors. All three compounds are predicted to bind in either site 1 or 3 of the 2E98 crystal structure (Figure 5.3), although X-ray crystallographic studies will be required to confirm this binding mode (and our attempts to obtain crystal structures of these systems have not been successful). In any case, the three new inhibitors discovered represent UPPS inhibitors with "drug-like" physico-chemical properties, passing the common drug-like filters as described in the Methods section. The most potent of the 3 compounds was the 4-oxo-2-thioxo-1,3-thiazolidine **1** (IC_{50} ~2.6 μM against *S. aureus* UPPS), which in an initial screen for bioactivity was also found to be active against *B. subtilis*, MIC (Minimal Inhibitory Concentration) ~3 μg/mL (Table 5.1). For this reason, we chose to next investigate analogs based on the 4-oxo-2-thioxo-1,3-thiazolidine core.

Novel core SAR. We next obtained 16 additional compounds from Chembridge, Sigma-Aldrich and from the Drug Synthesis and Chemistry Branch, Developmental Therapeutics Program, Division of Cancer Treatment and Diagnosis, National Cancer Institute (**4**-**19**, Table 5.1) containing the 4-oxo-2-thioxo-1,3-thiazolidine core and tested them for activity against SaUPPS and EcUPPS, as well as a preliminary activity screen against *B. subtilis*, *E. coli* and *S. cerevisiae* (the latter as a general cytotoxicity control, since it lacks UPPS). The alkyl carboxylic acid-containing compounds with the 4-oxo-2-thioxo-1,3-thiazolidine core were active in assays against *B. subtilis* and the most potent compound was **4** (an analog of **1**). **4** was roughly equipotent against SaUPPS and EcUPPS with an IC_{50} of ~2 μM. Additionally, **4** was active against *B. subtilis* with an MIC ~0.43 μg/mL and was very weakly active (~200 μg/mL) against *S. cerevisiae*, indicating that **4** was not generally cytotoxic. Since **1** and **4** showed significant activity in enzymatic and bacterial growth assays, we subsequently tested them against several pathogens. Both **1** and **4** gave MIC values in the high ng/mL to low μg/mL range against *B. anthracis* Sterne, MRSA, VRE, and *L. monocytogenes*, Table 5.2. This promising anti-bacterial activity suggested the potential utility of these UPPS inhibitors in synergizing with other cell wall agents but where significant resistance has emerged, such as with methicillin (MRSA) and vancomycin (VRE).

Synergistic interactions. To investigate the possibility of synergistic interactions with known cell wall biosynthesis inhibitors, we determined the fractional inhibitory concentration index (FICI) values for three systems: MRSA, using **1** + methicillin; VRE, using **1** + vancomycin, and *B. anthracis*, using **1** + ampicillin. The FICI is defined as:

$$FICI = FIC(A) + FIC(B) = MIC(AB)/MIC(A) + MIC(BA)/MIC(B)$$

where FIC(A), FIC(B) are the fractional inhibitory concentrations of drugs A and B, MIC(A) and MIC(B) are the MIC values of drugs A and B acting alone, and MIC(AB) and MIC(BA) are the MIC values of the most effective combination of drug A or B in the presence of drug B or A. Using this method, FICI values of <0.5 represent synergism, >0.5 and <1.0 represent additivity, >1 and <2 represent an indifferent effect, and >2 represents drug antagonism. Isobolograms are shown in Figure 5.4. As can be seen in Figure 5.4A the FICI for **1** + methicillin in MRSA is 0.11, which indicates strong synergism. However, with both VRE (**1** + vancomycin) and *B. anthracis* (**1** + ampicillin) the FICI values are in the 1-2 range, which indicates an indifferent effect.

What is particularly interesting about the most active species investigated here (**1**) is that it has a structure that is very similar to that found in the drug Epalrestat, an aldolase reductase inhibitor[16] that is used to treat diabetic neuropathy and is approved for clinical use in Japan, China and India. This is encouraging because rhodanines as a class are known to often have activity in widely different assays and indeed computer programs such as PAINS[17] categorize e.g. **1**-**4** (as well as Epalrestat) as possible "pan assay interference compounds". This can mean that the compounds cause false positive in assays, or that they may be multi-target inhibitors. In some cases multi-targeting may be undesirable, however, in the context of anti-infective development, multi-targeting is expected to increase efficacy as well as decrease the possibility of resistance developing[18]-both very desirable features.

5.4 Conclusions

The results described above are of interest for several reasons. First, we carried out an *in silico* screen of ~100 known UPPS inhibitors and 1000 decoys using 12 reported UPPS X-ray structures. The two X-ray structures providing the best enrichment in an AUC-ROC analysis were then used to screen a subset of ~100,000 compounds selected for drug-like activity from an initial Chembridge library of ~450,000 compounds. We then tested the ~100 *in silico* hits *in vitro* against SaUPPS and EcUPPS leading to several μM UPPS inhibitors (as deduced from both PPi release and radioactive assays). The most potent lead was **1** which is structurally quite similar to Epalrestat, in clinical use to treat diabetic neuropathy. **1** (and its analog **4**) inhibited the growth of Gram positives; they did not inhibit the growth of Gram negatives (important with *E. coli* in the context of maintaining commensal microflora) and they had no activity against *S. cerevisiae*. Activity against *B. anthracis*, *S. aureus*, a vancomycin-resistant *Enterococcus* spp. as well as *Listeria monocytogenes* was good-in the 0.125-4 μg/mL range, and there was very strong synergy (FICI=0.11) with methicillin and **1** in a MRSA strain of *S. aureus* suggesting that **1** could be a promising lead (in combination therapies) for treating staph infections.

5.5 Experimental Section

Computational aspects. Following the methods described in previous work[12] we docked 112 known UPPS inhibitors having IC_{50} values <100 μM, together with 1000 decoys from the

Schrodinger decoy collection (having an average molecular weight of 400 Da), to *E. coli* UPPS (hereafter, EcUPPS). Docking was performed using the Glide[19,20,21] program and compounds were ranked by their Glide XP score. The proteins were prepared by stripping water and ligand molecules, capping and neutralizing any unsolved loops, followed by preparation with the Schrodinger protein preparation wizard using standard parameters.[22] After docking, compounds were ranked by their docking score, then area under the curve (AUC) analyses were performed. Retrospective enrichment was quite good for 2/12 structures (PDB codes 2E98 and 4H3A) so we docked into these structures for the prospective studies (Figure 5.1). 2E98 is an EcUPPS X-ray structure containing four lipophilic bisphosphonates (BPH-629; IC_{50} ~300 nM), which bind to sites 1-4, one inhibitor to each site.[8] 4H3A is an EcUPPS structure containing a diketo acid inhibitor (BPH-1330) which has a 2 μM IC_{50} and the inhibitor binds (in the solid-state) only to site 4.[10,12] These structures thus have significant differences: only site 4 is occupied in 4H3A, while in 2E98, all four sites are occupied and the protein is in a "wide-open" conformation (Figure 5.2).

To find new inhibitors, we began with a library of ~450,000 commercially available compounds, the Chembridge Experimental Library. The library was filtered to exclude compounds that had undesired, toxic or reactive functional groups; known promiscuous binders; MW >460 Da or MW <250 Da; more than 4 chiral centers; polar surface area (PSA) >150 $Å^2$ or PSA <50 $Å^2$; number of rotatable bonds >10; or clogP >5 or clogP <-2. Salts were also removed. Next, the selected compounds (~100,000) were loaded into Schrodinger's virtual screening workflow where they were prepared with Ligprep and then docked using the filtering procedure for efficiency and only retaining the top 20% of compounds in the two rapid, initial docking modules HTVS (top 20% retained) and SP (top 20% retained). Finally, Glide XP was used to assign a final docking score to each molecule. AUC analyses on active and decoy datasets were previously performed using the Glide XP module, however, this was impractical for the large filtered Chembridge library. Therefore, we relied on HTVS and SP modules to provide early filtering before employing the more time intensive XP protocol.

We then extracted the ~400 top scoring compounds (docking score less than -7 kcal/mol). Binary Molprint2D fingerprints were generated using Canvas and 40 clusters were generated using K-means clustering.[23,24] Of these 40 clusters, the top scoring compounds from each cluster were visually inspected and a representative was chosen from each cluster, resulting in a final list of 100 compounds. These were purchased from Chembridge (Chembridge Corporation, San Diego, CA)

and then assayed for UPPS inhibition activity. Three out of the 100 compounds were UPPS inhibitors. Similarity searches based on these active compounds were then performed using Pubchem and SciFinder and additional compounds were obtained and tested.

Enzyme and cell growth inhibition assays.

***Protein Expression and Purification*.** EcUPPS and SaUPPS were expressed and purified as described previously.[8] Molecular weights and purities were verified by mass spectrometry and SDS-PAGE, respectively.

***UPPS Inhibition Screening*.** The UPPS inhibition assays were carried out as described previously.[8] Briefly, the condensation of FPP with IPP catalyzed by UPPS was monitored by using a continuous spectrophotometric assay[25] in 96 well plates with 200 μL reaction mixtures containing 400 μM 2-amino-6-mercapto-7-methylpurine ribonucleoside (MESG), 350 μM IPP, 35 μM FPP, 20 mM Tris·HCl buffer (pH 7.5), 0.01 % v/v Triton X-100, and 1 mM $MgCl_2$. The IC_{50} values were obtained by fitting the inhibition data to a rectangular hyperbolic dose-response function using GraphPad PRISM 4.0 software (Graphpad Software, San Diego, CA). The IC_{50} values for the most active hits were verified using a radiometric assay[26] with 2.5 μM FPP, 25 μM [^{3}H] IPP and 0.01 % v/v Triton X-100.

Cell strains. *Bacillus subtilis* subsp. *subtilis* (ATCC® 6051™), *Escherichia coli* (ATCC® 29425™), and *Saccharomyces cerevisiae* (ATCC® 208352™) were purchased from the American Type Culture Collection. *Bacillus subtilis* strain 168, *Bacillus anthracis* strain Sterne, *Listeria monocytogenes* strain 4b F2365, *Staphylococcus aureus* USA300 (methicillin-resistant), *E. coli* MC400, *Pseudomonas putida* and *Enterococcus faecalis* U503 (vancomycin-resistant) were from our laboratory strain collection[27].

E. coli* ATCC® 29425™ *growth inhibition assay. IC_{50} values for *E. coli* growth inhibition were determined by using a micro-broth dilution method. A 16 h culture of *E. coli* was diluted 50-fold into fresh Luria-Bertani (LB) broth and grown to an OD_{600} of ~0.4. The culture was then diluted 500-fold into fresh LB medium and 100 μL was inoculated into a 96-well flat bottom culture plate (Corning Inc., Corning, NY). The starting concentration of each compound was 0.3 mM and this was 2-fold serially diluted. Plates were incubated for 3 h at 37 °C to mid-exponential phase. An (3-(4, 5-dimethylthiazole-2-yl)-2, 5-diphenyltetrazolium bromide (MTT) cell proliferation assay (ATCC) was then carried out to obtain bacterial viability dose-response curves. 10 μL MTT

reagent was added into each well, followed by incubation for 2-4 h until a purple precipitate was visible. Then, 100 μL detergent reagent was added and plates were further incubated in the dark at 23 °C for 2 h. The absorbance was recorded at 570 nm. A non-linear regression analysis was then carried out using Origin 6.1. For each inhibitor, two independent experiments were performed and the IC_{50} values found were averaged.

B. subtilis* ATCC® 6051™ *growth inhibition assay. A 16 h culture of *B. subtilis* was diluted 50-fold into fresh Luria-Bertani (LB) broth and incubated to an OD_{600} of ~ 0.4. The culture was then diluted 500-fold into fresh LB medium and 100 μL were inoculated into a 96 well flat bottom culture plate (Corning Inc., Corning, NY). The starting concentration of each compound was 0.5 mM and was then serial diluted. Plates were incubated for 12-16 h at 37 °C. The absorbance was recorded at 570 nm. A non-linear regression analysis was carried out on the data obtained using Origin 6.1. For each inhibitor, two independent experiments were performed and the IC_{50} values found were averaged.

S. cerevisiae growth inhibition assay. The protocol was the same as with the *B. subtilis* assay protocol except that YPD medium was used and the 96-well plate was incubated for 36 h instead of 12-16 h.

Evaluation of 1 and 4 inhibitory activity and synergy. *B. subtilis* strain 168, *B. anthracis* strain Sterne, *E. coli* MC400, and *P. putida* were grown to stationary phase in 10 mL of Bb broth at 37 °C. *S. aureus* USA300 (methicillin-resistant), *E. faecalis* U503 (vancomycin-resistant), and *L. monocytogenes* strain 4b F2365 were grown to stationary phase in 10 mL brain-heart infusion (BHI) medium at 37 °C. The cultures were adjusted to an OD_{600} of 0.016 in the designated medium before being added to 96-well microplates. Successive two-fold dilutions of compounds **1** and **4** were added to the cultures (0.25–64 μg mL^{-1}). As a control, kanamycin (1–32 μg mL^{-1}) was added to samples of *E. coli*, *B. subtilis*, *B. anthracis*, *P. putida* and *L. monocytogenes*. Gentamycin was used as a control for *S. aureus* and *E. faecalis* with dilutions from 1-64 μg mL^{-1}. As a negative control, an equal volume of DMSO lacking antibiotic was used. Plates were covered and incubated at 37 °C for 16 h with shaking. The minimum inhibitory concentration (MIC) that suppressed at least 99% of bacterial growth was established based on culture turbidity in the micro-broth dilution assay. The assay was repeated in three replicates and values were averaged. Isobolograms were carried out as previously described.[28]

Inhibitor characterization.

The purities of the key compounds investigated, obtained from Chembridge (**1** and **4**), were determined by high-performance liquid chromatography and structures verified by NMR spectroscopy and high resolution mass spectrometry (Figure 5.5-5.12) and were consistent with the structures provided by the vendor. Purities were >95% by HPLC.

5.6 Schemes, Charts, Tables and Figures

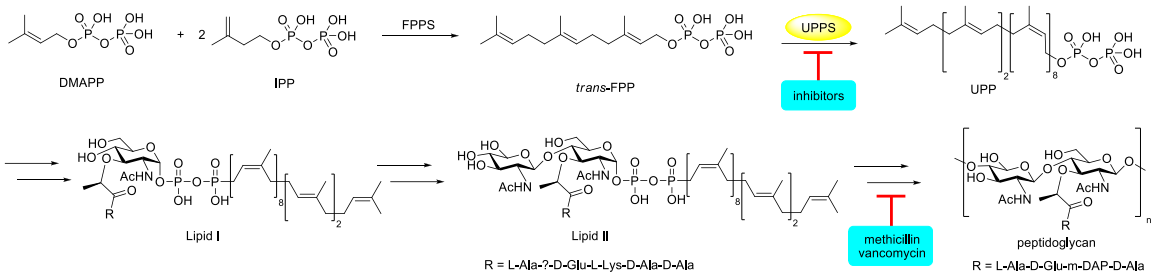

Figure 5.1. Undecaprenyl diphosphate synthase reaction and relationship of UPP to bacterial cell wall biosynthesis.

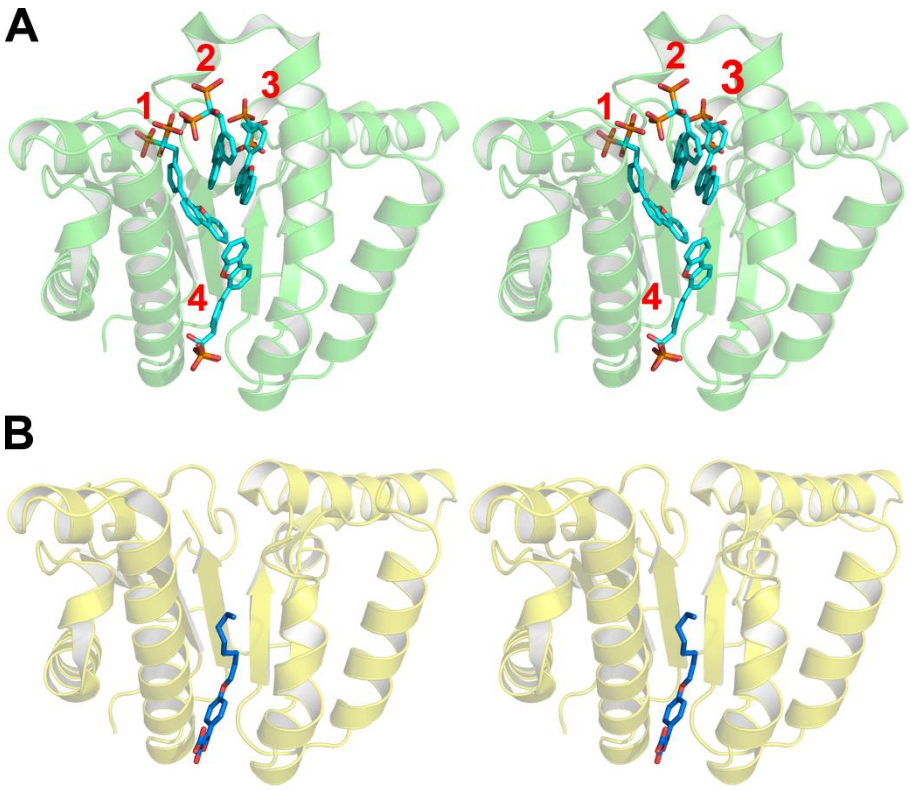

Figure 5.2. Stereo presentation of the X-ray structures chosen for further virtual screening from docking and ROC analysis. A, 2E98 showing all four inhibitor binding sites. B, 4H3A showing one inhibitor bound to site 4.

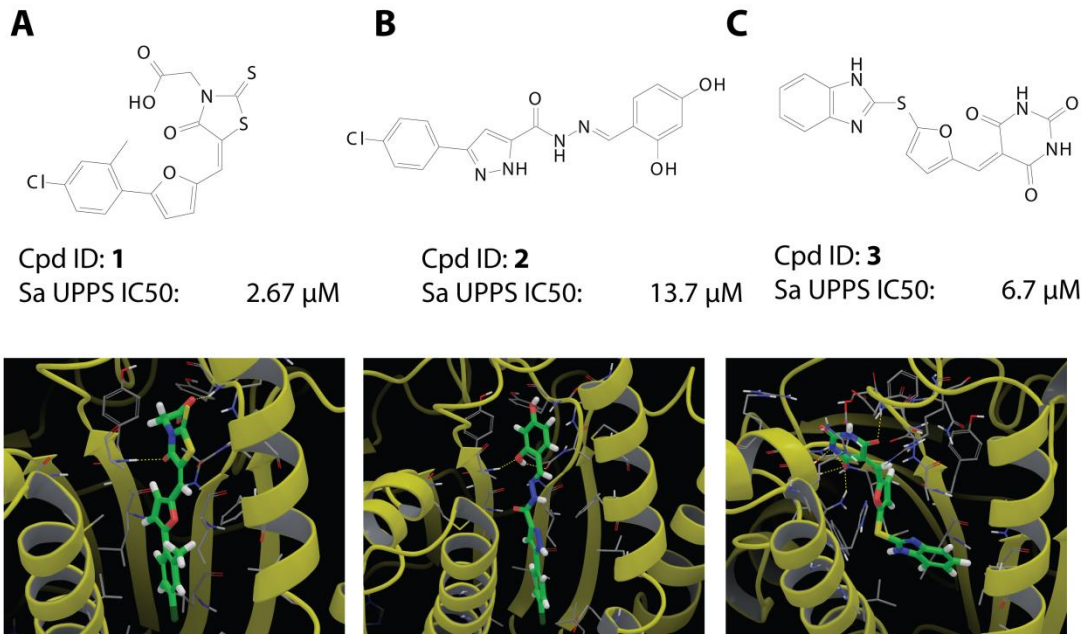

Figure 5.3. Three new classes of UPPS inhibitors discovered via virtual screening. A, chemical structure and computed docking mode of compound **1**, a rhodanine derivative. B, chemical structure and docking mode of compound **2**, a resorcinol derivative. C, same for compound **3**, a barbiturate.

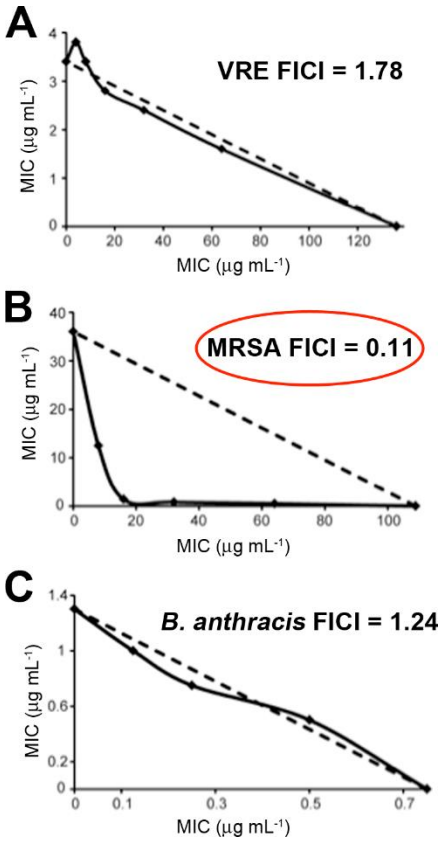

Figure 5.4. *In vitro* synergy assays. Isobolograms for growth inhibition of VRE, MRSA, and *B. anthracis* strain Sterne. A, **1** and vancomycin inhibition of *E. faecalis* U503 (vancomycin-resistant, VRE). FICI = 1.78. B, **1** and methicillin inhibition of *S. aureus* (USA300). FICI = 0.11. C, **1** and ampicillin inhibition of *B. anthracis* strain Sterne. FICI =1.24.

ID	Structure	Vendor #	EcUPPS IC_{50}	SaUPPS IC_{50}	*B. subtilis*	*E. coli*	*S. cerevisiae*
1	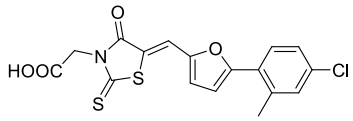	CB 7471392	260	2.7	2.9	>200	>200
4	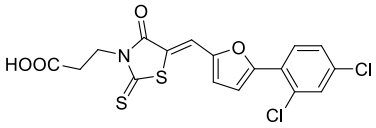	CB 5523169	2.1	2.4	0.43	>200	180
5	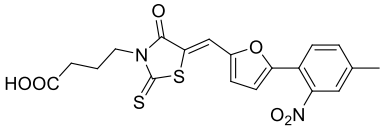	L339644	>100	5.7	3.2	>200	>200
6	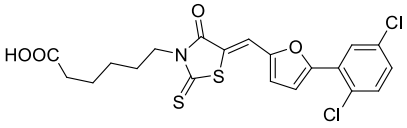	L339822	>100	3.8	5.6	>200	>200
7	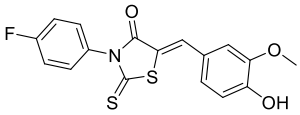	CB 5674456	41	150	>200	>200	>200
8	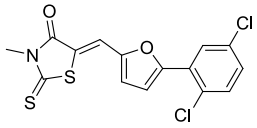	CB 5143717	>200	>200	>200	>200	>200
9	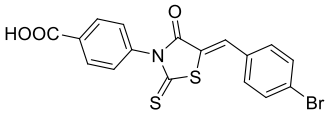	CB 5280379	>200	170	>200	>200	>200
10	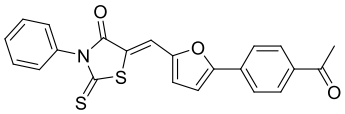	CB 5377413	85	32	>200	>200	>200
11	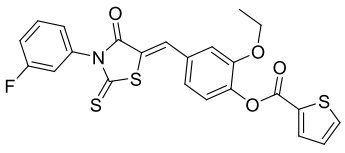	CB 6824270	>200	>200	>200	>200	>200

Table 5.1. 4-oxo-2-thioxo-1,3-thiazolidines investigated in UPPS and bacterial cell growth inhibition assays. All concentrations are in µM.

ID	Structure	Vendor #	EcUPPS IC_{50}	SaUPPS IC_{50}	*B. subtilis*	*E. coli*	*S. cerevisiae*
12	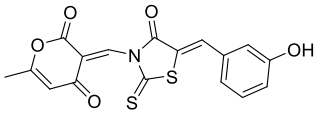	NCI 660017	>100	>100	>200	>200	>200
13	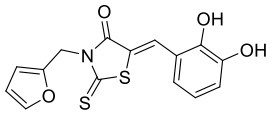	NCI 343985	>100	5.3	>200	>200	>200
14	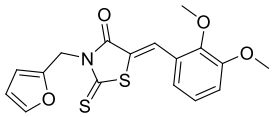	NCI 337736	>100	>100	>200	>200	>200
15	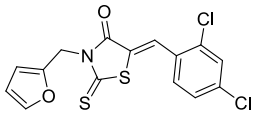	NCI 320208	>100	>100	>200	>200	>200
16	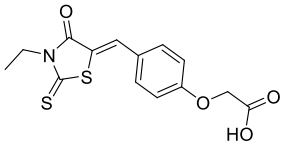	NCI 90950	>100	>100	>200	>200	>200
17	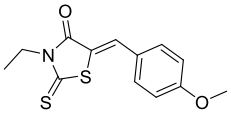	NCI 36005	>100	>100	>200	>200	>200
18	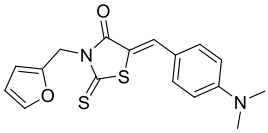	NCI 320207	>100	>100	>200	>200	>200
19	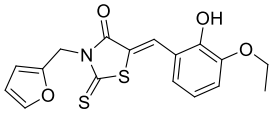	NCI 318219	>100	>100	>200	>200	>200

Table 5.1 (cont.). 4-oxo-2-thioxo-1,3-thiazolidines investigated in UPPS and bacterial cell growth inhibition assays. All concentrations are in μM.

	Compound **1**	Compound **4**
	MIC (μg/mL)	MIC (μg/mL)
	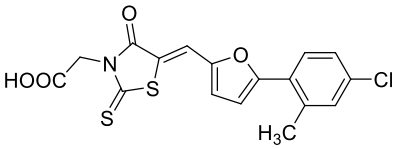	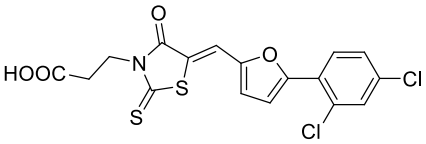
Bacillus subtilis	1	0.125
Bacillus anthracis	1	0.25
Staphylococcus aureus (MRSA)	8	4
Enterococcus faecalis (VRE)	1	4
Listeria monocytogenes	4	0.125
Pseudomonas putida	>64	>64
Escherichia coli	>64	>64

Table 5.2. MIC values for two 4-oxo-2-thioxo-1,3-thiazolidine analogs, compounds **1** and **4,** tested in diverse bacterial cell growth inhibition assays. The compounds were tested against a panel of both Gram-positive (top five) and Gram-negative (lower two) bacteria.

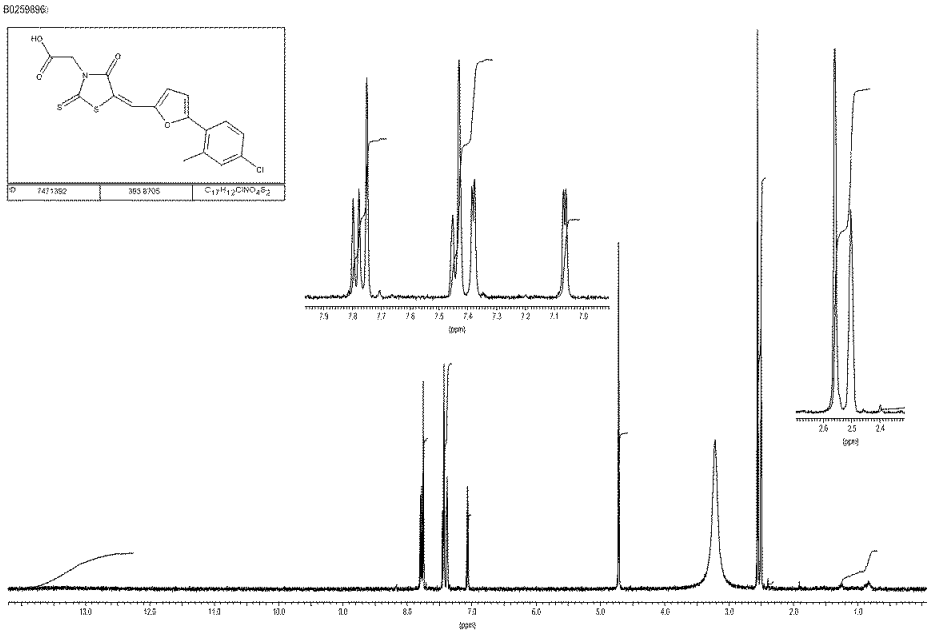

Figure 5.5. ^{1}H NMR of compound **1**

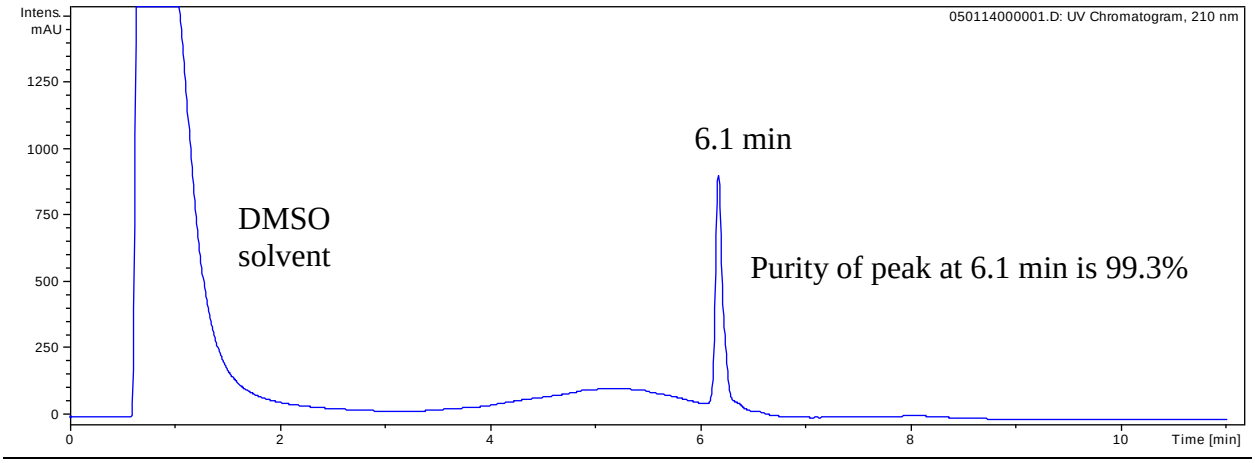

Figure 5.6. LC/MS analysis of compound **1**: UV chromatogram at 210

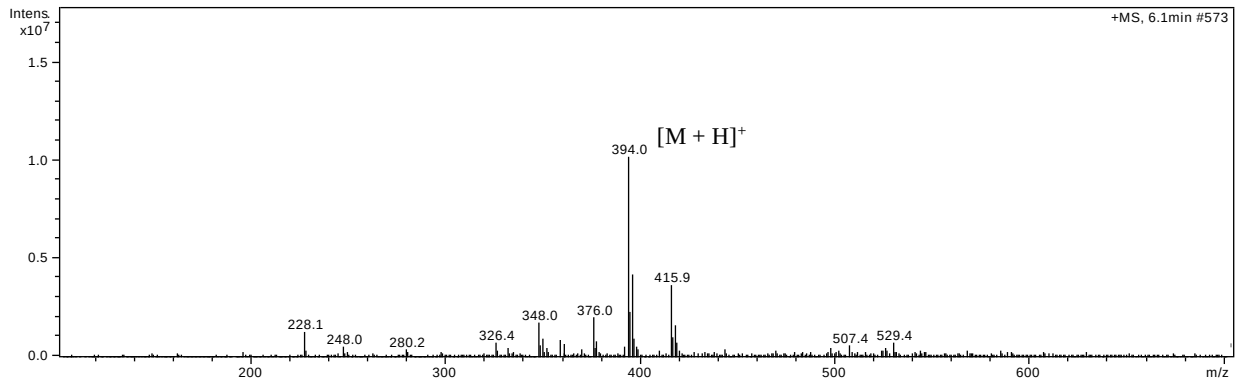

Figure 5.7. Mass spectrum for the peak at 6.1 min (compound **1**)

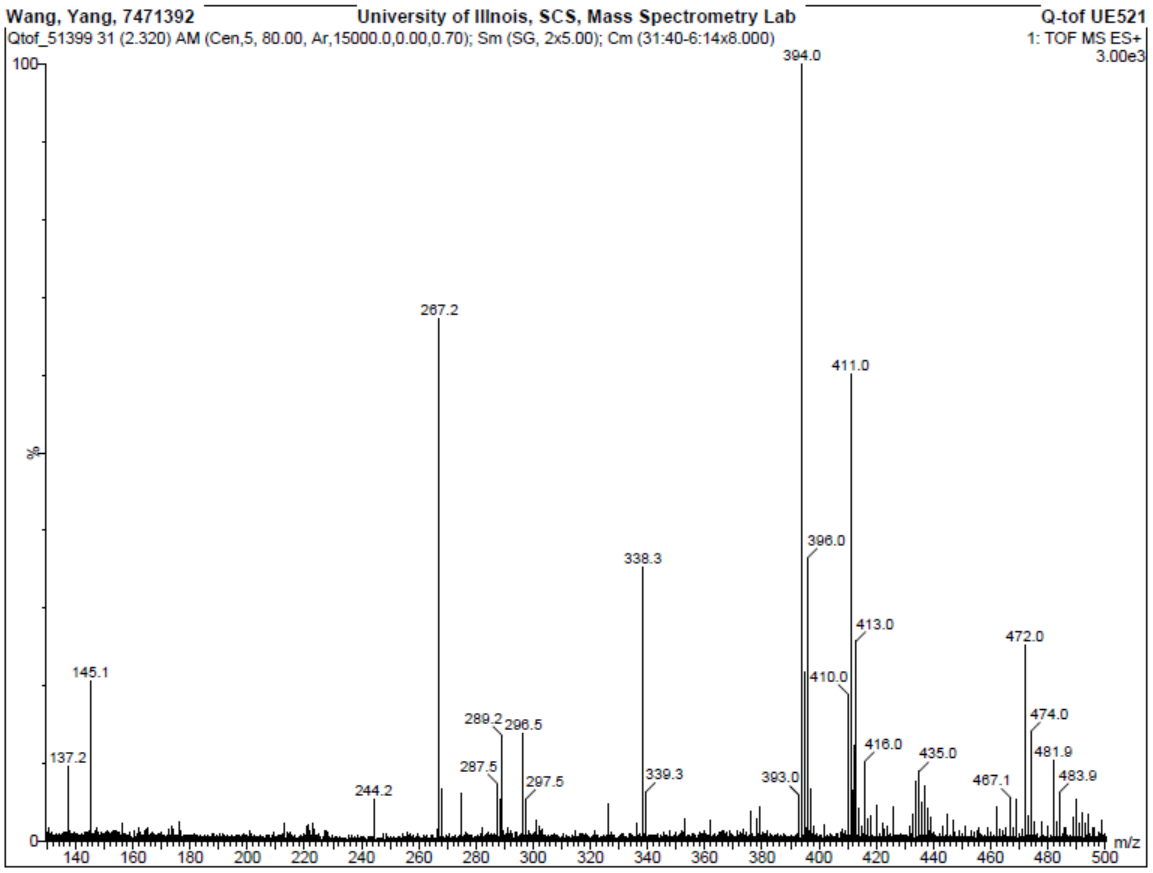

Elemental Composition Report

Single Mass Analysis
Tolerance = 10.0 PPM / DBE: min = -1.5, max = 600.0
Element prediction: Off
Number of isotope peaks used for i-FIT = 3

Monoisotopic Mass, Even Electron Ions
23 formula(e) evaluated with 1 results within limits (all results (up to 1000) for each mass)
Elements Used:
C: 0-125 H: 0-250 N: 0-1 O: 3-5 S: 2-2 Cl: 1-1

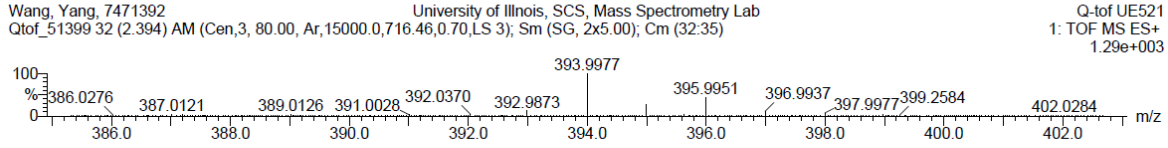

Minimum:				-1.5		
Maximum:		5.0	10.0	600.0		
Mass	Calc. Mass	mDa	PPM	DBE	i-FIT	Formula
393.9977	393.9975	0.2	0.5	11.5	6.2	C17 H13 N O4 S2 Cl

Figure 5.8. High-resolution mass spectrum of compound **1**

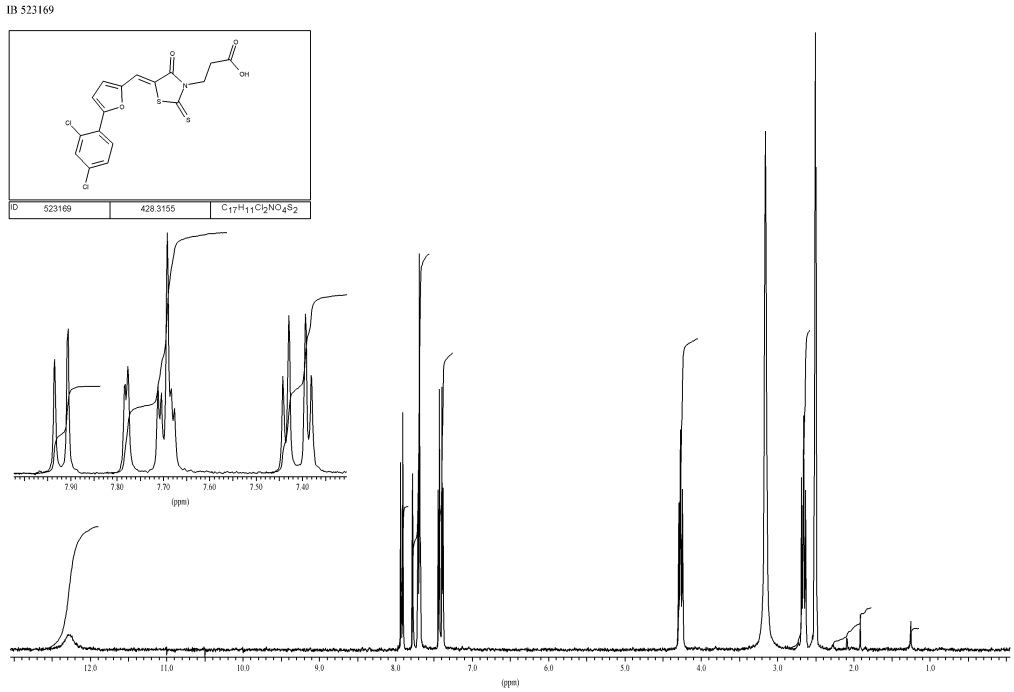

Figure 5.9. ^{1}H NMR of compound **4**

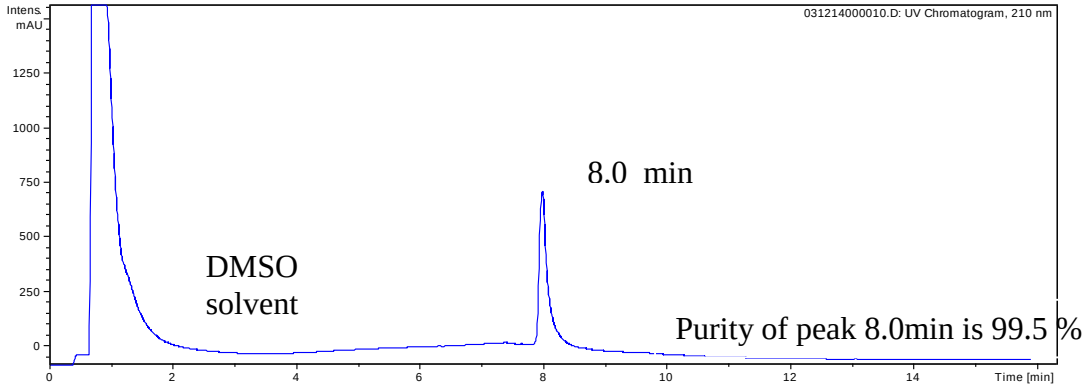

Figure 5.10. LC/MS analysis of compound **4**: UV chromatogram at 210

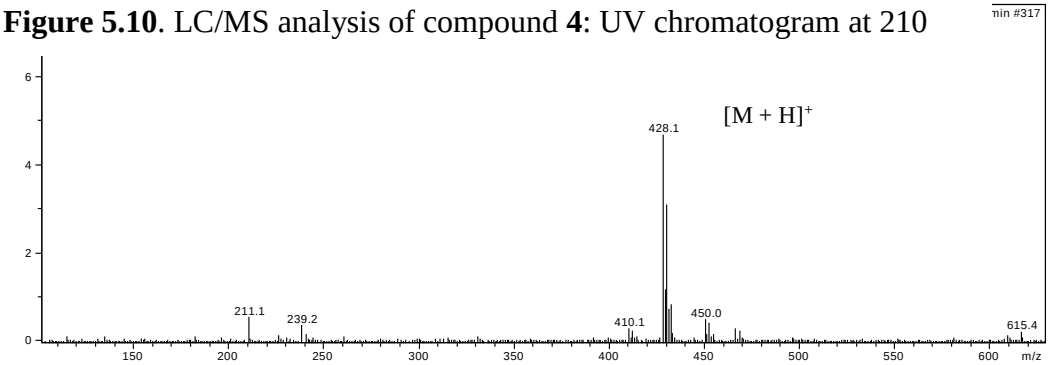

Figure 5.11. Mass spectrum for the peak at 8.0 min (compound **4**)

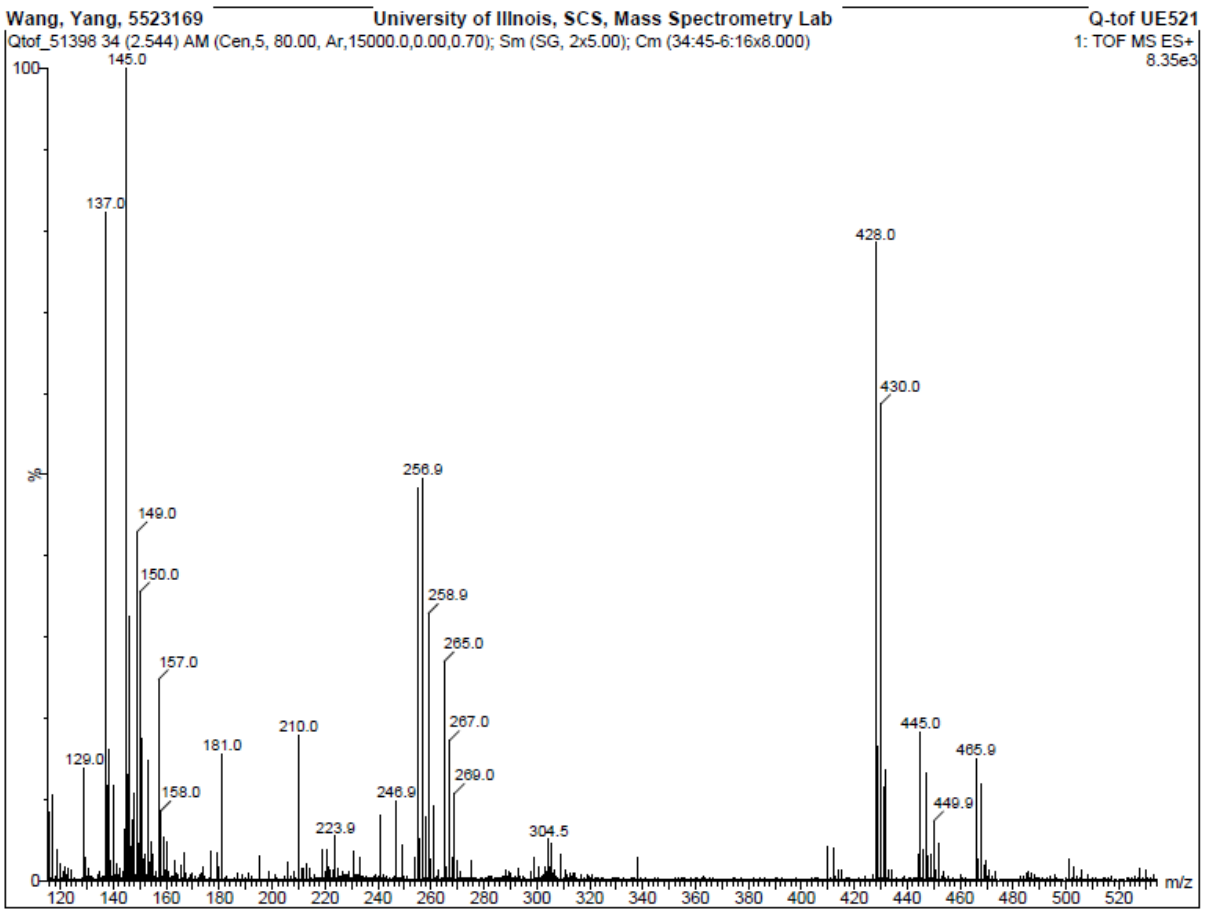

Elemental Composition Report

Single Mass Analysis
Tolerance = 10.0 PPM / DBE: min = -1.5, max = 600.0
Element prediction: Off
Number of isotope peaks used for i-FIT = 3

Monoisotopic Mass, Even Electron Ions
22 formula(e) evaluated with 1 results within limits (all results (up to 1000) for each mass)
Elements Used:
C: 0-125 H: 0-250 N: 0-1 O: 3-5 S: 2-2 Cl: 2-2

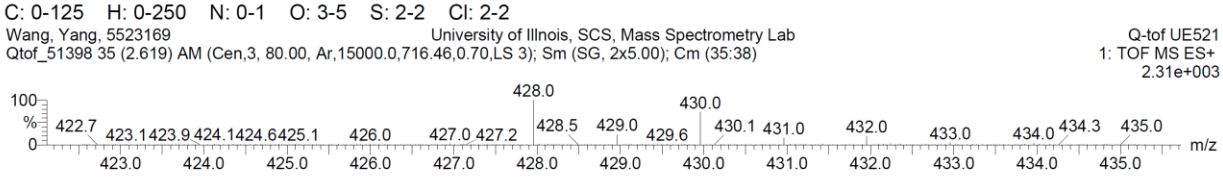

Minimum:				-1.5		
Maximum:		5.0	10.0	600.0		
Mass	Calc. Mass	mDa	PPM	DBE	i-FIT	Formula
427.9586	427.9585	0.1	0.2	11.5	2.2	C17 H12 N O4 S2 Cl2

Figure 5.12. High-resolution mass spectrum of compound **4**

5.7 References

1. Fischbach, M. A.; Walsh, C. T. Antibiotics for emerging pathogens. *Science* **2009**, *325*, 1089-1093.
2. Butler, M. S.; Cooper, M. A. Antibiotics in the clinical pipeline in 2011. *J. Antibiot. (Tokyo)* **2011**, *64*, 413-425.
3. van Heijenoort, J. Lipid intermediates in the biosynthesis of bacterial peptidoglycan. *Microbiol. Mol. Biol. Rev.* **2007**, *71*, 620-635.
4. Apfel, C. M.; Takacs, S.; Fountoulakis, M.; Stieger, M.; Keck, W. Use of genomics to identify bacterial undecaprenyl pyrophosphate synthetase: Cloning, expression, and characterization of the essential uppS gene. *J. Bacteriol.* **1999**, *181*, 483-492.
5. Payne, D. J.; Gwynn, M. N.; Holmes, D. J.; Pompliano, D. L. Drugs for bad bugs: confronting the challenges of antibacterial discovery. *Nat. Rev. Drug Discov.* **2007**, *6*, 29-40.
6. Peukert, S.; Sun, Y. C.; Zhang, R.; Hurley, B.; Sabio, M.; Shen, X. Y.; Gray, C.; Dzink-Fox, J.; Tao, J. S.; Cebula, R.; Wattanasin, S. Design and structure-activity relationships of potent and selective inhibitors of undecaprenyl pyrophosphate synthase (UPPS): Tetramic, tetronic acids and dihydropyridin-2-ones. *Bioorg. Med. Chem. Lett.* **2008**, *18*, 1840-1844.
7. Lee, L. V.; Granda, B.; Dean, K.; Tao, J. S.; Liu, E.; Zhang, R.; Peukert, S.; Wattanasin, S.; Xie, X. L.; Ryder, N. S.; Tommasi, R.; Deng, G. J. Biophysical Investigation of the Mode of Inhibition of Tetramic Acids, the Allosteric Inhibitors of Undecaprenyl Pyrophosphate Synthase. *Biochemistry* **2010**, *49*, 5366-5376.
8. Guo, R. T.; Cao, R.; Liang, P. H.; Ko, T. P.; Chang, T. H.; Hudock, M. P.; Jeng, W. Y.; Chen, C. K. M.; Zhang, Y. H.; Song, Y. C.; Kuo, C. J.; Yin, F. L.; Oldfield, E.; Wang, A. H. J. Bisphosphonates target multiple sites in both cis- and trans-prenyltransferases. *Proc. Natl. Acad. Sci. U. S. A.* **2007**, *104*, 10022-10027.
9. Durrant, J. D.; Cao, R.; Gorfe, A. A.; Zhu, W.; Li, J. K.; Sankovsky, A.; Oldfield, E.; McCammon, J. A. Non-Bisphosphonate Inhibitors of Isoprenoid Biosynthesis Identified via Computer-Aided Drug Design. *Chem. Biol. Drug. Des.* **2011**, *78*, 323-332.
10. Zhang, Y. H.; Lin, F. Y.; Li, K.; Zhu, W.; Liu, Y. L.; Cao, R.; Pang, R.; Lee, E. H.; Axelson, J.; Hensler, M.; Wang, K.; Molohon, K. J.; Wang, Y.; Mitchell, D. A.; Nizet, V.; Odfied, E. HIV-1 Integrase Inhibitor-Inspired Antibacterials Targeting Isoprenoid Biosynthesis. *ACS Med. Chem. Lett.* **2012**, *3*, 402-406.
11. Lindert, S.; Zhu, W.; Liu, Y. L.; Pang, R.; Oldfield, E.; McCammon, J. A. Farnesyl Diphosphate Synthase Inhibitors from *In Silico* Screening. *Chem. Biol. Drug. Des.* **2013**, *81*, 742-748.
12. Zhu, W.; Zhang, Y. H.; Sinko, W.; Hensler, M. E.; Olson, J.; Molohon, K. J.; Lindert, S.; Cao, R.; Li, K.; Wang, K.; Wang, Y.; Liu, Y. L.; Sankovsky, A.; de Oliveira, C. A. F.; Mitchell, D. A.; Nizet, V.; McCammon, J. A.; Oldfield, E. Antibacterial drug leads targeting isoprenoid biosynthesis. *Proc. Natl. Acad. Sci. U. S. A.* **2013**, *110*, 123-128.
13. Sinko, W.; de Oliveira, C.; Williams, S.; Van Wynsberghe, A.; Durrant, J. D.; Cao, R.; Oldfield, E.; McCammon, J. A. Applying molecular dynamics simulations to identify rarely sampled ligand-bound conformational states of undecaprenyl pyrophosphate synthase, an antibacterial target. *Chem. Biol. Drug. Des.* **2011**, *77*, 412-420.

14. Triballeau, N.; Acher, F.; Brabet, I.; Pin, J. P.; Bertrand, H. O. Virtual screening workflow development guided by the "receiver operating characteristic" curve approach. Application to high-throughput docking on metabotropic glutamate receptor subtype 4. *J. Med. Chem.* **2005**, *48*, 2534-2547.
15. Christofferson, A. J.; Huang, N. *How to Benchmark Methods for Structure-Based Virtual Screening of Large Compound Libraries*; Computational Drug Discovery and Design, 2012; Vol. 819.
16. Ramirez, M. A.; Borja, N. L. Epalrestat: An aldose reductase inhibitor for the treatment of diabetic neuropathy. *Pharmacotherapy* **2008**, *28*, 646-655.
17. Baell, J. B.; Holloway, G. A. New Substructure Filters for Removal of Pan Assay Interference Compounds (PAINS) from Screening Libraries and for Their Exclusion in Bioassays. *J. Med. Chem.* **2010**, *53*, 2719-2740.
18. Li, K.; Schurig-Briccio, L. A.; Feng, X. X.; Upadhyay, A.; Pujari, V.; Lechartier, B.; Fontes, F. L.; Yang, H. L.; Rao, G. D.; Zhu, W.; Gulati, A.; No, J. H.; Cintra, G.; Bogue, S.; Liu, Y. L.; Molohon, K.; Orlean, P.; Mitchell, D. A.; Freitas-Junior, L.; Ren, F. F.; Sun, H.; Jiang, T.; Li, Y. J.; Guo, R. T.; Cole, S. T.; Gennis, R. B.; Crick, D. C.; Oldfield, E. Multitarget Drug Discovery for Tuberculosis and Other Infectious Diseases. *J. Med. Chem.* **2014**, *57*, 3126-3139.
19. Friesner, R. A.; Murphy, R. B.; Repasky, M. P.; Frye, L. L.; Greenwood, J. R.; Halgren, T. A.; Sanschagrin, P. C.; Mainz, D. T. Extra precision glide: docking and scoring incorporating a model of hydrophobic enclosure for protein-ligand complexes. *J. Med. Chem.* **2006**, *49*, 6177-6196.
20. Halgren, T. A.; Murphy, R. B.; Friesner, R. A.; Beard, H. S.; Frye, L. L.; Pollard, W. T.; Banks, J. L. Glide: a new approach for rapid, accurate docking and scoring. 2. Enrichment factors in database screening. *J. Med. Chem.* **2004**, *47*, 1750-1759.
21. Schrödinger, L. L. C. *Suite 2011: Glide, version 5.7*; Schrödinger LLC: New York 2011.
22. Sastry, G. M.; Adzhigirey, M.; Day, T.; Annabhimoju, R.; Sherman, W. Protein and ligand preparation: parameters, protocols, and influence on virtual screening enrichments. *J Comput. Aided Mol. Des.* **2013**, *27*, 221-234.
23. Duan, J. X.; Dixon, S. L.; Lowrie, J. F.; Sherman, W. Analysis and comparison of 2D fingerprints: Insights into database screening performance using eight fingerprint methods. *J. Mol. Graph. Model.* **2010**, *29*, 157-170.
24. Sastry, M.; Lowrie, J. F.; Dixon, S. L.; Sherman, W. Large-Scale Systematic Analysis of 2D Fingerprint Methods and Parameters to Improve Virtual Screening Enrichments. *J. Chem. Inf. Model.* **2010**, *50*, 771-784.
25. Webb, M. R. A continuous spectrophotometric assay for inorganic phosphate and for measuring phosphate release kinetics in biological systems. *Proc. Natl. Acad. Sci. U. S. A.* **1992**, *89*, 4884-4887.
26. Li, H.; Huang, J.; Jiang, X.; Seefeld, M.; McQueney, M.; Macarron, R. The effect of triton concentration on the activity of undecaprenyl pyrophosphate synthase inhibitors. *J. Biomol. Screen* **2003**, *8*, 712-715.
27. Molohon, K. J.; Melby, J. O.; Lee, J.; Evans, B. S.; Dunbar, K. L.; Bumpus, S. B.; Kelleher, N. L.; Mitchell, D. A. Structure determination and interception of biosynthetic intermediates for the plantazolicin class of highly discriminating antibiotics. *ACS Chem. Biol.* **2011**, *6*, 1307-1313.

28. Leon, A.; Liu, L.; Yang, Y.; Hudock, M. P.; Hall, P.; Yin, F. L.; Studer, D.; Puan, K. J.; Morita, C. T.; Oldfield, E. Isoprenoid biosynthesis as a drug target: Bisphosphonate inhibition of *Escherichia coli* K12 growth and synergistic effects of fosmidomycin. *J. Med. Chem.* **2006**, *49*, 7331-7341.

Chapter 6: Bacterial Cell Growth Inhibitors Targeting Undecaprenyl Diphosphate Synthase and Undecaprenyl Diphosphate Phosphatase

6.1 Notes and Acknowledgements

Y.W. and E.O. designed research; Y.W. and K.W. synthesized the compounds; Y.W. and J.D. performed enzyme inhibition experiments; Y.W. and J.D. performed cell growth inhibition experiments; Y.W. J.D. and E.O. analyzed data.

This work was supported by the United States Public Health Service (National Institutes of Health Grants GM065307, CA158191, GM08326, GM31749 and HD071600.

6.2 Introduction

There is without doubt a pressing need for the development of novel antibiotics having new structures and new targets, to help combat the development of drug resistance.[1] Over the past ~70 years, many antibiotics that target bacterial cell wall biosynthesis, compounds such as penicillin, methicillin and bacitracin, have been discovered and developed and so the enzymes that are used in cell wall biosynthesis are attractive drug targets. A simplified version of cell wall biosynthesis is shown in Figure 6.1. Initial steps involve formation of the (C_5) isoprenoids dimethylallyl diphosphate (DMAPP, **1**) and isopentenyl diphosphate (IPP, **2**), formed in either the mevalonate pathway (in e.g. *Staphylococcus aureus*) or the 2-*C*-methyl-D-erythritol 4-phosphate (MEP) pathway (in e.g. *E. coli*), with fosmidomycin inhibiting the MEP pathway.[2]

DMAPP then condenses, sequentially, with two molecules of IPP to form the (C_{15}) species, farnesyl diphosphate (FPP, **3**) in a reaction catalyzed by farnesyl diphosphate synthase (FPPS). The FPP so produced then condenses with 8 additional IPP molecules to form (C_{55}) undecaprenyl diphosphate (UPP, **4**) in a reaction catalyzed by undecaprenyl diphosphate synthase (UPPS). UPPS is an attractive drug target since it is not used by humans and several inhibitors (tetramic/tetronic acids; diamidines and benzoic acids) have been reported.[3-4] UPP is then converted by undecaprenyl diphosphate phosphatase (UPPP) to undecaprenyl phosphate (UP, **5**) which acts as a membrane "anchor" for formation of glycosylated products (Lipid I, Lipid II) which are then converted to peptidoglycan cell-wall products, as outlined in Figure 6.1. Antibiotics such as bacitracin, vancomycin and methicillin target these later stages in cell wall biosynthesis, again as shown in Figure 6.1. In this work, we sought to find novel benzoic acid inhibitors of UPPS and potentially

UPPP since in earlier work[4] we had found that (2-(3-(decyloxy)benzamido)-5-nitrobenzoic acid, **6**) inhibited UPPS. We thus synthesized 30 analogs of **6**, **7**-**36**, primarily benzoic acids but also, four phosphonic acid analogs, and tested them for activity against *Staphylococcus aureus* and *Bacillus subtilis*. We also investigated their possible synergistic activity with a range of known antibiotics that either target, or do not target, bacterial cell wall biosynthesis, in order to narrow down possible targets, in addition to testing them for activity against UPPS and UPPP and in several cases, FPPS.

6.3 Results and Discussion

In previous work we found that the benzoic acid **6** was a promising inhibitor of both *E. coli* UPPS (EcUPPS; IC_{50} = 3 μM) and *S. aureus* UPPS (SaUPPS; IC_{50} = 0.49 μM), but there was no activity against the Gram-negative bacterium, *E. coli*, presumably because of poor cell penetration. However, in later work we found that several related lipophilic benzoic acids had activity against Gram positive (but not Gram negative) bacteria, leading us to synthesize the 30 compounds whose structures and activities are shown in Table 6.1. Full synthesis and characterization details are in the Supporting Information. We investigated the cell growth inhibition activity of these compounds against *S. aureus* and *B. subtilis* and IC_{50} values (in μg/mL) are shown in Table 6.1. Typical dose response curves for 3 compounds: benzoic acids with electron withdrawing (**7**) or electron donating (**13**) ring substituents, plus a phosphonic acid analog (**18)**, are shown in Figure 6.1. There were several active compounds with in the case of **11**, an IC_{50} value of 0.082 μg/mL (180 nM) against *S. aureus*. The most active bacterial cell growth inhibitors were all lipophilic benzoic acids with highly electron-withdrawing (-NO_2, -OCF_3) ring substituents, Table 6.1.

The question then arises: what might be the targets of these inhibitors? Such lipophilic, anionic species could be isosteres of e.g. intermediates in fatty acid biosynthesis, or of isoprenoid phosphates or diphosphates, and as noted above we previously found that **6** inhibited and bound to UPPS (PDB ID code 4H2O; 4), so UPPS inhibition appeared likely, but FPPS and UPPP inhibition also seemed possible (with some carboxylic acids being known, potent FPPS inhibitors,[5] binding to an allosteric site). Moreover, if these molecules have a similar pharmocophore to e.g. FPP, then there could be other targets, such as MenA, involved in quinone biosynthesis, as well as enzymes involved in heme A biosynthesis.[6] To try and narrow down the possibilities as well as open up potential routes to synergistic combinations, we next investigated whether or not one of

the most active compounds, the fluoro-benzoic acid **7**, exhibited synergistic, additive, indifferent or antagonistic activity with a broad range of antibiotics that act either by inhibiting bacterial cell wall biosynthesis, or by other mechanisms. This is basically the approach used previously to discover the novel SaUPPS inhibitor, clomiphene.[7] The antibiotics that act by targeting cell wall biosynthesis were fosmidomycin, carbenicillin, vancomycin, ampicillin, bacitracin, fosfomycin, and cefotaxime. The compounds that do not target bacterial cell wall biosynthesis were kanamycin, tetracycline, sulfamethoxazole, trimethoprim, spectinomycin, and chloramphenicol.

We determined the fractional inhibitory concentration index (FICI) values for each combination using the FICI formula[8-9]:

$$FICI = FIC_A + FIC_B = \frac{MIC(AB)}{MIC(A)} + \frac{MIC(BA)}{MIC(B)}$$

where FIC_A, FIC_B are the fractional inhibitory concentrations of drugs A and B, MIC(A) and MIC(B) are the MIC values of drugs A and B acting alone, and MIC(AB) and MIC(BA) are the MIC values of the most effective combination of drug A or B in the presence of drug B or A. Using this method, FICI values of <0.5 represent synergy, >0.5 and <1.0 represent additivity, >1 and <2 represent an indifferent effect, and ≥2 represents antagonism.[10] In addition, we evaluated isobolograms using the method of Berenbaum.[11] FICI values are shown in Table 6.2 and representative isobolograms in Figure 6.3.

As can be seen in Table 6.2, there are very clear-cut differences between the FICI values obtained with **7** and the cell-wall biosynthesis inhibitors, and those obtained with **7** and the non cell-wall biosynthesis inhibitors. For *S. aureus*, the mean FICI with a cell wall biosynthesis inhibitor is 0.32, for *B. subtilis*, 0.37. This represents a synergistic effect (i.e. the FICI is <0.5) and suggests that **7** acts in the cell wall biosynthesis pathway. With the non cell-wall biosynthesis inhibitors, the mean FICI for *S. aureus* in 1.42, and for *B. subtilis*, 1.47, meaning an indifferent effect, as expected. Clearly then, in both *S. aureus* as well as in *B. subtilis*, **7** is targeting an enzyme involved in cell wall biosynthesis (and not e.g. MenA or heme A synthase) and likely candidates that utilize long, lipophilic anionic substrates are FPPS, UPPS and UPPP. We thus next tested all compounds against UPPS (from *S. aureus*), since in earlier work we had found **6** was a UPPS inhibitor, plus, we tested all compounds against a UPP-phosphatase. UPPP is a membrane protein and we used the fusion hybrid of *E. coli* UPPP with *Haloarcula marismortui* bacteriorhodopsin,[12] since this was available in our lab. We also tested the most active compounds against an EcFPPS, but there

was no inhibition (up to 100 μM). Typical dose-response curves for SaUPPS and EcUPPP are shown in Figure 6.4 and include for UPPP, results for the known inhibitor, bacitracin, which has an IC_{50} = 32 μM, as also reported by Chang et al.[13]

As can be seen in Table 6.1, the most active cell growth inhibitors are also some of the most potent UPPS and UPPP inhibitors with IC_{50} values as low as 320 nM (for UPPS) and 1.3 μM (for UPPP). Interestingly, as can be seen in Figure 6.5A, there is a very good correlation between the pIC_{50} (= $-\log_{10} IC_{50}$[M]) values for *S. aureus* and *B. subtilis* cell growth inhibition (a Pearson r-value correlation-coefficient r = 0.90), strongly suggesting that the same targets are involved in both systems. And as shown in Figure 6.5B, the correlation for *S. aureus* cell growth versus SaUPPS inhibition is also high with an r = 0.85. Figure 6.5C shows a Pearson r-value correlation-coefficient matrix[14] for all cell and enzyme activities as well as for logD (estimated using chemicalize.org web portal, http://www.chemaxon.com), from which it can be seen that both UPPS inhibition as well as UPPP inhibition correlates with cell growth inhibition. There are weaker correlations between cell growth inhibition and logD, and the enzyme inhibition results are essentially uncorrelated with logD so, as expected, permeability/transport plays a role in overall activity in cell growth inhibition. The enzyme/cell correlations are better than those we discussed in a previous study[15] where we found for 10 different cell growth/putative enzyme target inhibition assays (3 from our group, 7 randomly chosen from the literature) that on average the correlation between the enzyme and cell assay results was r~0.55.

What is also apparent from the results shown in Table 6.1 is that, in general, the IC_{50} values for UPPP inhibition are larger than the IC_{50} values for UPPS inhibition, suggesting that in cells, UPPS and not UPPP is the primary target. This is, however, likely to be an over-simplification since the enzyme assays were all detergent based; substrate concentrations in cell are not known; UPPP is a membrane protein; and we used an EcUPPP-bacteriorhodopsin fusion in our assay together with FPP and not UPP. Nevertheless, as can be seen in Table 6.1, several of the most potent cell growth inhibitors do target both enzymes, and inhibition of two consecutive enzymes in the bacterial cell wall biosynthesis pathway is expected to result in enhanced activity over single target inhibition. Moreover, we do find good enzyme inhibition/cell growth correlations, plus, as shown in Figure 6.3, addition of any of the known cell wall biosynthesis inhibitors to **7** results in synergistic cell growth inhibition with, on average, FICI values of ~0.35.

6.4 Conclusions

The results we have reported above are of interest since we find that several lipophilic benzoic acids (with electron-withdrawing ring substituents) have activity against *S. aureus* and *B. subtilis* cell growth. One of the most potent compounds exhibited synergistic activity with numerous known cell wall biosynthesis inhibitors (FICI~0.35, n=13 different cell/inhibitor combinations), but an indifferent effect (FICI=1.45, n=12 cell/inhibitor combinations) with non cell-wall biosynthesis antibiotics. We tested all compounds against UPPS and UPPP and in some cases FPPS finding several promising UPPS as well as UPPP inhibitors. The most potent UPPP inhibitor **11** was ~40x more active than the known UPPP inhibitor, bacitracin, and also inhibited UPPS and was active against *S. aureus* (IC_{50} ~82 ng/mL). Non-polar electron-withdrawing substituents were essential for enzyme/cell inhibition by the benzoic acids, presumably because they make the benzoates much stronger acids (that are fully dissociated) and more akin to the phosphate/diphosphate enzyme substrates. Surprisingly, the phosphonic acids were worse UPPS/UPPP inhibitors and were mostly inactive in cells. There were good correlations between cell growth inhibition and UPPS as well as UPPP inhibition, but UPPS inhibition was more potent. Overall, the results are of interest since we show for the first time that lipophilic benzoic acids inhibit both UPPS and UPPP and are active in cells where they act synergistically with known cell wall biosynthesis inhibitors and as such, they may represent new leads for targeting bacterial cell wall biosynthesis.

6.5 Experimental Section

Chemical Syntheses and Characterization: General Methods. All chemicals were reagent grade. ^{1}H NMR and ^{13}C NMR spectra were obtained on Varian (Palo Alto, CA) Unity spectrometers at 400 and 500 MHz for ^{1}H. HPLC/MS analyses were performed by using an Agilent LC/MSD Trap XCT Plus system (Agilent Technologies, Santa Clara, CA) with an 1100 series HPLC system including a degasser, an autosampler, a binary pump, and a multiple wavelength detector. All final compounds were ≥95% pure as determined by or HPLC-MS and structures were characterized by ^{1}H NMR and HRMS. We synthesized 26 benzoic acids and 4 phenylphosphonates using the general methods shown in Scheme 6.1A, 6.1B.

5-Fluoro-2-(3-(octyloxy)benzamido)benzoic acid (7)

The scheme used to synthesize **7** is as shown in Scheme 6.1A. 1-Bromooctane **b** (7.7 g, 40 mmol) was added to a solution of methyl 3-hydroxybenzoate **a** (3.0 g, 20 mmol) in 20 mL DMF followed by addition of potassium carbonate (5.5 g, 20 mmol). The solution was heated to 80 ^{o}C and stirred for 12 h. After cooling to room temperature, the solution was washed with water (100 mL), extracted with ethyl acetate (50 mL ×3). The organic layer was the dried with Na_2SO_4 and solvent was removed under vacuum. The residue was purified by flash chromatography on a silica (hexane/EtOAc = 20:1) to give methyl 3-(octyloxy)benzoate **c** as a colorless oil (4.8 g, 90%). Compound c (4.0 g, 15 mmol) was dissolved in 20 mL of THF, and aqueous LiOH (1.8 g in 10 mL water) added. The reaction mixture was stirred at room temperature for 12 h, then concentrated under vacuum to remove solvent. The aqueous solution was acidified with HCl to pH 1, upon which a white solid precipitated. The suspension was extracted with ethyl acetate (30 mL ×3). The organic layer was dried with Na_2SO_4 and solvent removed under vacuum. The 3-(octyloxy)benzoic acid **d** was obtained as a white solid (2.5 g, 95%). Compound **d** (2.5 g, 10 mmol) was dissolved in 20 mL of CH_2Cl_2, and 2 mL of oxalyl chloride added. Then, one drop of DMF was added as a catalyst. The reaction mixture was stirred at room temperature for 12 h, then concentrated under vacuum. The residue 3-(octyloxy)benzoyl chloride **e** was obtained as a yellow liquid (3.4 g, 90%). Compound e (2.7 g, 10 mmol) was dissolved in 20 mL of CH_2Cl_2, then 2-amino-5-fluorobenzoic acid **f** (1.6 g, 10 mmol) added. After stirring for 5 min, 2 mL of NEt_3 was added. The reaction mixture was stirred at room temperature for 12 h. The reaction mixture was then washed with 2 M HCl (30 mL ×2) and water (30 mL). The residue was concentrated under vacuum to give the final product **g** (**7**) as a light yellow solid (3.0 g, 80%).^{1}H NMR (DMSO-d_6, 500 MHz) δ (ppm): 8.66 (dd, J =5, 9.5 Hz, 1 H), 7.75 (d, J =9.5 Hz, 1 H), 7.54 (t, J =9.5 Hz, 1 H), 7.48 (m, 3 H), 7.19 (d, J =8.0 Hz, 1 H), 4.03 (t, J =6.5 Hz, 2 H), 1.72 (m, 2 H), 1.41 (m, 2 H), 1.26–1.22 (m, 8 H), 0.84 (t, J =7.0 Hz, 3 H). ESI HRMS: m/z $[M+H]^+$ calculated for $C_{22}H_{27}FNO_4^+$: 388.1924, found: 388.1924. Purity of the product determined by HPLC (Phenomenex C6-Phenyl 110A. 100x2 mm, 3 μm, 250 nm, retention time = 8.1 min): 99.7%.

2-(*N*-methyl-3-(octyloxy)benzamido)phenylphosphonic acid (31)

The scheme used to synthesize **31** is as shown in Scheme 6.1B. Compound **e** (540 mg, 2.0 mmol) was dissolved in 20 mL of CH_2Cl_2, and then diethyl(2-aminophenyl)phosphonate **h** (460 mg, 2.0 mmol) was added. After stirring for 5 min, 2 mL of NEt_3 was added. The reaction mixture was stirred at room temperature for 12 h. The reaction mixture was then washed with 2 M HCl (30 mL

×2) and water (30 mL). The residue was concentrated under vacuum to give compound **i** as a white solid (780 mg, 85%). Compound **i** (460 mg, 1 mmol) was dissolved in dry DCM (15 mL), cooled to 0 ^{o}C and Me_3SiBr (1.2 mL, 9 mmol) added drop-wise over 30 min. The mixture was then stirred for 2 d at room temperature. The solvent was evaporated, and the residue dried in vacuum for approximately 1 h. Then, 20 mL dry methanol was added, and the mixture stirred for 20 min at room temperature. The solvent was removed, and the residue dried overnight to give the final product **j** (**31**) as a white solid (390 mg, 95%). ^{1}H NMR (DMSO-d_6, 500 MHz) δ (ppm): 12.14 (s, 1 H), 8.64 (dd, *J* =4.5, 8.5 Hz, 1 H), 7.65 (dd, *J* =7.5, 14.5 Hz, 1 H), 7.59 (d, *J* =7.5 Hz, 1 H), 7.54 (m, 2 H), 7.44 (t, *J* =8.0 Hz, 1 H), 7.16 (m, 2 H), 4.03 (t, *J* =6.5 Hz, 2 H), 1.73 (m, 2 H), 1.42 (m, 2 H), 1.26–1.22 (m, 12 H), 0.85 (t, *J* =7.0 Hz, 3 H). ESI HRMS: m/z [M-H]$^-$ calculated for $C_{21}H_{27}NO_5P^-$: 404.1627, found: 404.1622. Purity of the product determined by HPLC (Phenomenex C6-Phenyl 110A. 100x2 mm, 3 μm, 250 nm, retention time = 7.3 min): 93.1%.

5-Nitro-2-(3-(octyloxy)benzamido)benzoic acid (8)

Compound **8** was made by following the same procedure as described for the synthesis of compound **7**. ^{1}H NMR (DMSO-d_6, 500 MHz) δ (ppm): 12.60 (s, 1 H), 8.89 (d, *J* =9.5 Hz, 1 H), 8.73 (d, *J* =3.0 Hz, 1 H), 8.47 (dd, *J* =9.5, 3.0 Hz, 1 H), 7.48 (m, 3 H), 7.20 (dd, 1 H), 4.00 (t, *J* =8.0 Hz, 2 H), 1.69 (m, 2 H), 1.38 (m, 2 H), 1.26–1.22 (m, 8 H), 0.81 (t, *J* =7.0 Hz, 3 H). ESI HRMS: m/z [M-H]$^-$ calculated for $C_{22}H_{25}N_2O_6^-$ 413.1713; found 413.1714. Purity of the product determined by HPLC (Phenomenex C6-Phenyl 110A. 100x2 mm, 3 μm, 250 nm, retention time = 8.1 min): 99.6%.

5-Bromo-2-(3-(octyloxy)benzamido)benzoic acid (9)

Compound **9** was made by following the same procedure as described for the synthesis of compound **7**. ^{1}H NMR (DMSO-d_6, 500 MHz) δ (ppm): 8.62 (d, *J* =9.0 Hz, 1 H), 8.08 (d, *J* =2.5 Hz, 1 H), 7.81 (dd, *J* =9.0, 2.5 Hz, 1 H), 7.44 (m, 3 H), 7.17 (m, 1 H), 3.99 (t, *J* =6.0 Hz, 2 H), 1.71 (m, 2 H), 1.38 (m, 2 H), 1.26–1.22 (m, 8 H), 0.82 (t, *J* =7.0 Hz, 3 H). ESI HRMS: m/z [M-H]$^-$ calculated for $C_{22}H_{25}BrNO_4^-$: 446.0967, found: 446.0965. Purity of the product determined by HPLC (Phenomenex C6-Phenyl 110A. 100x2 mm, 3 μm, 250 nm, retention time = 8.4 min): 98.1%.

5-Chloro-2-(3-(octyloxy)benzamido)benzoic acid (10)

Compound **10** was made by following the same procedure as described for the synthesis of compound **7**. ^{1}H NMR (DMSO-d_6, 400 MHz) δ (ppm): 8.65 (d, *J* =9.2 Hz, 1 H), 7.95 (d, *J* =2.8 Hz, 1 H), 7.64 (dd, *J* =8.8, 2.8 Hz, 1 H), 7.48-7.42 (m, 3 H), 7.15 (d, *J* =8.8 Hz, 1 H), 4.00 (t, *J* =6.4 Hz, 2 H), 1.73 (m, 2 H), 1.38 (m, 2 H), 1.26–1.22 (m, 8 H), 0.82 (t, *J* =6.8 Hz, 3 H). ESI HRMS: m/z [M-H]$^-$ calculated for $C_{22}H_{25}ClNO_4^-$: 402.1472, found: 402.1469. Purity of the product determined by HPLC (Phenomenex C6-Phenyl 110A. 100x2 mm, 3 μm, 250 nm, retention time = 8.3 min): 99.7%.

2-(3-(octyloxy)benzamido)-5-(trifluoromethoxy)benzoic acid (11)

Compound **11** was made by following basically the same procedure as described for the synthesis of compound **7**. ^{1}H NMR (CD_3CN, 500 MHz) δ (ppm): 12.06 (s, 1 H), 8.99 (d, *J* =9.5 Hz, 1 H), 8.02 (d, *J* =3.0 Hz, 1 H), 7,61 (dd, *J* =9.5, 3.0 Hz, 1 H), 7.52 (m, 2 H), 7.18 (dd, *J* =3.0, 8.5 Hz, 1 H), 4.09 (t, *J* =6.5 Hz, 2 H), 1.82–1.78 (m, 2 H), 1.50–1.46 (m, 2 H), 1.36–1.32 (m, 8 H), 0.94 (t, *J* =7.0 Hz, 3 H). ESI HRMS: m/z [M+H]$^+$ calculated for $C_{23}H_{27}F_3NO_5^+$: 454.1841, found: 454.1834. Purity of the product determined by HPLC (Phenomenex C6-Phenyl 110A. 100x2 mm, 3μm, 250 nm, retention time = 8.4min): 99.6%.

4,5-difluoro-2-(3-(octyloxy)benzamido)benzoic acid (12)

Compound **12** was made by following the same procedure as described for the synthesis of compound **7**. ^{1}H NMR (DMSO-d_6, 500 MHz) δ (ppm): 12.16 (s, 1 H), 8.67 (dd, *J* =4.5, 17 Hz, 1 H), 7.96 (dd, 1 H), 7.45-7.38 (m, 3 H), 7.16 (m, 1 H), 3.99 (t, *J* =6.5 Hz, 2 H), 1.68 (m, 2 H), 1.37 (m, 2 H), 1.26–1.22 (m, 8 H), 0.82 (t, *J* =7.0 Hz, 3 H). ESI HRMS: m/z [M-H]$^-$ calculated for $C_{22}H_{24}F_2NO_4^-$: 404.1673, found: 404.1675. Purity of the product determined by HPLC (Phenomenex C6-Phenyl 110A. 100x2 mm, 3 μm, 250 nm, retention time = 8.3 min): 99.8%.

5-hydroxy-2-(3-(octyloxy)benzamido)benzoic acid (13)

Compound **13** was made by following the same procedure as described for the synthesis of compound **7**. ^{1}H NMR (DMSO-d_6, 400 MHz) δ (ppm): 11.70 (s, 1 H), 9.62 (s, 1 H), 8.44 (d, *J* =8.8 Hz, 1 H), 7.38-7,43 (m, 4 H), 7.13 (d, *J* =6.4 Hz, 1 H), 7.03 (dd, *J* =2.4, 8.8 Hz, 1 H), 3.98 (t, *J* =6.5 Hz, 2 H), 1.69 (m, 2 H), 1.37 (m, 2 H), 1.26–1.22 (m, 8 H), 0.81 (t, *J* =6.8 Hz, 3 H). ESI HRMS: m/z [M-H]$^-$ calculated for $C_{22}H_{26}NO_5^-$: 384.1811, found: 384.1812. Purity of the product determined by HPLC (Phenomenex C6-Phenyl 110A. 100x2 mm, 3 μm, 250 nm, retention time = 7.8 min): 99.7%.

5-Methoxy-2-(3-(octyloxy)benzamido)benzoic acid (14)

Compound **14** was made by following the same procedure as described for the synthesis of compound **7**. ^{1}H NMR (DMSO-*d*$_6$, 500 MHz) δ (ppm): 11.76 (s, 1 H), 8.53 (d, *J* =11.5 Hz, 1 H), 7.40-7.47 (m, 4 H), 7.25 (dd, *J* =4.0, 11.5 Hz, 1 H), 7.14 (d, *J* =8.5 Hz, 1 H), 3.98 (t, *J* =6.5 Hz, 2 H), 3.76 (s, 3 H), 1.71 (m, 2 H), 1.38 (m, 2 H), 1.26–1.22 (m, 8 H), 0.81 (t, *J* =7.0 Hz, 3 H). ESI HRMS: m/z [M-H]$^-$ calculated for $C_{23}H_{28}NO_5^-$: 398.1967, found: 398.1963. Purity of the product determined by HPLC (Phenomenex C6-Phenyl 110A. 100x2 mm, 3 μm, 250 nm, retention time = 8.1 min): 99.5%.

2-(3-(octyloxy)benzamido)benzoic acid (15)

Compound **15** was made by following the same procedure as described for the synthesis of compound **7**. ^{1}H NMR (DMSO-*d*$_6$, 500 MHz) δ (ppm): 8.69 (d, *J* =8.5 Hz, 1 H), 8.04 (dd, *J* =1.5, 8.0 Hz, 1 H), 7.64 (t, *J* =8.0 Hz, 1 H), 7.45-7.50 (m, 3 H), 7.18 (m, 2 H), 4.03 (t, *J* =6.5 Hz, 2 H), 1.71 (m, 2 H), 1.40 (m, 2 H), 1.33–1.25 (m, 8 H), 0.85 (t, *J* =6.5 Hz, 3 H). ESI HRMS: m/z [M-H]$^-$ calculated for $C_{22}H_{26}NO_4^-$: 368.1862, found: 368.1859. Purity of the product determined by HPLC (Phenomenex C6-Phenyl 110A. 100x2 mm, 3 μm, 250 nm, retention time = 8.1 min): 96.7%.

5-(methylsulfonyl)-2-(3-(octyloxy)benzamido)benzoic acid (16)

Compound **16** was made by following the same procedure as described for the synthesis of compound **7**. ^{1}H NMR (DMSO-*d*$_6$, 500 MHz) δ (ppm): 12.17 (s, 1 H), 9.16 (d, *J* =1.6 Hz, 1 H), 9.24 (d, *J* =8.4 Hz, 1 H), 7.70 (dd, *J* =1.6, 8.4 Hz, 1 H), 7.45-7.48 (m, 3 H), 7.19 (d, *J* =8.4 Hz, 1 H), 4.01 (t, *J* =6.8 Hz, 2 H), 3.25 (s, 3 H), 1.76 (m, 2 H), 1.36 (m, 2 H), 1.26–1.22 (m, 8 H), 0.82 (t, *J* =6.8 Hz, 3 H). ESI HRMS: m/z [M-H]$^-$ calculated for $C_{23}H_{28}NO_6S^-$: 446.1637, found: 446.1632. Purity of the product determined by HPLC (Phenomenex C6-Phenyl 110A. 100x2 mm, 3 μm, 250 nm, retention time = 8.1 min): 91.0%.

2-(3-(hexyloxy)benzamido)benzoic acid (17)

Compound **17** was made by following the same procedure as described for the synthesis of compound **7**. ^{1}H NMR (DMSO-*d*$_6$, 400 MHz) δ (ppm): 8.66 (d, *J* =8.0 Hz, 1 H), 8.01 (dd, *J* =7.6 Hz, 1 H), 7.55 (t, *J* =7.6 Hz, 1 H), 7.45-7.50 (m, 3 H), 7.14 (t, *J* =7.2 Hz,, 1 H), 4.00 (t, *J* =6.5 Hz, 2 H), 1.71 (m, 2 H), 1.39 (m, 2 H), 1.26 (m, 4 H), 0.84 (t, *J* =6.5 Hz, 3 H). ESI HRMS: m/z [M+H]$^+$

calculated for $C_{20}H_{24}NO_4^+$: 342.1705, found: 342.1702. Purity of the product determined by HPLC (Phenomenex C6-Phenyl 110A. 100x2 mm, 3 μm, 250 nm, retention time = 7.8 min): 99.5%.

5-bromo-2-(3-(octyloxy)benzamido)phenylphosphonic acid (18)

Compound **18** was made by following the same procedure as described for the synthesis of compound **31**. ^{1}H NMR (DMSO-d_6, 500 MHz) δ (ppm): 7.69 (dd, *J* =2.4, 14.8 Hz, 1 H), 7.54 (dd, *J* =2.4, 8.8 Hz, 1 H), 7.19 (t, *J* =8.0 Hz, 1 H), 7.09 (s, 1 H), 6.98 (m, 2 H), 6.76 (dd, *J* =2.4, 8.0 Hz, 1 H), 5.14 (s, 2 H), 3.85 (t, *J* =6.5 Hz, 2 H), 1.62 (m, 2 H), 1.33 (m, 2 H), 1.21 (m, 12 H), 0.80 (t, *J* =7.0 Hz, 3 H). ESI HRMS: m/z [M-H]$^-$ calculated for $C_{21}H_{27}BrO_5P^-$: 469.0779, found: 469.0783. Purity of the product determined by HPLC (Phenomenex C6-Phenyl 110A. 100x2 mm, 3 μm, 250 nm, retention time = 7.5 min): 98.2%.

2-(3-(octyloxy)benzamido)-5-phosphonobenzoic acid (19)

Compound **19** was made by following the same procedure as described for the synthesis of compound **31**. ^{1}H NMR (CD_3CN, 500 MHz) δ (ppm): 11.39 (s, 1 H), 8.83 (dd, *J* =2.5. 8.0 Hz, 1 H), 8.38 (d, *J* =14 Hz, 1 H), 7.88 (t, *J* =10.0 Hz, 1 H), 7.48 (d, *J* =7.5 Hz, 1 H), 7.45 (s, 1H), 7.41 (t, *J* =7.5 Hz, 1 H), 7.08 (dd, *J* =2.5, 8.5 Hz, 1 H), 4.01 (t, *J* =6.5 Hz, 2 H), 1.74 (m, 2 H), 1.47–1.43 (m, 2 H), 1.26–1.22 (m, 8 H), 0.85 (t, *J* =7.0 Hz, 3 H). ESI HRMS: m/z [M-H]$^-$ calculated for $C_{22}H_{27}NO_7P^-$: 448.1525, found: 448.1524. Purity of the product determined by HPLC (Phenomenex C6-Phenyl 110A. 100x2 mm, 3μm, 250 nm, retention time = 7.4 min): 98.7%.

3-fluoro-2-(3-(octyloxy)benzamido)benzoic acid (20)

Compound **20** was made by following the same procedure as described for the synthesis of compound **7**. ^{1}H NMR (DMSO-d_6, 500 MHz) δ (ppm): 10.11 (s, 1 H), 7.68 (d, *J* =8.0 Hz, 1 H), 7.50-7.54 (m, 2 H), 7.38-7.43 (m, 2 H), 7.14 (dd, *J* =3.0, 8.5 Hz, 1 H), 4.04 (t, *J* =6.5 Hz, 2 H), 1.72 (m, 2 H), 1.42 (m, 2 H), 1.26–1.22 (m, 8 H), 0.83 (t, *J* =7.5 Hz, 3 H). ESI HRMS: m/z [M-H]$^-$ calculated for $C_{22}H_{25}FNO_4^-$: 386.1768, found: 386.1763. Purity of the product determined by HPLC (Phenomenex C6-Phenyl 110A. 100x2 mm, 3 μm, 250 nm, retention time = 7.7 min): 99.8%.

5-(diethoxyphosphoryl)-2-(3-(octyloxy)benzamido)benzoic acid (21)

Compound **21** was made by following the same procedure as described for the synthesis of compound **7**. ^{1}H NMR ($CDCl_3$, 500 MHz) δ (ppm): 12.18 (s, 1 H), 9.03 (dd, *J* =4.5, 10.5 Hz, 1 H), 8.56 (dd, *J* =2.5, 14.5 Hz, 1 H), 7.95 (m, 1 H), 7.57 (m, 2 H), 7.40 (t, *J* =10.5 Hz, 1 H), 7.10

(dd, *J* =3.0, 10.5 Hz, 1 H), 4.13 (m, 4), 4.03 (t, *J* =6.5 Hz, 2 H), 1.80 (m, 2 H), 1.47–1.43 (m, 2 H), 1.32 (t, *J* =8.0, 6H), 1.26–1.22 (m, 8 H), 0.86 (t, *J* =7.0 Hz, 3 H). ESI HRMS: m/z $[M-H]^-$ calculated for $C_{26}H_{35}NO_7P^-$: 504.2151, found: 504.2156. Purity of the product determined by HPLC (Phenomenex C6-Phenyl 110A. 100x2 mm, 3 μm, 250 nm, retention time = 7.9 min): 99.1%.

3-(3-(octyloxy)benzamido)phthalic acid (22)

Compound **22** was made by following the same procedure as described for the synthesis of compound **7**. ^{1}H NMR (DMSO-*d*$_6$, 500 MHz) δ (ppm): 10.45 (s, 1 H), 7.99 (s, 1 H), 7,56 (m, 2 H), 7.45 (m, 3 H), 7.15 (dd, *J* =2.0. 8.0 Hz, 1 H), 4.02 (t, *J* =6.5 Hz, 2 H), 1.73 (m, 2 H), 1.47–1.43 (m, 2 H), 1.26–1.22 (m, 8 H), 0.85 (t, *J* =7.0 Hz, 3 H). ESI HRMS: m/z $[M-H]^-$ calculated for $C_{23}H_{26}NO_6^-$: 412.1760, found: 412.1757. Purity of the product determined by HPLC (Phenomenex C6-Phenyl 110A. 100x2 mm, 3 μm, 250 nm, retention time = 7.5 min): 97.4%.

5-fluoro-2-(3-(hexyloxy)benzamido)benzoic acid (23)

Compound **23** was made by following the same procedure as described for the synthesis of compound **7**. ^{1}H NMR (DMSO-*d*$_6$, 500 MHz) δ (ppm): 8.65 (d, *J* =10.0 Hz, 1 H), 8.02 (d, *J* =9.5 Hz, 1 H), 7.41-7.59 (m, 4 H), 7.13 (m, 2 H), 3.99 (t, *J* =7.5 Hz, 2 H), 1.72 (m, 2 H), 1.38 (m, 2 H), 1.26–1.22 (m, 4 H), 0.84 (t, *J* =6.5 Hz, 3 H). ESI HRMS: m/z $[M-H]^-$ calculated for $C_{20}H_{21}FNO_4^-$: 358.1455, found: 358.1451. Purity of the product determined by HPLC (Phenomenex C6-Phenyl 110A. 100x2 mm, 3 μm, 250 nm, retention time = 7.9 min): 99.5%.

4-hydroxy-3-(3-(octyloxy)benzamido)benzoic acid (24)

Compound **24** was made by following the same procedure as described for the synthesis of compound **7**. ^{1}H NMR (DMSO-*d*$_6$, 400 MHz) δ (ppm): 10.64 (s, 1 H), 9.52 (s, 1 H), 8.26 (d, *J* =2.0 Hz, 1 H), 7.66 (dd, *J* =2.0, 8.5 Hz, 4 H), 7.48-7.51 (m, 2 H), 7.41 (t, *J* =8.5 Hz, 1 H), 7.14 (dd, *J* =2.5, 8.5 Hz, 1 H), 6.97 (d, *J* =8.5 Hz, 1 H), 4.02 (t, *J* =6.5 Hz, 2 H), 1.72 (m, 2 H), 1.41 (m, 2 H), 1.26–1.22 (m, 8 H), 0.85 (t, *J* =6.5 Hz, 3 H). ESI HRMS: m/z $[M+H]^+$ calculated for $C_{22}H_{28}NO_5^+$: 386.1967, found: 386.1965. Purity of the product determined by HPLC (Phenomenex C6-Phenyl 110A. 100x2 mm, 3 μm, 250 nm, retention time = 7.9 min): 99.7%.

2-methoxy-6-(3-(octyloxy)benzamido)benzoic acid (25)

Compound **25** was made by following the same procedure as described for the synthesis of compound **7**. ^{1}H NMR (CD_3CN, 500 MHz) δ (ppm): 11.33 (s, 1 H), 8.12 (d, *J* =8.5 Hz, 1 H), 8.12

(t, *J* =8.5 Hz, 1 H), 7.39-7.46 (m, 3 H), 7.11 (m, 1 H), 6.91 (d, *J* =8.5 Hz, 1 H), 4.02 (t, *J* =6.5 Hz, 2 H), 3.92 (s, 3 H), 1.74 (m, 2 H), 1.43 (m, 2 H), 1.26–1.22 (m, 8 H), 0.85 (t, *J* =7.0 Hz, 3 H). ESI HRMS: m/z $[M-H]^-$ calculated for $C_{23}H_{28}NO_5^-$: 398.1967, found: 398.1966. Purity of the product determined by HPLC (Phenomenex C6-Phenyl 110A. 100x2 mm, 3 μm, 250 nm, retention time = 8.0 min): 98.9%.

2-(3-(3,3-dimethylbut-1-ynyl)benzamido)-5-bromobenzoic acid (26)

Compound **26** was made by following the same procedure as described for the synthesis of compound **7**. ^{1}H NMR (DMSO-d_6, 500 MHz) δ (ppm): 12.02 (s, 1 H), 8.51 (d, *J* =9.0 Hz, 1 H), 8.05 (s, 1 H), 7.81 (m, 3 H), 7.54 (m, 2 H), 1.26 (s, 9 H). ESI HRMS: m/z $[M-H]^-$ calculated for $C_{20}H_{17}BrNO_3^-$: 398.0392, found: 398.0387. Purity of the product determined by HPLC (Phenomenex C6-Phenyl 110A. 100x2 mm, 3 μm, 250 nm, retention time = 8.4 min): 99.2%.

5-(3-(octyloxy)benzamido)isophthalic acid (27)

Compound **27** was made by following the same procedure as described for the synthesis of compound **7**. ^{1}H NMR (DMSO-d_6, 500 MHz) δ (ppm): 10.52 (s, 1 H), 8.67 (s, 1 H), 8.64 (s, 1 H), 7.55 (m, 2 H), 7.43 (t, *J* =8.5 Hz, 1 H), 7.16 (dd, *J* =2.0, 8.5 Hz, 1 H), 4.09 (t, *J* =6.5 Hz, 2 H), 1.71 (m, 2 H), 1.41 (m, 2 H), 1.26–1.22 (m, 8 H), 0.86 (t, *J* =7.0 Hz, 3 H). ESI HRMS: m/z $[M+H]^+$ calculated for $C_{23}H_{28}NO_6^+$: 414.1917, found: 414.1918. Purity of the product determined by HPLC (Phenomenex C6-Phenyl 110A. 100x2 mm, 3 μm, 250 nm, retention time = 7.6 min): 99.8%.

2-(*N*-methyl-3-(octyloxy)benzamido)benzoic acid (28)

Compound **28** was made by following the same procedure as described for the synthesis of compound **7**. ^{1}H NMR (DMSO-d_6, 500 MHz) δ (ppm): 7.69 (d, *J* =7.5, 1H), 7.47 (d, *J* =6.0 Hz, 1 H), 7.36 (d, *J* =7.5, 1 H), 7.28 (t, *J* =8.0, 1 H), 7.02 (t, *J* =8.0, 1 H), 6.70 (m, 3 H), 3.70 (t, *J* =3.5 Hz, 2 H), 3.31 (s, 3H), 1.54 (m, 2 H), 1.26–1.22 (m, 10 H), 0.85 (t, *J* =8.0 Hz, 3 H). ESI HRMS: m/z $[M+H]^+$ calculated for $C_{23}H_{30}NO_4^+$: 384.2175, found: 384.2168. Purity of the product determined by HPLC (Phenomenex C6-Phenyl 110A. 100x2 mm, 3 μm, 250 nm, retention time = 7.5 min): 97.7%.

4-(3-(octyloxy)benzamido)isophthalic acid (29)

Compound **29** was made by following the same procedure as described for the synthesis of compound **7**. ^{1}H NMR (DMSO-d_6, 500 MHz) δ (ppm): 10.49 (s, 1 H), 8.05 (s, 1 H), 7.98 (dd, *J* =2.0, 8.5 Hz, 1 H), 7.74 (d, *J* =8.0, 1 H), 7.49 (m, 3 H), 7.14 (dd, *J* =2.0, 8.5 Hz, 1 H), 4.04 (t, *J*

=6.5 Hz, 2 H), 1.71 (m, 2 H), 1.42 (m, 2 H), 1.26–1.22 (m, 8 H), 0.85 (t, *J* =6.5 Hz, 3 H). ESI HRMS: m/z $[M+H]^+$ calculated for $C_{23}H_{28}NO_6^+$: 414.1917, found: 414.1921. Purity of the product determined by HPLC (Phenomenex C6-Phenyl 110A. 100x2 mm, 3 μm, 250 nm, retention time = 7.5 min): 99.7%.

5-methoxy-4-(2-methoxyethoxy)-2-(3-(octyloxy)benzamido)benzoic acid (30)

Compound **30** was made by following the same procedure as described for the synthesis of compound **7**. ^{1}H NMR (CD_3CN, 500 MHz) δ (ppm): 12.38 (s, 1 H), 8.57 (s, 1 H), 7.56 (s, 1 H), 7.40-7.52 (m, 3 H), 7.11 (dd, *J* =3.0, 8.5 Hz, 1 H), 4.19 (t, *J* =4.5 Hz, 2 H), 4.03 (t, *J* =6.5 Hz, 2 H), 3.81 (s, 3 H), 3.72 (t, *J* =4.5 Hz, 2 H), 3.35 (s, 3 H), 1.75 (m, 2 H), 1.47–1.43 (m, 2 H), 1.26–1.22 (m, 8 H), 0.86 (t, *J* =7.0 Hz, 3 H). ESI HRMS: m/z $[M-H]^-$ calculated for $C_{26}H_{34}NO_7^-$: 472.2335, found: 472.2339. Purity of the product determined by HPLC (Phenomenex C6-Phenyl 110A. 100x2 mm, 3 μm, 250 nm, retention time = 8.1 min): 91.9%.

***N*-(2-carbamoylphenyl)-3-(octyloxy)benzamide (32)**

Compound **32** was made by following the same procedure as described for the synthesis of compound **7**. ^{1}H NMR (DMSO-*d*$_6$, 500 MHz) δ (ppm): 8.68 (d, *J* =7.0 Hz, 1 H), 8.42 (s, 1 H), 7.88 (m, 2 H), 7.54 (m, 4 H), 7.17 (m, 2 H), 4.03 (t, *J* =6.5 Hz, 2 H), 1.72 (m, 2 H), 1.40 (m, 2 H), 1.26–1.22 (m, 8 H), 0.86 (t, *J* =7.0 Hz, 3 H). ESI HRMS: m/z $[M+H]^+$ calculated for $C_{22}H_{29}N_2O_3^+$: 369.2178, found: 369.2175. Purity of the product determined by HPLC (Phenomenex C6-Phenyl 110A. 100x2 mm, 3 μm, 250 nm, retention time = 7.9 min): 99.8%.

2-(3,4-bis(2-methoxyethoxy)benzamido)-5-bromobenzoic acid (33)

Compound **33** was made by following the same procedure as described for the synthesis of compound **7**. ^{1}H NMR (DMSO-*d*$_6$, 500 MHz) δ (ppm): 12.03 (s, 1 H), 8.64 (d, *J* =9.0 Hz, 1 H), 8.01 (d, *J* =2.5 Hz, 1 H), 7.83 (dd, *J* =9.0, 2.5 Hz, 1 H), 7.51 (m, 2 H), 7.17 (d, *J* =8.5 Hz, 1 H), 4.19 (t, *J* =4.5 Hz, 2 H), 4.17 (t, *J* =4.5 Hz, 2 H), 3.69 (t, *J* =4.5 Hz, 2 H), 3.67 (t, *J* =4.5 Hz, 2 H), 3.33 (s, 3H), 3.32 (s, 3H). ESI HRMS: m/z $[M-H]^-$ calculated for $C_{20}H_{21}BrNO_7^-$: 466.0501, found: 466.0495. Purity of the product determined by HPLC (Phenomenex C6-Phenyl 110A. 100x2 mm, 3 μm, 250 nm, retention time = 7.2 min): 96.8%.

3-(3-(octyloxy)benzamido)benzoic acid (34)

Compound **34** was made by following the same procedure as described for the synthesis of compound **7**. ^{1}H NMR (DMSO-*d*$_6$, 500 MHz) δ (ppm): 10.36 (s, 1 H), 8.40 (s, 1 H), 8.02 (d, *J*

=8.0 Hz, 1 H), 7.65 (d, *J* =7.5, 1 H), 7.47 (m, 4 H), 7.14 (dd, *J* =8.0, 3.0 Hz, 1 H), 4.04 (t, *J* =6.5 Hz, 2 H), 1.71 (m, 2 H), 1.42 (m, 2 H), 1.26–1.22 (m, 8 H), 0.85 (t, *J* =6.5 Hz, 3 H). ESI HRMS: m/z $[M+H]^+$ calculated for $C_{22}H_{28}NO_4^+$: 370.2018, found: 370.2018. Purity of the product determined by HPLC (Phenomenex C6-Phenyl 110A. 100x2 mm, 3 μm, 250 nm, retention time = 7.9 min): 99.8%.

3,4,5-trimethoxy-2-(3-(octyloxy)benzamido)benzoic acid (35)

Compound **35** was made by following the same procedure as described for the synthesis of compound **7**. ^{1}H NMR (CD_3CN, 500 MHz) δ (ppm): 7.52 (d, *J* =7.5 Hz, 1 H), 7.50 (t, *J* =2.5 Hz, 1 H), 7.42 (t, *J* =7.5 Hz, 1 H), 7.32 (s, 1 H), 7.13 (dd, *J* =2.5, 7.5 Hz, 1 H), 4.07 (t, *J* =6.5 Hz, 2 H), 3.91 (s, 3 H), 3.90 (s, 3 H), 3.84 (s, 3 H), 1.80 (m, 2 H), 1.49 (m, 2 H), 1.33-1.28 (m, 8 H), 0.91 (t, *J* =7.0 Hz, 3 H). ESI HRMS: m/z $[M+H]^+$ calculated for $C_{25}H_{34}NO_7^+$: 460.2335, found: 460.2328. Purity of the product determined by HPLC (Phenomenex C6-Phenyl 110A. 100x2 mm, 3 μm, 250 nm, retention time = 7.6 min): 99.7%.

3-(3-(octyloxy)benzamido)phenylphosphonic acid (36)

Compound **36** was made by following the same procedure as described for the synthesis of compound **31**. ^{1}H NMR (D_2O, 500 MHz) δ (ppm): 7.34 (d, *J* =13.2 Hz, 1 H), 7.14-7.23 (m, 4 H), 6.91-6.98 (m, 2 H), 6.61 (d, *J* =8.0 Hz, 1 H), 3.58 (2 H), 1.42 (2 H), 1.11 (m, 10 H), 0.71 (t, *J* =6.8 Hz, 3 H). ESI HRMS: m/z $[M-H]^-$ calculated for $C_{21}H_{27}NO_5P^-$: 404.1627, found: 404.1624. Purity of the product determined by HPLC (Phenomenex C6-Phenyl 110A. 100x2 mm, 3 μm, 250 nm, retention time = 7.1 min): 99.6%.

***B. subtilis* growth inhibition assay.** IC_{50} values for *B. subtilis* cell growth inhibition were determined using a microdilution method. A stationary overnight starter culture of *B. subtilis* (*Bacillus subtilis* subsp. *subtilis* (Ehrenberg) Cohn ATCC 6051) was diluted 100-fold and grown to an OD_{600} of ~0.3. This log-phase culture was again diluted 500-fold into fresh LB broth to generate the "working solution". 200 μL of working solution was transferred into each well of a 96-well culture plate (Corning 3370). Inhibitors were then added at 1 mM and sequentially diluted 3x to 46 nM, keeping volume and culture broth composition constant. Plates were incubated for 12 hours at 37°C, shaking at 200 RPM, and then absorbance at 600 nm was measured to assess bacterial cell growth. IC_{50} values were determined using nonlinear regression whereas, minimum

inhibitory concentration (MIC) values for each antibiotic and **7** in the synergy assays were calculated by using a Gompertz function in Prism 5 (GraphPad Software, Inc, La Jolla, CA).

***S. aureus* growth inhibition assay.** As with the *B. subtilis* growth inhibition assay, an overnight starter culture of *S. aureus* (Newman strain) was diluted 1000-fold to create a "working solution". Working solutions were transferred into flat-bottom 96-well plates and inhibitors added at 1 mM and sequentially diluted 3x to 46 nM. Plates were incubated at 37°C, shaking at 200 RPM for 24 hours. The OD_{600} was measured the next day to determine bacterial growth.

Synergy/Antagonism Assays. In order to investigate possible synergistic interactions between compound **7** and a range of antibiotics, we carried out two-drug combination assays using a mid-point method. Bacterial cells were incubated with a 3x gradient of antibiotic typically ranging from 40 μg/mL to 18 ng/mL (200 μg/mL to 90 ng/mL for bacitracin, fosfomycin, and sulfamethoxazole) in the presence half-MIC concentrations of **7**, in addition to a 3x gradient of **7** ranging from 40 μg/mL to 18 ng/mL in the presence of half-MIC concentrations of each antibiotic. New MIC values were calculated by using a Gompertz function in Prism 5 (GraphPad Software, Inc, La Jolla, CA).

Enzyme Inhibition Assays. SaUPPS and EcUPPP were expressed and purified as described previously[4, 13]. UPPS assays were carried out using a phosphate release assay[4]. Benzoic acid and phosphonic acid derivatives were prepared as 10 mM stock solutions in DMSO, and were then serially diluted from 1 mM to 1 nM. Inhibitors were incubated with 25 ng of SaUPPS at room temperature for 10 minutes in a pH 7.5 buffer (50 mM HEPES, 150 mM NaCl, 10 mM $MgCl_2$, and 0.02% dodecyl-maltopyranoside as detergent) before adding "reaction mixture" containing 5 μM FPP, 50 μM IPP, 3 U/mL purine nucleoside phosphorylase, 1 U/mL inorganic phosphatase, and ~600 μM MESG, again in the same buffer. Reactions were monitored for 15 minutes with the rate of increase in absorbance at 360 nm taken as the rate of UPP synthesis. IC_{50} values were calculated by using Prism 5 (GraphPad Software, Inc, La Jolla, CA).

The UPPP inhibition assay was carried out using a malachite-green reagent as described previously[16]**.** The same 10 mM inhibitor stock solutions and assay buffer as for the SaUPPS assays were used to test for UPPP inhibition. Inhibitors were incubated with 20 nM EcUPPP at room temperature for 15 minutes before adding FPP to 35 μM. Reaction mixtures were incubated at 37 °C for 20 minutes, then quenched by adding 30 μL of malachite-green reagent. In this assay,

the phosphate released from FPP reacts with ammonium molybdate to form phosphomolybdate (yellow) which then forms a green complex (λ_{max}~620 nm), used to assess phosphatase activity. Phosphate release was measured at 620 nm and quantified based on a phosphate standard curve, and the OD values used to construct dose-response curves.

6.6 Schemes, Charts, Tables and Figures

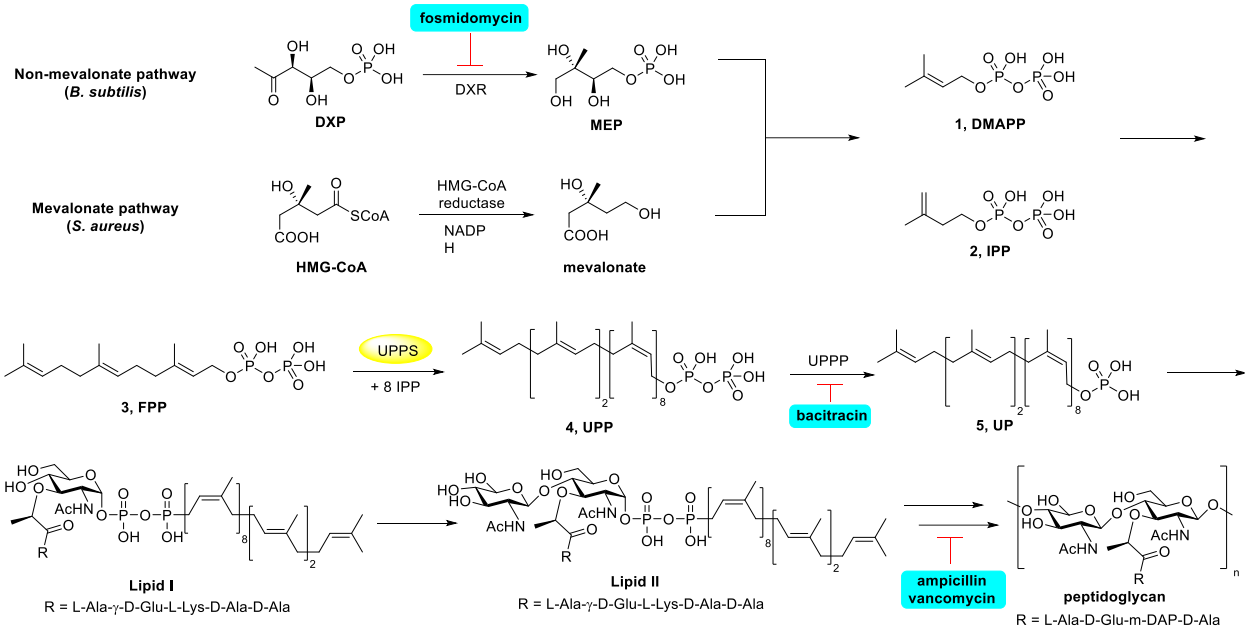

Figure 6.1. Schematic outline of cell wall biosynthesis (in most bacteria) delineating the role of isoprenoid biosynthesis in the early stages of peptidoglycan formation, together with the reaction targeted by several antibiotics discussed in the Text.

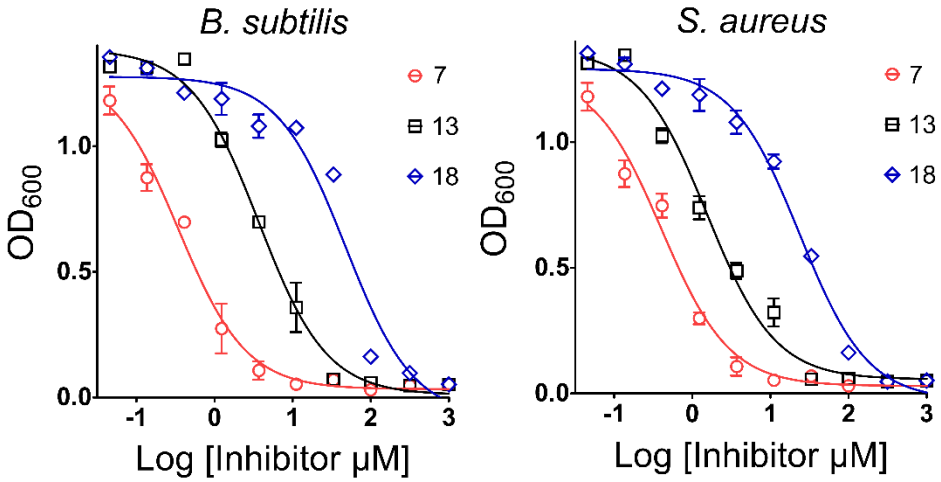

Figure 6.2. Representative dose-response curves for three inhibitors (**7, 13 and 18**) against *B. subtilis* and *S. aureus.*

Compound	logD	*B. subtilis*	*S. aureus*	SaUPPS	EcUPPP	Compound	logD	*B. subtilis*	*S. aureus*	SaUPPS	EcUPPP
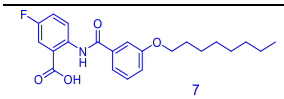 7	3.5	0.14	0.16	0.32	2.7	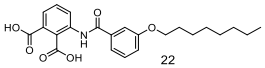 22	2.6	>100	>100	4.5	>200
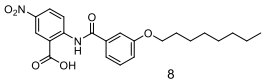 8	3.2	0.21	0.24	0.33	1.3	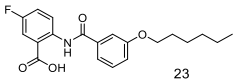 23	2.8	3.6	1.3	4.9	20
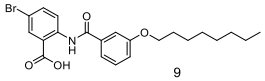 9	4.2	>100	>100	0.54	4.2	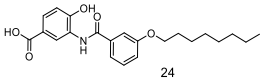 24	3.1	>100	>100	4.9	31
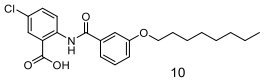 10	4.0	0.56	0.23	0.60	3.0	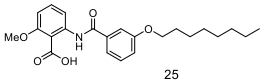 25	3.1	3.0	1.6	6.0	>200
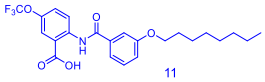 11	4.7	0.21	0.082	0.78	0.83	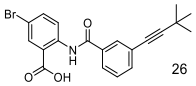 26	-0.28	3.4	0.6	6.9	>200
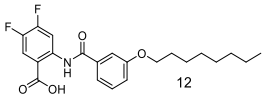 12	3.7	0.53	0.18	0.96	3.4	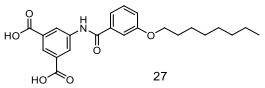 27	2.6	>100	>100	7.0	>200
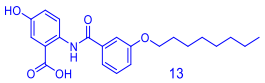 13	3.0	1.4	0.42	1.3	11	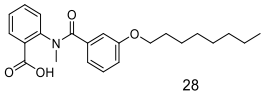 28	0.46	20	18	8.0	>200
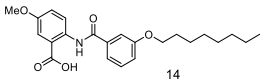 14	3.1	1.2	0.64	1.3	>200	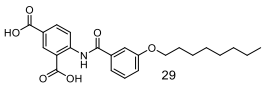 29	3.1	>100	3.0	8.5	>200
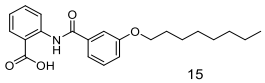 15	3.3	0.85	1.2	1.6	10	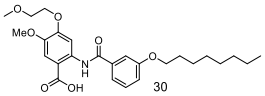 30	2.5	2.7	2.2	10	>200
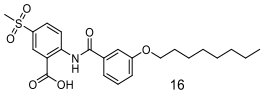 16	2.3	2.5	1.4	2.0	9.8	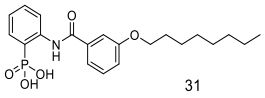 31	2.1	>100	41	39	6.5
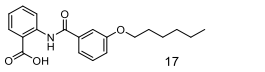 17	2.7	4.1	0.82	2.4	45	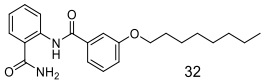 32	5.6	>100	>100	60	>200
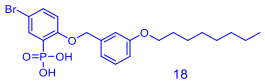 18	-1.6	23	11	2.5	6.7	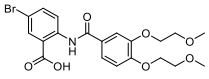 33	0.79	>100	33	130	>200
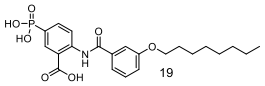 19	3.6	>100	>100	3.0	4.2	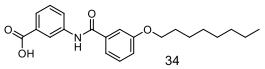 34	2.8	20	42	>200	73
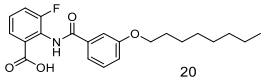 20	3.2	2.7	3.1	3.2	8.5	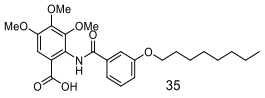 35	2.9	>100	>100	>200	>200
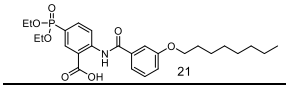 21	0.80	2.3	3.9	3.4	>200	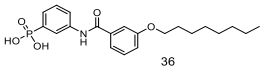 36	1.5	>100	>100	>200	7.1

Table 6.1. IC_{50} values of benzoic acids and phosphonic acids inhibtiors against *B. subtilis* and *S. aureus* cell growth (in µg/mL) and against SaUPPS and EcUPPP enzymes (in µM). Inhibitors discussed in the Text are shown in blue. logD values were estimated using chemicalize.org server (http://www.chemaxon.com).

B. subtilis

	Antibiotic	MIC antibiotic (μg/mL)	FIC antibiotic	MIC 7 (μg/mL)	FIC 7	FIC Index
Cell Wall Biosynthesis Inhibitors	Fosmidomycin	5	0.039 ± 0.0053	1	0.13 ± 0.056	0.17 ± 0.056
	Carbenicillin	5	0.22 ± 0.073	1	0.15 ± 0.071	0.37 ± 0.10
	Cefotaxime	2.5	0.17 ± 0.026	1	0.14 ± 0.081	0.31 ± 0.085
	Vancomycin	0.5	0.27 ± 0.24	1	0.17 ± 0.063	0.44 ± 0.25
	Fosfomycin	200	0.16 ± 0.15	1	0.063 ± 0.022	0.22 ± 0.15
	Ampicillin	0.5	0.30 ± 0.072	1	0.23 ± 0.084	0.53 ± 0.11
	Bacitracin	200	0.18 ± 0.089	1	0.36 ± 0.14	0.53 ± 0.17
Protein Biosynthesis Inhibitors	Chloramphenicol	0.5	0.75 ± 0.18	1	0.97 ± 0.42	1.72 ± 0.46
	Kanamycin	1.5	0.64 ± 0.14	1	0.71 ± 0.30	1.36 ± 0.33
	Tetracycline	5	0.48 ± 0.047	1	0.57 ± 0.50	1.04 ± 0.50
Nucleic Acid Inhibitors	Sulfamethoxazole	200	0.78 ± 0.21	1	0.94 ± 0.64	1.72 ± 0.67
	Trimethoprim	0.5	0.66 ± 0.13	1	0.85 ± 0.29	1.51 ± 0.32

S. aureus

	Antibiotic	MIC antibiotic (μg/mL)	FIC antibiotic	MIC 7 (μg/mL)	FIC 7	FIC Index
Cell Wall Biosynthesis Inhibitors	Carbenicillin	15	0.23 ± 0.048	1	0.077 ± 0.026	0.30 ± 0.055
	Cefotaxime	2	0.18 ± 0.055	1	0.084 ± 0.031	0.27 ± 0.063
	Vancomycin	1.5	0.14 ± 0.034	1	0.15 ± 0.062	0.29 ± 0.071
	Fosfomycin	200	0.20 ± 0.11	1	0.091 ± 0.034	0.29 ± 0.36
	Ampicillin	0.5	0.41 ± 0.17	1	0.15 ± 0.071	0.56 ± 0.18
	Bacitracin	200	0.16 ± 0.11	1	0.044 ± 0.019	0.20 ± 0.11
Protein Biosynthesis Inhibitors	Spectinomycin	40	0.75 ± 0.43	1	0.81 ± 0.32	1.56 ± 0.54
	Chloramphenicol	5	0.88 ± 0.47	1	0.81 ± 0.31	1.69 ± 0.56
	Kanamycin	1.5	0.89 ± 0.68	1	0.83 ± 0.29	1.72 ± 0.74
	Tetracycline	0.5	0.24 ± 0.11	1	0.51 ± 0.24	0.75 ± 0.26
Nucleic Acid Inhibitors	Sulfamethoxazole	200	0.54 ± 0.13	1	0.98 ± 0.37	1.53 ± 0.39
	Trimethoprim	15	0.69 ± 0.32	1	0.57 ± 0.25	1.26 ± 0.41

Mean FICIs:	*B. subtilis*	inhibitors targeting cell wall biosynthesis	0.37 ± 0.14
		inhibitors targeting nucleic acids and protein biosynthesis	1.47 ± 0.28
	S. aureus	inhibitors targeting cell wall biosynthesis	0.32 ± 0.12
		inhibitors targeting nucleic acids and protein biosynthesis	1.42 ± 0.37

Table 6.2. Combinations of 7 and antibiotics against *B. subtilis* and *S. aureus*

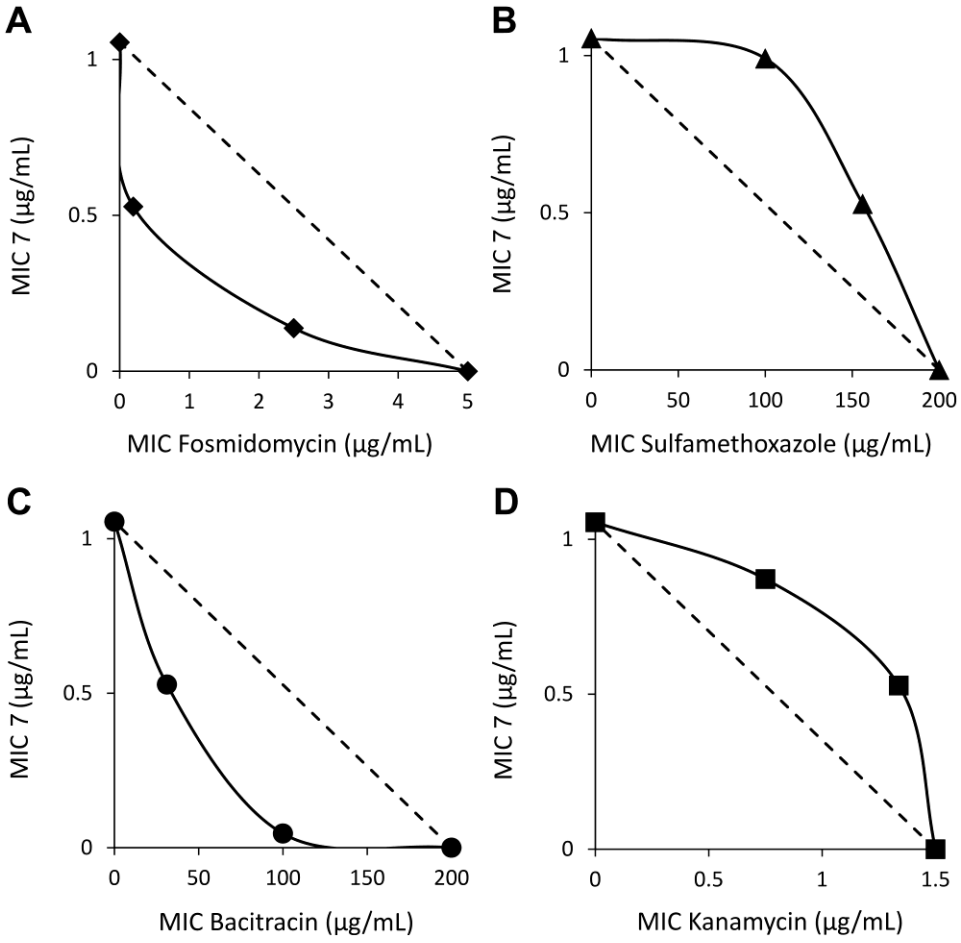

Figure 6.3. Representative isobolograms for **7** with antibiotics having known mechanisms of action. A, **7**+fosmidomycin in *B. subtilis* showing synergy (FICI=0.17) of **7** with a cell wall biosynthesis inhibitor (that targets DXR, 1-deoxy-D-xylulose 5-phosphate reductoisomerase, in the non-mevalonate pathway). B, **7**+sulfamethoxazole in *B. subtilis* showing an indifferent effect (FICI=1.72) of **7** with a nucleic acid biosynthesis inhibitor (that targets dihydropteroate synthase). C, **7**+bacitracin in *S. aureus* showing synergy (FICI=0.20) of **7** with a cell wall biosynthesis inhibitor (that targets UPPP). D, **7**+ kanamycin in *S. aureus* showing an indifferent ffect (FICI=1.72) of **7** with a protein biosynthesis inhibitor (that targets ribosome function).

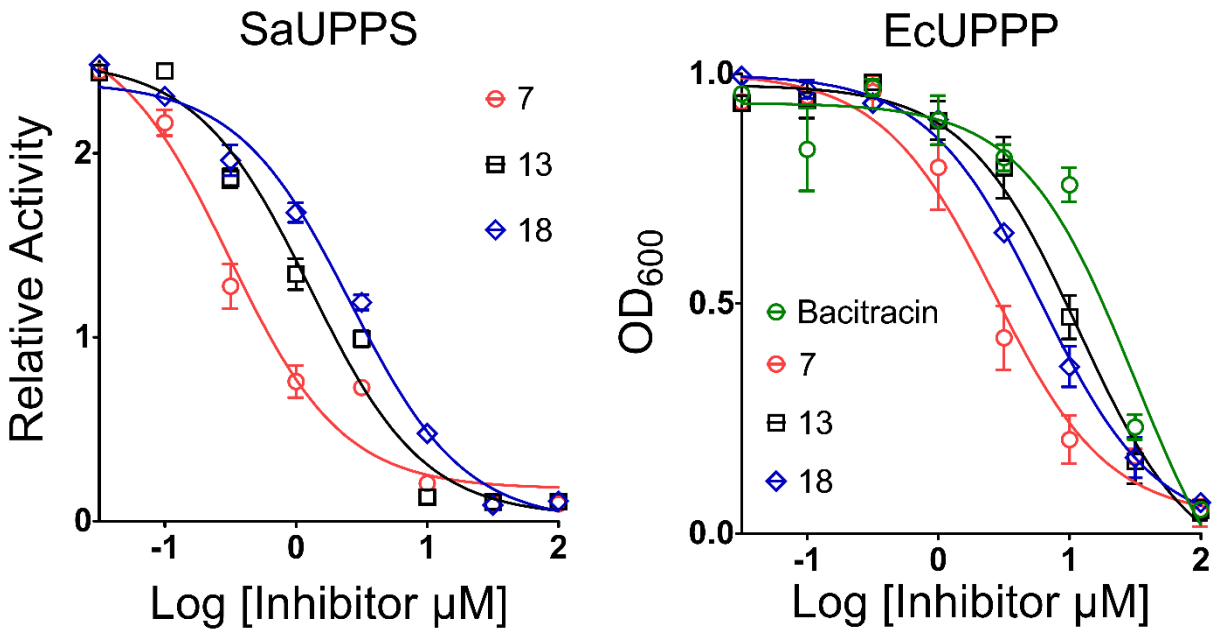

Figure 6.4. Dose-response curves of various benzoic acid and phenyl phosphonic acid derivatives against SaUPPS and EcUPPP. The benzoic acids were ~40x more potent UPPP inhibitors than bacitracin, a known UPPP inhibitor used as a topical antibiotic.

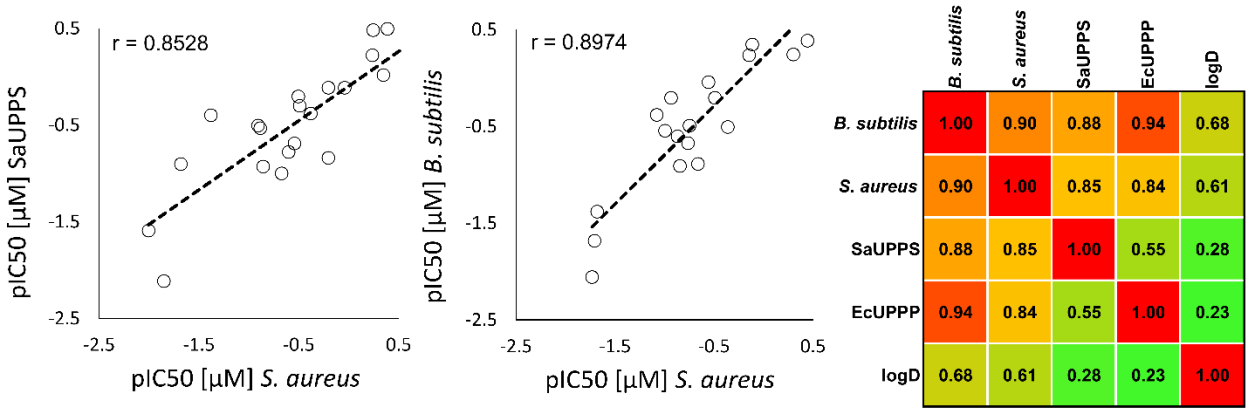

Figure 6.5. Correlations between cell growth and enzyme inhibition results. A, Correlation between *S. aureus* and *B. subtilis* cell growth inhibition based on pIC_{50} (=-$\log_{10}IC_{50}$[M]) results. B, Correlation between *S. aureus* cell growth inhibition and SaUPPS inhibition. C, Pearson r-value correlation matrix/heat map for *S. aureus* cell growth inhibition, *B. subtilis* cell growth inhibition, SaUPPS and EcUPPP enzyme inhibition (all based on pIC_{50} values). The Pearson r-values are indicated and red/orange=high correlation, green=low correlation.

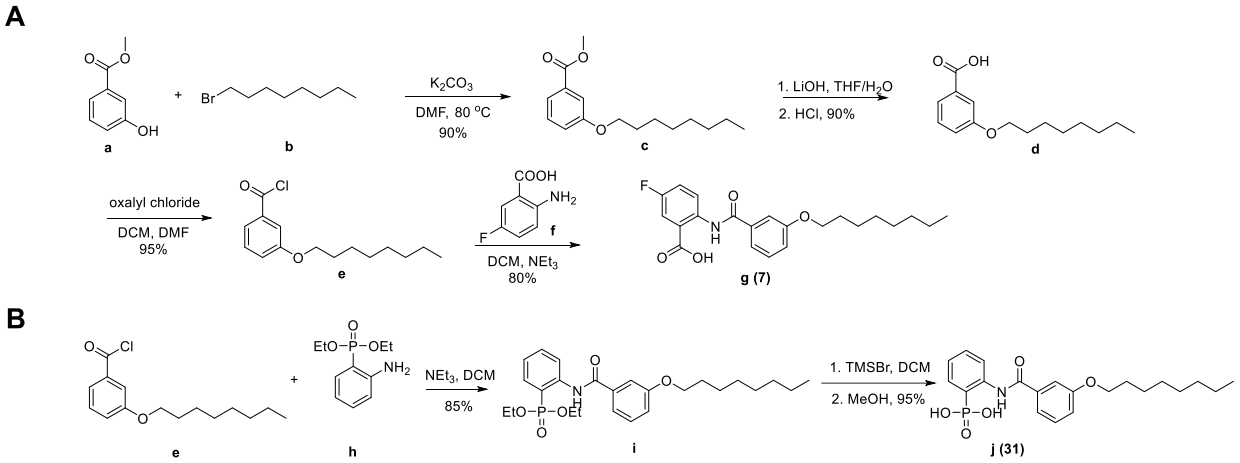

Scheme 6.1. A. route to benzoic acids (**7**). B. route to phenyl phosphonates (**31**).

6.7 References

1. *Antibiotics resistance threats in the United States, 2013.* Executive Summary. http://www.cdc.gov/drugresistance/pdf/ar-threats-2013-508.pdf
2. Jomaa, H.; Wiesner, J.; Sanderbrand, S.; Altincicek, B.; Weidemeyer, C.; Hintz, M.; Turbachova, I.; Eberl, M.; Zeidler, J.; Lichtenthaler, H. K.; Soldati, D.; Beck, E., Inhibitors of the nonmevalonate pathway of isoprenoid biosynthesis as antimalarial drugs. *Science* **1999,** *285* (5433), 1573-1576.
3. Peukert, S.; Sun, Y.; Zhang, R.; Hurley, B.; Sabio, M.; Shen, X.; Gray, C.; Dzink-Fox, J.; Tao, J.; Cebula, R.; Wattanasin, S., Design and structure-activity relationships of potent and selective inhibitors of undecaprenyl pyrophosphate synthase (UPPS): tetramic, tetronic acids and dihydropyridin-2-ones. *Bioorg. Med. Chem. Lett.* **2008,** *18* (6), 1840-4.
4. Zhu, W.; Zhang, Y.; Sinko, W.; Hensler, M. E.; Olson, J.; Molohon, K. J.; Lindert, S.; Cao, R.; Li, K.; Wang, K.; Wang, Y.; Liu, Y. L.; Sankovsky, A.; de Oliveira, C. A.; Mitchell, D. A.; Nizet, V.; McCammon, J. A.; Oldfield, E., Antibacterial drug leads targeting isoprenoid biosynthesis. *Proc. Natl. Acad. Sci. U. S. A.* **2013,** *110* (1), 123-8.
5. Jahnke, W.; Rondeau, J. M.; Cotesta, S.; Marzinzik, A.; Pelle, X.; Geiser, M.; Strauss, A.; Gotte, M.; Bitsch, F.; Hemmig, R.; Henry, C.; Lehmann, S.; Glickman, J. F.; Roddy, T. P.; Stout, S. J.; Green, J. R., Allosteric non-bisphosphonate FPPS inhibitors identified by fragment-based discovery. *Nat. Chem. Biol.* **2010,** *6* (9), 660-666.
6. Hederstedt, L., Heme A biosynthesis. *Biochim. Biophys. Acta.* **2012,** *1817* (6), 920-927.
7. Farha, M. A.; Czarny, T. L.; Myers, C. L.; Worrall, L. J.; French, S.; Conrady, D. G.; Wang, Y.; Oldfield, E.; Strynadka, N. C.; Brown, E. D., Antagonism screen for inhibitors of bacterial cell wall biogenesis uncovers an inhibitor of undecaprenyl diphosphate synthase. *Proc. Natl. Acad. Sci. U. S. A.* **2015,** *112* (35), 11048-53.
8. Eliopoulos, G. M.; Moellering, R. C., *In Antibiotics in Laboratory Medicine, 4th Ed.* 1998.
9. Singh, P. K.; Tack, B. F.; McCray, P. B.; Welsh, M. J., Synergistic and additive killing by antimicrobial factors found in human airway surface liquid. *Am. J. Physiol. Lung Cell Mol. Physiol.* **2000,** *279* (5), L799-L805.
10. Susc, E. C. A., Terminology relating to methods for the determination of susceptibility of bacteria to antimicrobial agents. *Clin. Microbiol. Infec.* **2000,** *6* (9), 503-508.
11. Berenbaum, M. C., What Is Synergy. *Pharmacol. Rev.* **1989,** *41* (2), 93-141.
12. Hsu, M. F.; Yu, T. F.; Chou, C. C.; Fu, H. Y.; Yang, C. S.; Wang, A. H. J., Using Haloarcula marismortui Bacteriorhodopsin as a Fusion Tag for Enhancing and Visible Expression of Integral Membrane Proteins in Escherichia coli. *Plos One* **2013,** *8* (2), e56363.
13. Chang, H. Y.; Chou, C. C.; Hsu, M. F.; Wang, A. H. J., Proposed Carrier Lipid-binding Site of Undecaprenyl Pyrophosphate Phosphatase from Escherichia coli. *J. Biol. Chem.* **2014,** *289* (27), 18719-18735.
14. Feng, X. X.; Zhu, W.; Schurig-Briccio, L. A.; Lindert, S.; Shoen, C.; Hitchings, R.; Li, J. K.; Wang, Y.; Baig, N.; Zhou, T. H.; Kim, B. K.; Crick, D. C.; Cynamon, M.; McCammon, J. A.; Gennis, R. B.; Oldfield, E., Antiinfectives targeting enzymes and the proton motive force. *Proc. Natl. Acad. Sci. U. S. A.* **2015,** *112* (51), E7073-E7082.
15. Mukkamala, D.; No, J. H.; Cass, L. A.; Chang, T. K.; Oldfield, E., Bisphosphonate Inhibition of a Plasmodium Farnesyl Diphosphate Synthase and a General Method for Predicting Cell-Based Activity from Enzyme Data. *J. Med. Chem.* **2008,** *51* (24), 7827-7833.

16. Baykov, A. A.; Evtushenko, O. A.; Avaeva, S. M., A malachite green procedure for orthophosphate determination and its use in alkaline phosphatase-based enzyme immunoassay. *Anal. Biochem.* **1988,** *171* (2), 266 –270.